Experimental and Theoretical Investigation of Characteristics of Triangular Patch Antennas on Composite, Suspended and Multilayered Media

THESIS SUBMITTED BY

Mihir Dam

DOCTOR OF PHILOSOPHY (ENGINEERING)

ELECTRONICS AND TELECOMMUNICATION ENGINEERING,
FACULTY COUNCIL OF ENGINEERING & TECHNOLOGY
JADAVPUR UNIVERSITY
KOLKATA, INDIA

2019

CERTIFICATE FROM THE SUPERVISOR

This is to certify that the thesis entitled "*Experimental and Theoretical Investigation of Characteristics of Triangular Patch Antennas on Composite, Suspended and Multilayered Media.*" submitted by Mr. Mihir Dam, who got his name registered on *31 January, 2013* for the award of Ph.D. (Engg.) degree of Jadavpur University is absolutely based upon his own work under the supervision of *Dr. Manotosh Biswas* and that neither his thesis nor any part of the thesis has been submitted for any degree/diploma or any other academic award anywhere before.

(DR. MANOTOSH BISWAS)

Signature of the Supervisor
and date with office Seal

JADAVPUR UNIVERSITY

KOLKATA – 700032

INDEX NO: 125/13/ E

1. Title of the thesis:

Experimental and Theoretical Investigation of Characteristics of Triangular Patch Antennas on Composite, Suspended and Multilayered Media

2. Name, Designation & Institution of the Supervisor:

Dr. Manotosh Biswas

Professor

Department of Electronics and Telecommunication Engineering

Jadavpur University, Kolkata – 700032

3. List of Publications:

Journal Articles

I. M. Biswas and ***M. Dam***, "Closed-form model to determine the co-axial probe reactance of an equilateral triangular patch antenna," ***Microwave and Wireless Technologies Lett****er (Cambridge University)*, Vol. 10, no.7, pp. 801-813, May, 2018.

II. M. Biswas and ***M. Dam*****,** "CAD oriented improved cavity model to investigate a 30^0-60^0-90^0 right angled triangular patch antenna on single, composite and suspended substrate for the application in portable wireless equipments," ***IET Microwave Antennas and Propagation***., Vol. 12, no. 3, pp. 425-434, January, 2018.

III. ***M. Dam*** and M. Biswas, "Investigation of a right-angled isosceles triangular patch antenna on composite and suspended substrates based on a CAD-oriented cavity model," ***IETE Journal of Research (Taylor & Francis)****,* Vol. 63, pp. 248-259, January, 2017.

IV. M. Biswas and ***M. Dam***, "Theoretical and experimental studies on characteristics of an equilateral triangular patch antenna with and without variable air gaps," ***Microwave and Optical Technology Lett****ers(Wiley)*, Vol. 55, pp. 2271-2277, July, 2013.

V. M. Biswas and ***M. Dam***, "Characteristics of equilateral triangular patch antenna on suspended and composite substrates," ***Electromagnetics (Taylor & Francis)***, Vol. 33, pp. 99–115, February, 2013.

VI. M. Biswas and ***M. Dam***, "Fast and accurate model of equilateral triangular patch antennas with and without suspended substrates," ***Microwave and Optical Technology Lett****ers (Wiley),* Vol. 54, 2663-2668, August, 2012.

Conference Articles

I. ***M. Dam*** and M. Biswas, "Fast and accurate model to compute the resonant frequency of 30^0-60^0-90^0 right angle triangular patch antenna on composite and suspended substrate," ***Proc. of*** **4th International Conference on Science, Technology & Management (*ICSTM-2017*)***,* Nov 2017

II. ***M. Dam*****,** S. Mazumder, and M. Biswas, "CAD model to compute input impedance and bandwidth of tunable right angle isosceles triangular patch antenna " ***Proc. of International Conference on Computer, Communication, Control and Information Theory (C3IT-2015)***, Feb. 7-8, 2015, Hooghly, India. ISBN no. 978-1-4799-4445-3/15.

III. ***M. Dam*****,** B. Chakraborty, and M. Biswas, "Accurate resonant frequency of 30^0-60^0-90^0 right angle triangular patch with and without suspended substrate," ***Proc.*** **of International Conference *IESA-2014***, Feb. 02-04, 2014, pp. 219-222, Durgapur, India. ISBN no. 978-93-80813-27-1.

IV. ***M. Dam*** and M. Biswas, "Improved model to compute resonant frequency of right angle isosceles triangular patch antenna with and without suspended substrate," ***Proc. of Antenna Test and Measurement Society conference (ATMS-2014)****,* Feb, 2014, Chennai, India

V. ***M. Dam***, S. Sabiruddin, and M. Biswas, "Accurate model to compute of resonant frequency of right angle isosceles triangular patch antenna," ***IEEE Applied Electromagnetics Conference* (*AEMC-2013*)**, Bhubaneswar, pp. 1-2, 2013.

VI. ***M. Dam***, S. Mazumder, and M. Biswas. "Accurate CAD model for computation of input impedance of equilateral triangular patch antenna on suspended and composite substrates." ***International Conference on Microwave and Photonics (ICMAP-2013),*** 2013.

VII. ***M. Dam*** and M. Biswas, "CAD model to compute the effect of air gap on the band width of an equilateral triangular patch antenna," ***Proc. of Antenna Test and Measurement Society Conference (ATMS-2013)***, pp.180-183, Feb. 2013, Kolkata, India.

VIII. ***M. Dam*,** P. Ghosh, and M. Biswas, "Improved cavity model to compute the resonant resistance of an equilateral triangular patch antenna with and without air gap," ***Proc. of International Conference on Computation and Communication Advancement (IC3A-2013)***, pp.302-305 Jan. 11-12, 2013, Nadia, India.

IX. ***M. Dam*** and M. Biswas, "Fast and accurate model to compute the resonant frequency of triangular patch antenna on suspended and composite substrates," ***Proc. of International Conference on Communications, Devices and Intelligent Systems (CODIS-2012),*** pp.224-227, Dec. 28-29, *2012*, Kolkata, India, ISBN no. 978-1-4673-4698-6.

X. ***M. Dam*,** S. Mazumder, and M. Biswas, "Improved computation of resonant resistance of a tunable equilateral triangular patch antenna," ***Proc. of 13th National Symposium on Antenna and Propagation (APSYM-2012)***, pp.151-155, Dec. 14-16, 2012, Cochin, India. ISBN: 978-93-80095-40-0

XI. ***M. Dam*** and M. Biswas, "CAD model to compute the resonant frequency of triangular patch antenna with and without air gap," ***Proc. of Antenna Test and measurement Society conference (ATMS-2012)***, pp.153-156, Feb.2-3, 2012, Mumbai, India.

XII. ***M. Dam***, and M. Biswas, "CAD model to compute the input impedance of tunable triangular patch antenna," ***Applied Electromagnetics Conference & Indian Antenna Week* (*AEMC & IAW – 2011)***, Dec.16-18, 2011, Kolkata, India.

XIII. M. Biswas and ***M. Dam***, "CAD model to compute the resonant frequency of a tunable equilateral triangular patch antenna," ***12th National Symposium on Antenna and Propagation (APSYM-2010),*** pp. 23-29, Dec.14-16, 2010, Cochin, India.

4. List of Patents: Nil

ACKNOWLEDGEMENT

First and foremost , I would like to express my deep and sincere regards for my supervisor, Dr. Manotosh Biswas, Professor, Department of Electronics and Telecommunication Engineering for providing me the opportunity, support and freedom to carry on this research work. His passion, guidance and discipline have been indispensable to my growth as a researcher and as a person over the period of my research work. I would also like to express my heartfelt gratitude to him for his painstaking patience in correcting all the articles. His guidance helped me in all the time of research and writing of this thesis.

Besides my supervisor I would like to thank Prof. B. Gupta, Dept. of ETCE, Jadavpur University for his valuable suggestions during the research work. I also want to thank Mr. P. K. Sarkar, Electronic science, University of Calcutta for his encouragement during the research work.

I would like to thank the research committee members for their insightful comments and encouragement, but also for the hard question which incented me to widen my research from various perspectives.

My fellow research scholars Sourav Banik, Anirban Mandal and Mausumi Sen deserve special thanks for their continuous help and encouragement throughout the research study. I also want to mention Ardhendu, Kausik, Suman, Amartya, Biplob and all others who helped me a lot in laboratory for measurement purpose. Finally, I would like to pay my heartiest gratitude to all who are directly or indirectly associated in my research work.

I would like to acknowledge specially my colleague Dr. Srobonti Chattapadhyay, Dept. of Economics and my beloved students of Vidyasagar College For Women for their cordial help and support.

Last but not the least, I owe a lot to my parents, who encouraged and helped me at every stage of my personal and academic life. I also appreciate the role of my sister and brother-in-law in this regards and thank them all for their good wishes.

I am very much indebted to my wife Piyali and son Mayukh, who supported me in every possible way to see the completion of this work.

Above all, I owe it all to Almighty God for granting me the wisdom, health and strength to undertake this research task and enabling me to its completion.

Mihir Dam

Contents

LIST OF FIGURES

LIST OF TABLES

CHAPTER 1

Introduction

Content:

1. 1 Microstrip patch antenna (MPA)

Microstrip patch antennas (MPAs) are used as embedded antennas in portable wireless devices such as cellular phones and other communication equipments like missile, radar, satellite etc. [1-5]. The simplest form of microstrip antenna configuration may be defined as a radiating patch of any shape at one side of a dielectric substrate (e.g. PTFE) and a ground plane (metal) on the other side of the substrate as shown in Fig. 1.1. The thickness (h) of the substrate is usually in the range $0.003\ \lambda_0 \leq h \leq 0.05\ \lambda_0$. The dielectric constant (ε_r) of the substrate is typically in the range $2.2 \leq \varepsilon_r \leq 12$. The patch is generally made of conducting material such as gold, copper or silver and can take any possible shape. The radiating patch is fabricated by photo etching method. The typical shape of the patch is generally square, rectangular, circular, triangular and elliptical or some other common shapes.

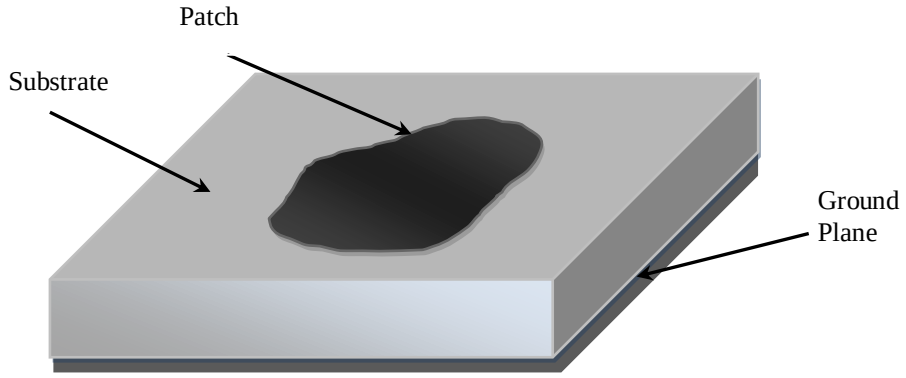

Figure 1.1: A simple microstrip patch antenna

1. 2. Advantages and Disadvantages of Microstrip Antenna

Some of the principal advantages of microstrip antennas are given below:

- Light weight and low fabrication cost.
- Linear and circular (left hand or right hand) polarizations are possible with simple changes in feed position.
- Can be easily integrated with microwave integrated circuits.
- Capable of dual and triple frequency operations and provides flexibility to be constructed in any shape.
- Mechanically robust when mounted on rigid surfaces.

- Can be made thin hence they do not perturb the aerodynamics of host aerospace vehicles.

The main advantage of the microstrip antenna is that it is usually low profile, in the sense that the substrate is fairly thin. If the substrate is thin enough, the antenna actually becomes "conformal," meaning that the substrate can be bent to conform to a curved surface.

However, microstrip antennas have some drawbacks including narrow bandwidth, power handling capability and low gain. These problems are overcome gradually by employing the advanced technology.

1. 3 Antenna Materials

The materials required to design the microstrip antenna are mainly divided into two sections. i) Materials for microstrip patch and ground plane and ii) Materials for dielectric Substrate.

1.3.1 Microstrip patch and ground plane

The highly conductive materials like Copper, Silver or Gold are used to design the patch and ground plane. Now, Silver has higher conductivity than copper or gold. But copper is much harder than the other two and also, it is cheaper than Gold and Silver. So, Copper is the mostly used material for this purpose.

1.3.2. Dielectric Substrate

In order to design a microstrip antenna the initial requirement is to choose appropriate dielectric substrate. The substrates mainly provide mechanical stability to the antenna. At the same time it also improves the electrical characteristics of the antenna [5]. So, the proper selection of substrate materials is very crucial and are chosen based on i) its inherent properties like relative permittivity (ε_r), loss tangent ($tan\delta$) etc. and ii) type of application of the antenna. For example flexible substrates are required to implement conformal microstrip antenna. For low frequency applications, substrates with high dielectric constant are suitable to reduce the antenna size, whereas in higher frequency application the antennas with low dielectric constant substrate are used. Different materials like Ceramic, Semiconductor, Ferromagnetic, Synthetic and Composite types [5] may be used as substrates of antenna. Among them, most widely used materials are composite substrates as it combines the properties of other basic materials to attain

desired mechanical and electrical properties. Commonly used materials are RT/Duried ($2.2 \leq \varepsilon_r \leq 10.5$, $tan\delta \leq 0.0024$), Arlon DiClad ($2.2 \leq \varepsilon_r \leq 10.5$, $tan\delta \leq 0.0019$), Arlon Cuclad ($\varepsilon_r \approx 2.17\text{-}2.6$, $tan\delta \leq 0.0018$), Ultralum2000 ($\varepsilon_r \approx 2.5$, $tan\delta \approx 0.0022$), Taconic ($\varepsilon_r \approx 2.33$, $tan\delta \approx 0.001$), Epoxy Glass FR4 ($\varepsilon_r \approx 4.0\text{-}6.0$, $tan\delta \approx 0.01$) and Rogers materials ($2.4 \leq \varepsilon_r \leq 10.2$, $tan\delta \leq 0.0022$) etc [5].

1.4 Feeding technique

In order to get radiation from microstrip antenna, the radiating patch is excited by RF signal. To accomplish this work, a number of feeding techniques are available. Among them, predominant techniques are microstrip feed, co-axial feed, aperture coupled feed and proximity coupled feed [1-5].

1. 4.1 Microstrip feed

In microstrip feed technique, a conducting strip is connected directly to the edge of the microstrip patch as shown in Fig. 1.2. The conducting strip is smaller in width as compared to the patch. This kind of feed arrangement has the advantage that the feed can be etched on the same substrate to provide a planar structure. So, it is very easy to fabricate. For higher substrate thickness the surface waves and spurious feed radiation become significant for this configuration. This disadvantage limits the bandwidth of the antenna after design.

1.4.2 Coaxial feed

The inner conductor of the coaxial probe is attached to the radiation patch while the outer conductor is connected to the ground plane in coaxial feed technique. This feeding technique is depicted in Fig. 1.3. The coaxial probe feed is also easy to fabricate and simple to find impedance matching between co-axial probe and radiating patch. It provides also low spurious radiation. However, it also has narrow bandwidth and it is slightly complicated to previous feed, especially for thick substrates. Longer probe is required for thick substrates which results in an increase in feed reactance.

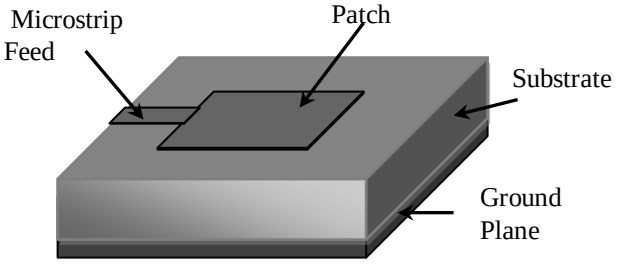

Figure 1.2: Microstrip feed

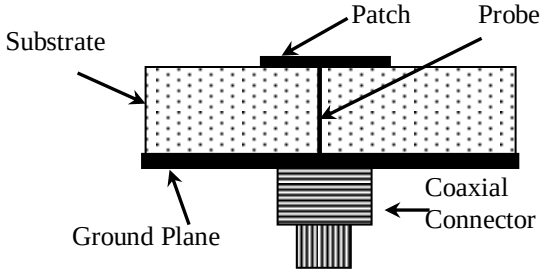

Figure 1.3: Co-axial feed

1.4.3 Aperture coupling feed

Figure 1.4 shows an aperture coupled feed structure. In this scheme, the radiating microstrip patch element is etched on the top of the antenna substrate, and the microstrip feed line is etched on the other side of the substrate as shown in Fig. 1.4. The coupling aperture is usually centered under the patch, leading to lower cross-polarization due to symmetry of the configuration. The amount of coupling from the feed line to the patch mainly depends on the size, shape and location of the aperture.

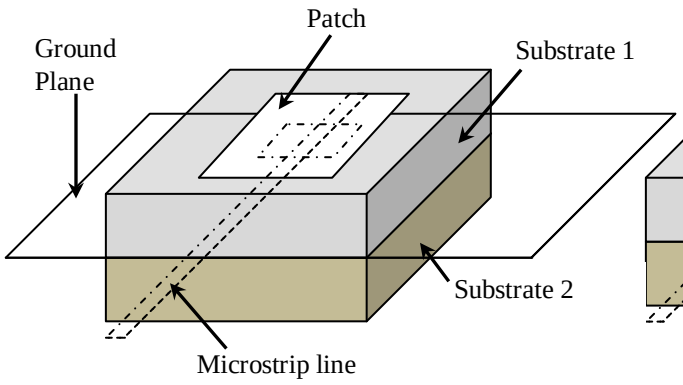

Figure 1.4: Aperture coupled feed

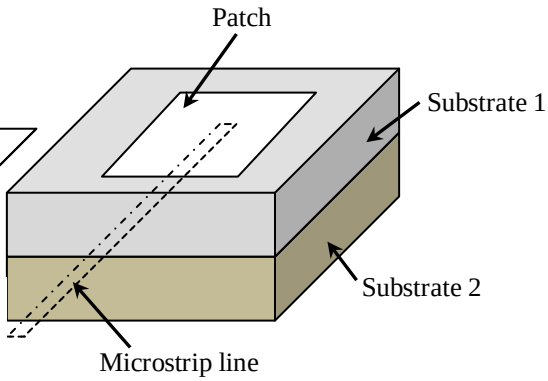

Figure 1.5: Proximity feed

By controlling the width of the feed line and the length of the slot typical matching is performed. The thickness and dielectric constants of these two substrates may thus be selected independently to optimize the distinct electrical functions of radiation. Since the ground plane separates the patch and the feed line, spurious radiation is moderate. The main problem of aperture coupling is that it is very difficult to design and provides the narrow bandwidth.

1.4.4 Proximity feed

The proximity feeding technique is shown in Fig. 1.5. In this technique the two dielectric substrates are used such that the feed line is between the two substrates and the radiating patch is on top of the upper substrate as shown in Fig. 1.5. This feeding technique eliminates spurious feed radiation and the same time provides very high bandwidth of about 13%. This technique very easily handles the electrically thick MPAs. This scheme also provides choices between two different dielectric media, one for the patch and one for the feed line to optimize the individual performances. This technique is also called the electromagnetic coupling scheme.

1.5 Methods of Analysis

The several well known approaches are available to analyze microstrip patch antenna. The transmission line model, cavity model, and full wave model (which include primarily integral equations/Moment Method) are the preferred models. Among them, the transmission line model is the simple. It gives good physical insight but it provides less accurate results. The full wave models give less insight as compared to the previous model mentioned above and they are very complex in nature. But the full wave models are more accurate. These models are applied to analyze the single elements, finite and infinite arrays, stacked elements, arbitrary shaped elements and coupling between the elements. The cavity model [1-5] is a little more complex than transmission line model but much simpler than full wave method and gives good physical insight. This model provides more accurate results compared to the transmission line model but error in this model increases for the increase of substrate thickness.

1.5.1 Transmission Line Model

In this model, the microstrip patch element is viewed as a transmission line resonator with the field only varying along the length (no transverse field variations). The radiation occurs mainly from the fringing fields at the open circuited ends.

This model represents the microstrip antenna by two slots of width *W* and height *h*, separated by a transmission line of length *L* as shown in Fig. 1.6 (a). The microstrip is essentially a non homogeneous line of two dielectrics, typically the substrate and air.

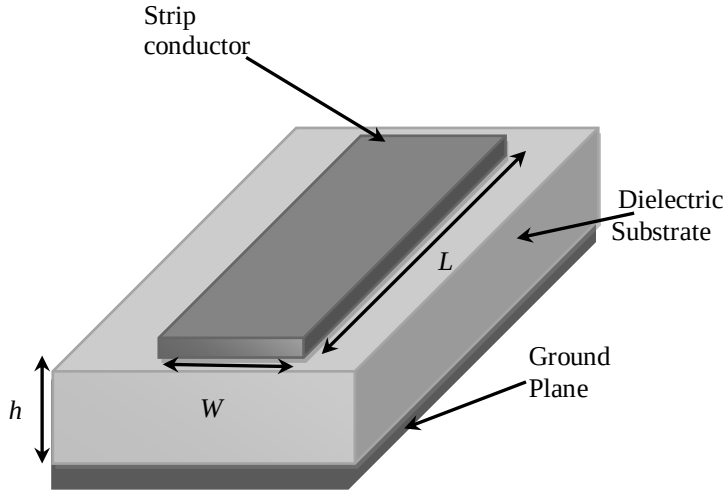

Figure 1.6(a): Microstrip Line

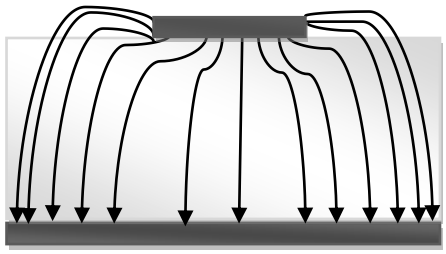

Figure 1.6(b): Electric Field Lines

In microstrip antenna, most of the electric field lines reside in the substrate and parts of some lines in air as shown in Fig. 1.6 (b). The phase velocities would be different in the air and the substrate, for this reason the transmission line cannot support pure transverse-electric-magnetic (TEM) mode of transmission. So, the dominant mode of propagation would be the quasi-TEM mode. In order to account for the fringing field an effective dielectric constant ($\varepsilon_{r,eff}$) must be obtained. The value of $\varepsilon_{r,eff}$ is slightly less than the actual dielectric constant ε_r because the fringing fields around the periphery of the patch are not confined in the dielectric substrate but are also appear in the air.

The microstrip patch antenna is represented by two slots, separated by a transmission line of length *L* and open circuited at both the ends as shown in Fig. 1.7(a). Along the width of the patch, the voltage is a maximum and the current is a minimum due to open ends. The fields at the edges can be resolved into normal and tangential components with respect to the ground plane. It is seen from Figure 1.7(b) that the normal components of the electric field at the two edges along the width are in opposite directions and thus out of phase since the patch is λ/2 long and hence they cancel each other in the broadside direction. The edges along the width can be represented as two radiating slots, which are $\lambda/2$ apart and excited in phase and radiating in the half space above the ground plane. The fringing fields along the width can be modeled as radiating slots and electrically the patch of the microstrip antenna looks greater than its physical dimensions.

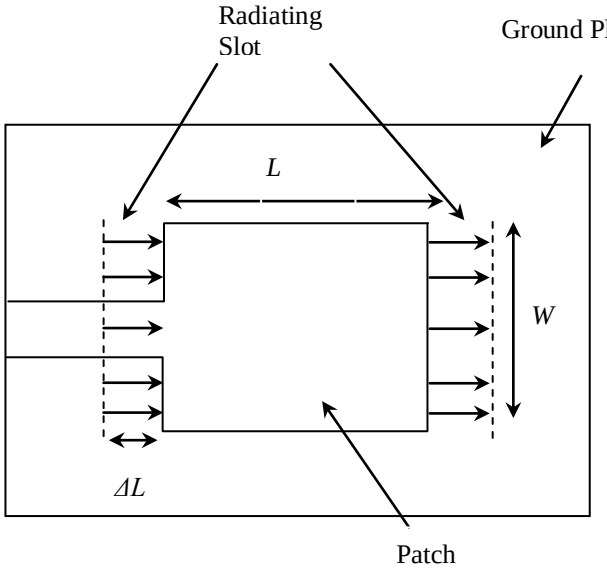

Figure 1.7(a): Top View of Antenna

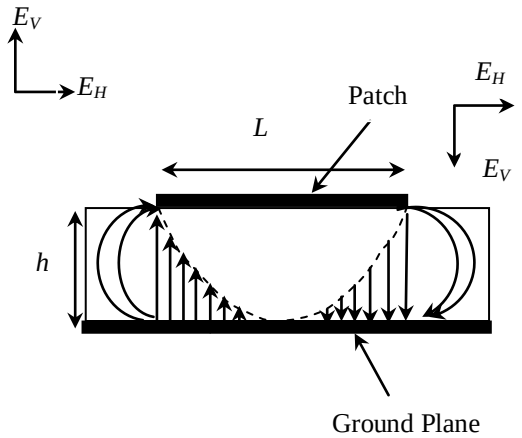

Figure 1.7(b): Side View of Antenna

1.5.2. Full wave Model

Method of Moments [6], the Finite Difference Time Domain method [7], the Finite element method (FEM) [8] all belong to this category. They are suitable for volumetric configurations. In Method of Moments (MoM) the surface currents are used to model the microstrip patch and the volume polarization currents are used to model the fields in the dielectric slab. The MoM is also very useful to solve electromagnetic scattering and radiation problems. This method is based on reducing the operator equations to a set of linear equations that is written in matrix form. The Finite Element Method (FEM) is more popular amongst these methods. In this method the region of interest is divided into any number of finite surfaces or volume elements depending upon the planar or volumetric structures to be analyzed. These discretized units, generally referred to as finite elements, are well defined geometrical shapes, such as triangular elements for planar configurations and tetrahedral and prismatic elements for three dimensional configurations.

1.5.3. Cavity Model

In this model the region between the patch and the ground plane is treated as a cavity, which is surrounded by magnetic walls around the periphery and by electric walls from the top and bottom sides as shown in Fig. 1.8.

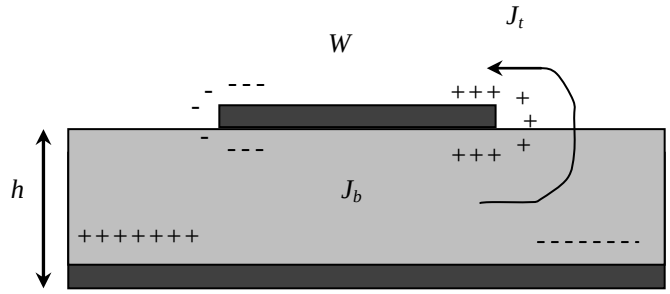

Figure 1.8: Charge distribution and current density creation on microstrip patch.

Since the thin substrates are used, the field inside the cavity is assumed to be uniform along the thickness of the substrate. In cavity model, the analysis is made simple, by expressing the electromagnetic fields within the patch substrate, as a summation of the various resonant modes of the two dimensional radiating patch. The cavity model makes the following assumptions:

• For a thin substrate, fields in the cavity do not vary with z-axis.

• Tangential component of the magnetic field is negligible at the edge of patch.

• The existence of a fringing field can be accounted for by slightly extending the edges of the patches

1.6. Motivation of the work

The concept of microstrip radiators was first proposed by Deschamps [9] in 1953. After two years, a patent was reported in [10] on planar radiator. Couple of works on MPA are reported during late 1960's and early 1970's [11, 12] but it took nearly two decades after first reported work [9] for practical implementation of MPA by Howell [13] and Munson [14]. Since this period, the microstrip patch drew much attention of the researchers in investigating the structure as planar circuit elements [15-19] and as radiating elements on conventional [20-70] and other improved configurations [71-115]. Few contemporary articles of the 70's and the 80's [14-16, 35, 36] provide very significant information about different MPA which is still used by the researchers. These developments of MPA from 70's to few subsequent decades is well documented in different books [1-5, 116-122]. Among them the developments of MPAs were first reported in two books [1, 2] in 1980 and 1981. Later two handbooks published in 1989 [3] and 2001 [5] are very noteworthy to mention because these are very well documented and cover most of the aspects of MPA research of the contemporary period. Few other recent developments of MPA technologies like strip-slot-foam-inverted patch (SSFIP) to expand the operating frequency range of microstrip antennas, multi resonators in planar and stacked configurations for dual band response, wired antennas, microstrip reflect array antennas, reconfigurable microstrip antennas, wearable antennas for body area networks etc. are documented in the books reported in [116-122]. Initially most of the researchers concentrated their investigations of MPA with conventional geometry as mentioned earlier. Different theoretical models are available to compute resonant frequency, input impedance, quality factor, band width, gain, efficiency and radiation performance of conventional MPA [20-70]. Recently, some new structures e.g. patch on suspended substrate, patch loaded with dielectric cover, stacked patch configuration etc. have drawn attention of the researchers due to improved performance over conventional configuration and few additional important characteristics. For example, structures like patch on suspended substrate [71-78] provide tunability in characteristics and also

improve the impedance bandwidth. The microstrip radiator with one or more dielectric cover layers [79-101] provide good support against the environmental hazard and also improves radiation performance, The two or more patches are in stacked configuration [102-115] is used to enhance the bandwidth and the gain of an antenna.

Different geometries like rectangular, circular, triangular, elliptical etc. has been considered for the design and analysis of MPA. Among these structures, the rectangular and the circular geometries are widely investigated till now [1, 5, 11-15, 20-54, 63, 73, 75-84, 86, 94, 97-101, 104-110, 112-115]. The triangular microstrip patch is the least investigated geometry compared to rectangular and circular patches till now. The radiation characteristics (fundamental mode) of triangular patch are similar to that of a rectangular patch. It is used to design the narrow band pass filter due to its narrow impedance bandwidth. Also, it can receive the signal of interest in the presence of noise. This patch shape is also well suitable to use in compact arrays on a conformal surface of satellite, missile, radar etc. [62]. So, the current work is mainly concentrated on different triangular geometries.

The antenna must be operated around its resonant frequency for improving the bandwidth, efficiency and gain. So, the accurate computation of resonant frequency is very essential. Except resonant frequency another important parameter of MPA is the input impedance. To improve the radiation efficiency, better impedance matching is required between coaxial probe and radiating patch. So, the accurate computation of input impedance at any feed location is very important. A number of studies have been carried out for predicting the resonant frequency of an equilateral triangular patch antenna [16-19, 55-67] on conventional structure but the investigation on other triangular geometry is still at an initial stage. Today, the patch antenna on composite and suspended substrate is being received a great deal of attention due to its frequency tunability features. The patch antenna on suspended substrate provides improved bandwidth, efficiency and gain. The increase in the bandwidth of triangular geometry is essential because of its very narrow bandwidth. The triangular patch antenna on suspended substrate has been investigated by [74]. But this study does not contain any experimental investigation of resonant frequency, input impedance and bandwidth with air gap. Parameters of different triangular patch on composite substrate are also not well investigated. A few

investigations are available to find the performance of triangular patch including the effect of dielectric cover [85, 95, 96]. Neither any design guide line nor any experimental result is available in open literature to predict the important parameters of a triangular patch covered with more than one dielectric layers. Electromagnetically coupled stack patch configuration is another promising area of research to improve the bandwidth and gain of triangular patch antenna. But the investigation of triangular geometry in stack patch configuration is still least investigated [102-104]. The full wave analysis was used to predict the important parameter of the stacked triangular patch in [102] and this article also provide some experimental results. The articles [103,104] are totally experiment based. Any closed form model is not available to analyse the stacked triangular patch. Therefore, these areas of investigation require serious attention of researchers.

It is already mentioned earlier that several models are available to investigate the parameters of MPA in different configuration. The preferred models for the studies are the transmission line model, cavity model, and full wave model. Among them, the most accurate approach is full wave model as discussed in section 1.4.2. Several studies of MPA based on different full wave models have been reported in [6-8, 18, 24, 85]. Several commercial softwares like HFSS, CFDTD, IE3D [123-125] may be used for the analysis of the microstrip patch antenna. But some limitations are associated with full wave approaches mentioned in section 1.4.2. Additionally the full wave analysis [4-6, 18, 24, 85] and commercial softwares [123-125] do not provide the closed form expressions and take large computational time. So, the full wave analysis and commercial softwares are not useful for direct synthesis of patch antennas. Whereas, the CAD oriented transmission line and cavity model are ideal for design purposes because it involves less mathematical steps and takes less computational time. It is also easy to implement and provide closed form expressions.

Considering all these aspects of triangular patch antennas, we have proposed a fast and accurate CAD oriented model based on transmission line, conformal technique and cavity model to investigate the characteristics of different triangular shaped patch antenna (i.e. equilateral, isosceles and 30^0-60^0-90^0 right angled triangle) on conventional and improved structure. The proposed theories are verified with experimental results of the fabricated prototypes throughout this dissertation.

The thesis is organised as: investigation of (i) *resonant frequency, quality factor, bandwidth, gain, probe reactance and input impedance of a co-axial probe fed equilateral triangular microstrip patch antenna (chapter 2 and 3), right angled isosceles (chapter 4) as well as* 30^0-60^0-90^0 *right angled triangular (chapter 5) microstrip patch antennas on single layered and double layered substrates,* (ii) *Equilateral triangular microstrip patch antenna covered with several dielectric layers (chapter 6) and* (iii) *equilateral triangular microstrip patch antennas in stacked configuration (chapter 7).*

In Chapter 2, Coaxial probe fed equilateral triangular microstrip patch on single and double layered substrate has been meticulously investigated, as shown in Fig. 1.9. A comprehensive design guide line based on CAD oriented cavity model and single resonant parallel *R-L-C* circuit has been proposed to predict the resonant frequency, input impedance, quality factor, bandwidth and gain.

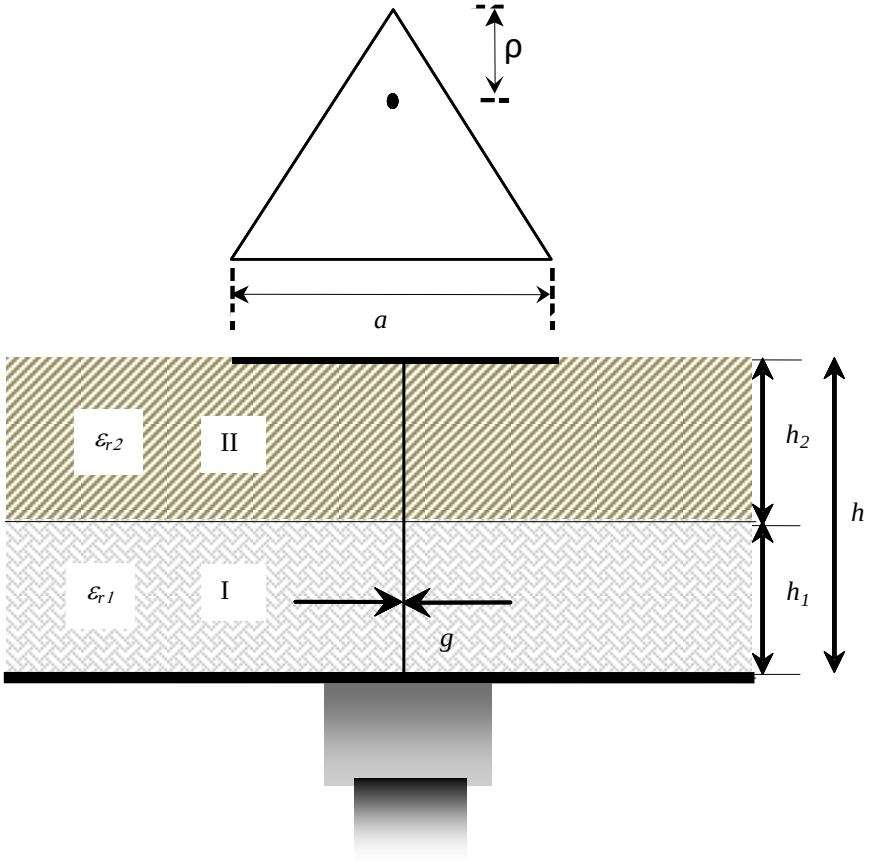

Figure 1.9: A schematic diagram of probe-fed equilateral triangular microstrip.

A series of experiments is performed using a Network Analyzer Agilent- E5071B with fabricated prototypes. The commercial softwares (IE3D, HFSS and CFDTD) are also used to validate present models.

In **Chapter 3,** a simple closed form analytical formula is proposed to compute the probe reactance of an equilateral triangular patch antenna (ETPA). For a probe fed patch antenna, the total input impedance is the series combination of probe reactance and the patch impedance as shown in Fig. 1.10. The computation of input impedance will be incomplete without consideration of the probe reactance. The effect of probe reactance is negligible when it is located at the edge of the patch but it becomes significant when the probe is located near the center of the patch and the thickness of the substrate is high. The patch reactance very much depends on the thickness and permittivity of the substrate.

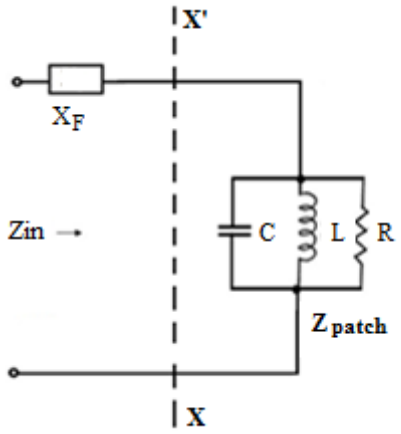

Figure 1.10: Equivalent resonant parallel *R-L-C* circuits of probe-fed equilateral triangular microstrip patch antenna.

To the best of our knowledge no model is available to compute probe reactance of an ETPA. For the first time, a very simple and efficient formula is proposed to accurately predict the probe reactance of an equilateral triangular patch antenna. The variation of the probe reactance with the variation of antenna dimension, substrate electrical parameters and probe location is examined thoroughly. The computed values employing the present model is verified with performed experiments using a Network Analyzer Agilent-E5071B. The **chapter 2** and **chapter 3** as a whole provide a complete model to accurately compute the input impedance characteristics of an ETPA.

In **chapter 4**, a set of simple and fast CAD oriented cavity model and single resonant parallel *R-L-C* circuit has been proposed to predict the characteristics of a right angle isosceles triangular patch antenna (RAITPA) on single, composite and suspended substrate as shown in Fig. 1.11. The endeavour of this work is to eliminate the drawbacks of the models reported in [64, 67]. To the best of our knowledge this is the first time the effect of composite and suspended substrate on resonant frequency, input impedance, gain and bandwidth of a RAITPA has been investigated. The model is verified with our experimental result and experimental result available in open literature. Also HFSS simulator is used to generate the simulated results.

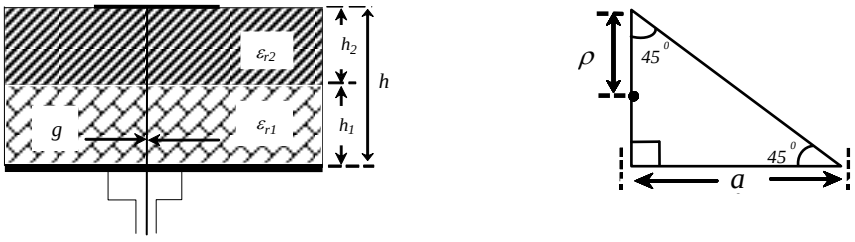

(a) (b)

Figure 1.11: A schematic diagram of probe-fed right angled isosceles triangular patch antenna. (a) Cross sectional view, (b) Patch shape.

Chapter 5 presents an improved model for resonant frequency, input impedance, bandwidth and gain for a 30^0-60^0-90^0 right angled triangular patch antenna printed on a single, composite and suspended substrate as shown in Fig 1.12. Merits of this model are the low computation cost and mathematical simplicity. It is useful for direct application in computer aided design (CAD) programs. The model is based on the classical methods: (i) the cavity model determining the resonant frequency and input resistance at resonance, (b) the dynamic and effective permittivity to take into account the influence of fringing field at the edge of the patch and (c) the equivalent resonant parallel *R-L-C* circuit for determination of input impedance. The prototypes have been etched on Roggers and Taconic substrates. The Network Analyzer Agilent- E5071B is used to test the prototypes.

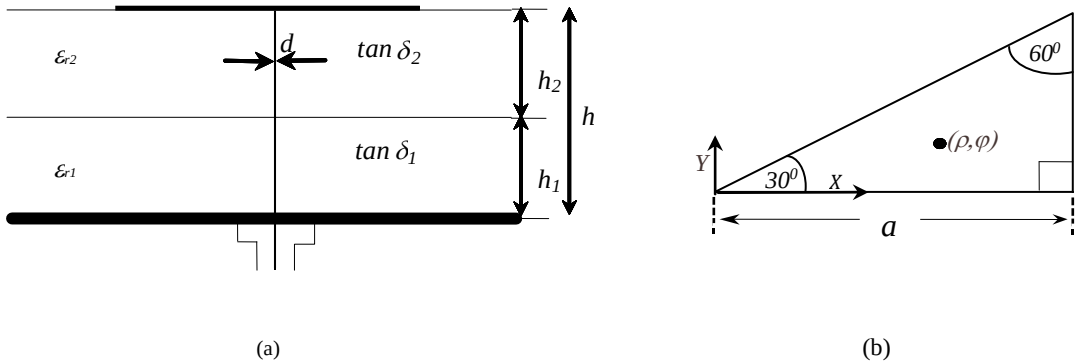

(a) (b)

Figure 1.12: (a). A schematic diagram of a probe-fed 30^0-60^0-90^0 right angled triangular patch antenna (RATPA) (b) Patch shape

In chapter 2 to chapter 5, we have primarily reflected the investigation of microstrip antenna with three different triangular shaped patches printed on single, composite and suspended substrate. Today it is well known that MPA finds extensive application in the design of many useful sensors [94, 97, 98, 126-132] both on fixed and portable devices like aircraft radome, missiles, radars and satellites etc. [98]. So in those outdoor applications the patch antenna must be covered with dielectric layers to protect the patch against environmental hazards. But due to imposition of dielectric cover layer the important parameters such as resonant frequency, quality factor, bandwidth, input impedance and gain of the patch are changed. So, the effect of dielectric cover layers must be considered accurately to properly install the antenna in wireless equipments. But so far triangular patch with one dielectric cover layer finds very few investigations [85, 95, 96]. But the models [85, 95, 96] have some serious drawbacks. In order to overcome the drawbacks of the earlier models we have introduced **Chapter 6.** A set of fast and simple closed-form expressions has been presented to compute the resonant frequency, quality factor, input impedance and gain of a triangular patch antenna covered with several dielectric layers as shown in Fig 1.13. A series of experiments is performed with designed prototypes using a Network Analyzer Agilent- E5071B. A HFSS simulation software has also been employed to validate the model.

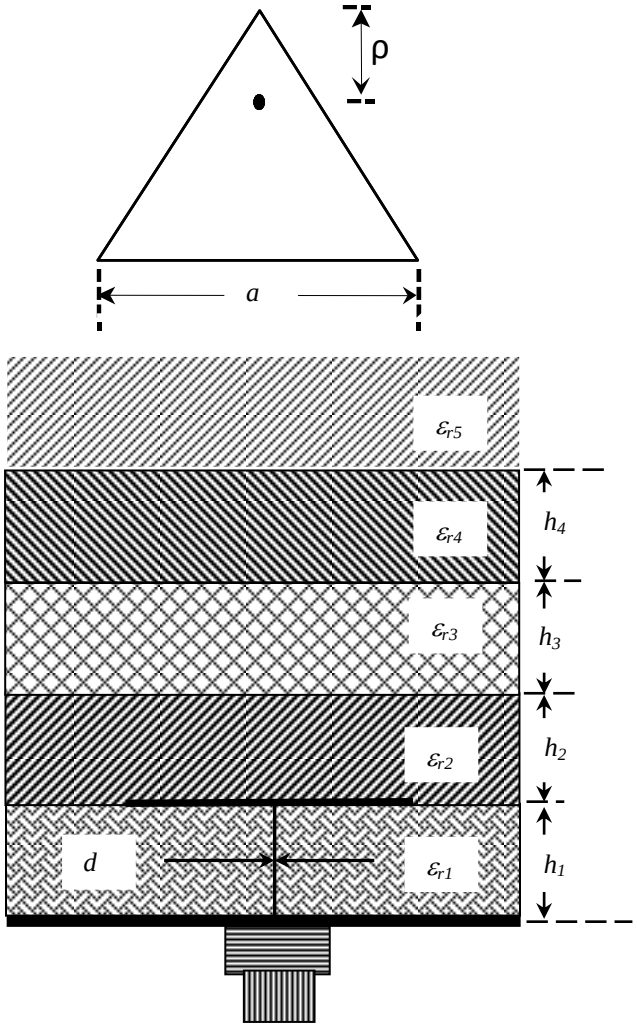

Figure 1.13: A schematic diagram of probe-fed equilateral triangular microstrip patch on multilayered structure

The triangular geometry is inherently narrow band structure. So, we cannot apply this shape of patch antenna in broadband application. The use of ETPAs in stacked configuration (shown in Fig. 1.14) enhanced the bandwidth up to 20% without degrading the other antenna performances as reported in [103]. So, the stacked patch configuration is the good choice for broad band application. But stacked ETPA find very little investigations [102-104] till now. The article [102] has employed full wave analysis to predict few parameters of the stacked triangular and this article also provide some experimental results. The articles [103,104] provide only experimental results of stacked ETPA. The CAD oriented closed form expression is very useful for practical implementation of ETPA in stack patch configuration. But any theoretical closed form expressions is not reported till now. In **Chapter 7,** accurate CAD oriented closed form

expressions have been proposed to compute resonant frequency, quality factor, band width, input impedance and gain of an ETPA in stacked configuration.

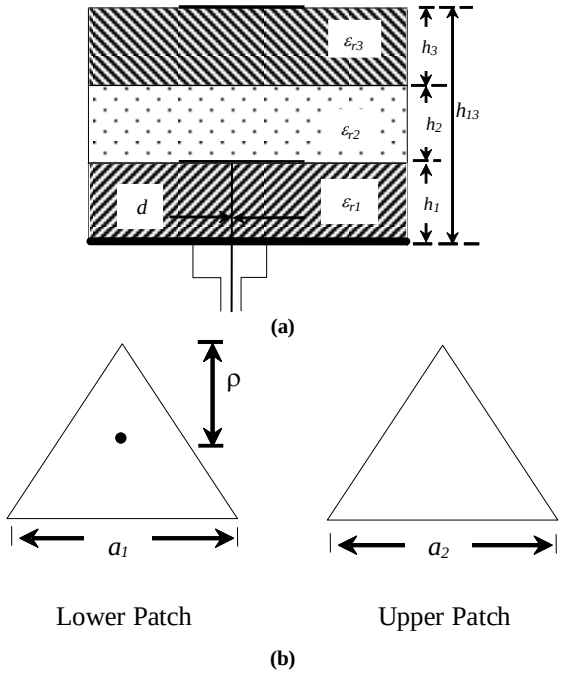

Figure 1.14 : A schematic diagram of probe-fed equilateral triangular microstrip patch in stacked patch configuration

This model is based on conformal mapping, transmission line model, cavity model analysis and single resonant parallel *R-L-C* circuit. To the best of our Knowledge this is the first time that we have proposed a closed form analytical model to compute the parameters of ETPAs in stacked configuration. Theoretical results employing the present model are compared with measured value [102, 103]. We have also performed some experiments with fabricated prototypes for further validation of the proposed model. Commercial software HFSS has also been employed to validate the model.

REFERENCES

[1] I. J. Bahl and P. Bhartia, "Microstrip antennas," *Artech House*, Dedham, MA, 1980.

[2] J. R. James, P. S. Hall, and C. Wood, "Microstrip antennas: theory and design," *UK, Peter Peregrinus*, London, 1981.

[3] J. R. James and P. S. Hall, "Handbook of microstrip antennas," *UK, Peter Peregrinus*, London, 1989.

[4] C. A. Balanis, "Antenna Theory: Analysis and Design," *John Wiley & Sons*, NY, 1997.

[5] R. Garg, P. Bhartia, I. J. Bahl, and A. Ittipiboon, "Microstrip antenna design handbook," *Artech house*, 2001.

[6] E.H. Newman and Tulyathan, "Analysis of microstrip antennas using method of moments," *IEEE Trans. Antennas Propagat*., vol. AP-29, pp.47-53, January 1981.

[7] A. Aflove, "Computational electrodynamics: The finite-difference time-domain method," Boston *MA : Artech House*, 2000.

[8] P. Silvester, "Finite element analysis of planar microwave network," *IEEE Trans. Microw. Theory Tech.*, vol. 21, pp. 104-108, 1973.

[9] G. A. Deschamps, "Microstrip microwave antennas," *presented at the Third USAF Symp. on Antennas*, 1953.

[10] H. Gutton and G. Baissinot, "Flat aerial for ultra high frequencies," *French Patent*, no. 703 113, 1955.

[11] J. Watkins, "Circular resonant structures in microstrip," *Electron Lett*., vol. 5, pp. 524–525, 1969.

[12] T. Itoh and R. Mitra, "Analysis of microstrip disk resonator," *Arch Eleck Ubertragung*, vol. 27, pp. 456–458, 1973.

[13] J. Q. Howell, "Microstrip antennas," *Dig. IEEE Int. Symp. Antennas Propagat.*, pp. 177-180, Dec. 1972.

[14] R. E. Munson, "Conformal microstrip antennas and microstrip phased arrays," *IEEE Trans. Antennas Propagat.*, vol. 22, pp. 74-78, 1974.

[15] I. Wolff and N. Knoppik, "Rectangular and circular microstrip disk capacitors and resonators," *IEEE Trans. Microwave Theory Tech.*, vol. 22, pp. 857-864, 1974.

[16] J. Helszajn and D. S. James, "Planar triangular resonators with magnetic walls," *IEEE Trans. Microwave Theory Tech*., vol. 26, pp. 95-100, Feb.1978.

[17] J. Helszajn, D. S. James, and W. T. Nisbet, "Circulators using triangular resonators," *IEEE Trans. Microw. Theory Tech*., vol. 27, pp.188-193, Feb. 1979.

[18] A. K. Sharma and B. Bhat, "Analysis of triangular microstrip resonator," *IEEE Trans. Microw. Theory Tech*., vol. 30, no. 11, pp. 2029 – 2031, Nov. 1982.

[19] J. S. Hong and M.J. Lancaster, "Theory and experiment of dual-mode microstrip triangular patch resonators and filters," *IEEE Trans. Microw. Theory Tech.*, vol. 52, no. 4, pp. 1237 – 1243, Apr. 2004.

[20] Y. T. Lo, D. Solomon, and W. F. Richards, "Theory and experiment on microstrip antennas," *IEEE Trans. Antennas Propagat.*, vol. 27, pp. 137-45, 1979.

[21] K. R. Carver and E. L. Coffey, "Theoretical investigation of the microstrip antenna," *Technical Report 00929 Physical Science Laboratory New Mexico State University,* 1979.

[22] W. F. Richards, Y. T. Lo, and D. D. Harrison, "An improved theory for microstrip antennas and application," *IEEE Trans. Antennas Propagat.*, vol. 29, pp. 38-46, 1981.

[23] K. R. Carver and J. W. Mink, "Microstrip antenna technology," *IEEE Trans. Antennas Propagat.,*vol. 29, pp. 2-24, 1981.

[24] A. Samet and A. Bouallegue, "Fast and rigorous calculation method for MoM matrix elements in planar microstrip structures," *Electron. Lett.*, vol. 36, no. 9, pp. 801-803, April 27, 2000.

[25] D. M. Pozar, "Input impedance and mutual coupling of rectangular microstrip antennas," *IEEE Trans. Antennas Propagat.*, vol. 30, pp. 1191-196, 1982.

[26] A. Khellaf, D. Thouroude, and J. P. Daniel, "Simple expression of rectangular patch's resistance at resonance," *Electron Lett.*, vol. 26, pp. 1188–190, 1990.

[27] D. Schaubert, D. M. Pozar, and A. Adrian, "Effect of microstrip antenna substrate thickness and permittivity: Comparison of theories with experiment," *IEEE Trans. Antennas Propagat.*, vol. 37, pp. 677-82, 1989.

[28] Z. Sipus, J. Bartolic, and B. Stipetic, "Input impedance of rectangular patch antenna fed by microstrip line," *Electron Lett.*, vol. 28, pp. 1886–888, 1992.

[29] M. Deshpande and M. Bailey, "Input impedance of microstrip antennas," *IEEE Trans. Antennas Propagat.*, vol. 30, pp. 645-650, 1982.

[30] W. C. Chew and Q. Liu, "Resonance frequency of a rectangular microstrip patch*," IEEE Trans. Antennas Propagat.*, vol. 36, pp. 1045–056, 1988.

[31] B. M. Alarjani and J. S. Dahele, "Feed reactance of rectangular microstrip patch antenna with probe feed" *Electron. Lett.*, vol. 36, pp. 388-390, 2000.

[32] A. K. Verma and Nasimuddin, "Input impedance of rectangular microstrip patch antenna with iso/anisopropic substrate-superstrate," *IEEE Microw. Wireless Components Lett.*, vol. 11, pp. 456-458, 2001.

[33] L.C. Shen, S.A. Long, M.R. Allerding, and M.D. Walton, "Resonant frequency of a circular disc, printed-circuit antenna," *IEEE Trans. Antennas Propagat.*, vol. 25, pp. 595–596, 1977.

[34] S. A. Long, L. C. Shen, and P. B. Morel, "Theory of the circular-disc printed-circuit antenna," *Inst. Elec. Eng. Proc.,* vol. 125, pt. H, no. 10, pp. 925-928, 1978.

[35] A.G. Derneryd, "Analysis of the microstrip disk antenna element," *IEEE Trans. Antennas Propagat*., vol. 27, pp. 660–664, 1979.

[36] W.C. Chew and J.A. Kong, "Effects of fringing field on the capacitance of circular microstrip disk," *IEEE Trans. Microw. Theory Tech*., vol. 28, pp. 98–104, 1980.

[37] S. Yano and A. Ishimaru, "A theoretical study of the input impedance of a circular microstrip disk antenna," *IEEE Trans. Antennas Propagat.*, vol. 29, pp. 77–83, 1981.

[38] H. A. Wheeler, "A simple formula for the capacitance of a disc on dielectric on a plane," *IEEE Trans. Microw. Theory Tech.*, vol. 30, pp. 2050-2054, 1982.

[39] R. W. Dearnley and A. R. F. Barel, "A broad-band transmission line model for a rectangular microstrip antenna," *IEEE Trans. Antennas Propagat.*, 37, pp. 6-15, Jan.1989.

[40] Y. S. Nanjing *et al.* "CAD formula for rectangular patch antenna on thick substrate," *Dig. IEEE Int. Symp. Antennas Propagat.*, pp. 866-869, 2002.

[41] K.F. Lee and J.S. Dahale, "Mode characteristics of annular-ring and circular-disc microstrip antenna with and without airgaps*," IEEE Antennas Propagat. Soc. Dig*., , pp. 55–58, 1983.

[42] J.S. Dahele and K.F. Lee, "Effect of substrate thickness on the performance of a circular-disk microstrip antenna," *IEEE Trans. Antennas Propagat*., vol. 31, pp. 358–360, 1983.

[43] M. J. Mehler, T. S. M. Maclean and A.K. Abbas, "Input impedance of a circular microstrip disc antenna using mode matching," *Electron Lett*., vol. 22, pp. 362–363, 1986.

[44] M. Davidovitz and Y. T. LO, "Input impedance of a probe-fed circular microstrip antenna with thick substrate," *IEEE Trans. Antennas Propag.*, vol.34**,** pp. 905-911. 1986.

[45] F. Abboud, J.P. Damiano, and A. Papiernik, "A new determination of the resonant frequency of a circular disc microstrip antenna: Application to the thick substrate," *Electron Lett*., vol. 24, pp. 1104–1106, 1988.

[46] K. Antoszkiewicz and L. Shafai, "Impedance characteristics of circular microstrip patches," *IEEE Trans. Antennas Propagat*., vol. 38, pp. 942–946, 1990.

[47] A. K. Bhattacharyya, "Characteristics of circular patch on thick substrate and superstrate," *IEEE Trans. Antennas Propagat*., vol. 39, pp. 1038–1041, 1991.

[48] K. F. Lee, K. M. Luk, and P.Y. Tam, "Cross polarization characteristics of circular patch antennas," *Elect. Lett.*, vol. 28, no. 6, pp. 587-589, Mar., 1992.

[49] J. A. Navarro and K. Chang, "A ka-band cavity-enclosed aperture coupled circular patch antenna and array for millimeter-wave circuit integration," *Proc. IEEE AP-S Int. Symp. Dig., Chicago, IL*, pp. 313–316, 1992.

[50] J. T. Aberle, "On the use of metallized cavities backing microstrip antennas," *Proc. IEEE AP-S Int. Symp. Dig.*, pp. 60–63, 1993.

[51] J.A. Navarro, L. Fun, and K. Chang, "Active integrated strip line circular patch antennas for spatial power combining," *IEEE Trans. Microw. Theory Tech.*, vol. 41, pp. 1856–1863, 1993.

[52] K.L. Wong and J.Y. Jan, "Broadband circular microstrip antenna with embedded loading," *Electron Lett.*, vol. 34, pp. 1804–1805, 1998.

[53] B.H. Uhl, M. Dawood, and S. Castillo, "Quadrature-modulated circular microstrip patch antenna for phased Arrays," *IEEE Antennas Wireless Propagat. Lett.*, vol. 9, pp. 958–961, 2010.

[54] D. Guha, M. Biswas, and J. Y. Siddiqui, "Harrington's formula extended to determine accurate feed reactance of probe-fed microstrip patches" *IEEE Antennas Wireless Propagat. Lett.*, vol. 6, pp. 33-35, 2007.

[55] E. F. Keuster and D. C. Chang, "A geometrical theory for the resonant frequencies and Q factors of some triangular microstrip patch antenna," *IEEE Trans. Antennas Propagat.*, vol. 31, pp.27-34, 1983.

[56] J. S. Dahele and K. F. Lee, "On the resonant frequencies of the triangular patch antenna," *IEEE Trans. Antennas Propagat.*, vol. 35, pp.100-101, 1987.

[57] K. F. Lee, K. M. Luk, and J. S. Dahele, "Characteristics of the equilateral triangular patch antenna," *IEEE Trans. Antennas Propagat.*, vol. 36, no.11, pp.1510-1518, Nov. 1988.

[58] X. Gang, "On the resonant frequencies of microstrip antennas," *IEEE Trans. Antennas Propagat.*, vol. 37, pp. 245-247, 1989.

[59] W. Chen, K. F. Lee, and J. S. Dahele, "Theoretical and experimental studies of the resonant frequencies of equilateral triangular microstrip antenna," *IEEE Trans. Antennas Propagat.*, vol. 40, pp.1253-1256, Oct. 1992.

[60] D. Karaboğa, K.Güney, N. Karaboğa, and A. Kaplan, "Simple and accurate effective side length expression obtained by using a modified genetic algorithm for the resonant frequency of an equilateral triangular microstrip antenna," *Int. J. Electron.*, vol. 83, pp. 99-108, Jan.1997.

[61] Nasimuddin, K. Esselle and A. K. Verma, "Resonant frequency of an equilateral triangular microstrip antenna," *Microw. Opt. Tech. Lett.*, vol. 47, no.5, pp.485-489, Dec. 2005.

[62] J.T.S. Sumantyo, K. Ito, and M. Takahashi, "Dual-band circularly polarized equilateral triangular-patch array antenna for mobile satellite communications," *IEEE Trans. Antennas Propagat.*, vol. 53, no. 11, pp. 3477 – 3485, Nov. 2005.

[63] K. Guney and N. Sarikaya, "A hybrid method based on combining artificial neural network and fuzzy inference system for simultaneous computation of resonant frequencies of rectangular, circular, and triangular microstrip antennas," *IEEE Trans. Antennas Propagat.*, vol. 55, pp. 659–668, 2007.

[64] M. M. Olaimat and N. I. Dib, "Improved formulae for the resonant frequencies of triangular microstrip patch antennas," *Int. J. Electron.*, vol. 98, pp. 407-424, 2011.

[65] M. M. Olaimat and N. I. Dib, "A study of 15^0-75^0-90^0 angles triangular patch antenna," *Prog. In Electromag. Res. Lett.*, vol. 21, pp. 1-9. 2011.

[66] K. Guney and E. Kurt, "Effective side length formula for resonant frequency of equilateral triangular microstrip antenna," *Int. J. Electron.*, vol. 103, pp. 261-268, 2016.

[67] P. L. Overfelt and D. J. White, "TE and TM Modes of some triangular cross-section waveguides using superposition of plane waves," *IEEE Trans. Microw. Theory Tech.*, vol. 34, pp. 161-167, 1986.

[68] S. Maity and B. Gupta, "Accurate resonant frequency of isosceles right-angled triangular patch antenna," *Microw. Opt. Technol. Lett.*, vol. 55, pp. 1306-1308, 2013.

[69] E. G. Lim, E. Korolkiewicz, S. Scott, A. Sambell, and B. Aljibouri, "An Efficient formula for the input impedance of a microstrip right-angled isosceles triangular patch Antenna," *IEEE Antennas Wireless Propagat. Lett.*, vol. 1, pp. 18-21, 2002.

[70] S. Maity and B. Gupta, "Cavity model analysis of 30°–60°–90° triangular microstrip antenna," *AEU-Int. J. Electron. Comm.*, vol. 69, pp. 923-932, 2015.

[71] K.F. Lee, K.Y. Ho, and J.S. Dahele, "Circular disc microstrip antenna with an air gap," *IEEE Trans. Antennas Propagat.*, vol. 32, pp. 880–884, 1984.

[72] S. Dahele, S. Mem, and K.F. Lee, "Theory and Experiment on microstrip antennas with air gaps," *Proc. Inst. Elect. Eng. pt H.*, vol. 132, pp. 455–460, 1985.

[73] F. Abboud, J. P. Damiano and A. Papiernik, "A new model for calculating the input impedance of coax-fed circular microstrip antennas with and without air gaps," *IEEE Trans. Antennas Propagat.*, vol. 38, pp. 1882–1885, 1990.

[74] C. S. Gurel and E. Yazgan, "New computation of the resonant frequency of a tunable equilateral triangular microstrip patch," *IEEE Trans. Microw. Theory Tech.*, vol. 48, pp. 334-338, Mar. 2000.

[75] S. Chattopadhyay, M. Biswas, J. Y. Siddiqui, and D. Guha, "Rectangular microstrips with variable air gap and varying aspect ratio: improved formulations and experiments," *Microw. Opt. Technol. Lett.*, vol. 51, pp. 169-173, 2009.

[76] S. Chattopadhyay, M. Biswas, J. Y. Siddiqui, and D. Guha, "Input impedance of probe-fed rectangular microstrip antennas with variable air gap and varying aspect ratio," *IET Microwave Antennas Propagat.*, vol. 3, pp. 1151–1156, 2009.

[77] M. Biswas and S. Banik, "Characteristics of circular patch antenna with and without air gaps," *Microw. Opt. Technol. Lett.*, vol. 54, pp. 1692-1699, 2012.

[78] M. Biswas and M. Sen, "Fast and accurate model for a coax-fed rectangular patch antenna with varying aspect ratio, feed location and substrate electrical parameters," *J. Electromagn. Waves Applicat.*, 2018.

[79] J. Bahl, P. Bhartia, and S. Stuchly, "Design of microstrip antennas covered with a dielectric layer," *IEEE Trans. Antennas Propagat*., vol. 30, pp. 314–318, 1982.

[80] J. Pribetich, "Modelling of microstrip antenna with dielectric protective layer for lossy medium," *Electron Lett.*, vol. 24, pp. 1464-1465, 1988.

[81] A. Benalla and K. C. Gupta, "Multiport network model for rectangular microstrip patches covered with a dielectric layer," *IEE Proc*., vol. 137, pp. 377-383, 1990.

[82] G. Qasim and S. Zhong, "Resonant frequency of a rectangular microstrip antenna covered with dielectric layer," *J. Shanghai Univ. Sci. Tech., vol*. 14, pp. 77-84, 1991.

[83] K. Verma, "Analysis of rectangular patch antenna with dielectric cover," *IEICE Trans.*, vol. 74, pp. 1270-1275, 1991.

[84] R. M. Nelson, D. A. Rogers and A. G. D'Assuncio, "Resonant frequency of a rectangular microstrip patch on several uniaxial substrates," *IEEE Trans. Antennas Propagat.*, vol. 38, pp. 978-981, 1990.

[85] H. R. Hassani and D. M. Syahkal, "Analysis of triangular patch antennas including radome effects" *IEE Proceedings H*, vol. 139, no. 3, pp.251-256, Jun. 1992.

[86] J. Svacina, "Analysis of multilayer microstrip lines by a conformal mapping method," *IEEE Trans. Microw. Theory Tech*., vol. 40, pp. 769–772, 1992.

[87] J. Svacina, "A simple quasi-static determination of basic parameters of multilayer microstrip and coplanar waveguide," *IEEE Microw. Guided Wave Lett*., vol. 2, pp. 385–387, 1992.

[88] R. Shavit, "Dielectric cover effect on rectangular microstrip antenna array," *IEEE Trans. Antennas Propagat*., vol. 42, pp. 1180–184, 1994.

[89] S. S. Zhong, G. Liu, and G. Qasim, "Closed form expressions for resonant frequency of rectangular patch antennas with multidielectric layers," *IEEE Trans. Antennas Propagat*., vol. 42, pp. 1360-1363, pp. 1994.

[90] J. T. Bernhard and C. J. Tousignant, "Resonant frequencies of rectangular microstrip antennas with flush and spaced dielectric superstrates," *IEEE Trans. Antennas Propagat*., vol. 47, pp. 302–308, 1999.

[91] V. Losada, R.R. Boix, and M. Horno, "Resonant modes of circular microstrip patches in multilayered substrates," *IEEE Trans. Microw. Theory Tech*., vol. 47, pp. 488–497, 1999.

[92] C.-S. Hong, "Gain-enhanced broadband microstrip antenna," *Proc. Natl. Sci. Counc. Rep. China A*, vol. 23, no. 5, pp. 609–611, 1999.

[93] A. Dreher and A. Ioffe, "Analysis of microstrip lines in multilayer structures of arbitrarily varying thickness" *IEEE Microwave Guided Wave Lett*.,; vol. 10, pp. 52–54, 2000.

[94] A. Ioffe, M. Thiel, and A. Dreher, "Analysis of microstrip patch antennas on arbitrarily shaped multilayers," *IEEE Trans. Antennas Propagat.*, vol. 51, pp. 1929–1935, 2003.

[95] M. Biswas and D. Guha, **"**Input impedance and resonance characteristic of superstrate loaded triangular microstrip patch," *IET Microw. Antennas Propagat.*, vol. 3, pp. 92 – 98, Feb. 2009.

[96] M.Biswas and A. Mandal, "CAD model to compute the input impedance of an equilateral triangular microstrip patch antenna with radome," *Prog. Electromag. Res. M.*, vol. 12, pp. 247-257, 2010.

[97] Y. Li and N. Bowler, "Resonant frequency of a rectangular patch sensor covered with multilayered dielectric structures," *IEEE trans. antennas propagat*. vol. 58, pp. 1883-1889, 2010.

[98] M. Biswas and M. Sen, "Design and development of rectangular patch antenna with superstrates for the application in portable wireless equipments and aircraft radome," *Microw. Optical Technol. Lett.* vol. 56, pp. 883-893, 2014.

[99] M. Biswas, S. Banik, M. Biswas, and A. Sukla, "CAD model to predict the effect of radome on the characteristics of rectangular patch antenna," *Microw. Opt. Technol. Lett.*, vol. 55, pp. 2460-2468, 2013.

[100] M. Biswas and A. Mandal, "Experimental and theoretical investigation of resonance and radiation characteristics of superstrate loaded rectangular patch antenna "*Microw. Opt. Technol. Lett*., vol. 57, pp. 791-799, 2014

[101] M. Biswas and A. Mandal, "Experimental and theoretical investigation to predict the effect of superstrate on the impedance, bandwidth, and gain characteristics for a rectangular patch antenna," *J. Electromagn. Waves Applicat*., vol. 29, no. 16, pp. 2093-2109, 2015.

[102] D. M. Syahkal and H. R. Hassani, "Characteristics of stacked rectangular and triangular patch antennas for dual band applications," *Eighth Int. Conf. on Antennas and Propagat.*, Edinburgh, vol. 2, pp. 728-731, 1993.

[103] P. S. Bhatnagar, J. P. Daniel, K. Mahdjoubi, and C. Terret, "Experimental study on stacked triangular microstrip antennas," *Electron. Lett.*, vol. 22, no. 16, pp. 864-865, July 31, 1986.

[104] J. Anguera, C. Puente, and C. Borja, "A procedure to design stacked microstrip patch antennas based on a simple network model," *Micro. Opt. Technol. Lett.*, vol. 30, 149–151, Aug. 2001.

[105] H. R. Hassani and D. M. Syahkal, "Study of electromagnetically coupled stacked rectangular patch antennas," *IEE Proc. Micro. Antennas Propagat.*, vol. 142, 7–13, Feb. 1995.

[106] M. Ali, T. M. Sayem, and V. K. Kunda, "A reconfigurable stacked microstrip patch antenna for satellite and terrestrial links," *IEEE Trans. Vehic. Technol*., vol. 56: 426–435, 2007.

[107] Z. Wang, S. Fang, S. Fu, and S. Lü, "Dual-band probe-fed stacked patch antenna for GNSS applications" *IEEE Antennas Wireless Propagat. Lett.*, vol. 8, pp. 100-103. 2009

[108] Z. Wang, S. Fang, S. Fu, and S. Jia, "Single-fed broadband circularly polarized stacked patch antenna with horizontally meandered strip for universal UHF RFID applications," *IEEE Trans. Microwave Theory Tech*., vol. 59, pp. 1066–1073. 2011.

[109] D. Li, P. Guo, Q. Dai, and Y. Fu, "Broadband capacitively coupled stacked patch antenna for GNSS applications" *IEEE Antennas Wireless Propagat*. *Lett*., vol. 11, pp. 701-04, 2012.

[110] O. P. Falade, M. U. Rehman, Y. Gao, X. Chen, and C. G. Parini, "Single stacked patch circular polarized antenna for triple band GPS receivers" *IEEE Trans. Antennas Propagat*., vol. 60, pp. 4479–484, 2012.

[111] Y. Jin and Z. Du, "Broadband dual-polarized F-probe fed stacked patch antenna for base stations" *IEEE Antennas Wireless Propagat. Lett.*, vol. 14, pp. 1121-1124, 2015.

[112] Q. Zhu, S. Yang, and Z. Chen, "Modified corner-fed dual-polarised stacked patch antenna for micro-base station applications" *Electron. Lett*., vol. 51, pp. 604–06, 2015.

[113] Y. Gao, R. Ma, Y. Wang, Q. Zhang, and C. Parini, "Stacked patch antenna with dual-polarization and low mutual coupling for massive MIMO," *IEEE Trans. Antennas Propagat*., vol. 64, pp. 4544–549, 2016.

[114] J. Hu, Z-C. Hao and W. Hong, "Design of a wideband quad-polarization reconfigurable patch antenna array using a stacked structure," *IEEE Trans. Antennas Propagat*., vol. 65, pp. 3014–3023, 2017.

[115] M. Biswas and M. Sen, "Design and development of coax-fed electromagnetically coupled stacked rectangular patch antenna for broad band application' *Prog. Electromag. Res. B*., vol. 79, pp. 21–44, 2017.

[116] Zürcher and F. E. Gardiol, "Broadband patch antennas," *Artech House*, Boston, 1995.

[117] K. F. Lee and W. Chen, "Advances in microstrip and printed antennas," *Wiley*, New York, 1997.

[118] K.-L. Wong, "Compact and broadband microstrip antennas," *Wiley*, NY, 2002.

[119] G. Kumar and K. P. Ray, "Broadband microstrip antennas," *Artech House*, Boston, 2003.

[120] Z. N. Chen and M. Y. W. Chia, "Broadband planar antennas design and applications," *Wiley*, 2006.

[121] D. Guha ancd Y. M. M. Antar, "Microstrip and printed antennas new trends, techniques and applications," *Wiley*, NY, 2011.

[122] D. M. Pozar, "Microwave engineering": *John Wiley & Sons Inc*, Hoboken, New Jersey, 2012.

[123] High Frequency Structure Simulator: *Ansoft Corp*.

[124] R. Mittra, W. Yu. "CFDTD," *Artech House*.

[125] Integral Equation Three-Dimensional (IE3D) software.

[126] E. Nyfors and P. Vainikainen, "Industrial microwave sensors," *Artech House*, 1989.

[127] H. Baltes , W. G.opel, and J. Hesse, " Sensors update," Wiley– Vch, Germany, Vol. 7, 2000.

[128] Zucchelli, M. Chimenti, and E. Bozzi, "Application of a coaxial-fed patch to microwave non-destructive porosity measurements in low-loss dielectrics," *Prog. Electromag. Res*., vol. 5, pp.1–14, 2008.

[129] M. Bogosanovich, "Microstrip patch sensor for measurement of the permittivity of homogeneous dielectric materials," *IEEE Trans. Instrum. Meas*., vol. 49, pp. 1144–1148, Oct. 2000.

[130] A. K. Verma, Nasimuddin, and A. S. Omar, "Microstrip resonator sensors for determination of complex permittivity of materials in sheet, liquid and paste forms," *Proc. Inst. Elect. Eng*., vol. 152, pp. 47–54, 2005.

[131] A. Cataldo, G. Monti, E. De Benedetto, G. Cannazza, and L. Tarricone, "A noninvasive resonance-based method for moisture content evaluation through microstrip antennas," *IEEE Trans. Instrum. Meas.*, vol. 58, pp. 1420–1426, May 2009.

[132] M. Biswas and A. Mandal, "Design and development of an equilateral patch sensor for determination of permittivity of homogeneous dielectric medium," *Microw. Optical Technol. Lett.,* vol. 56, pp. 1097-1104, May. 2014.

CHAPTER 2

Investigation of an Equilateral Triangular Patch Antenna with Varying Antenna Size, Substrate Electrical Parameters and Probe location

Content:

2.1. Introduction

The triangular geometry of the microstrip patch antenna is more compact than the rectangular geometry without any modification in radiation characteristic. So, the weight and dimension of an antenna structure can be reduced further with the use of triangular geometry. As the quality factor (*Q*) of the triangular patch antenna is high [1], it exhibits narrow band response. This narrow band feature supports its use in many applications like designing of microstrip band pass and band elimination filters [2-5], compact array [6-8] with reduced coupling between adjacent elements and also for being used on curved surfaces because of their easy conformability. Recently, the triangular patch antennas are being used in designing microstrip sensors [9, 10], ring antennas [11, 12], reconfigurable [13] and multiple input multiple output (MIMO) antennas [14].

The introduction of tunability feature in the characteristics of the patch antenna is a crucial issue for antenna developer. All the antenna parameters need to be changed for every change in resonant frequency. But it is a very difficult process. To avoid this difficulty an air gap is introduced between substrate and ground plane. This is called suspended type patch antenna. The change in resonant frequency, bandwidth, gain and efficiency is possible by changing the air gap height without altering the other antenna parameters [15-18].

The suspended substrate patch antenna is a special type of a patch antenna on the composite substrate (air layer is replaced by another dielectric layer). The patch on the composite substrate is encountered in many microstrip designs like i) the patch in multilayered media for improving the antenna performances and provide protection to the patch against the environmental hazards [19-25], ii) an electromagnetically coupled stacked patch antenna in two layers [26] and three layers composite substrates [27] for improving the bandwidth and radiation characteristic and iii) patch antenna made on a multilayered Monolithic Microwave Integrated Circuit (MMIC) [28-29].

The antenna must be operated around its resonant frequency to improve the bandwidth, efficiency and gain. So, the accurate computation of resonant frequency is very essential. Apart from the resonant frequency another important antenna parameter is the input impedance. The better impedance matching between coaxial probe and patch is required to improve the radiation efficiency. So, the accurate calculation of input impedance as a function of feed location under the patch is also very important.

The triangular patch antennas have been widely investigated by several researchers [1-14, 16-17, 20, 27, 30-47]. However, the majority of the studies concentrated only on equilateral shape. Some of the lower order field patterns and cutoff wave number for a triangular resonator were described in [30] for the first time. Different techniques like, full wave methods [20, 31, 36], geometrical theory [32], modified genetic algorithm [37] and differential evolution algorithm [38] have been employed to analyse the triangular microstrip patch antenna. The full wave method [20, 31, 36] are very much accurate than the other techniques [30, 32, 37]. But the full wave methods do not provide the closed form expression and equivalent circuit for design. Also, these techniques require large computational time for implementation. So, the full wave analysis and commercial softwares [48, 49] based on them are not useful for direct synthesis of patch antenna. The CAD oriented cavity model is ideal for design purpose because it takes less computational time, easy to implement, provide closed form expressions and equivalent circuit for design.

A number of researchers [16-17, 33-35, 39- 40, 42-44] have employed the cavity model analysis to compute the resonant frequency of an equilateral triangular patch antenna (ETPA). But these articles have not accurately incorporated the fringing field effects in the side length and effective permittivity computation. So, a big discrepancy is observed between measured and computed values for wide variation of antenna size and substrate electrical parameters.

The articles reported in [16-17, 33-35, 39- 40, 42-44] were mainly focussed on the equilateral patch on single substrate. Only a very few articles [16, 17] have theoretically studied the effect of suspended substrate on resonant frequency. But the effect of suspended substrate on input impedance, bandwidth and gain of a triangular patch was not investigated earlier. Also the effect of composite substrate on the characteristics of an ETPA was not reported earlier.

Few articles were available in [32, 35, 40, 41] for computing the losses in microstrip patch antennas. But these models involve large and rigorous mathematical steps. So, a simple closed form cavity model is required to compute the losses of an ETPA. The study on input impedance also finds a very few investigations till now [35, 40, 41]. Among them, the model reported in [35] provides rigorous mathematical steps for the first time to compute the input impedance of an ETPA on a single substrate. Also, there is a big discrepancy exist

between measured and theoretical values. Recently, Biswas [40, 41] has extended this model [35] to compute the input impedance of an ETPA with and without a cover layer.

In this chapter, these problems have been addressed carefully and proposed a simple model to predict the resonant frequency, quality factor, input impedance, bandwidth and gain of an ETPA on single, composite and suspended substrate. The present model based on CAD oriented cavity model and single resonant parallel *R-L-C* circuit. The advantage of the model is the mathematical simplicity and low computation cost. This efficient model is capable of predicting accurately the antenna characteristics for wide variation of antenna size, substrate electrical parameters and probe location under the patch. A series of experiments is performed with designed prototypes to validate the present model. We have also employed commercial softwares HFSS [48] and CFDTD [49] to validate the model.

2.2 Theory

This section introduces the expressions to compute equivalent relative permittivity, effective permittivity, effective side length, quality factors, bandwidth, gain, resonant frequency, resonant resistance based on the cavity model and single resonant parallel *R-L-C* circuit.

2.2.1. Resonant frequency

Based on cavity model analysis, the resonant frequency of an ETPA on composite, suspended and single substrate (Fig. 2.1) operated in TM_{nml} modes may be computed from [30] as

$$f_{r,nml} = \frac{2c}{3a_{eff}\sqrt{\varepsilon_{r,eff}}}\sqrt{n^2+nm+m^2} \tag{2.1}$$

where, c is the velocity of light in free space, a_{eff} is the effective side length of the ETPA , $\varepsilon_{r,eff}$ is the effective relative permittivity of the medium below the patch and m, n, l are integers which never zero simultaneously satisfying the condition $m+n+l=0$.

2.2.2. Effective permittivity $\varepsilon_{r,eff}$

The $\varepsilon_{r,eff}$ for this two layered structure is obtained as[50]

$$\varepsilon_{r,eff} = \varepsilon_{re} - \frac{\varepsilon_{re}-\varepsilon_{r,dyn}}{1+G\left(f_a/f_p\right)^2} \tag{2.2}$$

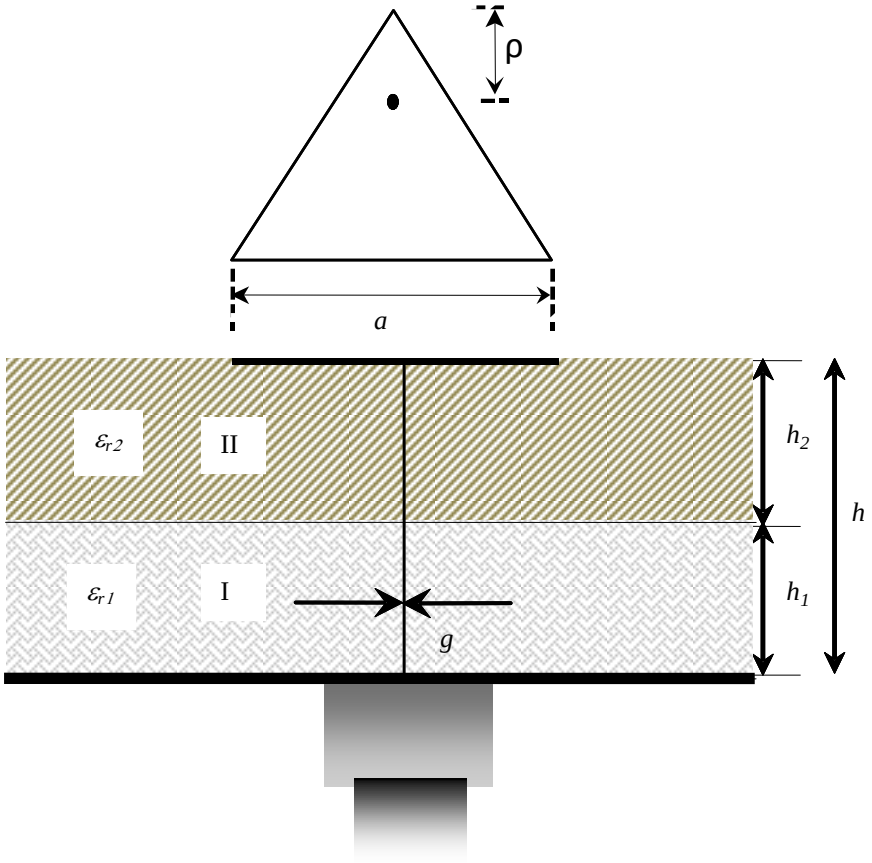

Figure 2.1: A schematic diagram of probe-fed equilateral triangular microstrip patch

where, G is a purely empirical term, $\varepsilon_{r,dyn}$ is the dynamic permittivity which depends on the dimensions, equivalent substrate relative permittivity ε_{re}, and field configurations of the mode under study, f_a is the frequency without fringing fields. The G, f_a and f_p are computed as

$$G = \sqrt{\frac{\varepsilon_{r,dyn}}{\varepsilon_{re}}} \tag{2.3}$$

$$f_a = \frac{2c}{3a\sqrt{\varepsilon_{re}}} \tag{2.4}$$

$$f_p = \frac{Z\left(\frac{a}{h}, h, \varepsilon_{re}\right)}{2\mu_0 h} \tag{2.5}$$

The $Z\ (a/h,\ h,\ \varepsilon_{re})$ is the characteristic impedance. The $Z\ (a/h,\ h,\ \varepsilon_{re})$ for an ETPA is obtained from originally formulated equation of rectangular geometry [1, 44] by employing an equivalence relation between an equilateral triangular (side length a) and a rectangular geometry (width W and length L). Here the equal surface area has been considered on the basis of equivalence, resulting in

$$W L=(\sqrt{3}/4)a^2 \tag{2.6}$$

Now equating the zeroth order resonant frequencies of rectangular patch and triangular patch without fringing we get

$$f_r=\frac{c}{2L\sqrt{\varepsilon_r}}=\frac{2c}{3a\sqrt{\varepsilon_r}} \tag{2.7}$$

Thus,

$$L=\left(3/4\right)a \tag{2.8}$$

The width (W) of rectangular patch is obtained from (2.6) and (2.8) as

$$W=\left(1/\sqrt{3}\right)a \tag{2.9}$$

Thus the $Z\ (a/h,\ h,\ \varepsilon_{re})$ for an ETPA after employing the equivalence relations (2.8) and (2.9) becomes

$$Z\left(\frac{a}{h},h,\varepsilon_{re}\right)=\frac{120\pi}{\sqrt{\varepsilon_{rp}}}\left[\frac{a}{\sqrt{3}h}+1.393+0.667\ln\left(\frac{a}{\sqrt{3}\,h}+1.444\right)\right]^{-1} \tag{2.10}$$

$$\varepsilon_{rp}=\frac{\varepsilon_{re}+1}{2}+\frac{\varepsilon_{re}-1}{2}\left(1+\frac{12h}{a/\sqrt{3}}\right)^{-1/2} \tag{2.11}$$

The ε_{re} for this two-layer structure is modeled as the single-layer one having substrate thickness of $h = h_1 + h_2$. The upper layer has thickness h_2 with relative permittivity ε_{r2} and lower layer has thickness h_1 with permittivity ε_{r1}. The ε_{re} can be computed as

$$\varepsilon_{re}=\frac{\varepsilon_{r1}\,\varepsilon_{r2}h}{\varepsilon_{r1}\,h_1+\varepsilon_{r2}\,h_1} \tag{2.12}$$

The $\varepsilon_{r,dyn}$ for this structure is computed as

$$\varepsilon_{r,dyn}=\frac{C_{dyn}\left(\varepsilon=\varepsilon_0\varepsilon_{re}\right)}{C_{dyn}\left(\varepsilon=\varepsilon_0\right)} \tag{2.13}$$

where, C_{dyn} (ε) is the total dynamic capacitance of the condenser formed by the conducting patch and the ground plane separated by a dielectric of permittivity ε. It takes into account the influence of the fringing field at the edge of the patch. The C_{dyn} (ε_0) is the total dynamic capacitance when $\varepsilon = \varepsilon_0$. The C_{dyn} (ε) can be written as

$$C_{dyn}(\varepsilon) = C_{0,dyn}(\varepsilon) + C_{e,dyn}(\varepsilon) \tag{2.14}$$

here, $C_{e,dyn}$ (ε) and $C_{0,dyn}$ (ε) are the total dynamic fringe and the main field capacitance respectively. The total dynamic fringe field capacitance $C_{e,dyn}$ (ε) for this geometry is obtained from originally formulated rectangular geometry [51] by employing equivalence relations (2.8) and (2.9). Thus the $C_{e,dyn}$ (ε) for an ETPA becomes

$$C_{e,dyn}(\varepsilon) = \frac{1}{2}\left[\frac{Z\left(a/h, h, \varepsilon_{re}=1\right)3a}{4cZ^2\left(a/h, h, \varepsilon_{re}\right)} - C_{0,stat}(\varepsilon)\right] \tag{2.15}$$

In (2.15), $C_{0,stat}$ is the static main field capacitance and may be obtained as

$$C_{0,stat}(\varepsilon) = \frac{\sqrt{3}\,\varepsilon_0\varepsilon_{re}\,a^2}{4h} \tag{2.16}$$

The total dynamic main field capacitance $C_{0,dyn}(\varepsilon)$ is computed as

$$C_{0,dyn}(\varepsilon) = \gamma_{nm} C_{0,stat}(\varepsilon) \tag{2.17}$$

γ_{nm} = 0.3525, for n = 1
= 0.2865 = 2
= 0.2450 = 3

2.2.3 Effective side length a_{eff}

The actual side length a of a triangular patch is enhanced due to the effect of fringing field at the edge of the patch. This new side length termed as effective side length a_{eff}. The most of the researchers [16, 17, 20, 30-37, 39-41, 43, 45-47] have reported that all the modes have the same a_{eff}. But the different modes have the different fringing fields [1]. So, the different modes have different a_{eff}. Thus, the mode dependent a_{eff} is expressed as

$$a_{eff} = a\left(1+\tau q\right)^{\frac{1}{2}} \tag{2.18}$$

In equation (2.18), q arises due to the fringing field at the edge of the patch and τ is the mode dependent factor.

The model reported in [36] has employed a curve fitting formula for computing *q*. But a large discrepancy is shown between measured and computed values with this *q*. We have proposed a new curve fitting formula for *q* based on the experimental [33, 36] and simulation [48, 49] results. This approach shows better agreement with the simulation and experimental results. The *q* for this geometry is proposed as

$$q = 7.146\frac{h}{a} - 16.485\left(\frac{1}{\sqrt{\varepsilon_{re}}}\right)\left(\frac{h}{a}\right) + 21.083\left(\frac{1}{\varepsilon_{re}}\right)\frac{h}{a} + 10.172\left(\frac{h}{a}\right)^2 - 16.121\left(\frac{1}{\sqrt{\varepsilon_{re}}}\right)\left(\frac{h}{a}\right)^2 \tag{2.19}$$

where, ε_{re} is the equivalent relative permittivity of the medium below the patch. The ε_{re} for a two layered structure is defined in (2.6)

$$\tau = 0.75^{m}\, n^{0.23} \tag{2.20}$$

2.2.4 Input Impedance

The better impedance matching is required between coaxial probe and patch for achieving the optimum performance. So, the accurate computation of input impedance of the patch antenna is very essential. The patch antenna can be treated as a resonant cavity modeled by a single resonant parallel of *L*, *C* and *R* circuit. The equivalent resonant parallel *L*, *C* and *R* circuit of an ETPA is shown in Fig. 2.2 Thus, the input resistance and reactance for an ETPA of side length *a* is seen a the coaxial probe, located at a distance ρ from the tip of the triangle (Fig. 2.1), may be written as

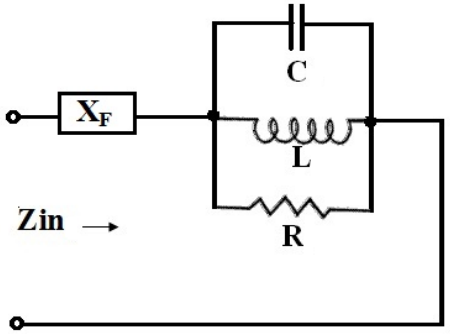

Figure 2.2: Equivalent resonant parallel R-L-C circuits of probe-fed equilateral triangular microstrip patch.

$$R_{in} = \frac{R(\rho)}{1+Q_T^2\left[\frac{f_{r,nml}}{f}-\frac{f}{f_{r,nml}}\right]^2} \tag{2.21}$$

$$X_{in} = X_f(f,\rho) + \frac{R(\rho)Q_T\left[\frac{f_{r,nml}}{f}-\frac{f}{f_{r,nml}}\right]}{1+Q_T^2\left[\frac{f_{r,nml}}{f}-\frac{f}{f_{r,nml}}\right]^2} \tag{2.22}$$

where, $R(\rho)$ is the input resistance at resonance and it is different for different modes [20, 35, 40, 41], Q_T is the total quality factor, $f_{r,\,nml}$ is the mode depended resonant frequency defined in (2.1), f is the working frequency and X_f is the feed reactance. The impact of X_f is described in detail in the next chapter.

$R(\rho)$ is the resonant resistance of the microstrip element which varies with ρ as:

$$R(\rho) = R_r P_{nml}(\rho) \tag{2.23}$$

where P_{nml} is the field factor. Here we have employed simple and efficient expression to compute the mode dependent R_r as

$$R_r = \left[\frac{(0.18+0.83^n)}{m+0.6^{nm}} - 1.6\,m(n-m)^2\right]\left(\frac{\eta\, h\, \lambda_{r,nm}\, \pi\, Q_T}{\sqrt{2}\, a^2 \sqrt{\varepsilon_{r,eff}}}\right) \tag{2.24}$$

The work reported in [35] has employed different mode dependent values for computing the input impedance. Here we have also introduced mode dependent factor for computing the input impedance. The first term indicates the mode dependent factor, η is the intrinsic impedance of the medium, Q_T is the total quality factor, $\lambda_{r,nml} = c/f_{r,\,nml}$, $f_{r,\,nml}$ is the mode dependent resonant frequency given by (2.1) and $\varepsilon_{r,eff}$ is effective dielectric constant defined in (2.2). The field factor $p_{nml}(\rho)$ may be computed as

$$P_{nml}(\rho) = (5\pi)^{-1}\left[\cos\frac{2\pi l\rho}{\sqrt{3}\,a} + \cos\frac{2\pi n\rho}{\sqrt{3}\,a} + \cos\frac{2\pi m\rho}{\sqrt{3}\,a}\right]^2 \tag{2.25}$$

2.2.5 Total quality factor Q_T

The total loss (Q_T) is defined as

$$Q_T = \left(\frac{1}{Q_r} + \frac{1}{Q_d} + \frac{1}{Q_c} \right)^{-1} \tag{2.26}$$

Basically three losses are pronounced in microstrip patch antennas. They are (i) quality factor due to radiation loss (Q_r), (ii) quality factor due to dielectric loss (Q_d) and (iii) quality factor due to conductor loss (Q_c). A geometrical theory has been employed in [33] for computing the Q factors but shows large discrepancy with measured value [35]. The model reported in [35] has employed rigorous and large mathematical steps for computing the different losses. The model reported in MB [40] employs an equivalence relation between rectangular and triangular geometry for computing the quantity Q. Here very simple formulas have been proposed to compute the loss factors.

The accurate computation of Q_r is very important because it determines the radiation efficiency. The computation of Q_r is very complex for a triangular patch antenna due to its shape. The Q_r depends on the field configuration under the mode [1]. Here we have taken a very simple and efficient expression to compute Q_r as proposed in [18, 53] and added a mode dependent correction factor. So, the Q_r for an ETPA is defined as

$$Q_r = \left[\left\{ 2(n + 0.6nm) - 1 \right\}^{0.6} - \frac{1.31(n-1)}{(n-0.6)} \right] \frac{\beta D(\delta) \varepsilon_{re}}{\mu_0 f_{r,nml} h} \tag{2.27}$$

where, the first term is the mode dependent facto rand the factor β is a constant. The value of β = 21.15 for circular patch antenna [18, 53] and we have employed β = 30 for an ETPA. ε_{re} is defined in (2.6), $f_{r,nml}$ is given by (2.1), $D(\delta)$ is the directivity and n and m are the mode indices.

Here we have proposed a new curve fitting formula for computing the directivity of the structure under study based on simulation and experimental results as

$$D(\delta) = 3.194 - 0.482\,\delta + 3.042\,\delta^2 - 3.213\,\delta^3 + 4.924\,\delta^4 - 1.526\,\delta^5 \tag{2.28}$$

where,

$$\delta = \frac{\pi f_{r,nml}}{2 f_{0,nml} \sqrt{\varepsilon_{re}}} \tag{2.29}$$

and

$$f_{0,nml} = \frac{2c}{3a\sqrt{\varepsilon_{re}}}\sqrt{n^2 + nm + m^2} \tag{2.30}$$

The quality factor due to conductor loss Q_c can be expressed as

$$Q_c = \frac{\pi\sqrt{\varepsilon_{r,eff}}}{\lambda_{r,nml}\,\alpha_c} \tag{2.31}$$

α_c is the conductor loss. The expression for α_c of a rectangular patch was reported in [54]. We have used this expression to calculate the α_c for an ETPA by employing the equivalent relations (2.8) and (2.9). Thus, the α_c for an ETPA becomes as

$$\alpha_c = \frac{R_s}{Z\left(\frac{a}{h}, h, \varepsilon_{re}\right) a/\sqrt{3}} \tag{2.32}$$

$$R_s = \sqrt{\frac{\pi\, f_{r,nml}\,\mu_0}{\sigma}} \tag{2.33}$$

where, σ is the conductivity and other variables have usual meaning. Q_d for this structure can be computed as

$$Q_d = \frac{1}{\tan\delta_e} \tag{2.34}$$

where, $tan\delta_e$ is the equivalent loss tangent of a triangular patch on two dielectric layer may be defined as

$$\tan\delta_e = \frac{h_1\,\varepsilon_{r1}\tan\delta_1 + h_2\,\varepsilon_{r2}\tan\delta_2}{h\,\varepsilon_{re}} \tag{2.35}$$

2.2.6. Bandwidth and Gain

The percentage bandwidth (V.S.W.R < 2) of the antenna is calculated as [1]

$$\frac{1}{\sqrt{2}\,Q_T}\,100\,\% \tag{2.36}$$

The gain of an ETPA on composite, suspended and single substrate as

$$G = \eta \times D(\delta) \tag{2.37}$$

where, η and $D(\delta)$ are the efficiency and directivity respectively. η may be expressed as

$$\eta = \frac{Q_T}{Q_r} \tag{2.38}$$

The mathematical expression for computing the directivity of an ETPA with and without air gap was not reported earlier. Directivity is computed from (2.28).

2.3 Antenna design and experimental tests

A number of prototypes of different *a* are etched on different substrates like i) Rogers with ε_{r2} = 2.4, h_2 = 0.8265 and 1.58 mm, $tan\delta_2$ = 0.0022, ii) Glass epoxy with ε_{r2} = 4.4, h_2 = 1.63 mm, $tan\delta_2$ = 0.02 and iii) Arlon with ε_{r2} = 10.0, h_2 = 1.63 mm, $tan\delta_2$ = 0.0035. Some of the fabricated prototypes and experimental setup is shown in Fig. 2.3. The patch was excited with a coaxial probe whose diameter *g* = 1.24 mm. To validate the proposed model, we have performed a series of experiments using Network Analyzer Agilent- E5071B.

Figure 2.3 (a)

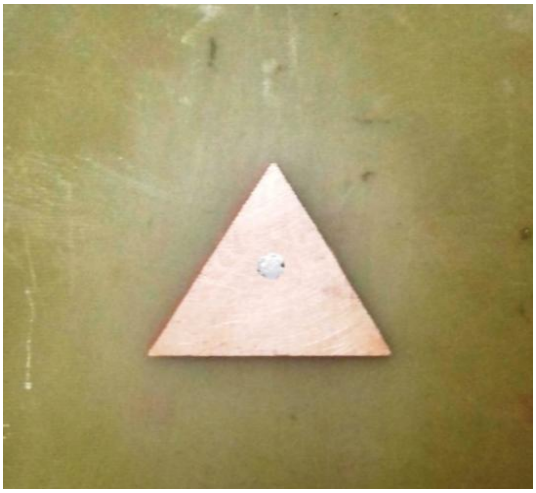

2.3(b)

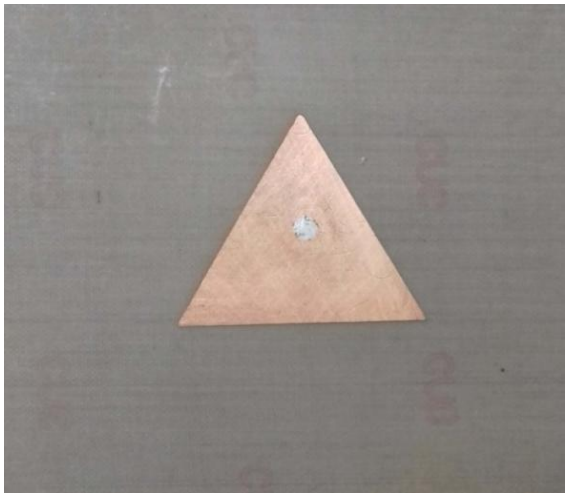

2.3(c)

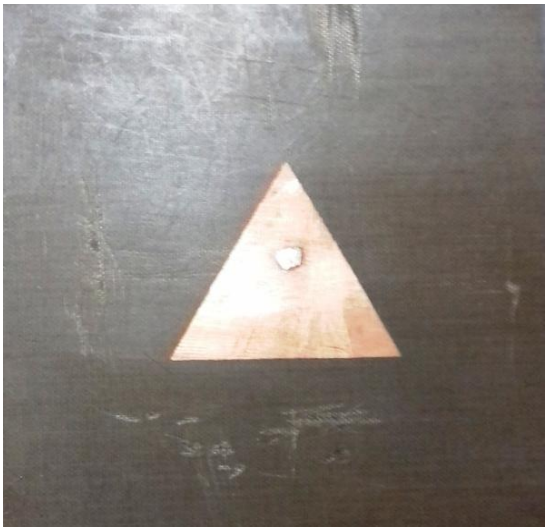

2.3(d)

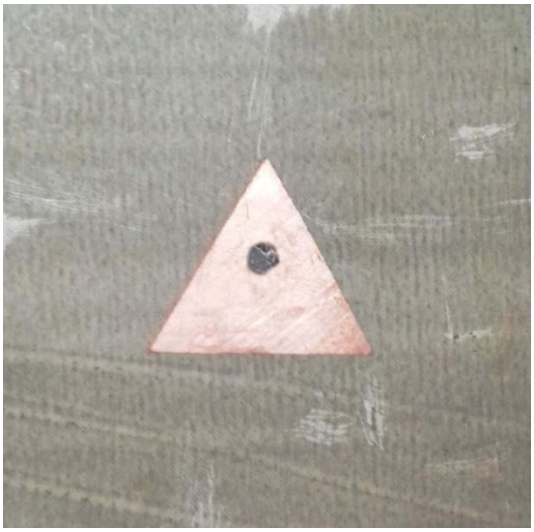

2.3(e)

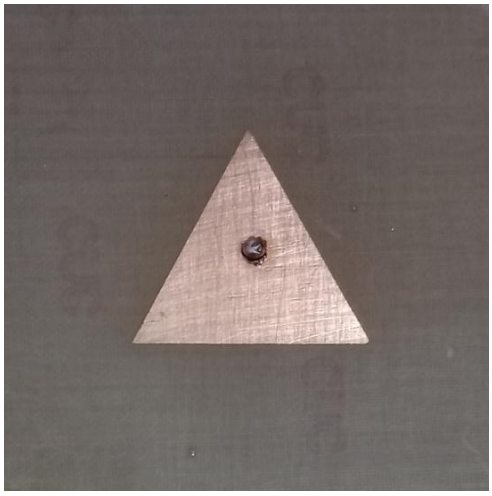

2.3(f)

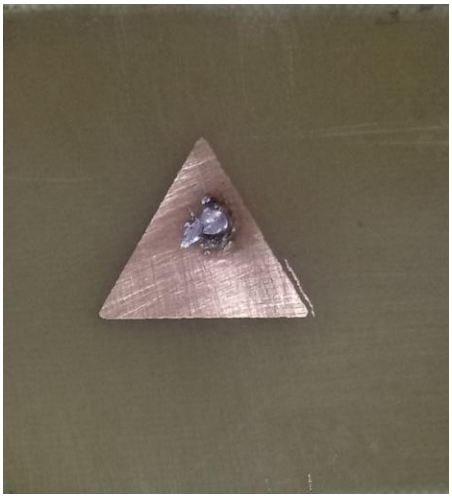

2.3(g)

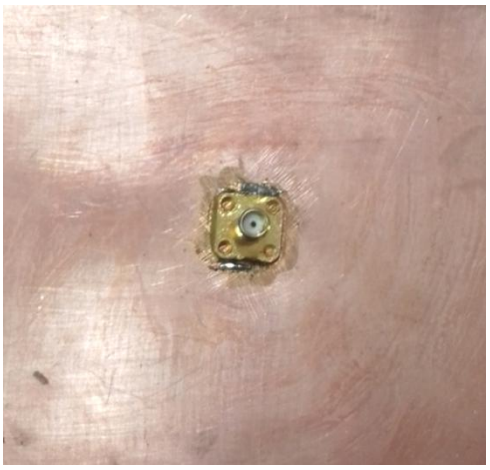

2.3(h)

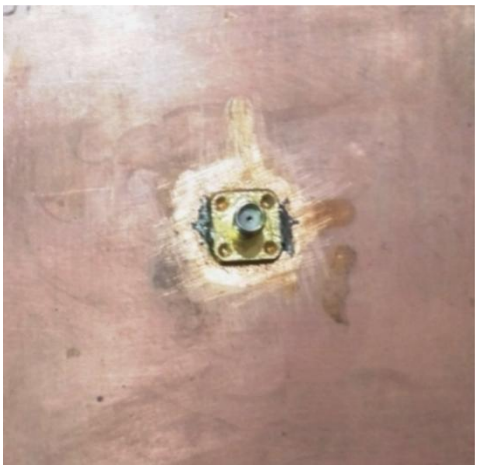

2.3(i)

2.3(j)

2.3(k)

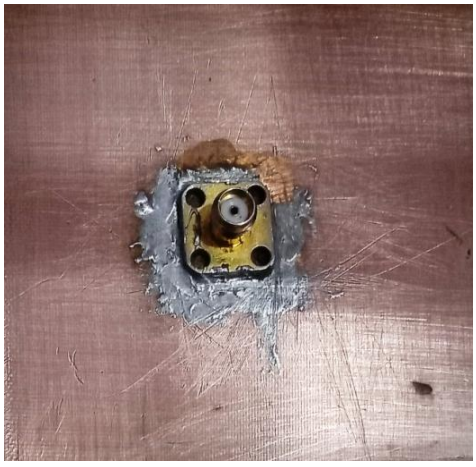

2.3(l)

2.3(m)

Figure 2.3: (a) Snapshot of experimental setup, (b-g) fabricated prototypes and (h-m) backside ground plane.

2.4 Results and discussions

Here, we have presented the theoretically predicted, simulated and measured results for the resonant frequency, quality factor, input impedance band width and gain of an ETPA printed on a single, composite and suspended substrate. It is important to mention that slight discrepancies in experimental results always remain due to unintended shift in feed position, BNC connector and fabrication error. It is also very difficult to maintain uniform air gap for an ETPA on suspended substrate and eradication of air gap between two composite substrates. So, we have considered ±1% tolerance in measured values of resonant frequencies.

2.4.1 Resonant frequency

In table 2.1, we have compared the computed resonant frequencies employing the present model with simulation [48, 49] and our experimental results for an ETPA printed on two dielectric layers operated in dominant and higher order modes. The total average error of the present model is computed against the simulated [48, 49] and measured results. From this comparison we observe that the model shows excellent agreement with experimental and simulation results.

TABLE 2.1

THEORETICAL, SOFTWARE COMPUTATIONAL AND EXPERIMENTAL [OUR] RESONANT FREQUENCIES FOR AN EQUILATERAL TRIANGULAR PATCH ON TWO LAYERS COMPOSITE SUBSTRATE OPERATED IN DIFFERENT MODES.

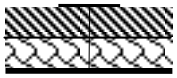

Resonant frequency (GHz)								
h_1 (mm)	Mode	EXP [I]	HFSS [II] [48]	CFDTD [III] [49]	Computed			
					Present	% Error with respect to I	% Error with respect to II	% Error With respect to III
0.8265	TM_{10}	2.403	2.398	2.409	2.388	0.624	0.209	0.042
	TM_{11}	4.273	4.347	4.333	4.247	0.608	0.000	-0.331
	TM_{20}	4.76	4.778	4.767	4.725	0.735	-1.005	-1.243
	TM_{21}	6.41	6.471	6.525	6.443	-0.515	-1.130	-1.866
	TM_{30}	7.178	7.173	7.237	7.05	1.783	0.325	1.219
1.58	TM_{10}	2.446	2.480	2.464	2.422	0.981	0.329	0.083
	TM_{11}	4.32	4.434	4.348	4.341	-0.486	-0.162	-2.189
	TM_{20}	4.885	4.875	4.892	4.772	2.313	-1.209	-1.705
	TM_{21}	6.519	6.647	6.672	6.558	-0.598	-1.722	-2.919
	TM_{30}	7.276	7.260	7.246	7.097	2.460	0.880	-1.545
Total Average % Error						1.110	0.693	1.314
a = 42 mm, ε_{r2} = 4.4, ε_{r1} = 2.4, h_2 = 1.63								

A comparison of computed values with simulated [48, 49] and our measured resonant frequencies for an ETPA on suspended substrate operated in dominant and higher order modes is presented in table 2.2. From this comparison we observe that the model shows good correlation with experimental and simulation results.

TABLE 2.2
THEORETICAL, SOFTWARE COMPUTATIONAL AND EXPERIMENTAL [OUR] RESONANT FREQUENCIES FOR AN EQUILATERAL TRIANGULAR PATCH ON SUSPENDED SUBSTRATE OPERATED IN DIFFERENT MODES.

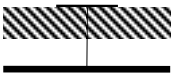

Resonant frequency (GHz)								
h_1 (mm)	Mode	EXP [I]	HFSS [II] [48]	CFDTD [III] [49]	Computed			
					Present	% Error with respect to I	% Error with respect to II	% Error With respect to III
0.5	TM_{10}	3.460	3.435	3.452	3.477	-0.491	-1.223	-0.724
	TM_{11}	6.127	6.09	6.143	6.169	-0.685	-1.297	-0.423
	TM_{20}	6.932	6.86	6.913	6.863	0.995	-0.044	0.723
	TM_{21}	9.283	9.255	9.115	9.331	-0.517	-0.821	-2.370
	TM_{30}	10.4	10.385	10.379	10.212	1.808	1.666	1.609
1.0	TM_{10}	3.550	3.546	3.521	3.544	0.169	0.056	-0.653
	TM_{11}	6.144	6.275	6.162	6.354	-3.418	-1.259	-3.116
	TM_{20}	7.015	7.105	7.147	6.946	0.984	2.238	2.812
	TM_{21}	9.629	9.485	9.422	9.553	0.789	-0.717	-1.390
	TM_{30}	10.488	10.675	10.546	10.288	1.907	3.625	2.446
Total Average % Error						1.176	1.295	1.627
a = 42 mm, ε_{r2} = 2.4, ε_{r1} = 1.0, h_2 = 0.8265								

In Fig. 2.4, the variation of dominant mode resonant frequency as a function of h_1/h for composite and suspended substrate patch antenna is visualized. For a composite substrate patch the effective dielectric constant is enhanced and the effective dielectric constant is lowered for a suspended substrate patch. This behavior is clearly investigated in Fig. 2.5. Thus, f_r is decreased for composite substrate patch whereas, f_r increases for suspended substrate patch with the increase of h_1/h. The computed curves are very well agreed with the HFSS simulated results for all values of h_1/h.

The effect of air gap on resonant frequency is depicted in Fig. 2.6. The effective permittivity is lowered due to introduction of air gap below the substrate (Fig. 2.5). Thus, the resonant frequency is increased. So, the tunability is achieved. The computed values compared with simulated [48, 49] and our measured values. The present model shows close agreement with measured and simulated results.

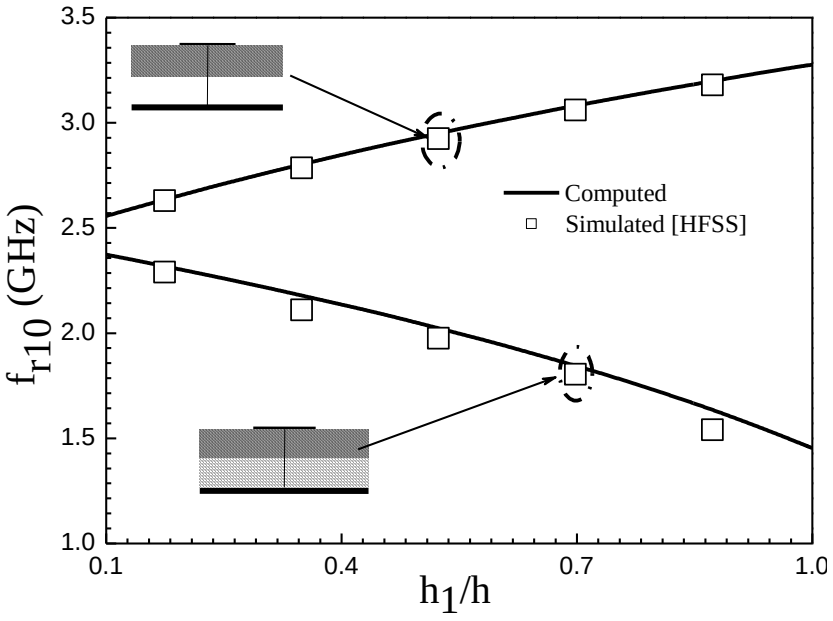

Figure 2.4: Variation of dominant mode resonant frequency as a function of thickness h_1/h I for an equilateral triangular patch on suspended and composite substrate. a = 50.0 mm, h = 2.865 mm, ε_{r2} = 2.32, ρ = 22.3 mm, g = 1.24 mm, ε_{r1} = 9.8 (for composite substrate), ε_{r1} = 1.0 (for suspended substrate).

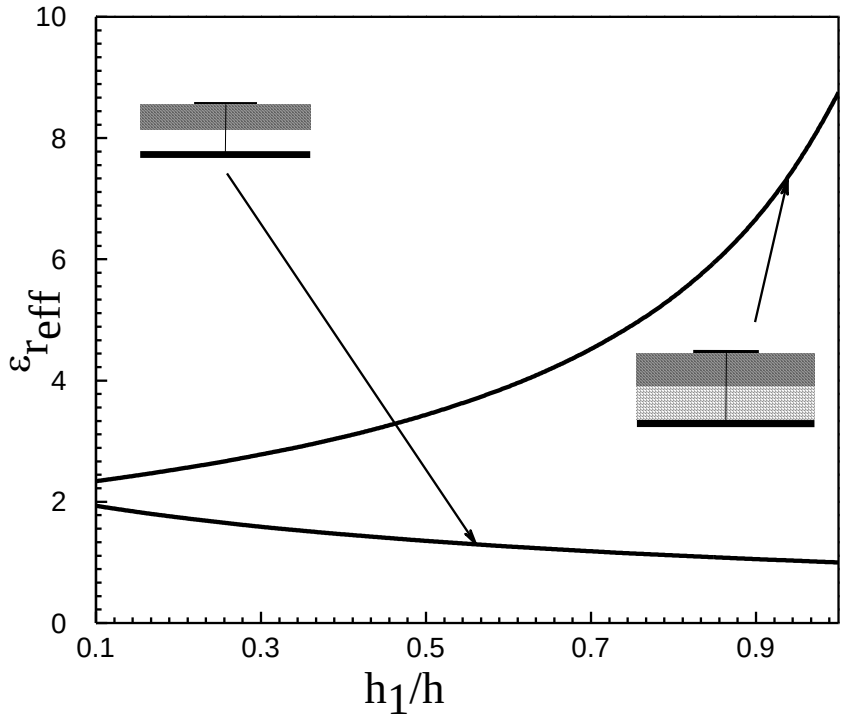

Figure 2.5: Theoretical variation of ε_{reff} and p with the variation of thickness of layer I for suspended and composite substrate. Parameters as in Fig. 2.4.

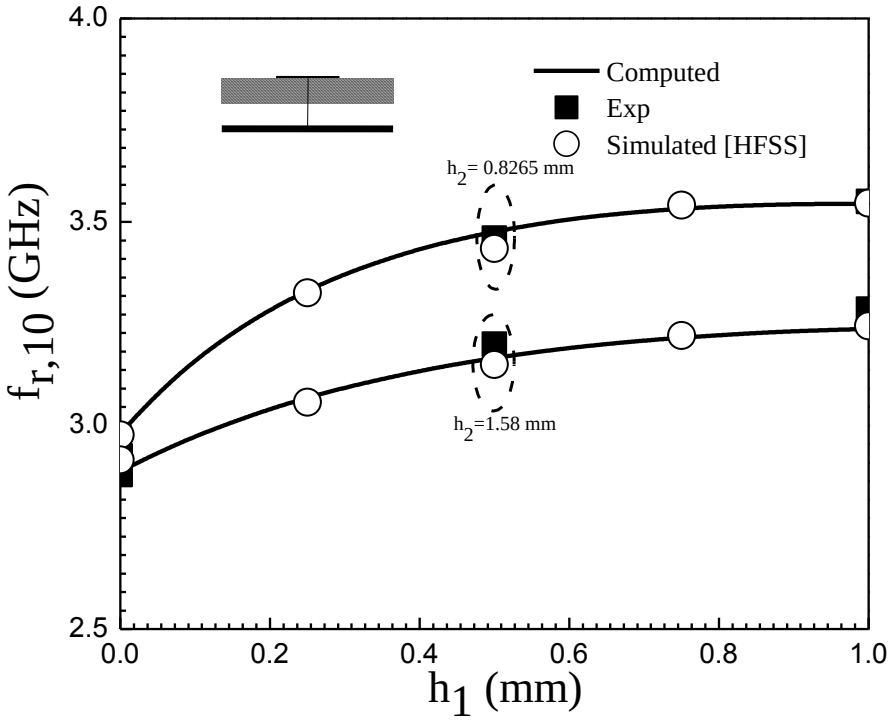

Figure 2.6: The computed, simulated and measured [our] variation of resonant frequency of an ETPA with the change of air gap thickness h_1 of layer I for different thickness of layer II. a = 42 mm, ε_{r2} = 2.4.

In table 2.3 and 2.4, we compare the computed resonant frequencies employing present the model with simulated and our measured results for an equilateral patch having a = 42 mm, 22 mm and 32 mm respectively printed on a single substrate with different ε_{re} and h operated in dominant and higher order modes. The model shows excellent correlation with experimental and simulation results.

Now the accuracy of the present model is verified against the other measured results [33] for an equilateral patch printed on a low dielectric constant substrate operated in dominant and higher order modes in table 2.5. Here the measured resonant frequencies [33] are compared with our model and the models reported in [16, 17, 30, 34, 36, 37, 39, 42]. The present model shows closer agreement with measured [36] results than the other models.

The variation of resonant frequency of an ETPA on single substrate with the change of substrate thickness ($h = h_2$) for different dielectric constant ($\varepsilon_{re} = \varepsilon_{r2}$) is visualized in Fig. 2.7. Here, we have compared our theoretical curves with MoM [36] and simulated [48] values. Very good agreement is observed between them for all substrate thickness except $h/a \geq 0.08$

mm for low dielectric constant substrate. This is due to the inherent limitation of cavity model because the cavity model is valid for small h/λ_r value.

TABLE 2.3

THEORETICAL, SOFTWARE COMPUTATIONAL AND EXPERIMENTAL [OUR] RESONANT FREQUENCIES FOR AN EQUILATERAL TRIANGULAR PATCH ON SINGLE SUBSTRATE OPERATED IN DIFFERENT MODES.

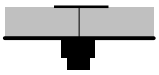

Resonant frequency (GHz)										
							Computed			
a (mm)	**$\varepsilon_{re} = \varepsilon_{r2}$**	**$h = h_2$ (mm)**	**Mode**	**EXP [I]**	**HFSS [II] [48]**	**CFDTD [III] [49]**	**Present**	**% Error with respect to [I]**	**% Error with respect to [II]**	**% Error with respect to [III]**
42	2.4	0.8265	TM_{10}	2.925	2.997	3.012	2.981	-1.915	0.534	1.029
			TM_{11}	5.173	5.117	5.289	5.225	-1.005	-2.111	1.210
			TM_{20}	5.861	5.916	6.00	5.936	-1.280	-0.338	1.067
			TM_{21}	7.871	8.035	7.933	7.961	-1.143	0.921	-0.353
			TM_{30}	8.786	8.869	8.959	8.885	-1.127	-0.180	0.826
	2.4	1.58	TM_{10}	2.879	2.955	2.963	2.888	-0.313	2.267	2.531
			TM_{11}	5.149	5.105	5.259	5.099	0.971	0.118	3.042
			TM_{20}	5.743	5.78	5.796	5.731	0.209	0.848	1.121
			TM_{21}	7.746	7.965	7.778	7.735	0.142	2.888	0.553
			TM_{30}	8.555	8.69	8.833	8.555	0.000	1.554	3.147
	4.4	1.63	TM_{10}	2.186	2.224	2.214	2.19	-0.183	1.529	1.084
			TM_{11}	3.889	3.865	3.912	3.861	0.720	0.103	1.304
			TM_{20}	4.364	4.364	4.407	4.359	0.115	0.115	1.089
			TM_{21}	5.855	5.956	5.829	5.884	-0.495	1.209	-0.944
			TM_{30}	6.543	6.446	6.547	6.526	0.260	-1.241	0.321
	10.0	1.63	TM_{10}	1.474	1.472	1.481	1.462	0.814	0.679	1.283
			TM_{11}	2.595	2.590	2.619	2.578	0.655	0.463	1.565
			TM_{20}	2.888	2.952	2.939	2.913	-0.866	1.321	0.885
			TM_{21}	3.901	3.958	3.972	3.934	-0.846	0.606	0.957
			TM_{30}	4.329	4.423	4.377	4.367	-0.878	1.266	0.228
22	2.4	0.8265	TM_{10}	5.531	5.505	5.478	5.513	0.325	-0.145	-0.639
			TM_{11}	9.731	9.725	9.822	9.753	-0.226	-0.288	0.703
			TM_{20}	11.007	11.045	11.101	10.927	0.727	1.068	1.567
			TM_{21}	14.965	15.335	14.647	14.809	1.042	3.430	-1.106
			TM_{30}	16.271	16.140	16.393	16.31	-0.240	-1.053	0.506
Total Average % Error								0.660	1.051	1.162
$\varepsilon_{r1} = 1.0$, $h_1 = 0.0$										

TABLE 2.4

THEORETICAL, SOFTWARE COMPUTATIONAL AND EXPERIMENTAL [OUR] RESONANT FREQUENCIES FOR AN EQUILATERAL TRIANGULAR PATCH ON SINGLE SUBSTRATE OPERATED IN DIFFERENT MODES.

Resonant frequency (GHz)									
$\varepsilon_{re} = \varepsilon_{r2}$	$h = h_2$ (mm)	Mode	EXP [I]	HFSS [II] [48]	CFDTD [III] [49]	Computed			
						Present	% Error with respect to I	% Error with respect to II	% Error with respect to III
2.4	0.8265	TM_{10}	3.893	3.850	3.934	3.871	0.565	-0.545	1.601
		TM_{11}	6.708	6.815	6.771	6.807	-1.476	0.117	-0.532
		TM_{20}	7.586	7.74	7.754	7.695	-1.437	0.581	0.761
		TM_{21}	10.249	10.37	10.311	10.36	-1.083	0.096	-0.475
		TM_{30}	11.339	11.49	11.646	11.507	-1.482	-0.148	1.194
2.4	1.58	TM_{10}	3.789	3.765	3.750	3.711	2.059	1.434	1.040
		TM_{11}	6.659	6.67	6.667	6.6	0.886	1.049	1.005
		TM_{20}	7.391	7.49	7.500	7.332	0.798	2.109	2.240
		TM_{21}	10.091	10.47	10.107	9.997	0.932	4.518	1.088
		TM_{30}	11.18	11.135	11.25	10.924	2.290	1.895	2.898
4.4	1.63	TM_{10}	2.882	2.865	2.889	2.828	1.874	1.291	2.111
		TM_{11}	5.056	5.045	5.101	5.01	0.910	0.694	1.784
		TM_{20}	5.69	5.66	5.667	5.615	1.318	0.795	0.918
		TM_{21}	7.685	7.61	7.611	7.621	0.833	-0.145	-0.131
		TM_{30}	8.464	8.39	8.378	8.394	0.827	-0.048	-0.191
10.0	1.63	TM_{10}	1.949	1.945	1.962	1.888	3.130	2.931	3.772
		TM_{11}	3.374	3.42	3.397	3.347	0.800	2.135	1.472
		TM_{20}	3.75	3.83	3.805	3.755	-0.133	1.958	1.314
		TM_{21}	5.168	5.15	5.124	5.099	1.335	0.990	0.488
		TM_{30}	5.646	5.685	5.745	5.621	0.443	1.126	2.158
Total Average % Error							1.230	1.230	1.359
a= 32 mm, ε_{r1} = 1.0, h_1 = 0.0									

TABLE 2.5

THEORETICAL AND EXPERIMENTAL VALUES OF RESONANT FREQUENCIES FOR AN ETPA ON SINGLE SUBSTRATE OPERATED IN DIFFERENT MODE.

a = 100 mm, $\varepsilon_{re} = \varepsilon_{r2}$ = 2.32, ε_{r1} = 1.0, $h = h_2$ = 1.59 mm, h_1 = 0.0, ρ = 3 mm

Mode	Resonant Frequencies (GHz)								
	Exp [33]	Computed							
		Present	[17]	[42]	[37]	[16]	[34]	[36]	[30]
TM_{10}	1.280	1.280 (0.000)	1.278 (0.156)	1.286 (-0.469)	1.281 (-0.078)	1.283 (-0.234)	1.306 (-2.031)	1.288 (-0.630)	1299 (-1.484)
TM_{11}	2.242	2.239 (0.134)	2.224 (0.803)	2.226 (0.714)	2.219 (1.025)	2.221 (0.936)	2.262 (-0.892)	2.259 (-0.758)	2252 (-3.702)
TM_{20}	2.550	2.550 0.000)	2.556 (-0.235)	2.551 (-0.039)	2.562 (-0.470)	2.565 (-0.588)	2.612 (-2.431)	2.610 (-2.350)	2599 (-1.921)
TM_{21}	3.400	3.413 (-0.382)	3.398 (0.059)	3.400 (0.0)	3.389 (0.323)	3.393 (0.205)	3.400 (0.000)	3.454 (-1.590)	3439 (-6.029)
TM_{30}	3.824	3.819 (0.130)	3.834 (-0.261)	3.802 (0.575)	3.843 (-0.496)	3.848 (-0.627)	3.824 (0.000)	3.875 (-1.330)	3899 (-1.961)
Avg. % Error		0.129	0.303	0.3594	0.478	0.518	1.071	1.3316	3.019

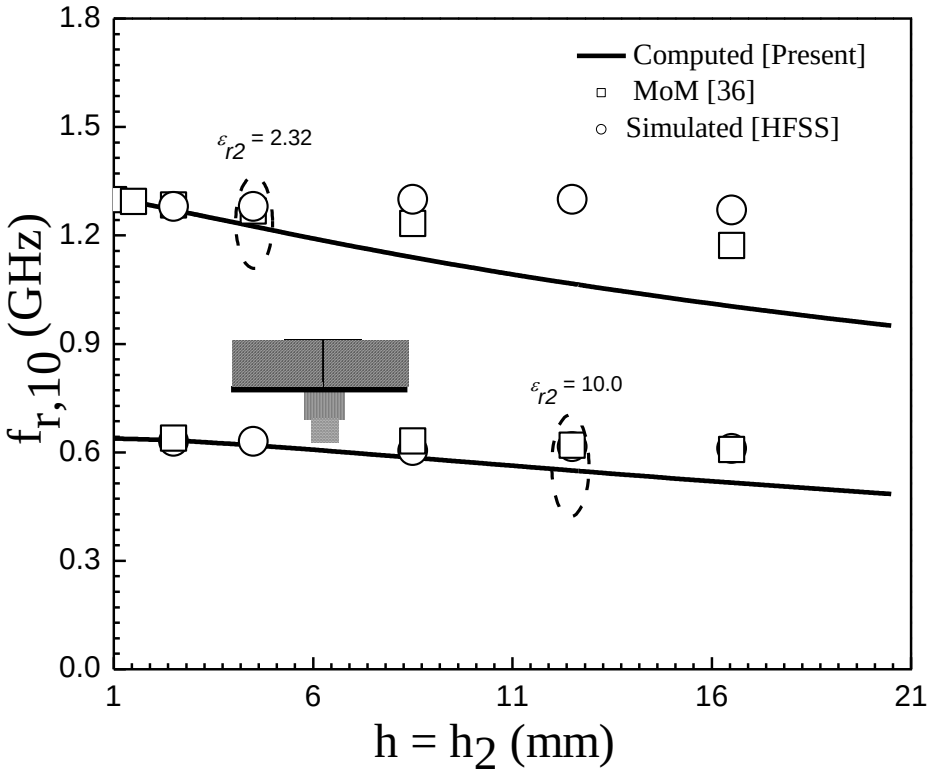

Figure 2.7: The variation of dominant mode resonant frequency with the variation of thickness of layer II for different substrate dielectric constants. a = 100 mm, h_1 = 0.0 mm.

The validity of the present model for an ETPA on a single substrate is further verified in Fig. 2.8 and 2.9. The variation of dominant mode resonant frequency with side length is visualized in Fig. 2.8. Here we have compared our theoretical curve with simulated [48] and our measured results. In Fig. 2.9 the computed values employing the present model is compared with experimental results reported in [31]. The very good agreement is revealed between computed, measured and simulated values.

From the above studies it is clear that the present formulae based on cavity model are valid for wide variation of antenna size and substrate electrical parameters. But slight discrepancy is observed for a patch having very small side length or large substrate thickness. Because the accuracy of the present model mainly depends on the value of h/λ_r and it is well suited for small value of h/λ_r. This is not the limitation of the present model but it is the inherent limitation of the cavity model.

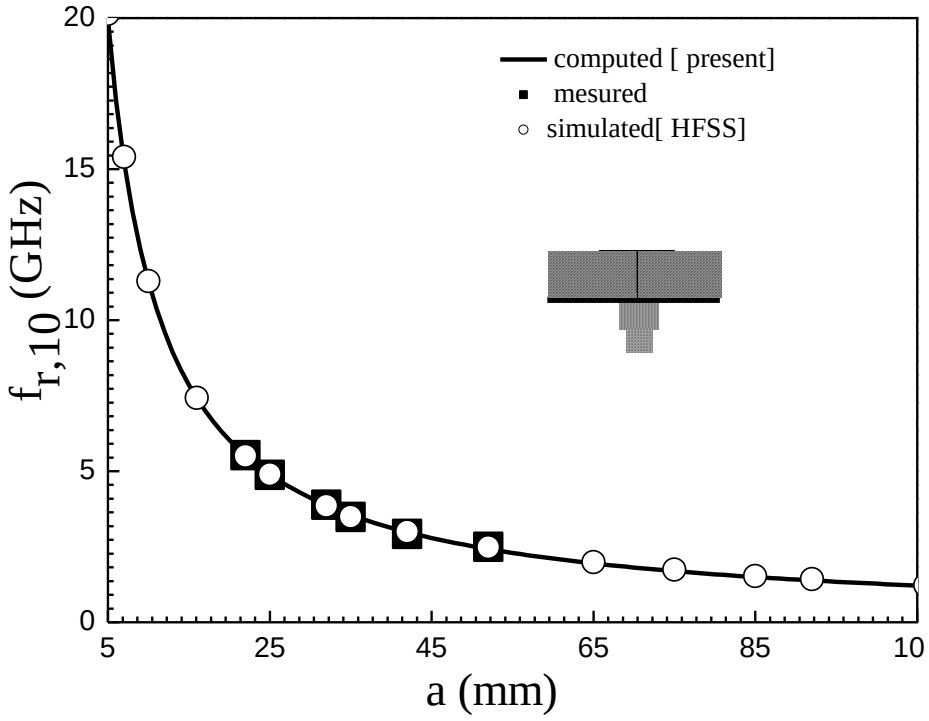

Figure 2.8: Computed, measured [our] and simulated variation of dominant mode resonant frequency as a function of side length of an ETPA on single substrate. h_1 = 0.0 mm, $h = h_2$ = 0.8265 mm, ε_{r1}= 1.0, $\varepsilon_{re} = \varepsilon_{r2}$ = 2.4.

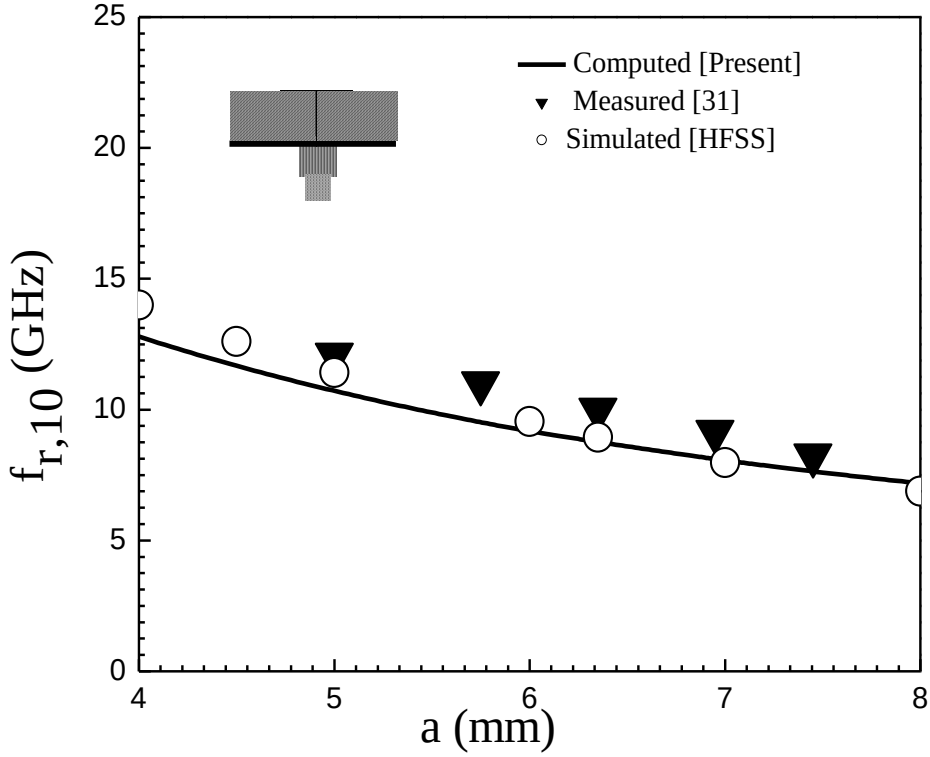

Figure 2.9: Computed, measured [31] and simulated variation of dominant mode resonant frequency as a function of side length of an ETPA on single substrate. h_1 = 0.0 mm, $h = h_2$ = 0.635 mm, ε_{r1} = 1.0, $\varepsilon_{re} = \varepsilon_{r2}$ = 10.2.

2.4.2. Input impedance

In Fig. 2.10, we have compared the computed impedance curve with simulated impedance curve foran ETPA on composite substrate for different value of h_1. This study shows that the present model agrees very well with the simulated results.

A comparison of theoretically predicted input impedance with our measured results for an equilateral patch printed on suspended substrate for three different h_1 is depicted in Fig. 2.11. The input impedance decreases a little with the increase of h_1 but significant increase in resonant frequency is observed with the increase of h_1. The computed curve employing the present model is closer to the measured results. The bandwidth is increases with the increase of h_1 is visualized from this figure.

The effect of composite and suspended substrate on both resonant frequency and input impedance of an ETPA operated in TM_{10} mode is visualized in Fig. 2.12. The resonant frequency is significantly shifted to the lower side of the frequency spectrum for composite substrate while for suspended substrate the resonant frequency is shifted to the upper side of frequency spectrum due to the increase of h_1 values with respect to single substrate patch antenna. The input impedance increases with the increase of h_1 for a patch on composite substrate whereas input impedance decreases with the increase of h_1 for a patch on suspended substrate with respect to single substrate patch.

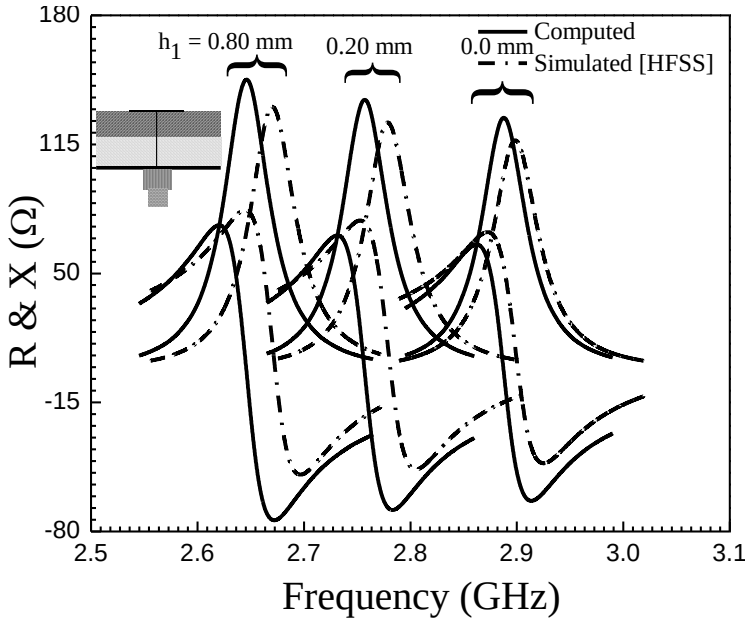

Figure 2.10: Computed and simulated dominant mode (TM_{10}) input impedance of an ETPA on composite substrate with different thickness of layer I. a = 42.0 mm, ε_{r2} = 2.4, h_2 = 1.58 mm, ρ = 19.2 mm, $tan\delta_1 = tan\delta_2$ = 0.0022, g = 1.25 mm.

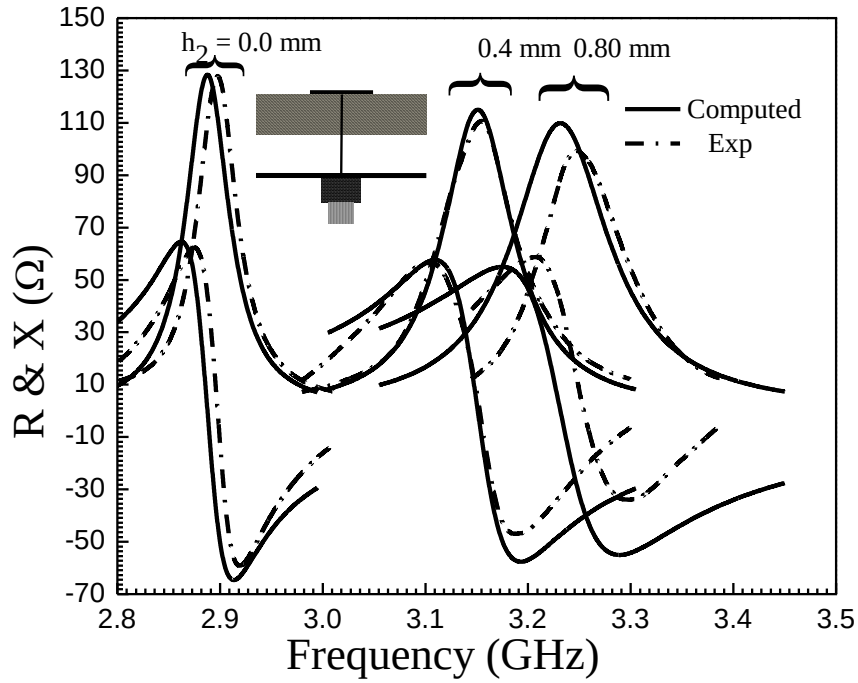

Figure 2.11: Measured [our] and computed dominant mode input impedance for a probe-fed ETPA having different thickness h_1 of layer I. a = 42 mm, ε_{r2} = 2.4, ε_{r1} = 1.0, h_2 = 1.58 mm, $tan\delta_1$ = 0.000, $tan\delta_2$ = 0.0022, ρ = 19.20 mm.

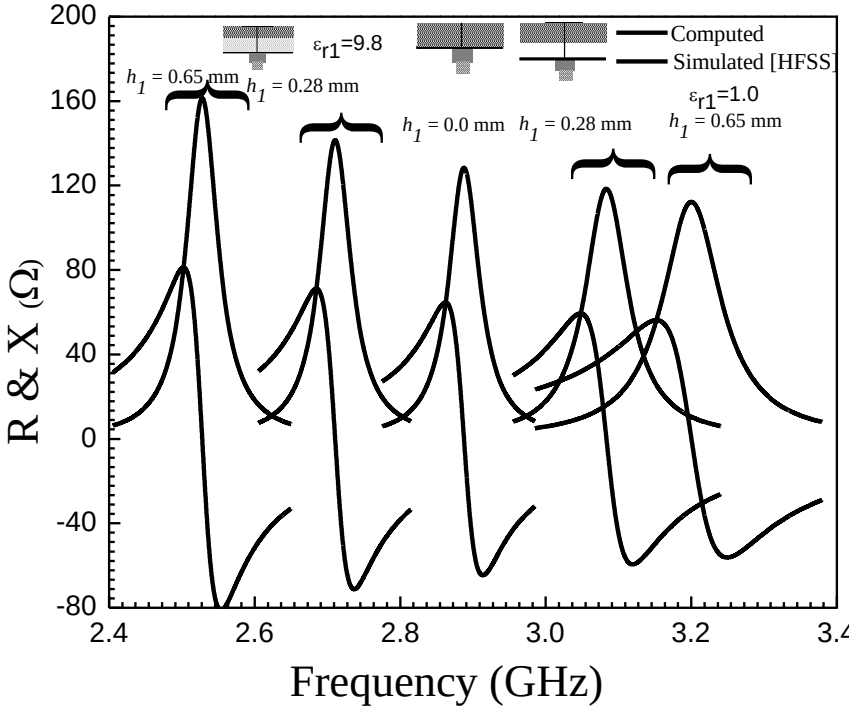

Figure 2.12: Computed dominant mode (TM_{10}) input impedance of an ETPA on composite and suspended substrate with different thickness of layer I. a = 42.0 mm, ε_{r2} = 2.4, h_2 = 1.58 mm, ρ = 19.2 mm, $tan\delta_1$ = $tan\delta_2$ = 0.0022, g = 1.25 mm.

Measured and computed TM_{10} mode input impedance as a function of frequency for a probe-fed ETPA on single substrate with two different patch size (a = 32 mm and a = 42 mm) is shown in Fig. 2.13 and Fig. 2.14 respectively. From these studies it is clear that the present model accurately computes the input impedance.

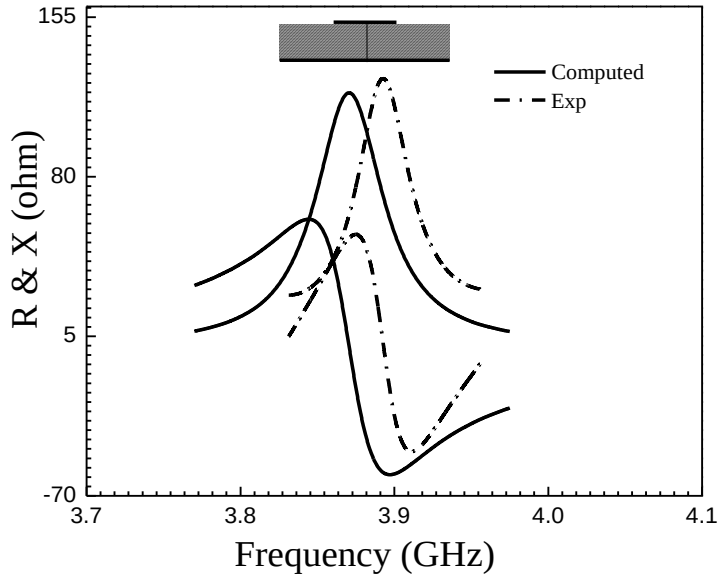

Figure 2.13: Measured [our] and computed TM_{10} mode input impedance for a probe-fed ETPA on single substrate. a = 32 mm, $\varepsilon_{re} = \varepsilon_{r2}$ = 2.4, ε_{r1} = 1.0, $h = h_2$ = 0.8265 mm, h_1 = 0.0 mm, ρ = 14.5 mm, $tan\delta_1$ = 0.000, $tan\delta_2$ = 0.0022.

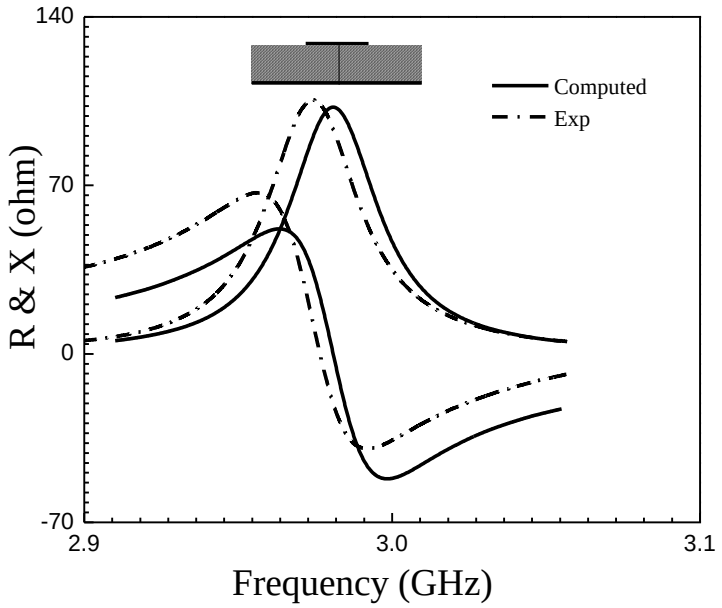

Figure 2.14: Measured [our] and computed TM_{10} mode input resistance and reactance as a function of frequency for a probe-fed ETPA on single substrate. a = 42 mm, $\varepsilon_{re} = \varepsilon_{r2}$ = 2.4, ε_{r1} = 1.0, $h = h_2$ = 0.8265 mm, h_1 = 0.0 mm, ρ = 19.1 mm, $tan\delta_1$ = 0.000, $tan\delta_2$ = 0.0022.

In table 2.6, we have compared the computed input impedances employing the present model and the model reported in [35] for an ETPA printed on a single substrate operated in dominant and higher order modes with experimental results [35]. Here the equilateral patch having side length a = 100 mm printed on a substrate whose h = 1.59 mm, ε_{re} = 2.32, $tan\delta_e$ = 0.0005, h/λ_r = 0.0068 and probe is located at a distance ρ = 3.0 mm from the tip of the triangle. The corresponding plots are depicted in Fig. 2.15. Here we have compared the computed input impedance curves employing the present model and the model reported in [35] with experimental curves [35]. From the study, we can say that the present model very accurately computes the input resistance at resonance for all modes.

TABLE 2.6
THEORETICAL AND EXPERIMENTAL [OUR] RESONANT FREQUENCIES AND INPUT IMPEDANCES FOR AN EQUILATERAL TRIANGULAR PATCH ON SINGLE SUBSTRATE OPERATED IN DIFFERENT MODES.

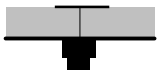

a = 100 mm, ε_{r1} = 1.0, $\varepsilon_{re} = \varepsilon_{r2}$ = 2.32, h_1 = 0.0, $h = h_2$ = 1.59 mm, ρ = 3 mm, $tan\delta_1$=0.000, $tan\delta_2$=0.0005

	Resonant Frequency (Ghz)			Input Impedance (Ω)		
Mode	Measured [35]	Theory		Measured [35]	Theory	
		Lee [35]	Present		Lee [35]	Present
TM_{10}	1.280	1.299	1.280	1510	1640	1509
TM_{20}	2.550	2.599	2.550	340	450	367
TM_{21}	3.400	3.439	3.413	949	909	933
Total % average error		1.519	0.127	Total % average error	15.059	3.231

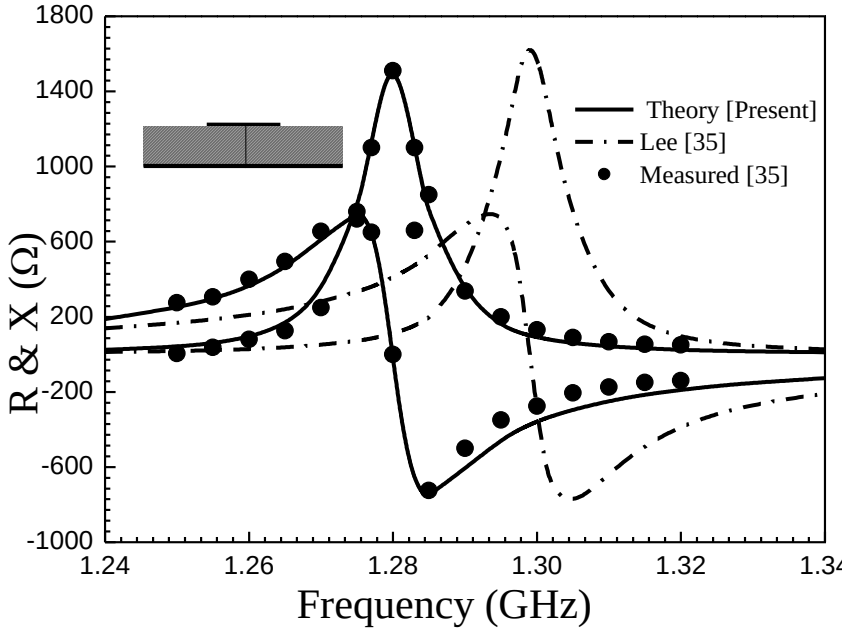

2.15 (a)

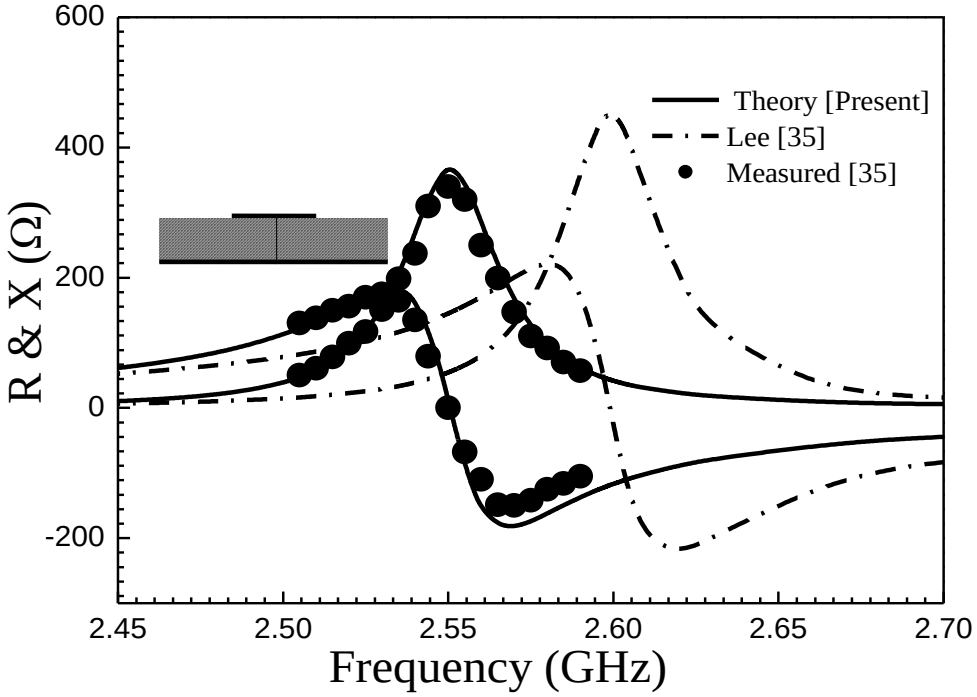

2.15 (b)

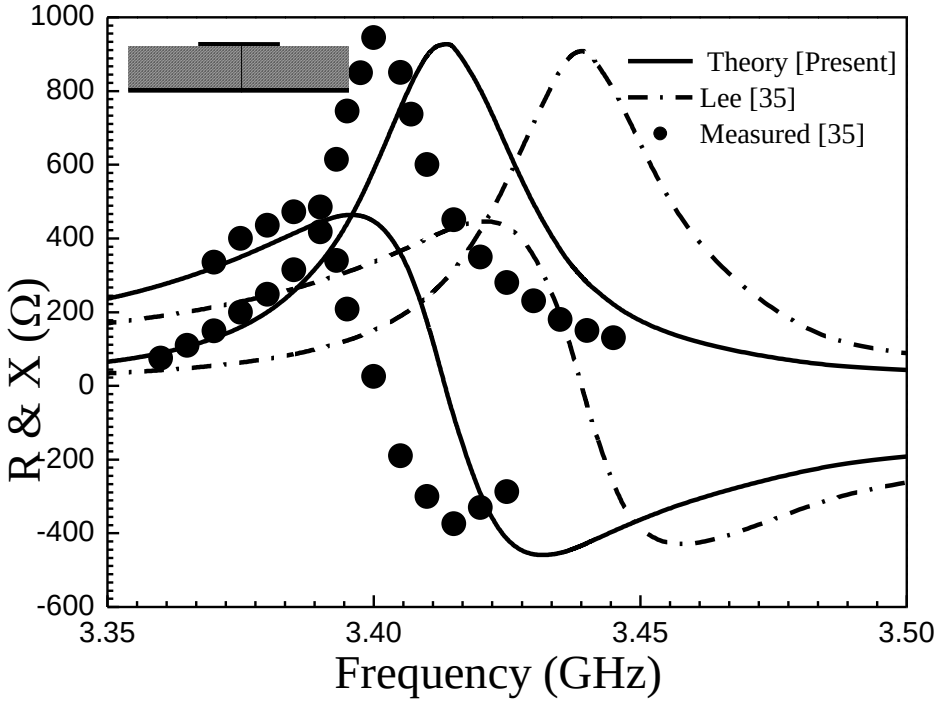

2.15 (c)

Figure 2.15: Measured [35] and computed input resistance and reactance as a function of frequency for a probe-fed ETPA on single substrate. (a) TM_{10} mode, (b) TM_{20} mode and (c) TM_{21}. a = 100 mm, ε_{r1} = 1.0, $\varepsilon_{re} = \varepsilon_{r2}$ = 2.32, $h = h_2$ =1.59 mm, h_1 = 0.0 mm, ρ = 3.0 mm, $tan\delta_1$ = 0.000, $tan\delta_2$ = 0.0005.

The validity of the present model is further verified in Fig. 2.16. The parameters for this study are for a = 54 mm, $\varepsilon_{re} = \varepsilon_{r2}$ = 2.5, $h = h_2$ =1.59 mm, $tan\delta_2$ = 0.0025, ρ = 40.0 mm. Here we have compared the computed values employing the present model with experimental result [20]. This study shows the computed input impedance is closed to measured [20] values.

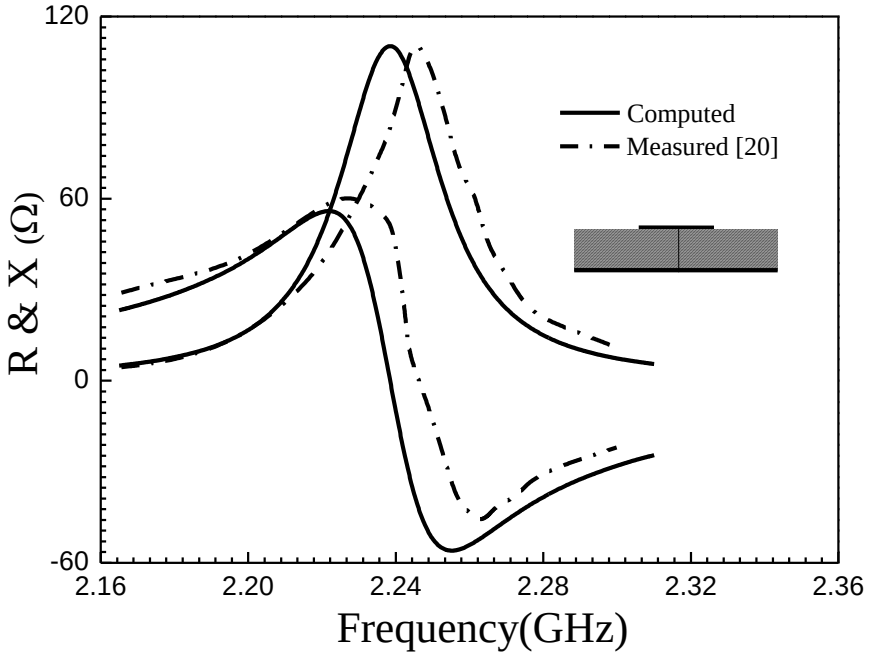

Figure 2.16: Measured [20] and computed TM_{10} mode input resistance and reactance as a function of frequency for a probe-fed ETPA on single substrate. a = 54 mm, ε_{r1} = 1.0, $\varepsilon_{re} = \varepsilon_{r2}$ = 2.5, $h = h_2$ =1.59 mm, h_1 = 0.0 mm, ρ = 40.0 mm $tan\delta_2$ = 0.0025, $tan\delta_1$ = 0.000.

In table 2.7, we have compared the computed input resistance at resonance employing the present model with our experimental results and experimental results available in [20, 35]. We have also employed the HFSS simulator to generate simulated results. The present model shows very close agreements with all measured and simulated results.

The variation of the resonant resistance as a function of feed location for different side length a is investigated in Fig. 2.17. The computed values are compared with simulated values [48] and shows close agreements between them for all ρ and a.

2.4.3. Quality Factor, Bandwidth and Gain

The total quality factor Q_T mainly depends on radiation loss. The radiation loss is different for different operating modes. A comparative study of Q_r is given in table 2.8. The table shows that the effect of modes on Q_r is more effective in [35] but negligible in [32]. The

computed Q_r employing the present model is mode dependent and significantly changes for changing of operating modes. It is important to mention that the article [35] has employed large and rigorous mathematical steps to compute mode dependent Q_r, whereas we have used a very simple formula for computing similar values of mode dependent Q_r [35]. The present model gives the almost same values [35] without employing the complex and rigorous mathematical steps.

TABLE 2.7
EXPERIMENTAL AND THEORETICAL VALUES OF INPUT IMPEDANCE OF AN ETPA ON SINGLE AND SUSPENDED SUBSTRATE OPERATED IN DOMINANT MODE

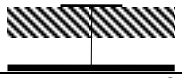

Input Impedance (Ω)									
a (mm)	**$\varepsilon_{re} = \varepsilon_{r2}$**	**$tan\delta_2$**	**h_2**	**h_1**	**ρ**	**Measured**		**Computed**	**Simulated (HFSS)**
100	**2.32**	**0.0005**	**1.59**	**0.0**	**3.0**	**1510**	**Lee [35]**	**1509**	**1416**
54	**2.5**	**0.0025**	**1.59**	**0.0**	**26**	**59**	**Hasani [20]**	**76**	**58**
					40	**112**		**114**	**90**
42	**2.2**	**0.0022**	**0.8265**	**0.0**	**19.1**	**106**		**103**	**105**
42	**2.2**	**0.0022**	**1.58**	**0.0**	**19.2**	**128**		**130**	**119**
35	**2.4**	**0.0022**	**0.8265**	**0.0**	**16.8**	**70**		**70**	**61**
32	**2.4**	**0.0022**	**0.8265**	**0.0**	**14.5**	**123**		**121**	**124**
32			**1.58**	**0.0**	**14.3**	**130**		**134**	**119**
32	**4.4**	**0.02**	**1.63**	**0.0**	**15**	**76.5**		**79**	**65**
32	**2.4**	**0.0022**	**0.8265**	**0.25**	**14.5**	**120**	**Our exp.**	**112**	**116**
				0.50		**104**		**109**	**112**
				1.0		**91**		**107**	**106**
			1.58	**0.25**	**14.7**	**119**		**122**	**109**
				0.50		**111**		**116**	**104**
				1.0		**101**		**110**	**99**
42	**2.4**		**1.58**	**0.45**	**19.2**	**111**		**115**	**104**
				0.90		**99.5**		**110**	**98**
ε_{r1} =1.0, $tan\delta_1$ = 0.00									

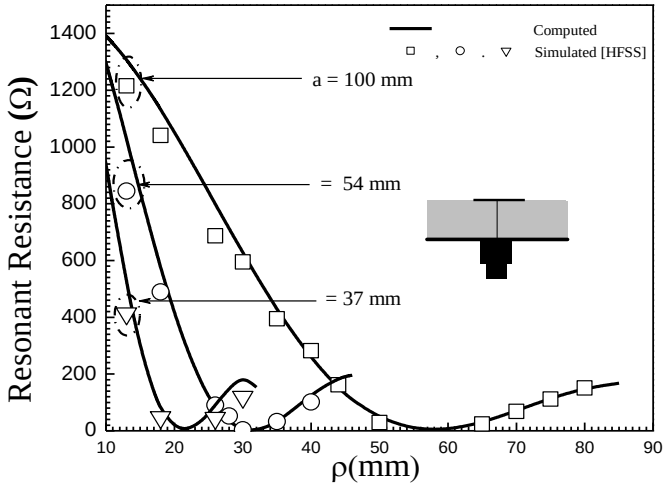

Figure 2.17: Computed, simulated and measured dominant mode input resistance at resonance versus feed location ρ of an ETPA with different side length. ε_{r1}= 1.0, ε_{r2} = 2.32, h_1= 0.00 mm, h_2= 1.59 mm, $tan\delta_1$ = 0.000, $tan\delta_2$ = 0.0005.

TABLE 2.8

THEORETICAL VALUES OF RADIATION QUALITY FACTOR DUE TO RADIATION LOSS (Q_r) OF AN ETPA ON SINGLE SUBSTRATE OPERATED IN DIFFERENT MODES.
a = 100 mm, $\varepsilon_{re} = \varepsilon_{r2}$ = 2.32, $h = h_2$ = 1.59

Mode	Geometrical Theory [32]	Lee [35]	Present
TM_{10}	75	163	163
TM_{20}	75	82	81
TM_{30}	75	84	83
TM_{40}	75	77	83
TM_{50}	75	81	83
TM_{60}	75	84	81
TM_{11}	63	151	151

The effect of composite and suspended substrate on total quality factor and bandwidth is visualized in Fig. 2.18. The total quality factor increases exponentially for composite substrate while the total quality factor decreases linearly for suspended substrate with the increase of h_1/h. This behavior is based on the fact that the effective dielectric constant is enhanced, the fringing fields effect decreases (Fig. 2.19), and therefore, the radiation emitted by the patch also decreases for composite substrate. But for suspended substrate, the effective dielectric constant is lowered, the fringing fields effect increases (Fig. 2.19), and, therefore, the radiation emitted by the patch also increases. Subsequently, the bandwidth is decreased for composite and bandwidth is increased for suspended substrate with increase of h_1/h. The computed values are well supported the simulated values.

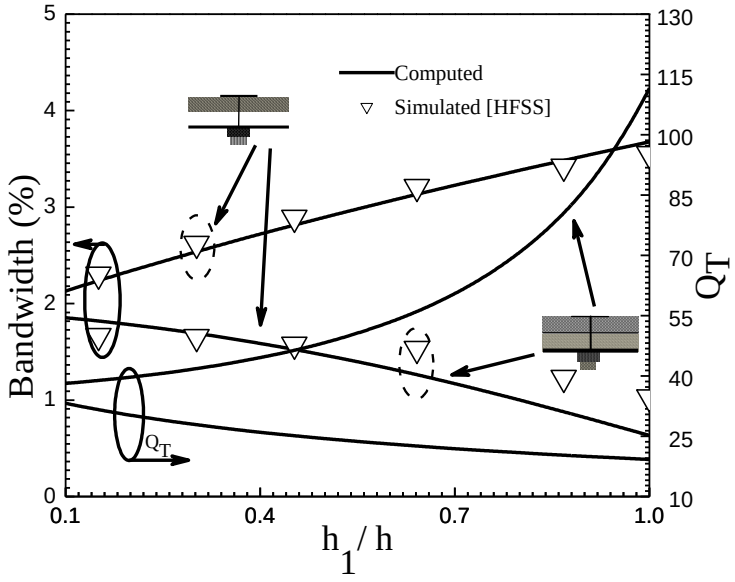

Figure 2.18: Computed and simulated variation of percentage B.W and Q_T with h_1 of an ETPA on composite (ε_{r1} = 4.4, $tan\delta_1$ = 0.0035) and suspended substrate (ε_{r1} = 1.0, $tan\delta_1$ = 0.000). a = 42.00 mm, h = 2.65 mm, ε_{r2} = 2.4, ρ = 19.20, $tan\delta_2$ = 0.0022, h_1 and h_2 variable but h is fixed.

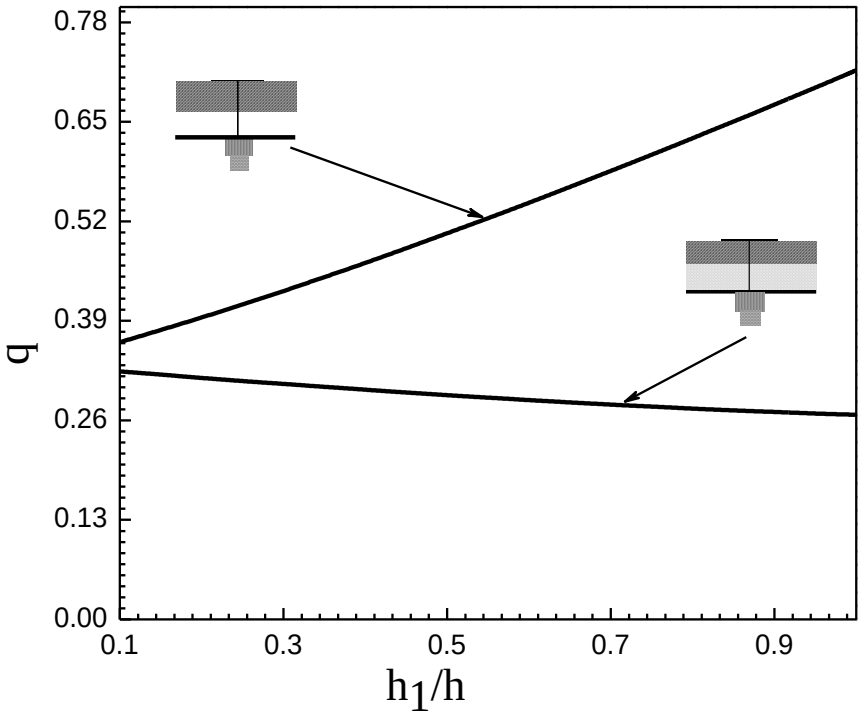

Figure 2.19: Theoretical variation of q of an ETPA on composite (ε_{r1} = 4.4, $tan\delta_1$ = 0.0035) and suspended substrate. (ε_{r1} = 1.0, $tan\delta_1$ = 0.000). h_1 and h_2 variable but h is fixed. Parameter as in Fig. 2.16.

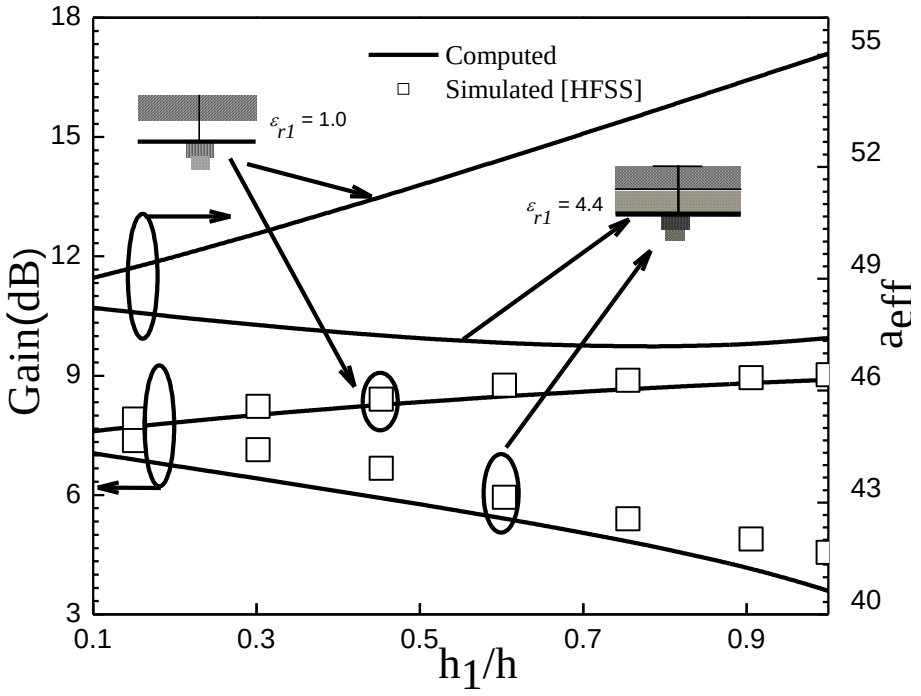

Figure 2.20: Theoretical variation of effective side length and gain of an ETPA on composite (ε_{r1} = 4.4, $tan\delta_1$ = 0.0035) and suspended substrate. (ε_{r1} = 1.0, $tan\delta_1$ = 0.000) as a function of h_1. Parameter as in Fig. 2.16.

In Fig. 2.20, the change of gain and effective side length (a_{eff}) with the change of h_1/h keeping the total height h constant of an ETPA on composite and suspended substrate have been plotted. The a_{eff} is decreased for composite and increased for suspended substrate, so, the effective aperture area decreases for composite and increases for suspended substrate, therefore, the gain is decreased for composite and increased for suspended substrate with increase of h_1/h. No theoretical and experimental value is available to predict the effect of composite and suspended substrate on gain. So, we have employed HFSS simulator [48] to validate the present model and good agreement is revealed between them.

The simulated gain pattern of an ETPA on composite, suspended and single substrate is depicted in Fig. 2.21. It is noticed that the gain is high for suspended substrate and low for composite substrate with respect to single substrate ETPA. This phenomena clearly explained in previous paragraph using theoretically predicted curve and simulated results in Fig 2.20.

Simulated gain pattern of an ETPA with different ε_{r1} is depicted in Fig. 2.22. It is observed that the effect of ε_{r1} on both co-polar and cross polar gain are significant. The gain increases with the decrease of ε_{r1}. The simulated gain pattern as a function of azimuth angle for an equilateral triangular patch antenna with different h_1 with fixed h_2 for suspended substrate patch is shown in Fig. 2.23. The slight improvement in gain is observed with the increase of h_1.

Measured and simulated gain pattern of an ETPA on single substrate is depicted in Fig. 2.24. The comparaison shows excellent correlation between measured and simulated gain pattern.

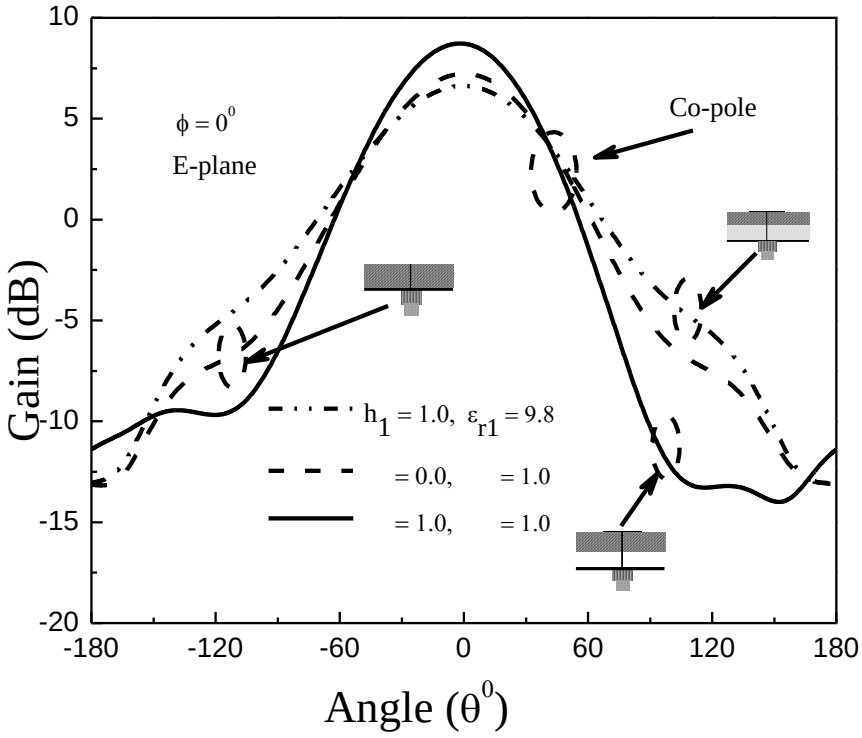

(a)

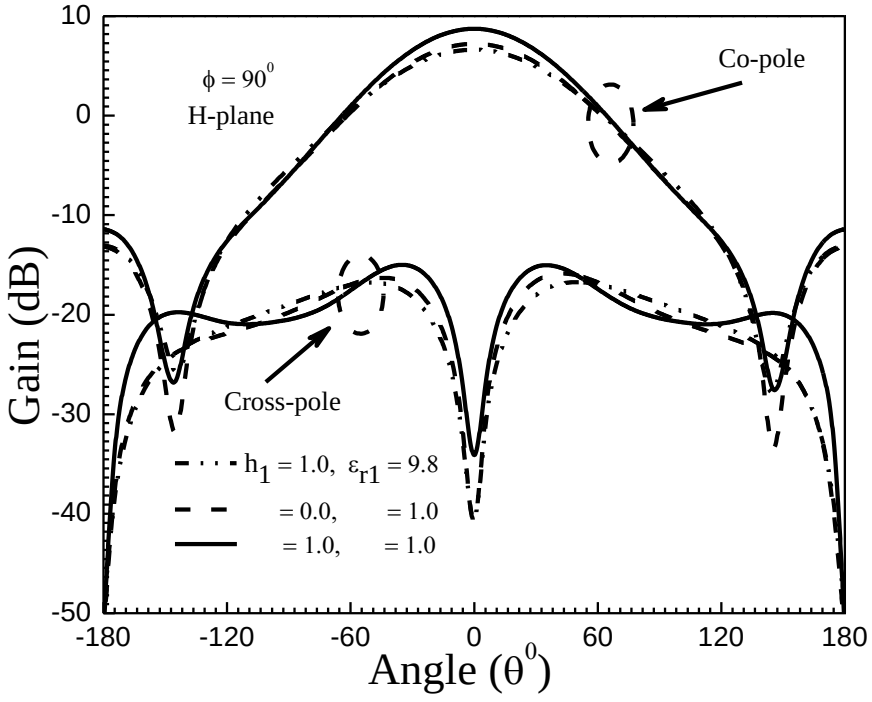

(b)

Figure 2.21: Simulated gain pattern as a function of azimuth angle for an ETPA on composite, suspended and single substrate. h_2 = 1.58 mm, ε_{r2} = 2.4 other parameters as in Fig. 2.11.(a) E- plane co-polar gain pattern (b) H- plane co-polar and cross polar gain pattern.

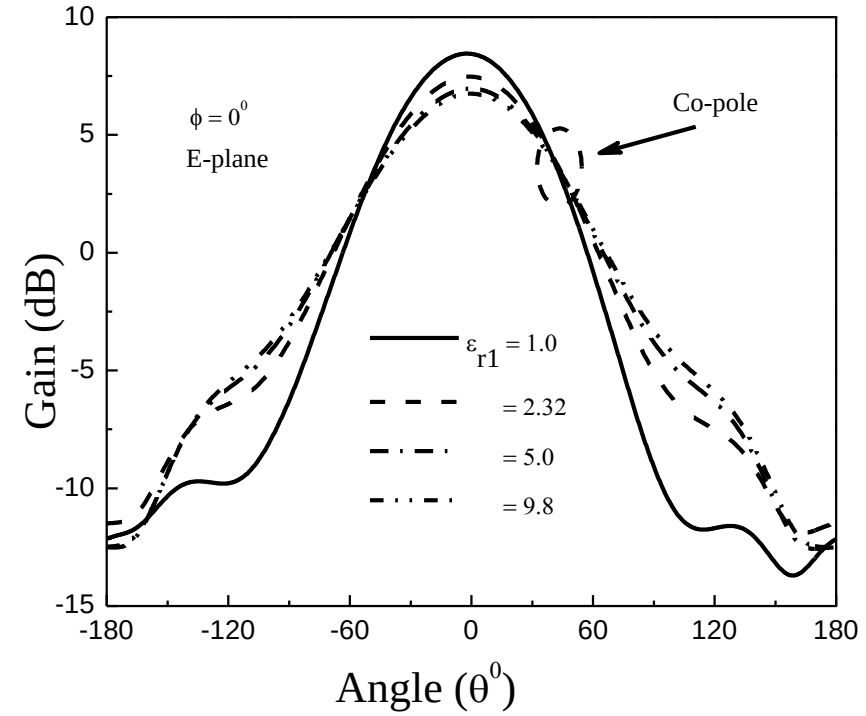

(a)

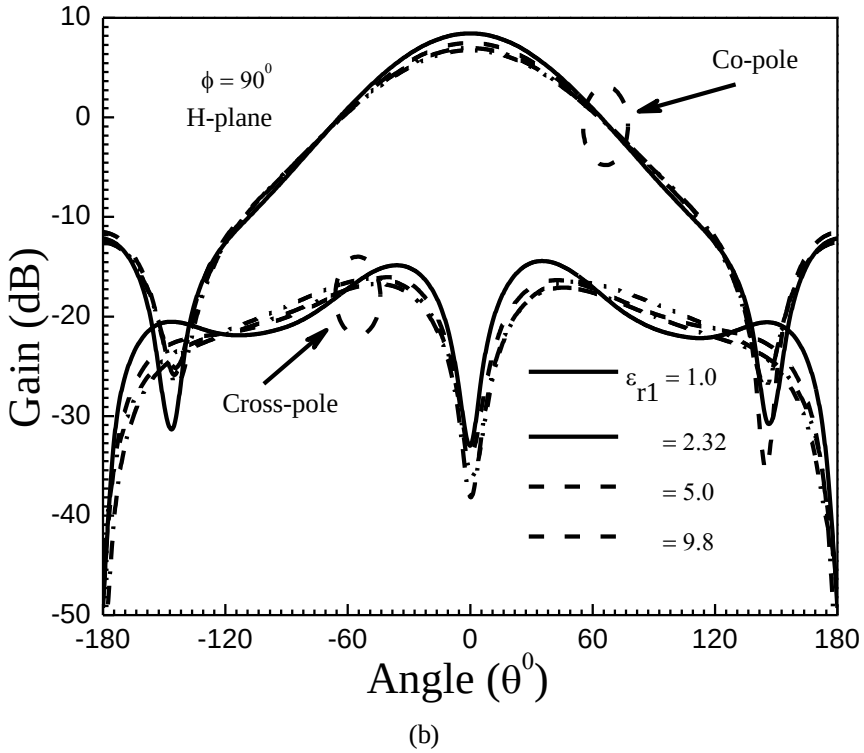

(b)

Figure 2.22: Simulated gain pattern as a function of azimuth angle for an ETPA with different ε_{r1} of layer I. h_1 = 0.7875 mm, h_2 = 1.58 mm, ε_{r2} = 2.4 other parameters as in Fig. 2.11. (a) E- plane co-polar gain pattern (b) H-plane co-polar and cross polar gain pattern.

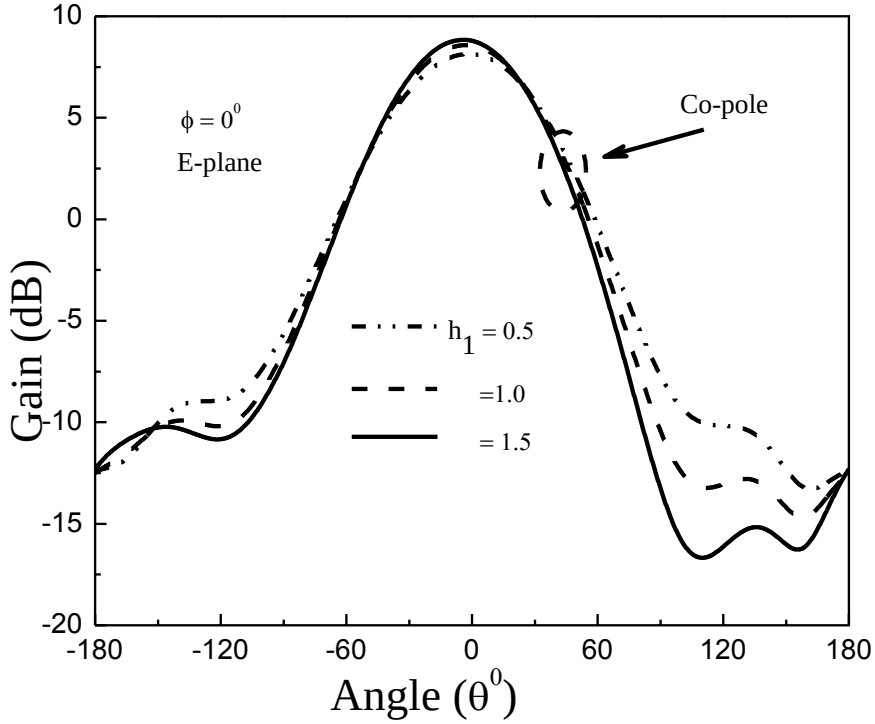

(a)

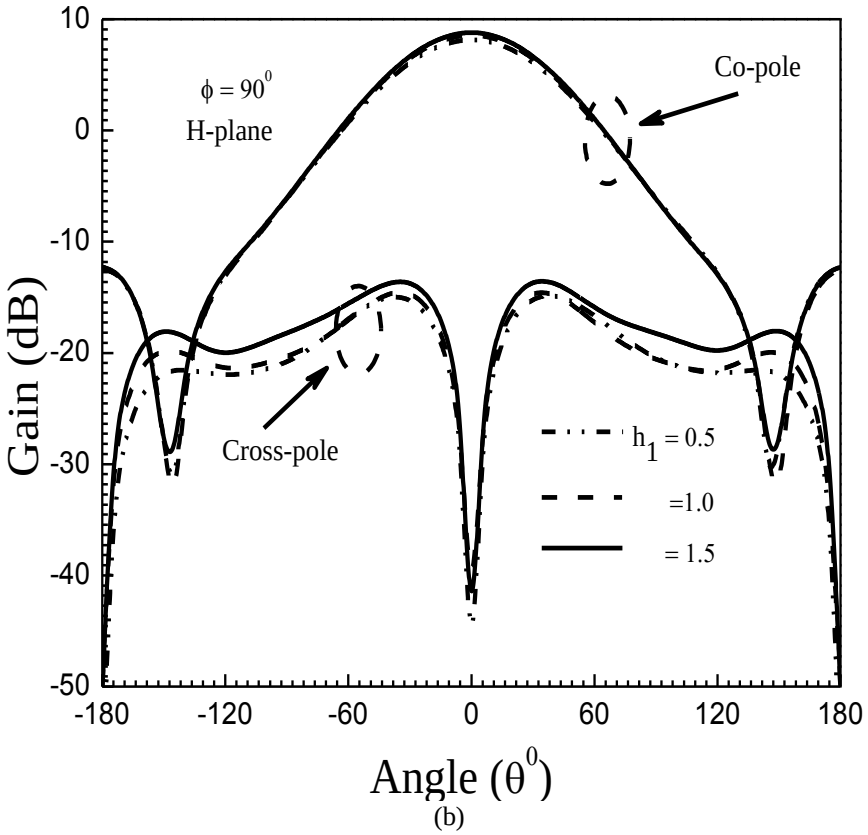

(b)

Figure 2.23: Simulated gain pattern as a function of azimuth angle for an ETPA with h_1 of layer I. a = 42 mm, h_1 = 1.58 mm, ε_{r1} = 2.4, $tan\delta_1$ = 0.0022. h_2 = 1.58 mm, ε_{r1} = 1.0, ε_{r2} = 2.4 other parameters as in Fig. 2.11. (a) E- plane co-polar gain pattern (b) *H*- plane co-polar and cross polar gain pattern.

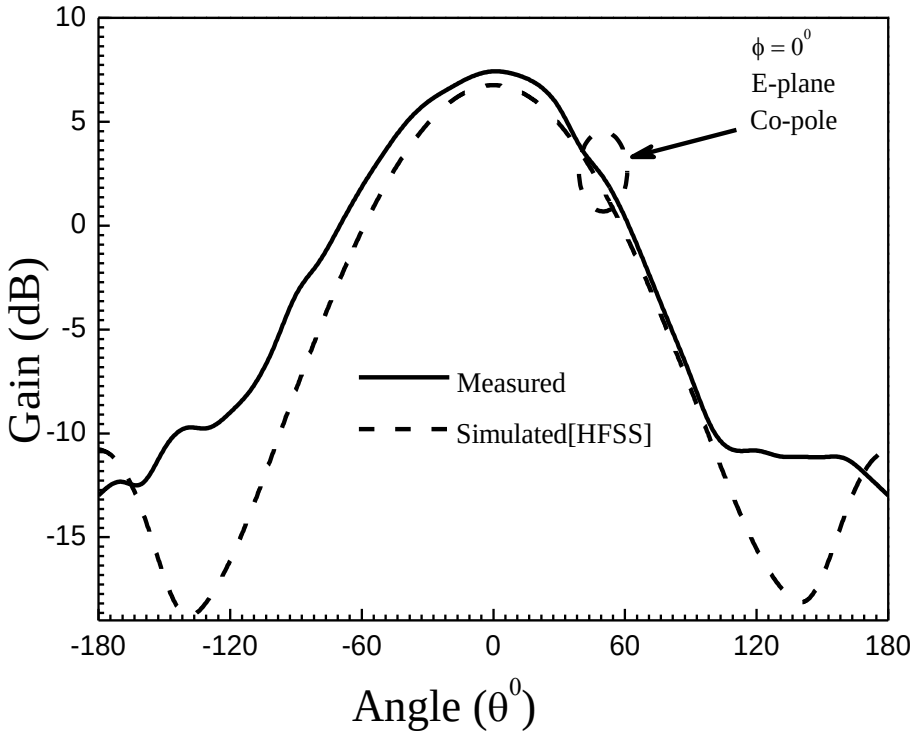

(a)

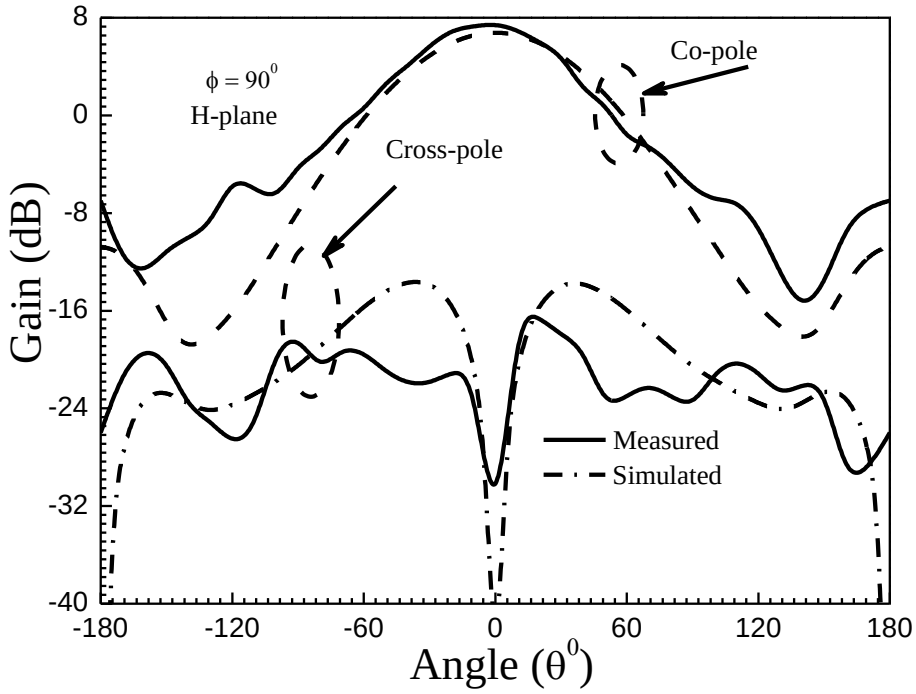

(b)

Figure 2.24: Measured [our] and simulated gain pattern as a function of azimuth angle for an ETPA on single substrate. Parameters are a = 22 mm, h_1 = 0.0, $h = h_2$ = 1.58 mm, ε_{r1} = 1.0 $\varepsilon_{re} = \varepsilon_{r2}$ = 2.4, $tan\delta_1$ = 0.00, $tan\delta_2$ = 0.0022. (a) *E*- plane co-polar gain pattern, (b) *H*- plane co-polar and cross polar gain pattern.

2.5. Conclusions

A very simple, fast and accurate CAD oriented cavity model is proposed to predict the resonant frequency, input impedance, bandwidth and gain of an ETPA on composite, suspended and single substrate. The present model is valid for a wide variation of antenna size, substrate electrical parameters and feed location under the patch. Neither any theoretical nor any experimental value is available of an ETPA on composite substrate. Also, the effect of suspended substrate on input impedance, bandwidth and gain was not investigated earlier. So, we have performed a series of experiments with fabricated prototypes and employed simulation softwares (HFSS and CFDTD) to validate the present model. We have also studied the gain patterns. The present model shows excellent agreements with measured and simulated values. This information is very useful for practical implementation of ETPA and designing the MIC on semiconductor materials with $\varepsilon_r \geq 10$.

REFERENCES:

[1] R. Garg, P. Bhartia, I. J. Bahl, and A. Ittipiboon, "Microstrip antenna design handbook," *Artech house*, 2001.

[2] Q. Liu, J. Wang, and Y. He, "Compact balanced band pass filter using isosceles right triangular patch resonator," *Electron Lett.*, vol. 53, pp. 253-254. 2017.

[3] S. Yadav, A. K. Gautam, B. K. Kanaujia, and K. Rambabu, "Design of band-rejected UWB planar antenna with integrated Bluetooth band," *IET Microw. Antennas Propagat.*, vol. 10, pp. 1528-1533. 2016.

[4] H. W. Liu, Z. Q. Cheng, and L. L. Sun, "Dual-mode triangular-patch band pass filter using spur-lines," *Electron Lett.*, vol. 42, pp. 762-763, 2006.

[5] J. S. Hong and M. J. Lancaster, "Theory and experiment of dual-mode microstrip triangular patch resonators and filters," *IEEE Trans. Microw. Theory Tech.*, vol. 52, no. 4, pp. 1237 – 1243, Apr. 2004.

[6] Q. Luo *et al.*, "Dual circularly polarized equilateral triangular patch array," *IEEE Trans. Antennas Propagat.*, vol. 64, no. 6, pp. 2255-2262, June 2016.

[7] J. T. S. Sumantyo and K. Ito, "Circularly polarised equilateral triangular patch array antenna for mobile satellite communications," *IEE Proc. Microw. Antennas Propagat.*, vol. 153, no. 6, pp. 544-550, Dec. 2006

[8] J.T.S. Sumantyo, K. Ito, and M. Takahashi, "Dual-band circularly polarized equilateral triangular-patch array antenna for mobile satellite communications," *IEEE Trans. Antennas Propagat.*, vol. 53, no. 11, pp. 3477 – 3485, Nov. 2005.

[9] M. Biswas and A. Mandal, "Design and development of an equilateral patch sensor for determination of permittivity of homogeneous dielectric medium," *Microw. Opt. Technol. Lett.*, vol. 56, pp. 1097-1104, May. 2014.

[10] M. Jobs and A. Rydberg, "Conformal dual patch antenna for diversity based sensor nodes," *Electron. Lett.*, vol. 48, pp. 306-307. 2012.

[11] T. Zhang, Y. Zhang, W. Hong, and K. Wu, "Triangular ring antennas for dual-frequency dual-polarization or circular-polarization operations," *IEEE Antennas Wireless Propagat. Lett.*, vol. 13, pp. 971-974, 2014.

[12] J.S. Chen, "Studies of CPW-fed equilateral triangular-ring slot antennas and triangular-ring slot coupled patch antennas," *IEEE Trans. Antennas Propagat.*, vol. 53, pp. 2208-2211, 2005.

[13] Y. Sung, "Investigation into the polarization of asymmetrical- feed triangular microstrip antennas and its application to reconfigurable antennas," *IEEE Trans. Antennas Propagat.*, vol. 58, pp. 1039-1046. 2010

[14] H. Zhang, Z. Wang, J. Yu, and J. Huang, "A compact MIMO antenna for wireless communication," *IEEE Antennas Propagat. Magaz.*, vol. 50, no. 6, pp. 104-107, Dec. 2008.

[15] S. Dahele, S. Mem, and K.F. Lee, "Theory and experiment on microstrip antennas with air gaps," *Proc. Inst. Elect. Eng. pt H.*, vol. 132, pp. 455–460, 1985.

[16] Nasimuddin, K. Esselle, and A.K.Verma, "Resonant frequency of an equilateral triangular microstrip antenna," *Microw. Opt. Technol. Lett.*, vol. 47, no.5, pp.485-489, Dec. 2005.

[17] C. S. Gurel and E. Yazgan, "New computation of the resonant frequency of a tunable equilateral triangular microstrip patch," *IEEE Trans. Microw. Theory Tech*., vol. 48, pp. 334-338, Mar. 2000.

[18] F. Abboud, J. P. Damiano, and A. Papiernik, "A new model for calculating the input impedance of coax-fed circular microstrip antennas with and without air gaps," *IEEE Trans. Antenna Propagat*., vol. 38, pp. 1882–1885, 1990.

[19] N. G. Alexopoulos and D. R. Jackson, "Fundamental superstrate (cover) effects on printed circuit antennas," *IEEE Trans. Antennas Propagat.*, vol. 32, pp. 807-816, 1984.

[20] H. R. Hassani and D. M. Syahkal, "Analysis of triangular patch antennas including radome effects" *IEE Proc. H*, vol. 139, no. 3, pp.251-256, Jun. 1992.

[21] J. Svacina, "Analysis of multilayer microstrip lines by a conformal mapping method," *IEEE Trans. Microw. Theory Tech*., vol. 40, pp. 769–772, 1992.

[22] V. Losada, R.R. Boix, and M. Horno, "Resonant modes of circular microstrip patches in multilayered substrates," *IEEE Trans. Microw. Theory Tech*., vol. 47, pp. 488–497, 1999.

[23] Y. Li and N. Bowler, "Resonant frequency of a rectangular patch sensor covered with multilayered dielectric structures," *IEEE Trans. Antennas Propagat*. vol. 58, pp. 1883-1889, 2010.

[24] M. Biswas and M. Sen, "Design and development of rectangular patch antenna with superstrates for the application in portable wireless equipments and aircraft radome," *Microw. Opt. Technol. Lett*. vol. 56, pp. 883-893, 2014.

[25] M. Biswas, S. Banik, M. Biswas, and A. Sukla, "CAD model to predict the effect of radome on the characteristics of rectangular patch antenna," *Microw. Opt. Technol. Lett*., vol. 55, pp. 2460-2468, 2013.

[26] R. Q. Lee and K. F. Lee, "Experimental study of two-layer electromagnetically coupled rectangular patch antenna" *IEEE Trans. Antennas Propagat*., vol. 38, pp. 1298-1302, 1990.

[27] P. S. Bhatnagar, J. P. Daniel, K. Mahdjoubi, and C. Terret, "Experimental study on stacked triangular microstrip antennas," *Electron. Lett.*, vol. 22, no. 16, pp. 864-865, July 31, 1986.

[28] R.K. Hoffmann, "Handbook of microwave integrated circuits," Norwood, MA , *Artech House*, pp. 243-245, 1987.

[29] M. J. Tsai, F. De Flaviis, O. Fordham, and N. G. Alexopoulos, "Modelling planer arbitrary shaped microstrip elements in multilayered MIC/MMIC media," *IEEE Trans.*

Microw. Theory Tech., vol. 45, pp. 330-337, 1997.

[30] J. Helszajn and D. S. James, "Planar triangular resonators with magnetic walls," *IEEE Trans. Microw. Theory Tech*., vol. 26, pp. 95-100, Feb.1978.

[31] A. K. Sharma and B. Bhat, "Analysis of triangular microstrip resonator," *IEEE Trans. Microw. Theory Tech*., vol. 30, no. 11, pp. 2029 – 2031, Nov. 1982.

[32] E. F. Keuster and D. C. Chang, "A geometrical theory for the resonant frequencies and Q factors of some triangular microstrip patch antenna," *IEEE Trans. Antennas Propagat.*, vol. 31, pp.27-34, 1983.

[33] J. S. Dahele and K. F. Lee, "On the resonant frequencies of the triangular patch antenna," *IEEE Trans. Antennas Propagat.*, vol. 35, pp.100-101, 1987.

[34] X. Gang, "On the resonant frequencies of microstrip antennas," *IEEE Trans. Antennas Propagat*., vol. 37, pp. 245-247, 1989.

[35] K. F. Lee, K. M. Luk, and J. S. Dahele, "Characteristics of the equilateral triangular patch antenna," *IEEE Trans. Antennas Propagat.*, vol. 36, no.11, pp.1510-1518, Nov. 1988.

[36] W. Chen, K. F. Lee, and J. S. Dahele, "Theoretical and experimental studies of the resonant frequencies of equilateral triangular microstrip antenna," *IEEE Trans. Antennas Propagat.*, vol. 40, pp.1253-1256, Oct. 1992.

[37] D. Karaboğa, K.Güney, N. Karaboğa, and A. Kaplan, "Simple and accurate effective side length expression obtained by using a modified genetic algorithm for the resonant frequency of an equilateral triangular microstrip antenna," *Int. J. Electron.*, vol. 83, pp. 99-108, Jan.1997.

[38] K. Guney and E. Kurt, "Effective side length formula for resonant frequency of equilateral triangular microstrip antenna," *Int. J. Electron.,* vol. 103, pp. 261-268, 2016.

[39] P. Mythili, A. Das, "Simple approach to determine resonant frequencies of microstrip antennas," *IEE Proc. Microw. Antennas Propagat.,* vol. 145, No. 2, April 1998.

[40] M. Biswas and D. Guha, **"**Input impedance and resonance characteristic of superstrate loaded triangular microstrip patch," *IET Microw. Antennas Propagat.,* vol. 3, pp. 92 – 98, Feb. 2009.

[41] M.Biswas and A. Mandal, "CAD model to compute the input impedance of an equilateral triangular microstrip patch antenna with radome," *Prog. Electromag. Res. M.*, vol. 12, pp. 247-257, 2010.

[42] M. M. Olaimat and N. I. Dib, "Improved formulae for the resonant frequencies of triangular microstrip patch antennas," *Int. J. Electron.,* vol. 98, pp. 407-424, 2011.

[43] M. M. Olaimat and N. I. Dib, "A study of 15^0-75^0-90^0 angles triangular patch antenna," *Prog. Electromag. Res. Lett.*, vol. 21, pp. 1-9, 2011.

[44] J. R. James and P. S. Hall, "Handbook of microstrip antennas," *UK, Peter Peregrinus*, London, 1989.

[45] S. Maity and B. Gupta, "Accurate resonant frequency of isosceles right-angled triangular patch antenna," *Microw. Opt. Technol. Lett.*, vol. 55, pp. 1306-1308, 2013.

[46] S. Maity and B. Gupta, "Cavity model analysis of 30°–60°–90° triangular microstrip antenna," *AEU-Int. J. Electron. Comm.,* vol. 69, pp. 923-932, 2015.

[47] S. Maity, B. Gupta, "Approximate investigation on isosceles triangular microstrip antenna in fundamental mode," *Microw. Opt. Technol. Lett.*, vol. 59, pp. 614-618, 2017.

[48] High Frequency Structure Simulator: *Ansoft Corp*. 2012.

[49] R. Mittra, W. Yu. "CFDTD," *Artech House,* 2004.

[50] T. C. Edwards and M. B. Steer, "Foundations of interconnect and microstrip design," *Third Edition, John Wiley & Sons Ltd.*, 2000.

[51] I. Wolff and N. Knoppik, "Rectangular and circular microstrip disk capacitors and resonators," *IEEE Trans. Microw. Theory Tech.*, vol. 22, pp. 857-864, 1974.

[52] F. Abboud, J.P. Damiano, and A. Papiernik, "Simple model for the input impedance of coax-fed rectangular microstrip patch antenna for CAD," *IEE Proc. Pt. H*., vol. 135, pp. 323-326, 1988.

[53] A.G. Derneryd, "Analysis of the microstrip disk antenna element," *IEEE Trans. Antennas Propagat*., vol. 27, pp. 660–664, 1979.

[54] D. M. Pozar, "Microwave engineering," *John Wiley & Sons Inc*, Hoboken, New Jersey, 2012.

CHAPTER 3

Theoretical and Experimental Investigation of Co-axial Probe Reactance for an Equilateral Triangular Patch Antenna with Varying Antenna Size, Substrate Electrical Parameter and Probe Location

Content:

3.1. Introduction

The impedance for a coaxial probe fed equilateral triangular microstrip patch on single substrate and double layered (composite and suspended) substrate has been thoroughly investigated in chapter 2. But the computation of input impedance is not fully accurate without consideration of coaxial probe reactance. For a co-axial probe feeding technique, the outer conductor of the probe is connected to the ground plane of the antenna and the central conductor is connected to the radiating patch by penetrating through the substrate as shown in Fig. 1(a). The excitation of the patch principally occurs through the coupling of the probe current to the patch. The current through a central conductor of the probe creates surface electric current under the patch which produces the electric field. This field provides an inductive reactance which is called the probe reactance X_f in series with the patch reactance itself. Therefore, the correct estimation of the probe reactance is very essential to match properly the input impedance between the coaxial probe and the patch.

It is mentioned in the previous chapter that the resonant frequency and input impedance of a triangular patch antenna have been investigated by several researchers [1-23] but those articles do not provide any information regarding the probe reactance. So, the works reported in [1-23] are insignificant for probe reactance computation of an equilateral triangular patch antenna. The coaxial probe feeding technique to a single microstrip element or arrays has become very popular and common in practice [24]. The probe reactance is highly sensitive to its location under the patch and it significantly affects the matching of input impedance [25, 26]. The various numerical techniques e.g. Green's function [26-28], Mode matching [29], Vector Hankel Transform [30], etc. have been employed to analyze the probe reactance of rectangular and circular patch antenna. These techniques provide reasonably accurate results. However, the numerical techniques are very complex, rigorous and time consuming for estimating the probe reactance.

Harrington [31] developed a simple formula for the reactance of a current carrying probe within a parallel plate waveguide taking the source as a cylindrical wave function. Due to its simplicity, many researchers have used this formula to analyze the probe reactance. But a group of researchers [32] have reported that the computed probe reactance employing the Harrington's formula [31] shows large discrepancy with respect

to the measured reactance. An additional static capacitance was introduced in series with probe reactance by a research group [32] to match the experimental and theoretical values of the probe reactance. This modified formulation shows better agreement near resonance and at a specific probe location. The works reported in [31, 32], do not consider the effect of the probe location variation under the patch on probe reactance. Recently, Guha *et. al*. [33] has modified the Harrington's formula [31] by multiplying it with the field factor to compute the probe reactance of rectangular and circular patch antenna. The works reported in [6, 8, 14, 15] have proposed different models for computation of input impedance but they have not considered the effect of probe reactance on input impedance computation. The work reported in [33] is focused on rectangular and circular geometry. To the best of our knowledge, neither any design guideline nor any experimental results of the probe reactance of an equilateral triangular patch antenna have yet been reported.

We have addressed this problem and proposed a very simple and efficient closed form analytical formula to predict accurately the probe reactance of an equilateral triangular patch antenna (ETPA). This efficient formula is capable for predicting accurately the probe reactance for wide variation of antenna geometric, substrate electrical parameters and probe location. This formula also computes accurately the probe reactance as a function of frequency and probe location under the patch. The accuracy of the proposed model has been verified with our experimental results. We have also employed HFSS to validate the present model.

3.2. Theory

The probe reactance as a function of frequency may be obtained as [31]

$$X_f(f) = \frac{\eta k_r h}{2\pi}\left[\ln\left(\frac{4}{k g}\right) - 0.577\right] \tag{3.1}$$

where, g is the probe diameter, η is the intrinsic impedance of the medium, h is the thickness of the substrate, and k_r is the wave number. It is previously mentioned that probe reactance is highly sensitive to its location under the patch and it significantly influences the input impedance of the patch. So the computation of probe reactance (X_f) is incomplete without consideration of probe location under the patch. The X_f as a function of probe location ρ (Fig.3.1a) and frequency can be derived as follows [33]:

Figure 3.1(b) shows an equivalent circuit of a probe-fed patch. Ideally the patch itself can be looked upon from XX′ and near resonance this can be represented by a simple resistive network as shown in Fig. 3.2(a).

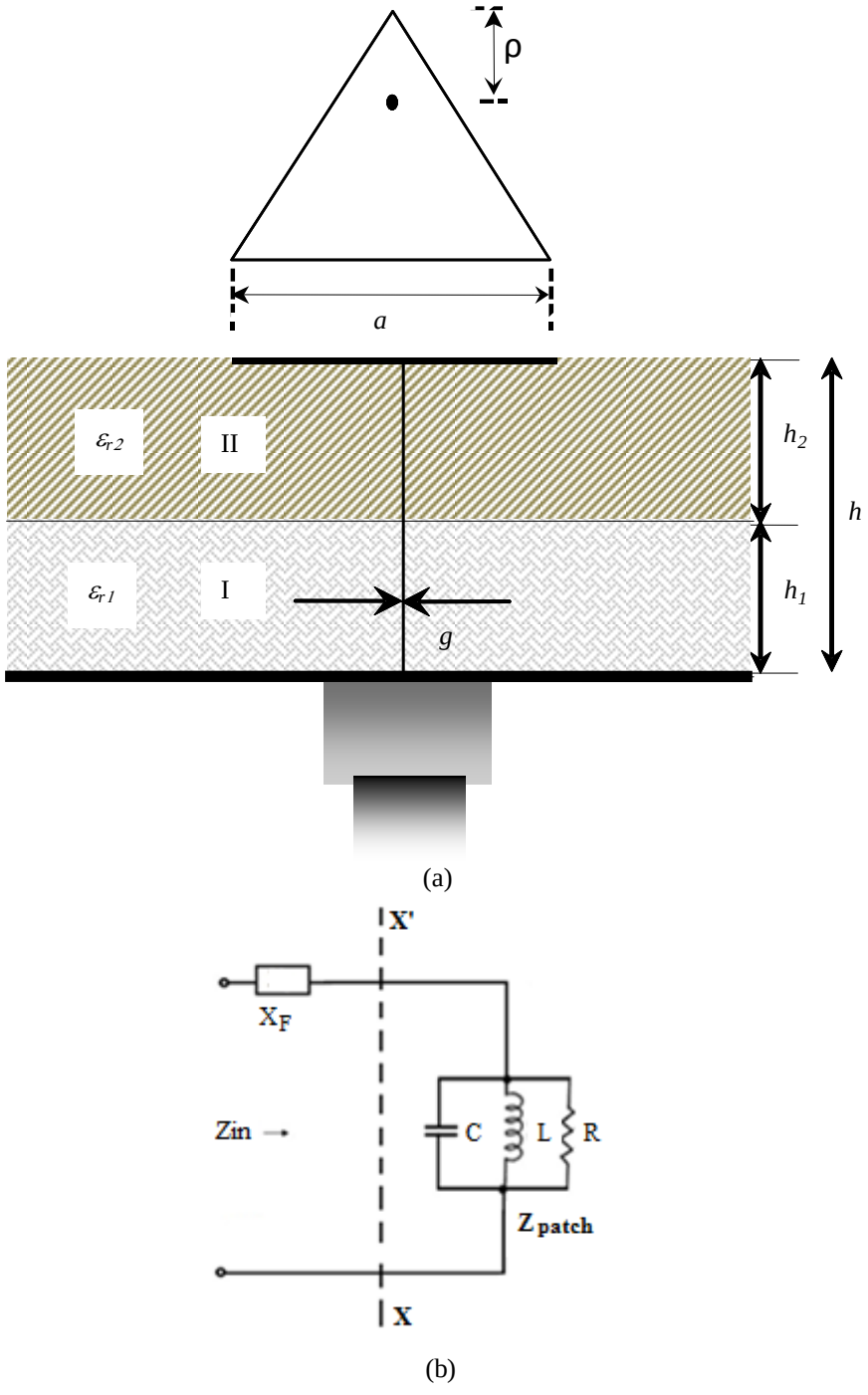

Figure 3.1: (a) A schematic diagram of probe-fed equilateral triangular microstrip patch, (b) Equivalent resonant parallel *R-L-C* circuits.

The quantity L_f is the probe inductance and $R(\rho)$ is the resonant resistance of the microstrip element which varies with ρ as:

$$R(\rho) = R_r P_{nml}(\rho) \tag{3.2}$$

$$P_{nml}(\rho) = (5\pi)^{-1}\left[\cos\frac{2\pi l\rho}{\sqrt{3}a} + \cos\frac{2\pi n\rho}{\sqrt{3}a} + \cos\frac{2\pi m\rho}{\sqrt{3}a}\right]^2 \tag{3.3}$$

where, R_r is the resonant resistance of the patch. This circuit excited by an RF source will have the voltage-current relation as

$$V_{YY'} = L_f\frac{dI}{dt} + V_{XX'} \tag{3.4}$$

where, $V_{XX'}$ can be expressed for different ρ values as

$$V_{XX'} = I_{\rho_1}R(\rho_1) = I_{\rho_2}R(\rho_2) \tag{3.5}$$

Equation (3.5) implies that the product of $I(\rho)$ and $R(\rho)$ is constant and the profile of $I(\rho)$ and $R(\rho)$ is complementary to each other that is when $I(\rho)$ increases then $R(\rho)$ decreases or vice-versa. So $I(\rho)$ or $R(\rho)$ anyone can be replaced by other. Thus, the element $R(\rho)$ can be replaced by a branch current $I(\rho)$ which must follow the complementary profile of $R(\rho)$ [33]. So, for an ETPA $I(\rho)$ may be represented as

$$I(\rho) = I_0 P'_{nml} \tag{3.6}$$

$$P'_{nml}(\rho) = (5\pi)^{-1}\left[\cos\pi l\left(\frac{a/\sqrt{3}-\rho}{a}\right) + \cos\pi n\left(\frac{a/\sqrt{3}-\rho}{a}\right) + \cos\pi m\left(\frac{a/\sqrt{3}-\rho}{a}\right)\right]^2 \tag{3.7}$$

where, I_0 is the current for $\rho = 0$.

When the element $R(\rho)$ is replaced by the branch current $I(\rho)$, then the equivalent circuit of Fig. 3.2 (a) reduces to a reactive network as shown in Fig. 3.2 (b) [33] and its terminal voltage can be written as

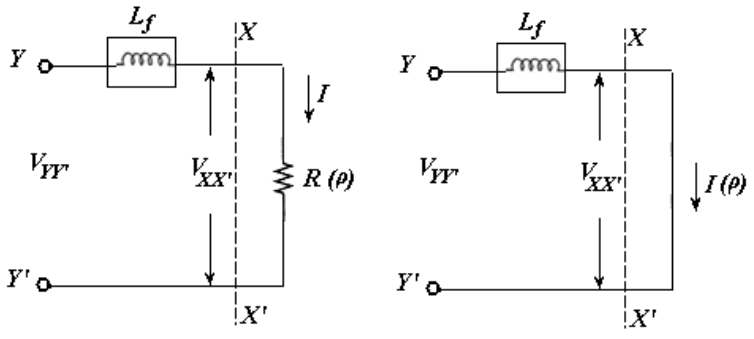

(a) (b)

Figure 3.2: Equivalent circuits for a microstrip patch fed by a coaxial probe. (a) Near resonance (b) Replacing $R(\rho)$ by $I(\rho)$ near resonance.

$$V_{YY'} = L_f \frac{dI(\rho)}{dt} \tag{3.8}$$

This equation with the help of (3.6) reduces to

$$V_{YY'} = L_{f,e} \frac{dI_0}{dt} \tag{3.9}$$

where, $L_{f,e}$ is expressed as

$$L_{f,e} = L_f P'_{nml}(\rho) \tag{3.10}$$

The equation (3.10) finally determines the equivalent feed reactance which can account for its variation with the change in ρ. The relation (3.10) thus can be extended to modify Harrington's formula (1) as:

$$X_f(f,\rho) = X_f(f) P'_{nml}(\rho) \tag{3.11}$$

The wave number k_r may be defined as

$$k_r = \frac{2\pi}{\lambda_{r,nml}} = \frac{2\pi f_{r,nml}}{c} \tag{3.12}$$

where, c is the velocity of light in free space and $f_{r,nml}$ is the resonant frequency of the antenna, computed from (2.1) in chapter 2.

3.3 Antenna design and experimental tests

A number of prototypes of different a has been etched on a Rogers substrate with ε_{r2} = 2.4, h_2 = 0.8265. One of the fabricated prototypes is shown in Fig. 3.3. The patch was excited with a coaxial probe whose diameter g = 1.24 mm. To validate the model developed in section 3.2 we have performed a series of experiments using Network Analyzer Agilent- E5071B. Here, we have presented the theoretically predicted, simulated and measured results for the probe reactance of an ETPA.

3.4 Results and discussions

In Fig. 3.4, we have compared the computed probe reactance X_f as a function of frequency employing the model with simulation [34] and our experimental results for an equilateral patch on single substrate and close agreement is revealed between them. The theoretical frequency is obtained by employing (2.1) in chapter 2. The change in resonant frequency is obtained by changing side length a keeping all the antenna parameters unchanged. For each frequency we have estimated the corresponding a. The

50 ohm probe location under the patch for every *a* is determined by employing (2.24) in chapter 2. The probe reactance increases with the increase of frequency.

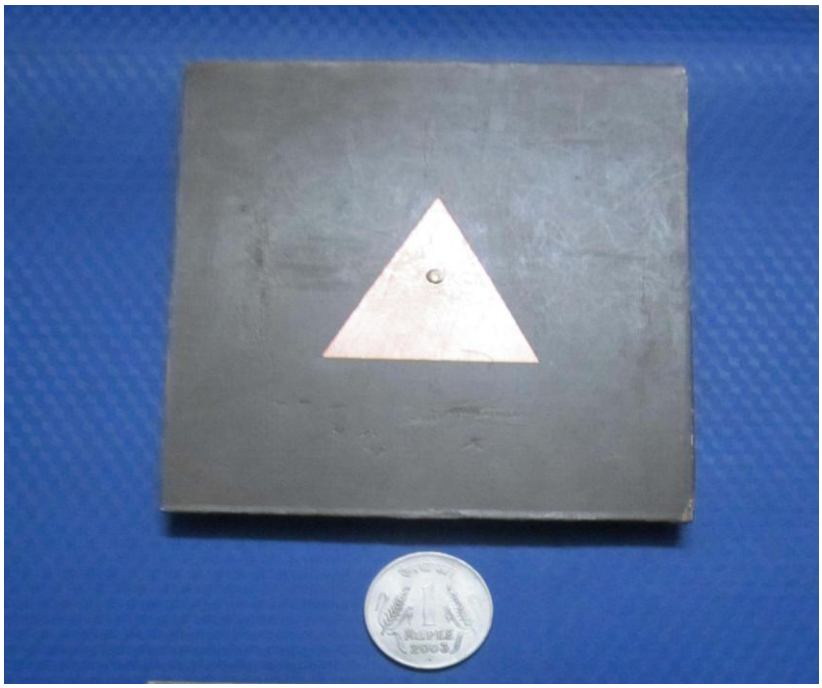

Figure 3.3: Snapshot of a fabricated prototype

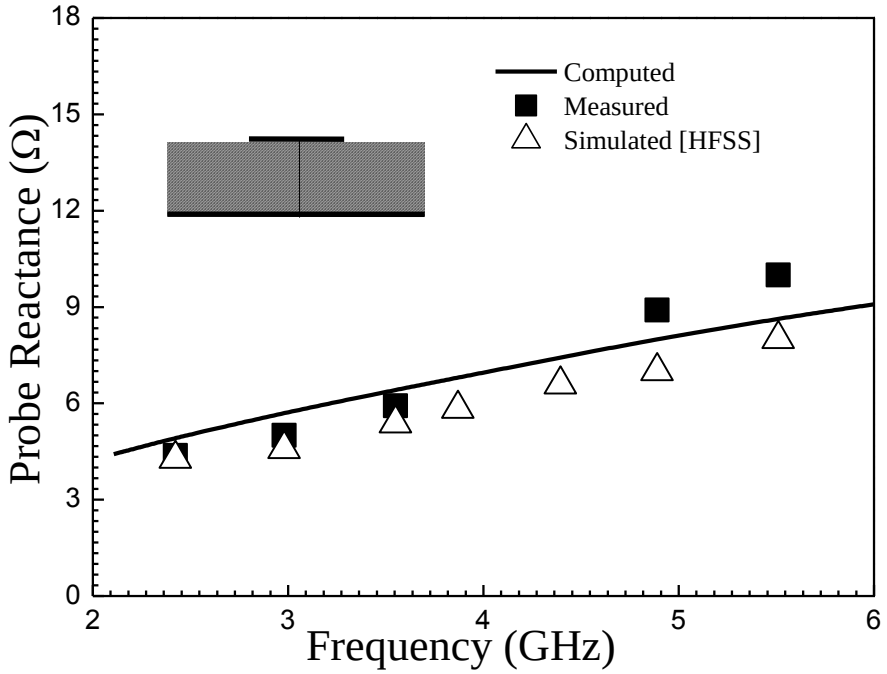

Figure 3.4: Experimental [our], simulation and theoretical variation of probe reactance as a function of frequency. $\varepsilon_{re} = \varepsilon_{r2} = 2.4$, $tan\delta_e = tan\delta_2 = 0.0022$, $h = h_2 = 0.8265$.

The variation of X_f as a function of probe position ρ for an equilateral patch on single substrate having different a is depicted in Fig. 3.5. Here we have compared the computed X_f with simulation and our experimental results. The computed reactance curves well agree with the measured and simulated results. This study shows that the probe reactance increases with the decrease of a. When the side length a of the patch increases then the frequency of that patch decreases, as a result the probe reactance X_f decreases.

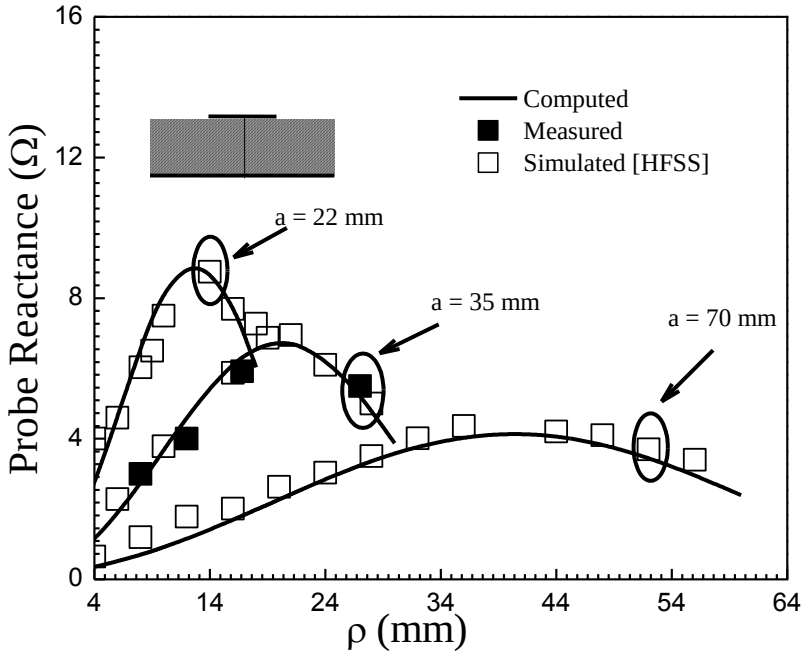

Figure 3.5: Computed, measured [our] and simulated variation of probe reactance as a function of probe location for different side length. $\varepsilon_{re} = \varepsilon_{r2} = 2.4$ $tan\delta_e = tan\delta_2 = 0.0022$, $h = h_2 = 0.8265$.

The effect of probe reactance X_f on input impedance is depicted in Fig. 3.6. Here measured input impedance is compared with the computed input impedance curve employing the model with and without probe reactance. A discrepancy is observed between measured and computed input impedances when probe reactance X_f is not considered but close agreement is seen between measured and computed input impedances when probe reactance X_f is considered.

In Fig. 3.7, authors present the variation of X_f as a function of probe location ρ under the patch for an equilateral patch on a single substrate having different substrate

thickness *h*. Here we have compared the computed X_f with simulated values [34] and close agreement is revealed between them.

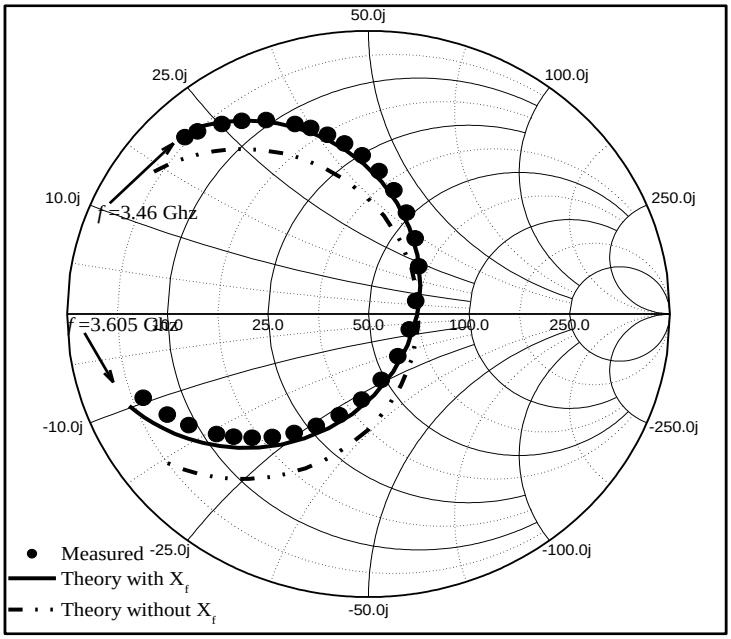

Figure 3.6: Theoretical and experimental [our] input impedance loci of a probe fed ETPA. a = 35 mm, h = h_2 = 0.8265, $\varepsilon_{re} = \varepsilon_{r2}$ = 2.4, ρ = 16.8, $tan\delta_e = tan\delta_2$ = 0.0022.

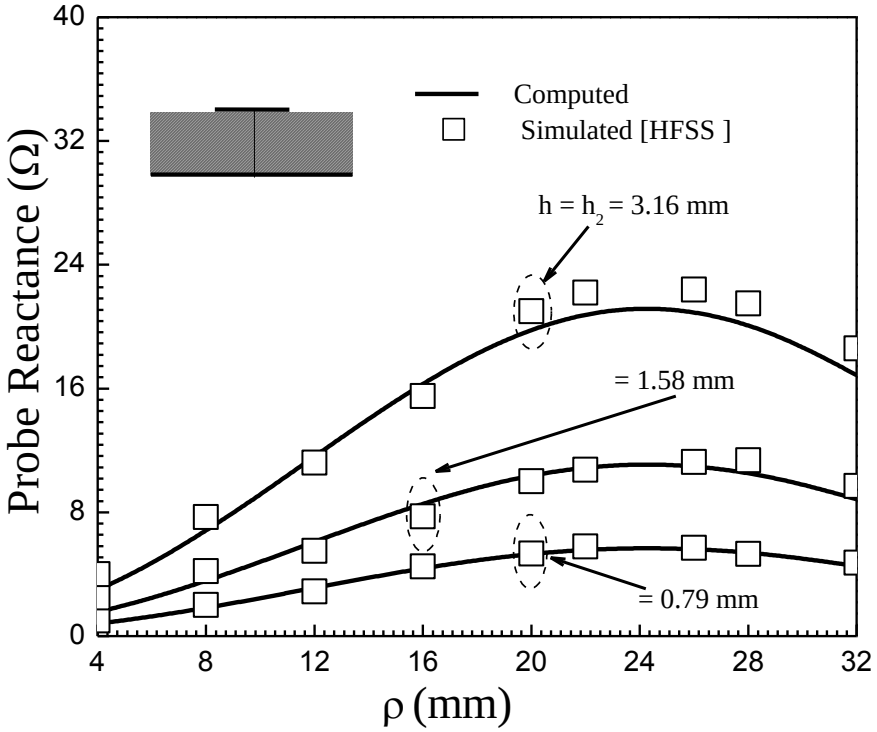

Figure 3.7: Computed and simulated variation of probe reactance as a function probe location for different substrate thickness. a = 42 mm, $\varepsilon_{re} = \varepsilon_{r2}$ = 2.4, $tan\delta_e = tan\delta_2$ = 0.0022.

The variation of X_f as a function of h for an equilateral patch is visualized in Fig. 3.8. In this study first we have determined the 50 ohm probe position under the patch for every h and then calculate the X_f. The X_f increases with increase of h. If the thickness of the substrate h increases, the length of the probe increases, the spurious radiation from the probe increases, the surface wave power increases and thus the probe reactance increases. Here the computed curve is compared with the HFSS simulated [34] results. The slight discrepancy is observed for higher thickness. This is due to the fact that the Harrington's formula is well valid for small h/λ_0.

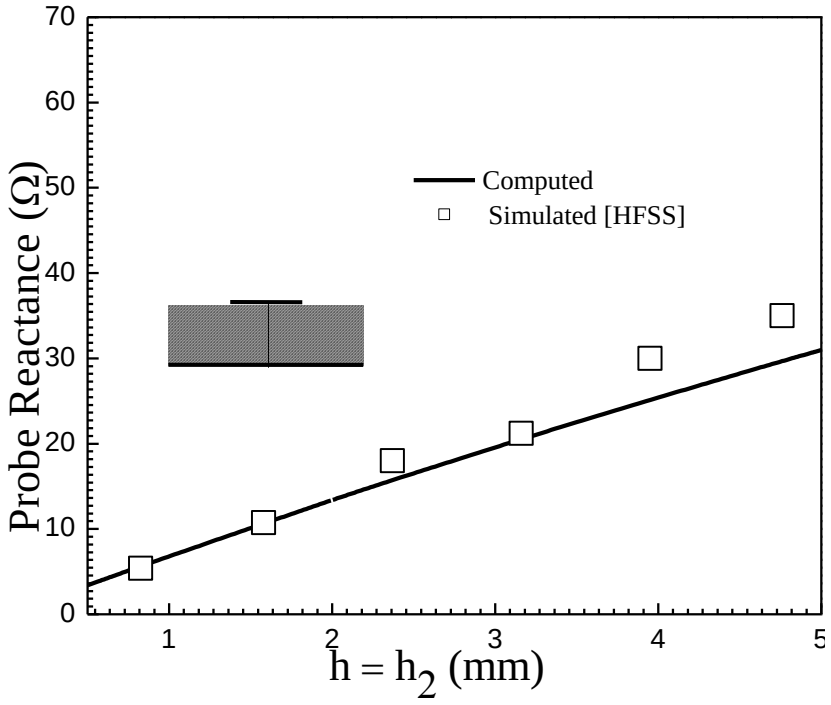

Figure 3.8: Computed and simulated variation of probe reactance as a function of substrate thickness. Parameters as in Fig. 3.7.

The variation of X_f with the variation of ρ for different ε_{re} of an equilateral patch on a single substrate is depicted in Fig. 3.9. In this study, we have compared the computed X_f curves with HFSS [34] simulation results. The computed curves well support the simulation results.

In Fig. 3.10, we present the variation of X_f as a function of ε_{re}. The X_f decreases with the increase of ε_{re}. Here we have first estimated the 50 ohm probe position under the patch and then calculate the probe reactance. If the relative permittivity of the

substrate ε_{re} increases, fringing field effect decreases, unwanted radiation from the probe decreases and surface wave power decreases as a result the probe reactance decreases. The computed curve compared with the simulated curve and very close agreement is observed between them for all values of ε_{re}.

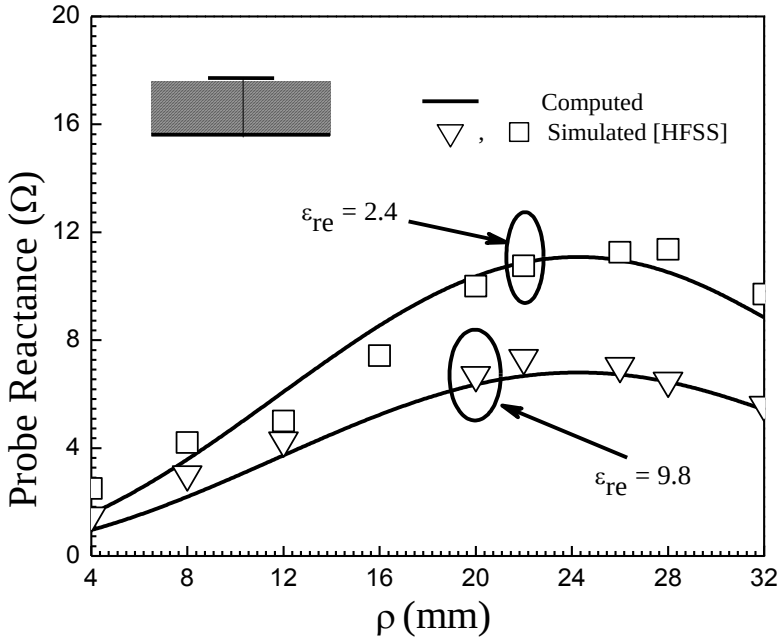

Figure 3.9: Computed and simulated variation of probe reactance as a function feed location for different dielectric constant. a = 42 mm, $h = h_2$ = 1.58 mm, $tan\delta_e = tan\delta_2$ = 0.0022.

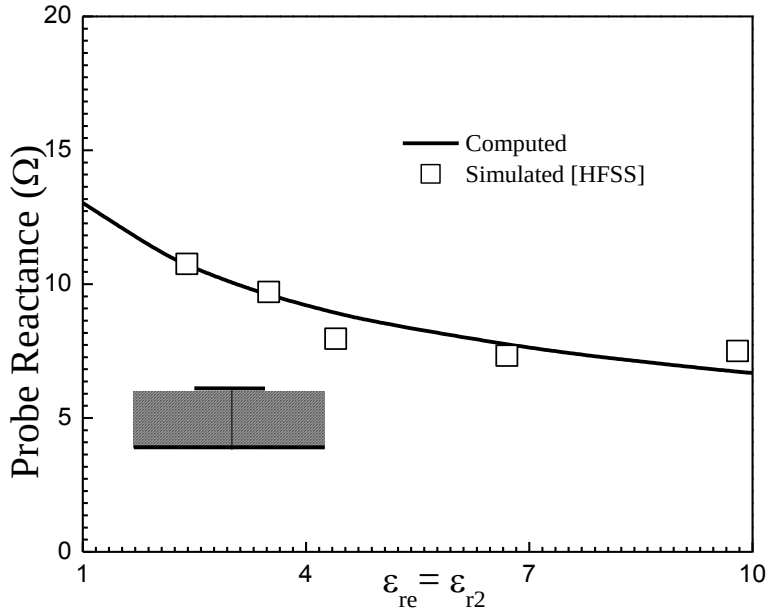

Figure 3.10: Computed and simulated variation of probe reactance as a function of dielectric constant of substrate. Parameters as in Fig. 3.9.

Figure 3.11 shows the variation of X_f as a function of a. The X_f decreases with the increase in a. The computed X_f is compared with simulated [34] and our measured results. The close agreement is observed between them. Thus the model is valid for a patch whose side length is varied from low to high value.

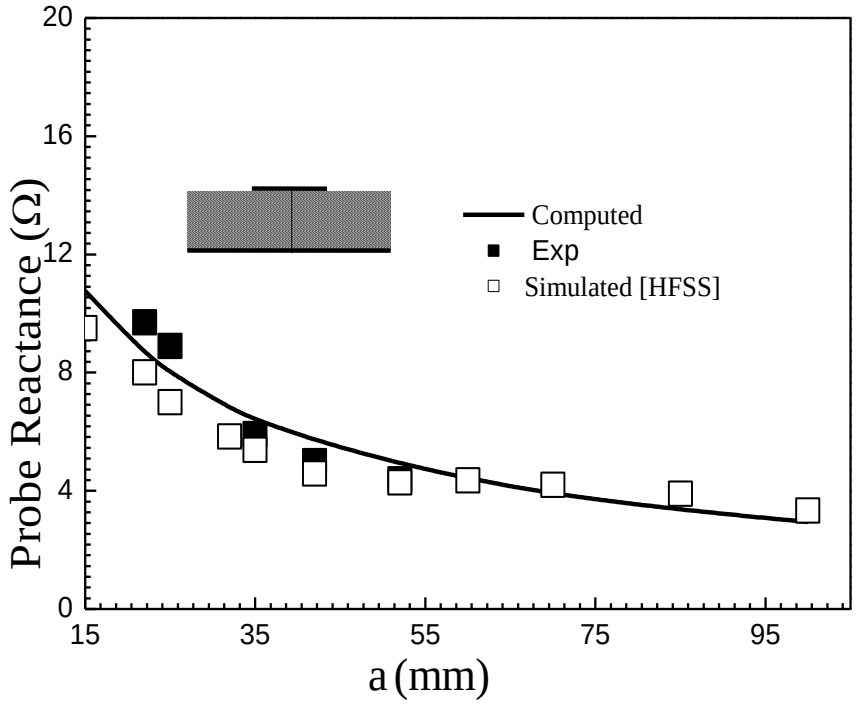

Figure 3.11: Computed, simulated and measured [our] variation of probe reactance as a function of side length a. $\varepsilon_{re} = \varepsilon_{r2} = 2.4$, $h = h_2 = 0.8265$ mm, $tan\delta_e = tan\delta_2 = 0.0022$.

The effect of composite and suspended substrate on X_f is depicted in Fig. 3.12. For suspended substrate the X_f is increased with the increase of h_1 whereas, X_f decreases with the increase of h_1 for composite substrate. The computed curves well support the simulated results for all h_1/h. The effective permittivity for a composite substrate is enhanced, fringing field effect decreases, surface wave power decreases so the probe reactance decreases. The exactly opposite behavior is occurred for suspended substrate.

Simulated impedance loci of a probe fed ETPA for different probe locations are shown in Fig. 3.13 and 3.14. The center of each locus marked as solid black dot indicates the value of corresponding probe reactance. These simulated probe reactances are used for validating computed values of probe reactances in the Fig. 3.4 to Fig. 3.12.

Now it is clear from the above that X_f increase with the increase of thickness h and frequency f. X_f decreases with the decrease of side length a and relative permittivity ε_{re}. This information is very useful for practical implementation of the ETPA.

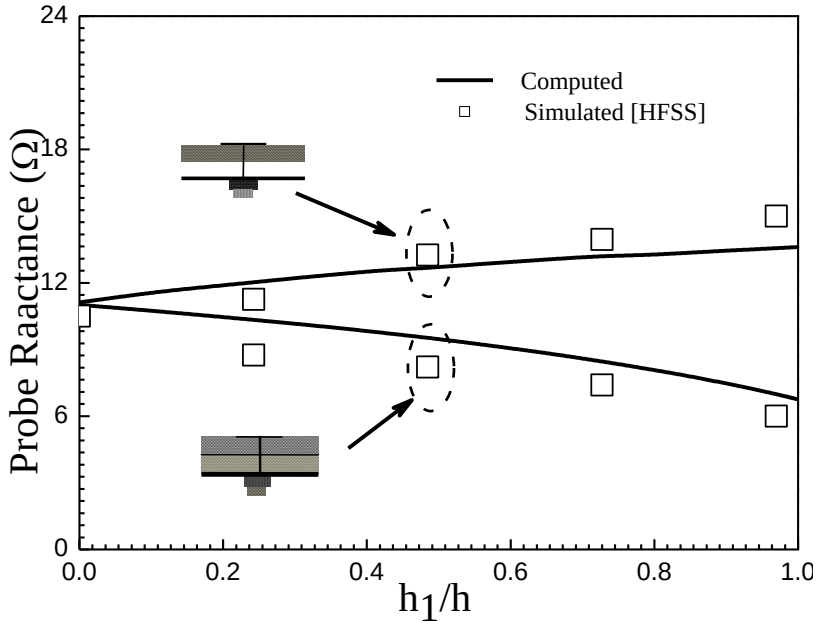

Figure 3.12: Computed and simulated variation of probe reactance as a function of suspended. (ε_{r1} = 1.0, $tan\delta_1$ = 0.000) and composite (ε_{r1} = 9.8, $tan\delta_1$ = 0.0035) substrate thickness. a = 42 mm, ε_{r2} = 2.4, $tan\delta_2$ = 0.0022.

3.5. Conclusion

The radiated power and impedance bandwidth of an ETPA mainly controlled by the input impedance. For probe fed patch antenna, the total input impedance consists of the probe reactance in series with the patch impedance. Good models for calculating patch impedance are available, but to the best of our knowledge no model is available to compute probe reactance of an ETPA. For the first time, a very simple and efficient formula is proposed to accurately predict the probe reactance of an equilateral triangular patch antenna. To overcome the drawback of earlier models as discussed detail in Section I, we have introduced the field factor in Harrington's formula. This efficient formula is capable of predicting accurately the probe reactance for wide variation of substrate electrical parameters, antenna geometric and probe position under the patch. Present theoretical analysis shows excellent agreement with our measured results. We have also employed electromagnetic software to validate the model.

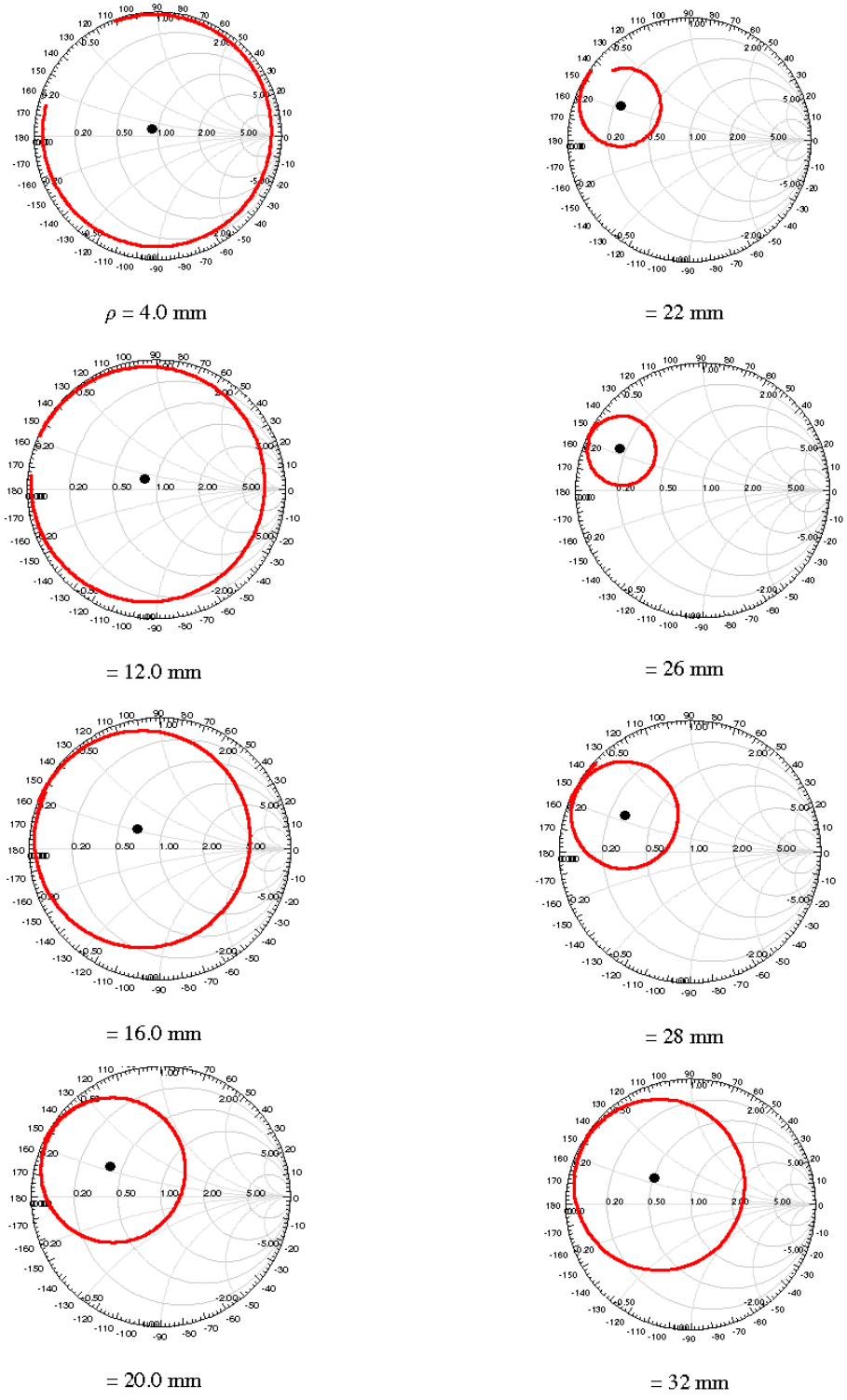

Figure 3.13: Simulated impedance loci of a probe fed ETPA for different feed locations. a = 42 mm, $\varepsilon_{re} = \varepsilon_{r2}$ = 2.4, $h = h_2$ = 1.58 mm, $tan\delta_e = tan\delta_2$ = 0.0022.

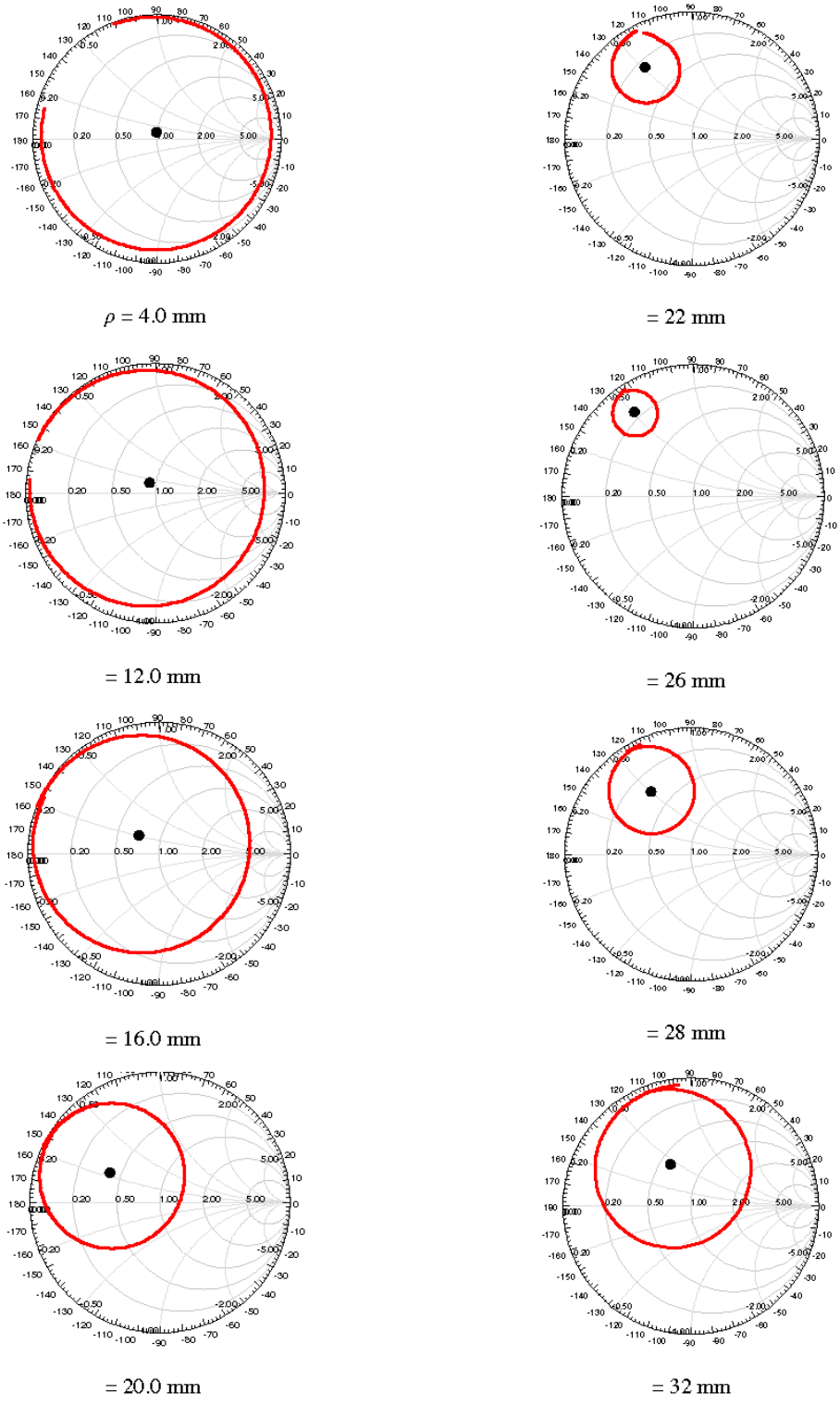

Figure 3.14: Simulated impedance loci of a probe fed ETPA for different feed locations. a = 42 mm, ε_{re} = ε_{r2} = 2.4, h = h_2 = 3.16 mm, $tan\delta_e$ = $tan\delta_2$ = 0.0022.

REFERENCES

[1] J. Helszajn and D. S. James, "Planar triangular resonators with magnetic walls," *IEEE Trans. Microw. Theory Tech.*, vol. 26, pp. 95-100, Feb.1978.

[2] A. K. Sharma and B. Bhat, "Analysis of tiangular microstrip resonator," *IEEE Trans. Microw. Theory Tech*., vol. 30, no. 11, pp. 2029 – 2031, Nov. 1982.

[3] E. F. Keuster and D. C. Chang, "A geometrical theory for the resonant frequencies and Q factors of some triangular microstrip patch antenna," *IEEE Trans. Antennas Propagat.*, vol. 31, pp.27-34, 1983.

[4] J. S. Dahele and K. F. Lee, "On the resonant frequencies of the triangular patch antenna," *IEEE Trans. Antennas Propagat.*, vol. 35, pp.100-101, 1987.

[5] X. Gang, "On the resonant frequencies of microstrip antennas," *IEEE Trans. Antennas Propagat*., vol. 37, pp. 245-247, 1989.

[6] K. F. Lee, K. M. Luk, and J. S. Dahele, "Characteristics of the equilateral triangular patch antenna," *IEEE Trans. Antennas Propagat.*, vol. 36, no.11, pp.1510-1518, Nov. 1988.

[7] W. Chen, K. F. Lee, and J. S. Dahele, "Theoretical and experimental studies of the resonant frequencies of equilateral triangular microstrip antenna," *IEEE Trans. Antennas Propagat.*, vol. 40, pp.1253-1256, Oct. 1992.

[8] H. R. Hassani and D. M. Syahkal, "Analysis of triangular patch antennas including radome effects" *IEE Proc. H*, vol. 139, no. 3, pp.251-256, Jun. 1992.

[9] D. Karaboğa, K.Güney, N. Karaboğa, and A. Kaplan, "Simple and accurate effective side length expression obtained by using a modified genetic algorithm for the resonant frequency of an equilateral triangular microstrip antenna," *Int. J. Electron.*, vol. 83, pp. 99-108, Jan.1997.

[10] P. Mythili, A. Das, "Simple approach to determine resonant frequencies of microstrip antennas," *IEE Proc. Microw. Antennas Propagat.*, vol. 145, No. 2, April 1998.

[11] C. S. Gurel and E. Yazgan, "New computation of the resonant frequency of a tunable equilateral triangular microstrip patch," *IEEE Trans. Microw. Theory Tech*., vol. 48, pp. 334-338, Mar. 2000.

[12] E. G. Lim, E. Korolkiewicz, S. Scott, A. Sambell, and B. Aljibouri, "An Efficient formula for the input impedance of a microstrip right-angled isosceles triangular patch Antenna," *IEEE Antennas Wireless Propagat. Lett*., vol. 1, pp. 18-21, 2002.

[13] K. E. Nasimuddin and A.K. Verma, "Resonant frequency of an equilateral triangular microstrip antenna," *Microwave Opt. Technol. Lett*., vol. 47, pp. 485-489, 2005.

[14] M. Biswas and D. Guha, **"**Input impedance and resonance characteristic of superstrate loaded triangular microstrip patch," *IET Microw. Antennas Propagat.*, vol. 3, pp. 92 – 98, Feb. 2009.

[15] M.Biswas and A. Mandal, "CAD model to compute the input impedance of an equilateral triangular microstrip patch antenna with radome," *Prog. Electromag. Res. M.*, vol. 12, pp. 247-257, 2010.

[16] M. M. Olaimat and N. I. Dib, "Improved formulae for the resonant frequencies of triangular microstrip patch antennas," *Int. J. Electron.*, vol. 98, pp. 407-424, 2011.

[17] M. M. Olaimat and N. I. Dib, "A study of 15^0-75^0-90^0 angles triangular patch antenna," *Prog. Electromag. Res. Lett.*, vol. 21, pp. 1-9, 2011..

[18] S. Maity and B. Gupta, "Simplified analysis for 30^o–60^o–90^o triangular microstrip antenna," *J. Electromag. Waves Appl.*, vol. 28, pp. 91–101, 2013.

[19] S. Maity and B. Gupta, "Accurate resonant frequency of isosceles right-angled triangular patch antenna," *Microw. Opt. Technol. Lett.*, vol. 55, pp. 1306-1308, 2013.

[20] S. Maity and B. Gupta, "Cavity model analysis of 30°–60°–90° triangular microstrip antenna," *AEU-Int. J. Electron. Comm.*, vol. 69, pp. 923-932, 2015.

[21] K. Guney and E. Kurt, "Effective side length formula for resonant frequency of equilateral triangular microstrip antenna," *Int. J. Electron.*, vol. 103, pp. 261-268, 2016.

[22] S. Maity and B. Gupta, "Approximate investigation on isosceles triangular microstrip antenna in fundamental mode," *Microw. Opt. Technol. Lett.*, vol. 59, pp. 614-618, 2017.

[23] R. Garg, P. Bhartia, I. J. Bahl, and A. Ittipiboon, "Microstrip antenna design handbook," *Artech house*, 2001.

[24] K. F. Lee and W. Chen, "Advances in Microstrip and Printed Antennas," *Wiley*, New York, 1997.

[25] W. F. Richards, Y.T. Lo, and D.D. Harrison, "An improved theory for microstrip antennas and applications," *IEEE Trans. Antennas Propagat.*, vol. 29, pp. 38–46, 1981.

[26] S. Yano and A. Ishimaru, "A theoretical study of the input impedance of a circular microstrip disk antenna," *IEEE Trans Antennas Propagat.*, vol. 29, pp. 77–83, 1981.

[27] W. Chen, K. F. Lee, and R. Q. Lee, "Input impedance of coaxially fed rectangular microstrip antenna on electrically thick substrate," *Microw. Opt Technol. Lett.*, vol. 6, pp. 387–390, 1993.

[28] J. T. Aberle, D. M. Pozar, and C. R. Birtcher, "Evaluation of input impedance and radar cross section of probe-fed microstrip patch elements using an accurate feed model," *IEEE Trans Antennas Propagat.*, vol. 39, pp. 1691–1696, 1991.

[29] M. Y. Davidovitz and T. Lo, "Input impedance of a probe-fed circular microstrip antenna with thick substrate," *IEEE Trans Antennas Propagat.*, vol. 34, pp. 905–911, 1986.

[30] W. C. Chew and J. A. Kong, "Analysis of a circular microstrip disk antenna with a thick dielectric substrate," *IEEE Trans Antennas Propagat*., vol. 29, pp. 68–76, 1981.

[31] R. F. Harrington, "Time-Harmonic Electromagnetic Fields" *New York: McGraw-Hill*, pp. 228, 1961.

[32] B. M Alarjani and J. S. Dahele, "Feed reactance of rectangular microstrip patch antenna with probe feed," *Electron Lett.,* vol. 36, pp. 388-390, 2000.

[33] D. Guha, M. Biswas, and J. Y. Siddiqui, "Harrington's formula extended to determine accurate feed reactance of probe-fed microstrip patches." *IEEE Antennas Wireless Propagat. Lett.,* vol. 6, pp. 33-35, 2007.

[34] High Frequency Structure Simulator: *Ansoft Corp*.

CHAPTER 4

Investigation of a Right Angle Isosceles Triangular Patch Antenna with Varying Antenna Size, Substrate Electrical Parameters and Probe Location: Theoretical and Experimental Study

Content:

4.1. Introduction

The triangular patch antenna is physically smaller than the rectangular patch antenna without any change in radiation characteristics. It is a well-known microwave network element due to its extensive application in the design of many useful microwave circuit components like circulator, resonators and filters [1]. High Q geometry of triangular microstrip patch antenna supports its application in array configuration with reduced coupling [2]. It is also suitable for use in curved surface due to its conformability.

Among all triangular geometry only equilateral shape has been widely investigated by several researchers [1-12]. Other geometry like right angled isosceles triangular patch antenna (RAITPA) is least investigated till now. The isosceles triangular patch antenna can provide better flexibility compared to the other triangular patch antenna in the design of microwave integrated circuit [12]. Only a few investigations are available in open literature for RAITPA [12-18]. Among them, the full wave methods [12], reflection of plane wave (i.e. geometrical theory) [13, 14], superposition of plane wave with snell's law [15] and cavity model [16, 17] have been reported to compute the resonant frequency of RAITPA.

But the disadvantages of the models presented in [12-17] are i) the effect of fringing field was not properly included, ii) the design guideline for computing the input impedance was not provided and iii) the effect of composite and suspended substrate on the characteristics of a RAITPA was not reported. To the best of our knowledge only one article [18], is available in open literature for computing the input impedance of a RAITPA. But the model reported in [18] has used complex and rigorous mathematical steps.

To make a tunable antenna, the microstrip patch with composite and suspended substrate is a good choice as it provides frequency, gain and bandwidth tunability features without any major change in antenna structure.

Full wave analysis [5, 7, 12, 19-21] and commercial softwares [22] can be used to predict the characteristics of patch antennas. But the numerical techniques are not efficient for direct synthesis of antennas due to their complexity and large computational time requirement.

Keeping these in view, we have addressed this problem into two objectives. i) A fast and accurate CAD model based on cavity model analysis and single resonant parallel *R-L-C* circuit is proposed to predict accurately the resonant frequency, quality factor, bandwidth, input impedance and gain of a RAITPA. This model very accurately calculates the above parameters for wide variation of antenna size, substrate electrical parameters and probe location. This is ideal for design purposes, because it involves less mathematical steps, takes less computational time and is easy to realize. ii) We have performed a set of experiments to validate the model.

4.2 Theory

In this section a set of closed form expressions has been presented to compute the effective permittivity, effective side length, resonant frequency, quality factor, input impedance, bandwidth and gain for a probe fed RAITPA on composite and suspended substrate as shown in Fig. 4.1

4.2.1. Resonant frequency

Based on cavity model analysis we have considered the side walls of the patch are perfectly magnetic. According to this assumption, the resonant frequency $f_{r,nm}$ of TM_{nml} modes for a RAITPA on two dielectric layers can be computed as [15-16, 23]:

$$f_{r,nml} = \frac{c}{2a\sqrt{\varepsilon_{re}}}\left(n^2 + m^2\right)^{1/2} \tag{4.1}$$

where, c is the velocity of light in free space, ε_{re} is the equivalent relative permittivity of the medium below the patch, a is the side length of the patch and m, n, l are the integers which are never zero simultaneously satisfying the condition $n+m+l=0$. The models presented in [12-17] were not properly included the fringing field effect for computing the resonant frequency. We have replaced a and ε_{re} by a_{eff} and $\varepsilon_{r,eff}$ respectively in equation (4.1) to account properly the effect of fringing field. Here, $\varepsilon_{r,eff}$ is the effective permittivity of the medium below the patch and a_{eff} is the effective side length of the patch.

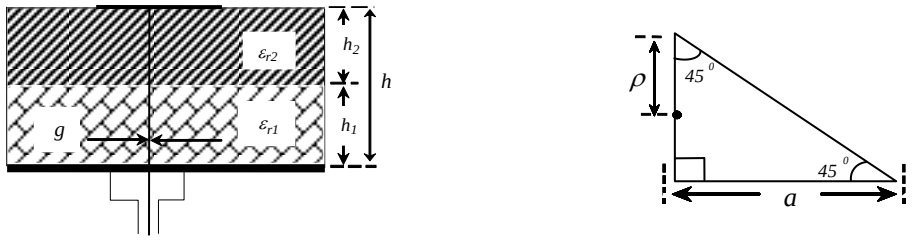

(a) (b)

Figure 4.1: (a). A schematic diagram of probe-fed right angled isosceles triangular patch antenna. (a) Cross sectional view, (b) Patch shape.

2.2.2. Effective permittivity $\varepsilon_{r,eff}$

The effective permittivity of the structure $\varepsilon_{r,eff}$ can be expressed as:

$$\varepsilon_{r,eff} = \varepsilon_{re} - \frac{\varepsilon_{re} - \varepsilon_{r,dyn}}{1 + G\left(f / f_p\right)^2} \tag{4.2}$$

where,

$$G = 0.6 + 0.009\,Z \tag{4.3}$$

$$f = \frac{c}{2a\sqrt{\varepsilon_{re}}} \tag{4.4}$$

$$f_p = \frac{Z\left(\frac{a}{h}, h, \varepsilon_{re}\right)}{2\mu_0 h} \tag{4.5}$$

$$Z\left(a/h, h, \varepsilon_{re}\right) = \frac{120\pi Z}{\sqrt{\varepsilon_{rp}}} \tag{4.6}$$

The $Z\,(a/h,\ h,\ \varepsilon_{re})$ in (4.6) for this geometry is derived from rectangular geometry. Here we have employed an equivalent relation between a rectangular geometry (width W and length L) and a right angle isosceles triangular geometry of side length a. To account for equal static fringing fields, equal surface area has been considered on the basis of equivalence. The surface area of rectangular patch is WL and surface area of RAITP is $1/2a^2$. So the equivalence relation become

$$WL = (1/2)a^2 \tag{4. 7}$$

Now equating the zeroth order resonant frequencies of rectangular patch and RAITP without fringing we get

$$f_{r,10} = \frac{c}{2L\sqrt{\varepsilon_{re}}} = \frac{c}{2a\sqrt{\varepsilon_{re}}} \tag{4. 8}$$

$$L = a \tag{4. 9}$$

Putting the value of L in equation (4.7) we get

$$W = \frac{1}{2}a \tag{4.10}$$

Thus the $Z\ (a/h,\ h,\ \varepsilon_{re})$ for a RAITPA, after employing the equivalent relation (4.9) and (4.10) becomes

$$Z = \left[\frac{a}{2h} + 1.393 + 0.667\ln\left(\frac{a}{2h} + 1.444\right)\right]^{-1} \tag{4.11}$$

$$\varepsilon_{rp} = \frac{\varepsilon_{re}+1}{2} + \frac{\varepsilon_{re}-1}{2}\left(1 + \frac{12h}{a/2}\right)^{-1/2} \tag{4.12}$$

The ε_{re} for this two-layer structure is modeled as the single-layer one having substrate thickness of $h = h_1 + h_2$. The upper layer has thickness h_2 with relative permittivity ε_{r2} and lower layer has thickness h_1 with permittivity ε_{r1}. The ε_{re} can be computed as

$$\varepsilon_{re} = \frac{\varepsilon_{r1}\varepsilon_{r2}h}{\varepsilon_{r1}h_2 + \varepsilon_{r2}h_2} \tag{4.13}$$

and $\varepsilon_{r,dyn}$ is the dynamic permittivity. The $\varepsilon_{r,dyn}$ depends on the dimensions, equivalent substrate relative permittivity ε_{re} and field configuration of the mode under study [24]. It can be expressed as

$$\varepsilon_{r,dyn} = \frac{C_{dyn}\left(\varepsilon = \varepsilon_0\varepsilon_{re}\right)}{C_{dyn}\left(\varepsilon = \varepsilon_0\right)} \tag{4.14}$$

In equation (4.14), $C_{dyn}\ (\varepsilon)$ is the total dynamic capacitance of the condenser formed by the conducting patch and the ground plane separated by a dielectric of permittivity ε. It takes into account the influence of the fringing field at the edge of the patch. The $C_{dyn}\ (\varepsilon_0)$ is the total dynamic capacitance when $\varepsilon = \varepsilon_0$. The $C_{dyn}\ (\varepsilon)$ can be written as

$$C_{dyn}(\varepsilon) = C_{0,dyn}(\varepsilon) + C_{e,dyn}(\varepsilon) \tag{4.15}$$

where, $C_{e,dyn}$ (ε) and $C_{0,dyn}$ (ε) are the total dynamic fringe and main field capacitance respectively.

The $C_{e,dyn}$ (ε) is defined as [24]:

$$C_{e,dyn}(\varepsilon) = \frac{1}{2}\left[\frac{Z\left(a/h,\, h,\, \varepsilon_{re}=1\right)a}{cZ^2\left(a/h,\, h,\, \varepsilon_{re}\right)} - C_{0,stat}(\varepsilon)\right] \tag{4.16}$$

where, $C_{0,stat}$ (ε) is the static main capacitance and Z $(a/h,\ h,\ \varepsilon_{re})$ can be obtained from equation (4.6).

The $C_{0,stat}$ (ε) is defined as:

$$C_{0,stat}(\varepsilon) = \frac{\varepsilon_0 \varepsilon_{re} a^2}{2h} \tag{4.17}$$

The total dynamic main field capacitance $C_{0,dyn}(\varepsilon)$ is taken in this study as [8]:

$$C_{0,dyn}(\varepsilon) = 0.5\, C_{0,stat}(\varepsilon) \tag{4.18}$$

4.2.3 Effective side length a_{eff}

The effective side length of the RAITPA is computed as

$$a_{eff} = a(1+p)^{1/2} \tag{4.19}$$

In equation (4.19), p arises due to the fringing fields at the edge of the patch. The p for this geometry is computed from originally formulated circular geometry [25] by employing an equivalent relation between a circular patch of radius r and a RAITP with side length a. To account for equal static fringing fields, equal area has been considered on the basis of equivalence. The surface area of circular patch is πr^2 and the surface area of RAITP is $1/2a^2$. So the equivalence relation between circular patch and RAITP is defined as

$$\pi r^2 = \frac{1}{2}a^2 \tag{4.20}$$

$$r = \sqrt{1/2\pi}\, a \tag{4.21}$$

Now, employing equation (4.21), p can be written as

$$p = \frac{2\sqrt{2}h}{\sqrt{\pi}\, a\, \varepsilon_{re}} \left(p_1 + p_2 + p_3\right) \tag{4.22}$$

$$p_1 = \log\left(\frac{\sqrt{1/2\pi}\, a}{2h}\right) \tag{4.23}$$

$$p_2 = 1.41\varepsilon_{re} + 1.77 \tag{4.24}$$

$$p_3 = \frac{h}{\sqrt{1/2\pi}\, a}\left(0.268\,\varepsilon_{re} + 1.65\right) \tag{4.25}$$

4.2.4 Input Impedance

Better impedance matching is required between coaxial probe and radiating patch to get the optimum performance. So, the accurate computation of input impedance for a probe fed RAITPA at a particular feed location is very important. The RAITPA can be treated as a single resonant parallel resonant *R-L-C* circuit (Fig. 4.2). The input impedance is seen by a coaxial probe located at a distance ρ as indicated in Fig. 4.1(a) may be obtained as

$$Z_{in} = \frac{R(\rho)}{1 + Q_T^2\left[\frac{f}{f_{r,nm}} - \frac{f_{r,nm}}{f}\right]^2} + j\left[X_F - \frac{R(\rho)\, Q_T\left(\frac{f}{f_{r,nm}} - \frac{f_{r,nm}}{f}\right)}{1 + Q_T^2\left(\frac{f}{f_{r,nm}} - \frac{f_{r,nm}}{f}\right)^2}\right] \tag{4.26}$$

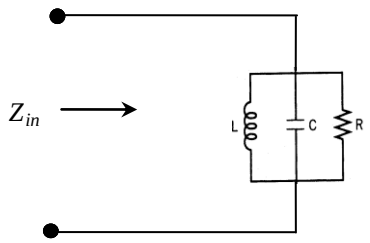

Figure 4.2: Equivalent resonant parallel R-L-C circuits of RAITPA.

In equation (4.26), Q_T and $R(\rho)$ are the total quality factor and the input resistance when the feed is located at a distance ρ as indicated in Fig.4.1. The value of the feed reactance X_L is negligible when the feed is located near the edge. So, we have not considered the feed reactance for computation of input impedance in this chapter.

The $R(\rho)$ can be computed as

$$R(\rho)=\frac{\eta_0}{7a^2}\frac{h}{\sqrt{\varepsilon_{r,eff}}}\frac{Q_T\lambda_r}{}P_{\ln m} \tag{4.27}$$

and $P_{\ln m}$ is the field factor for coaxial feed RAITPA.

$$P_{\ln m}=\left[\cos\frac{\pi l\rho}{a}+\cos\frac{\pi n\rho}{a}+\cos\frac{\pi m\rho}{a}\right]^2 \tag{4.28}$$

4.2.5 Total quality factor Q_T:

The total quality factor is given by

$$Q_T=\left(\frac{1}{Q_r}+\frac{1}{Q_d}+\frac{1}{Q_c}\right)^{-1} \tag{4.29}$$

where, Q_r, Q_c and Q_d are the quality factors due to radiation loss, conductor loss and dielectric loss respectively.

In this chapter, we have presented a very efficient formula to compute the quality factor. The quality factor due to radiation loss Q_r of a RAITPA may be computed as [25]:

$$Q_r=\frac{2.39}{4\mu_0 h f_{r,nm}G_r} \tag{4.30}$$

$$G_r=\frac{a}{240\lambda_r} \tag{4.31}$$

The quality factor due to dielectric loss Q_d can be computed as

$$Q_d=\frac{1}{\tan\delta_e} \tag{4.32}$$

where, $tan\delta_e$ is the equivalent loss tangent of a RAITPA on composite and suspended substrate and may be defined as

$$\tan\delta_e=\frac{h_1\varepsilon_{r1}\tan\delta_1+h_2\varepsilon_{r2}\tan\delta_2}{h\varepsilon_{re}} \tag{4.33}$$

The quality factor due to conductor loss Q_c, can be expressed as

$$Q_c=\frac{\pi\sqrt{\varepsilon_{r,eff}}}{\lambda_r\alpha_c} \tag{4.34}$$

α_c is the conductor loss and obtained from [26] as

$$\alpha_c = \frac{R_s}{Z\left(a/h, h, \varepsilon_{re}\right)a/2} \tag{4.35}$$

$$R_s = \sqrt{\frac{\pi f_{r,nm}\mu_0}{\sigma}} \tag{4.36}$$

where, σ is the conductivity and other variables have usual meaning.

4.2.4. Bandwidth and Gain

The percentage bandwidth (*V.S.W.R < 2*) of the patch can be obtained as

$$\frac{1}{\sqrt{2}\,Q_T}\,100\,\% \tag{4.37}$$

The gain (*G*) can be expressed as

$$G = \frac{\left(k_r a_{eff}\right)^2}{\pi \eta_0 G_r}\left(\frac{\varepsilon_{r,eff}}{\varepsilon_{re}}\right)^2 \tag{4.38}$$

$$k_r = \frac{2\pi}{\lambda_r} \tag{4.39}$$

$$\lambda_r = \frac{c}{f_r} \tag{4.40}$$

4.3 Patch fabrication and experimental tests

To verify the proposed theoretical model, the prototype have been etched on Roggers substrate whose thickness h = 0.8265 mm, permittivity ε_{re} = 2.4 and dielectric loss tangent $tan\delta_e$ = 0.0022. The photograph of the fabricated prototype is shown in 4.3. The measurements were performed using an Agilent E 5071B Network Analyzer. The resonant frequency is defined as the minimum return loss point.

4.4 Results and discussions

Here, we have presented the theoretically predicted, simulated and measured results for the resonant frequency, quality factor, input impedance band width and gain of an RAITPA on single, composite and suspended substrate

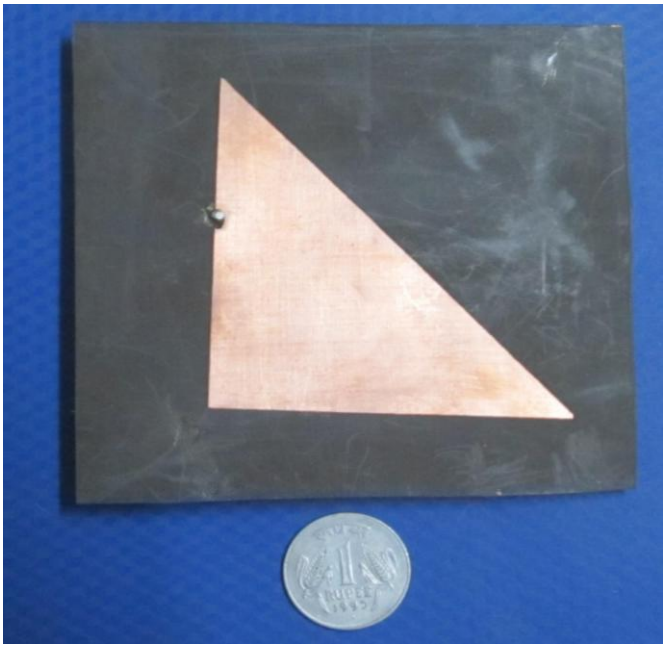

Figure 4.3: Snapshot of a fabricated prototype.

4.4.1 Resonant frequency

The variation of p and $\varepsilon_{r,eff}$ as a function of h_1 for a RAITPA on composite and suspended substrate are shown in 4.4. For a composite substrate RAITPA the $\varepsilon_{r,eff}$ is enhanced, p is decreased and $\varepsilon_{r,eff}$ is reduced, the p is increased for suspended substrate RAITPA.

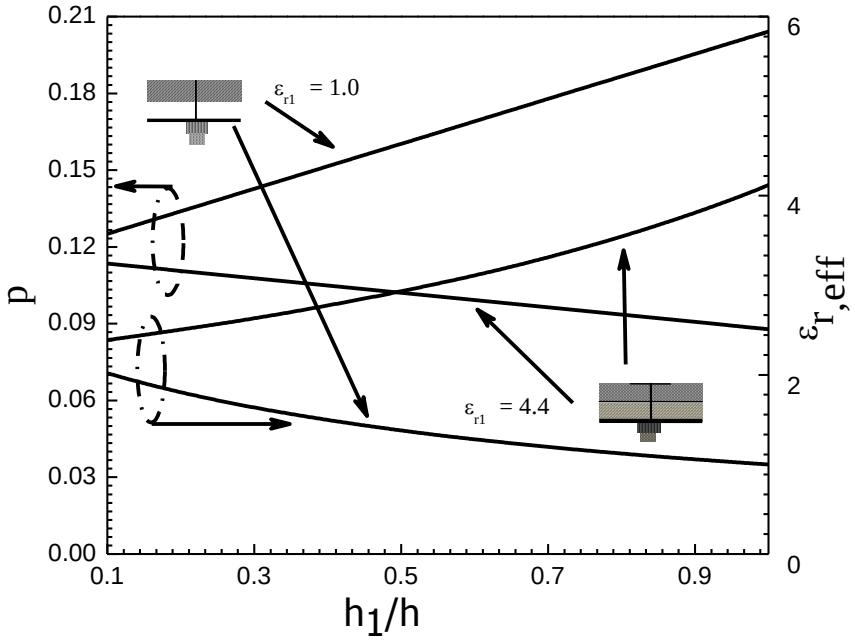

Figure 4.4: Theoretical variation of p and $\varepsilon_{r,eff}$ with h_1 for composite (ε_{r1} = 4.4) and suspended substrate (ε_{r1} = 1.0). a = 70.00 mm, $h = h_1 + h_2$ = 1.65 mm, h_1 and h_2 variable but h is fixed, ε_{r2} = 2.4.

Table 4.1 shows a comparative study of computed and simulated resonant frequencies of a RAITPA on composite and suspended substrate operated in different modes for different values of h_1. This comparison shows close agreement between computed and simulated values.

In table 4.2, we have compared the computed resonant frequencies employing the present model with corresponding HFSS [22] simulated and our measured resonant frequencies for a RAITPA on suspended substrate operated in different modes. The percentage error shows that the present model accurately computes the resonant frequency. The measured return loss for h_1 = 0.5 mm is depicted in Fig. 4.5.

TABLE 4.1

COMPUTED AND SIMULATED (HFSS) [22] VALUES OF RESONANT FREQUENCY OF A RAITPA (45^0-45^0-90^0) ON COMPOSITE AND SUSPENDED SUBSTRATE OPERATED IN DIFFERENT MODES.

a = 70.00 mm, h_2 = 0.8265 mm, ε_{r2} = 2.4, $tan\delta_1$ = 0.0035, $tan\delta_2$ = 0.0022, ρ = 30 mm

Resonant frequency (GHz)					
h_1	Mode	Composite Substrate (ε_{r1} = 4.4) 		Suspended Substrate (ε_{r1} = 1.0) 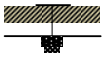	
		Computed	HFSS [22]	Computed	HFSS [22]
0.21	TM_{10}	1.296	1.297	1.522	1.517
	TM_{11}	1.833	1.806	2.153	2.103
	TM_{20}	2.592	2.549	3.045	3.968
	TM_{21}	2.899	2.911	3.404	3.411
	TM_{30}	3.888	3.832	4.567	4.520
0.42	TM_{10}	1.251	1.265	1.610	1.602
	TM_{11}	1.769	1.747	2.277	2.215
	TM_{20}	2.502	2.462	3.220	3.189
	TM_{21}	2.797	2.830	3.601	3.586
	TM_{30}	3.752	3.719	4.831	4.702
0.66	TM_{10}	1.217	1.230	1.663	1.648
	TM_{11}	1.721	1.713	2.352	2.297
	TM_{20}	2.434	2.408	3.326	3.226
	TM_{21}	2.712	2.763	3.719	3.713
	TM_{30}	3.650	3.618	4.989	4.846
0.8265	TM_{10}	1.192	1.205	1.694	1.690
	TM_{11}	1.686	1.688	2396	2.334
	TM_{20}	2.384	3.365	3.389	3.278
	TM_{21}	2.666	2.717	3.789	3.796
	TM_{30}	3.576	3.554	5.083	4.951

TABLE 4.2

COMPARISON OF EXPERIMENTAL [OUR], SIMULATION (HFSS) [22] AND THEORETICAL VALUES OF RESONANT FREQUENCIES OF A RAITPA (45^0-45^0-90^0) ON SUSPENDED SUBSTRATE OPERATED IN DIFFERENT MODES.
a = 70.00 mm, h_2 = 0.8265 mm, ε_{r1} = 1.0, ε_{r2} = 2.4

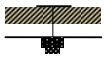

Resonant frequency (GHz)				
h_1 (mm)	Mode	Exp	Simulated [22]	Computed
0.5	TM_{10}	1.635	1.621	1.634
	TM_{11}	2.327	2.305	2.310
	TM_{20}	3.264	3.211	3.267
	TM_{21}	3.686	3.658	3.653
	TM_{30}	4.886	4.874	4.901
Avg. %Error with respect to Exp				0.417
Avg. %Error with respect to HFSS				0.691

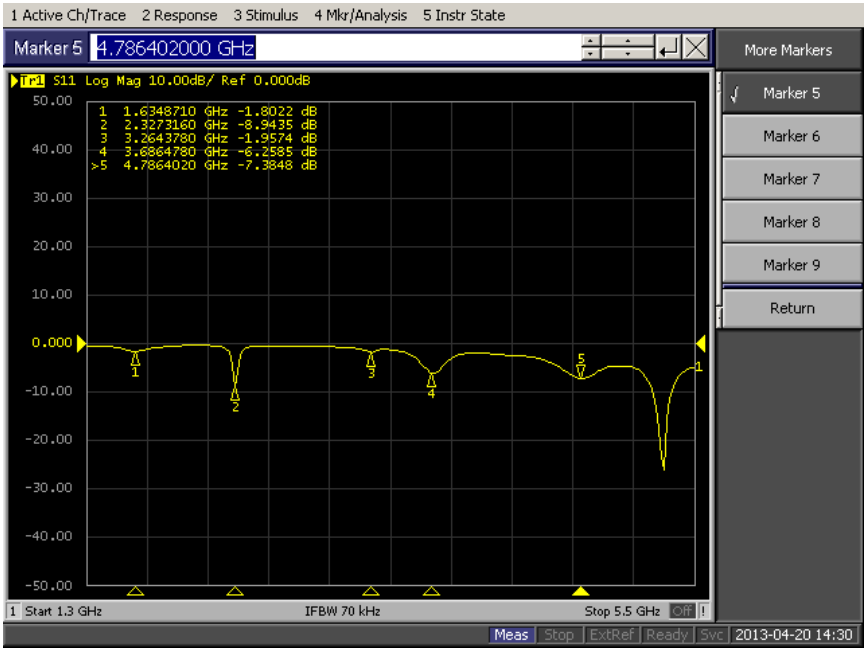

Figure 4.5: Measured return loss (S_{11} in dB) for a suspended substrate RAITPA. a = 70.00 mm, h_1 = 0.50 mm, h_2 = 0.8265 mm, $h = h_1 + h_2$, ε_{r1} = 1.0, ε_{r2} = 2.4.

Theoretical variation of resonant frequency for TM_{10} and TM_{11} mode of a RAITPA on composite substrate (ε_{r1} = 4.4) and suspended substrate (ε_{r1} = 1.0) as a function of h_1 is shown in Fig. 4.6. The resonant frequency decreases for composite substrate and increases for suspended substrate RAITPA. The computed curve well supported the software [22] computed data for all values of h_1.

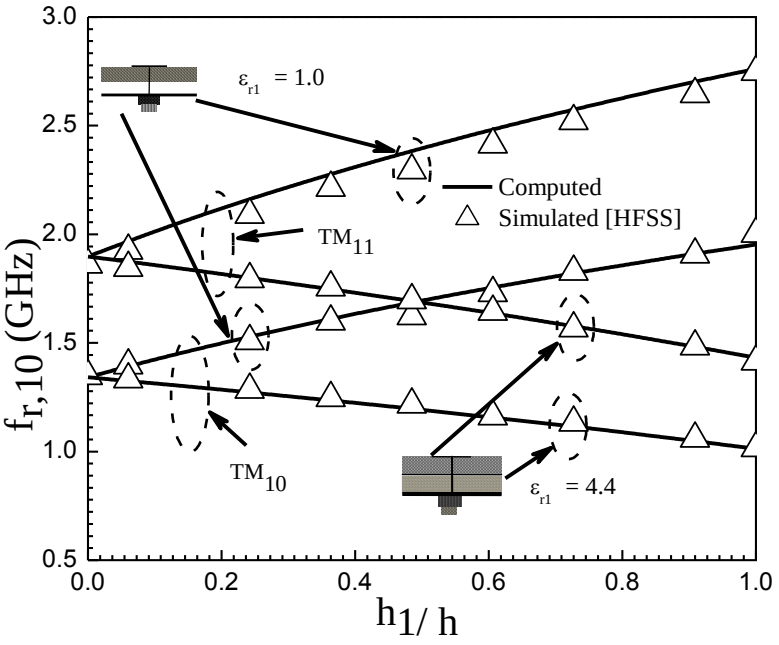

Figure 4.6: Computed and simulated [21] variation of resonant frequency as a function of h_1 for a RAITPA on composite (ε_{r1} = 4.4) and suspended substrate (ε_{r1} = 1.0) operated in TM_{10} and TM_{11} mode. Parameters as in Fig. 4.4.

The measured and HFSS simulated [22] resonant frequencies are compared with theoretically computed results employing the present model and another model [16] in table 4.3 for a RAITPA on sigle substrate. The computed resonant frequency employing the present model shows closer agreement with HFSS computation [22] and experimental values compared to [16]. The measured return loss for h_2 = 0.0 mm is shown in Fig. 4.7.

TABLE 4.3
COMPARISON OF MEASURED [OUR] SIMULATED [22] AND COMPUTED RESONANT FREQUENCIES OF A RAITPA (45^0-45^0-90^0) ON SINGLE SUBSTRATE OPERATED IN DIFFERENT MODES.
a = 70.00 mm, $h = h_2$ = 0.8265, mm ε_{r1} = 1.0, $\varepsilon_{r2} = \varepsilon_{re}$ = 2.4

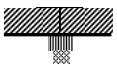

Resonant frequency (GHz)					
h_1 (mm)	Mode	Exp	Simulated [22]	Computed	
				Present	[16]
0.0	TM_{10}	1.369	1.364	1.361	1.383
	TM_{11}	1.926	1.899	1.925	1.956
	TM_{20}	2.699	2.681	2.722	2.766
	TM_{21}	3.051	3.045	3.044	3.093
	TM_{30}	4.043	4.027	4.084	4.149
Avg. %Error with respect to Exp				0.546	1.812
Avg. %Error with respect to HFSS				0.913	2.434

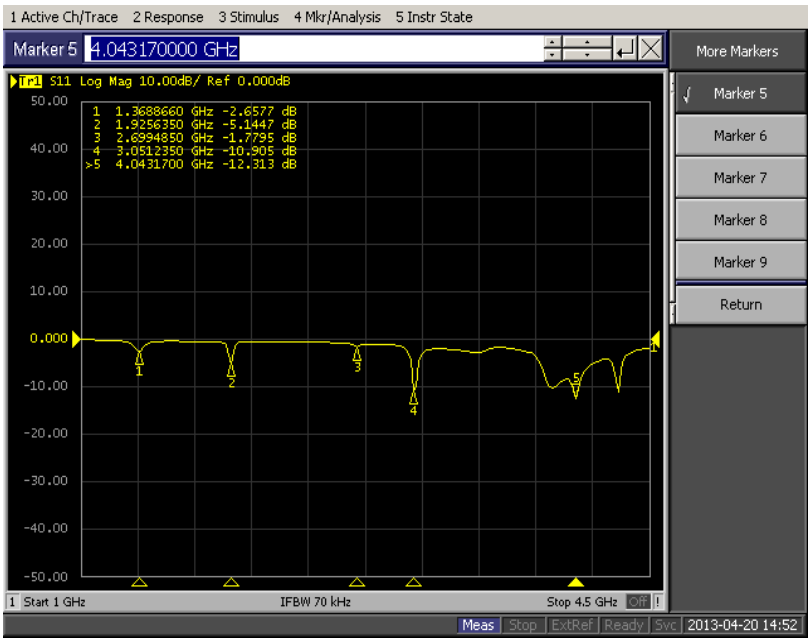

Figure 4.7: Measured return loss (S_{11} in dB) for single substrate RAITPA. a = 70.00 mm, h_1 = 0.0 mm, h = h_2 = 0.8265 mm, ε_{r1} = 1.0, ε_{r2} = ε_{re} = 2.4.

The theoretical, experimental [14] and HFSS simulation [22] variation of TM_{10} mode resonant frequency for a RAITPA on single substrate as a function of side length a is visualized in Fig. 4.8. Theoretical curve employing the present model shows very close agreement with measured and simulated results.

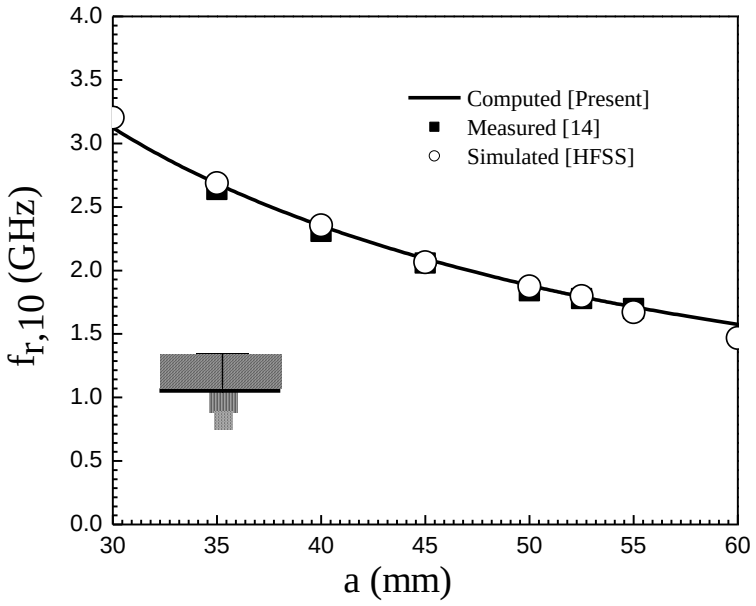

Figure 4.8: Experimental [13], software computational [21] and theoretical variation of resonant frequency for a RAITPA on single substrate operated in TM_{10} mode as a function of a. h_1 = 0.0 mm, h = h_1+ h_2 = 0.76 mm, ε_{r1} = 1.0, ε_{r2} = ε_{re} =2.45.

The variation of resonant frequency for a probe-fed RAITPA as a function of substrate thickness $h = h_2$ for different dielectric constant $\varepsilon_{re} = \varepsilon_{r2}$ is visualized in Fig. 4.9. Here we have compared the theoretically predicted curve employing the present model with simulated values [22] and it exhibits close correlation for a wide range of substrate thickness. But slight discrepancy is observed for low dielectric substrate when the substrate thickness is very high. This is due to the fact that the cavity model is well applicable for an antenna with small value of h/λ_0.model.

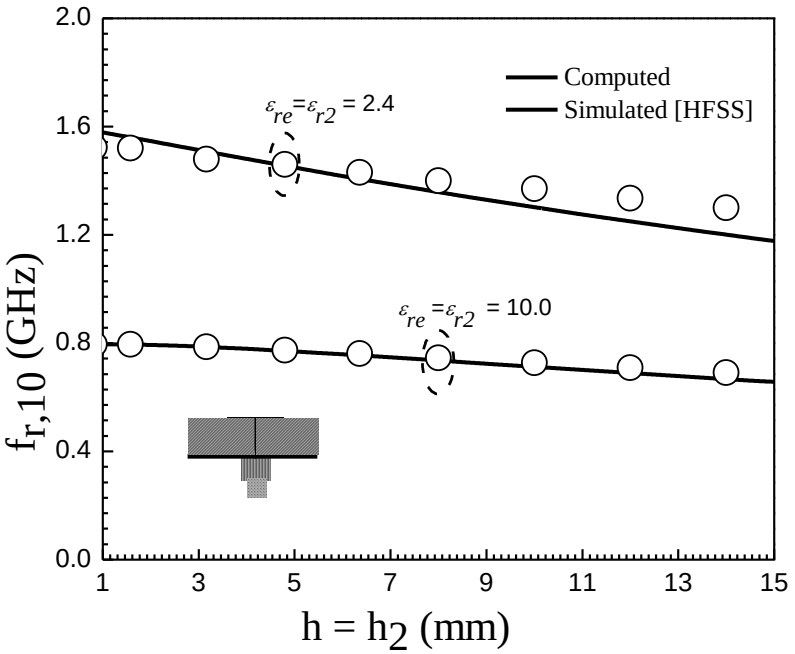

Figure 4.9: Computed and simulated [21] variation of TM_{10} mode resonant frequency of a RAITPA on single substrate as a function of h. a = 60.00 mm, h_1 = 0.0 mm, $h = h_1 + h_2 = h_2$, ε_{r1} = 1.0, $\varepsilon_{r2} = \varepsilon_{re}$ variable.

4.4.2. Quality Factor and Bandwidth

The variation of Q_T and percentage B.W. as a function of side length a for a RAITPA on composite substrate (ε_{r1} = 4.4, $tan\delta_1$ = 0.0035), suspended substrate (ε_{r1} = 1.0, $tan\delta_1$ = 0.000) and single substrate is shown in Fig. 4.10. It is clear from this study that Q_T is increasing with the increase of side length a, as a result B.W is decreasing accordingly. The computed curve employing the present model well supports the simulation [22] results. So, our model is valid for a RAITPA having a side length varied from very small to very large values. The Q_T is higher for composite substrate, so B.W. is lower with respect to single substrate. The opposite phenomenon is occurred for suspended substrate.

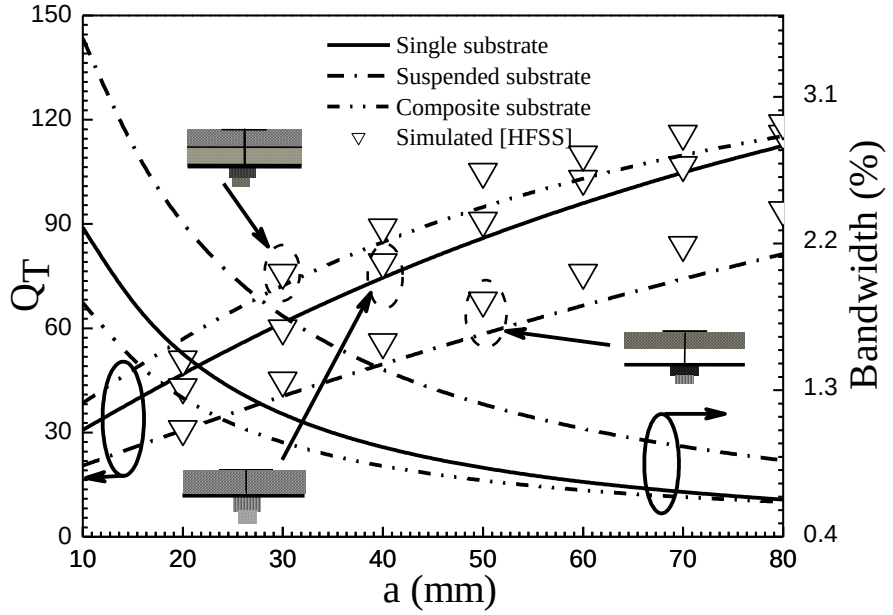

Figure 4.10: Computed and simulated [21] variation of Q_T and percentage B.W as function of a of a RAITPA on i) composite substrate (ε_{r1} = 4.4, $tan\delta_1$ = 0.0035, h_1 = 1.2 mm, h_2 = 0.45 mm) ii) suspended substrate (ε_{r1} = 1.0, $tan\delta_1$ = 0.0, h_1 = 1.2 mm, h_2 = 0.45 mm) iii) single substrate (h_1 = 0.0 mm, $h = h_2$). h = 1.65 mm, ε_{r2} = 2.4, ρ = 30.00, $tan\delta_2$ = 0.0022, h_1 and h_2 variable but h is fixed.

The validity of the model for Q_T and percentage B.W is further validated in Fig. 4.11. The variation of percentage B.W and Q_T with different values of h_1 for a RAITPA on composite substrate and suspended substrate is shown in Fig. 4.11. From this study it is observed that the quality factor (Q_T) increases; bandwidth decreases for composite subtrate while Q_T decreases; bandwidth increases for suspended subtrate. The computed curves employing the present model well supports the simulated [22] values.

4.4.3. Input impedance

The variation of TM_{10} mode input impedance as a function of frequency for a RAITPA on composite (ε_{r1} = 4.4, $tan\delta_1$ = 0.0035) and suspended substrate (ε_{r1} = 1.0, $tan\delta_1$ = 0.000) for different h_1 is shown in Fig. 4.12. This study indicates that both resonant frequency and input impedance significantly change with the change in h_1. The resonant frequency (f_r) and resonant resistance (R_r) increases for a RAITPA on suspended substrate while f_r decreases and R_r increases for the antenna on composite substrate with respect to the single substrate antenna. The increment in resonant resistance is more for RAITPA on composite substrate compared to suspended substrate and it is clearly visualized further in Fig. 4.13.

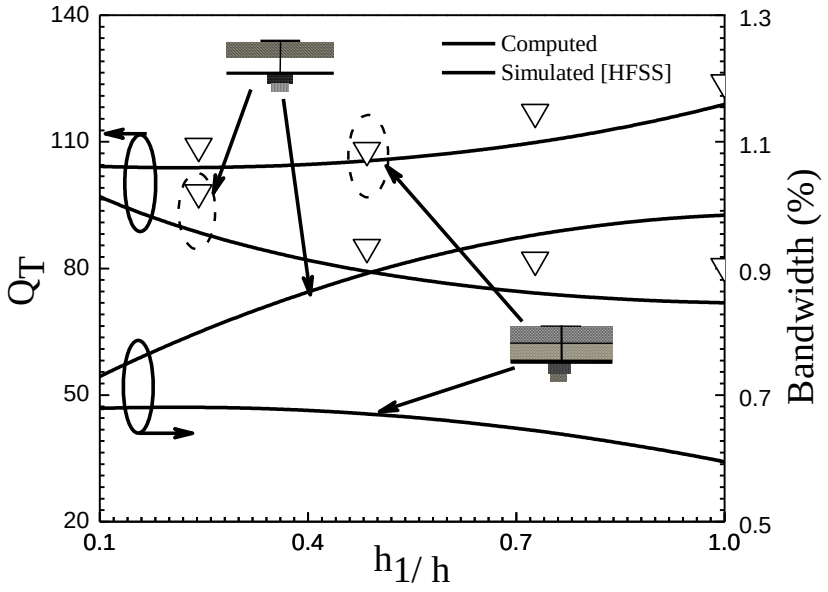

Figure 4.11: Computed and simulated [21] variation of Q_T and percentage B.W with h_1 of a RAITPA on composite (ε_{r1} = 4.4, $tan\delta_1$ = 0.0035) and suspended substrate (ε_{r1} = 1.0, $tan\delta_1$ = 0.000). a = 70.00 mm, h = 1.65 mm, ε_{r2} = 2.4, ρ = 30.00, $tan\delta_2$ = 0.0022, h_1 and h_2 variable but h is fixed.

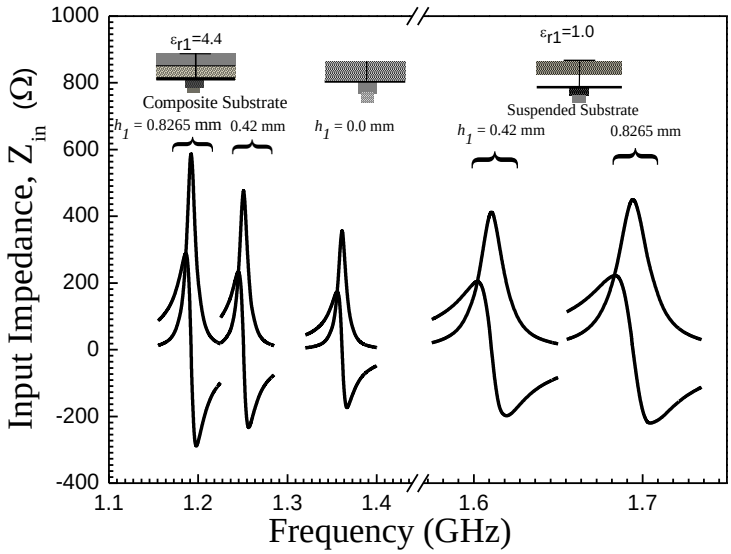

Figure 4.12: TM_{10} mode input impedance as a function of frequency for a RAITPA on composite (ε_{r1} = 4.4, $tan\delta_1$ = 0.0035) and suspended substrate (ε_{r1} = 1.0, $tan\delta_1$ = 0.000). a = 70.00 mm, h_2 = 0.8265 mm, h_1 variable, ε_{r2} = 2.4, $tan\delta_2$ = 0.0022, ρ = 30.00.

The computed TM_{10} mode input impedance as a function of frequency for a RAITPA on composite substrate (h_1 = 0.42 mm) is compared with simulated [22] input impedance in Fig. 4.14. The theoretical curves employing the present model exhibits good agreement with simulated [22] curves.

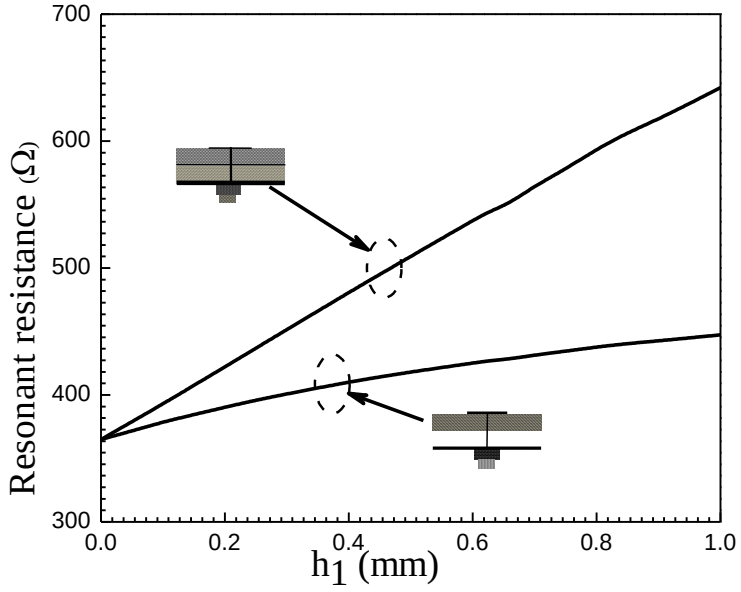

Figure 4.13: Theoretical variation of resonant resistance of a RAITPA on composite (ε_{r1} = 4.4) and suspended substrate (ε_{r1} = 1.0) as a function h_1. Other parameters as in Fig. 4.11.

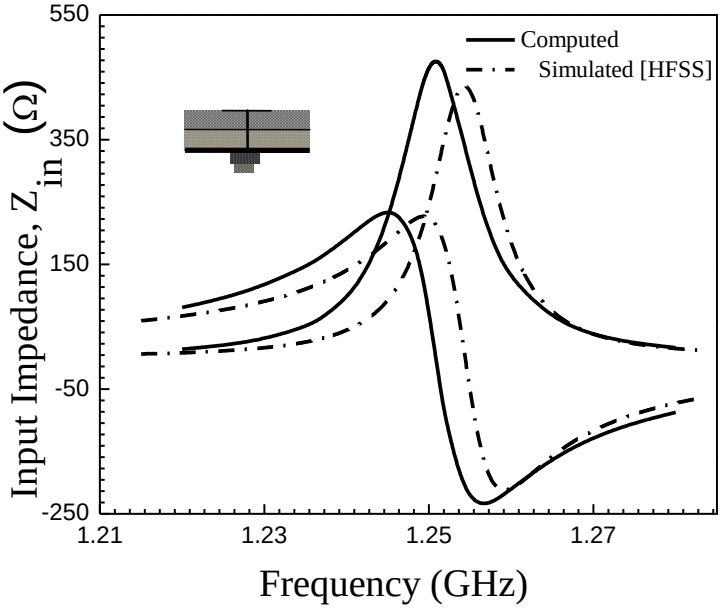

Figure 4.14: TM_{10} mode input impedance as a function of frequency for a RAITPA on composite substrate (ε_{r1} = 4.4, $tan\delta_1$ = 0.0035). a = 70.00 mm, h_1 = 0.42, h_2 = 0.8265 mm, ε_{r2} = 2.4, ρ = 30.00, $tan\delta_2$ = 0.0022.

The measured and computed TM_{10} mode input impedance as a function of frequency for a RAITPA on suspended substrate (ε_{r1} = 1.0, $tan\delta_1$ = 0.000) is shown in Fig. 4.15. (a). The theoretical curves employing the present model shows close correlation with our experimental curves. The measured impedance locus is depicted in Fig. 4.15. (b).

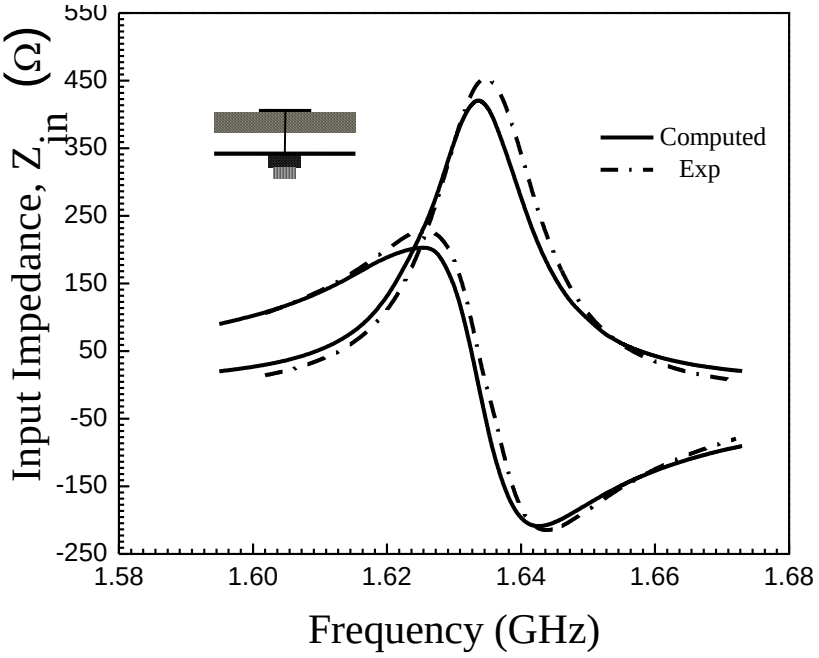

(a)

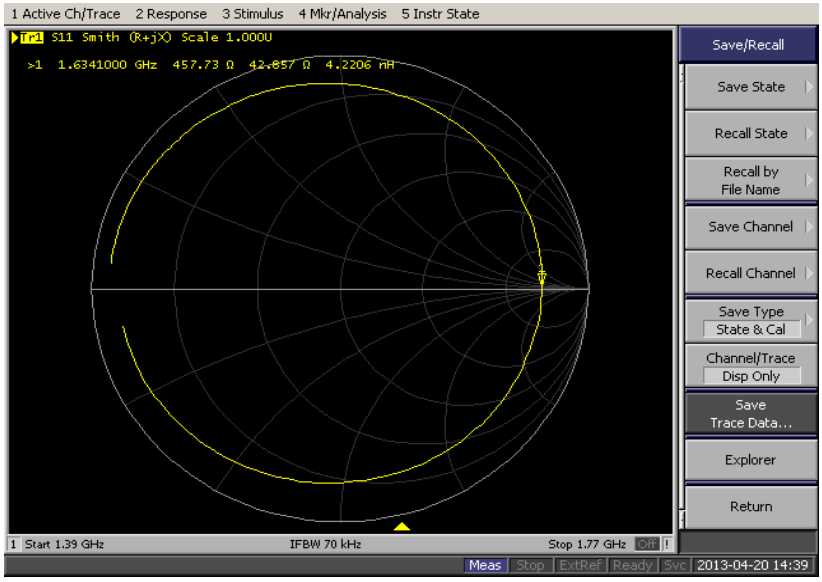

(b)

Figure 4.15: (a). Measured [our] and computed TM_{10} mode input impedance as a function of frequency for a RAITPA on suspended substrate. a = 70.00 mm, ε_{r1} = 1.0, ε_{r2} = 2.4, h_1 = 0.5 mm, h_2 = 0.8265 mm, ρ = 30.00 mm, $tan\delta_1$ = 0.000, $tan\delta_2$ = 0.0022. (b). Measured impedance locus for a RAITPA on suspended substrate Parameters as in Fig. (a).

The measured and computed TM_{10} mode input impedance as a function of frequency for a RAITPA on single substrate (h_1 = 0.0 mm) is shown in Fig. 4.16. (a) and good agreement is seen between them. The measured impedance locus is shown in Fig. 4.16. (b).

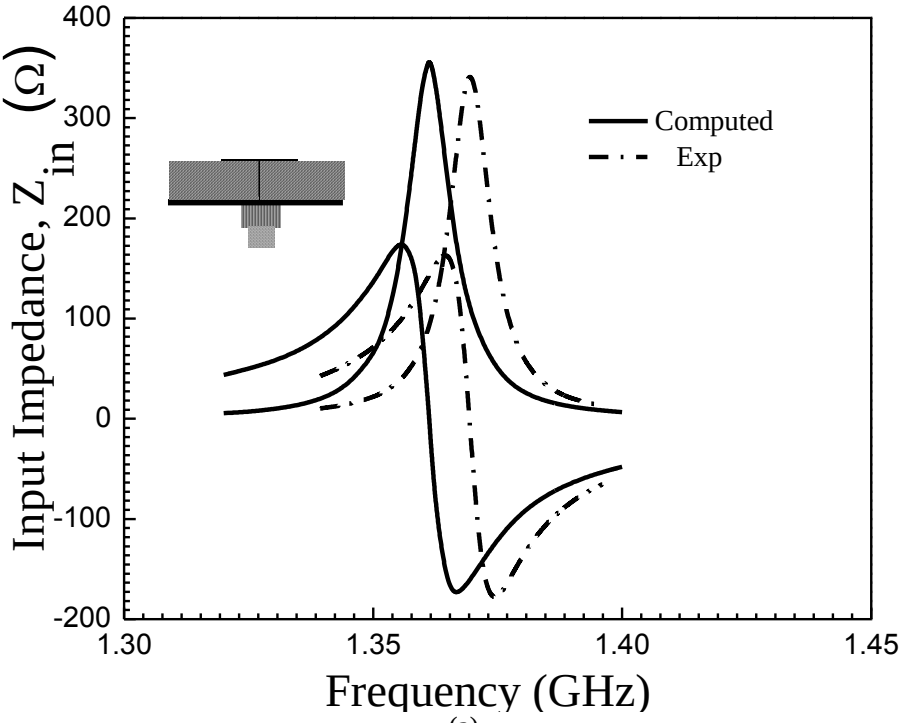

(a)

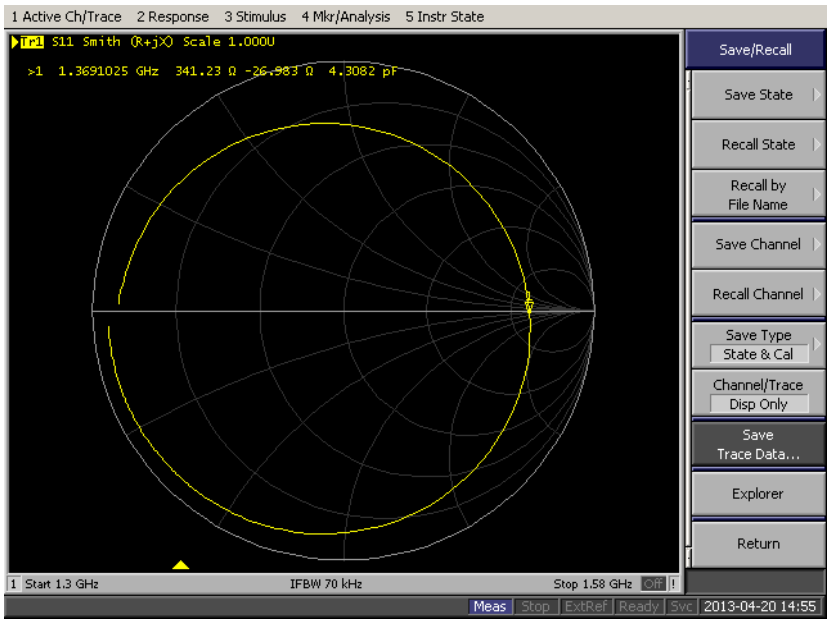

(b)

Figure 4.16: (a). Measured [our] and computed TM_{10} mode input impedance as a function of frequency for a RAITPA on single substrate. a = 70.00 mm, h_1 = 0.0 mm, $h = h_2$ = 0.8265 mm, ε_{r1} = 1.0, $\varepsilon_{r2} = \varepsilon_{re}$ = 2.4, ρ = 30.00 mm, $tan\delta_1$ = 0.000, $tan\delta_2$ = 0.0022. (b). Measured impedance locus for a RAITPA on single substrate. Parameters as in Fig. (a).

In Fig. 17 measured [18] and computed TM_{10} mode input impedance as a function of frequency for a RAITPA on single substrate is further verified for a patch with side

length a = 40 mm, ε_{r1} = 1.0, ε_{re} = ε_{r2} = 2.33, h_1 = 0.0 mm, $h = h_2$ = 0.79 mm, ρ = 16 mm, $tan\delta_1$ = 0.000, $tan\delta_2$ = 0.0012. The theoretical curves employing the present model shows good agreement with measured [18] curves.

The slight discrepancy is observed between theoretical and experimental resistance curve this is due to feed position, BNC connector, and unintended fabrication and measurement error.

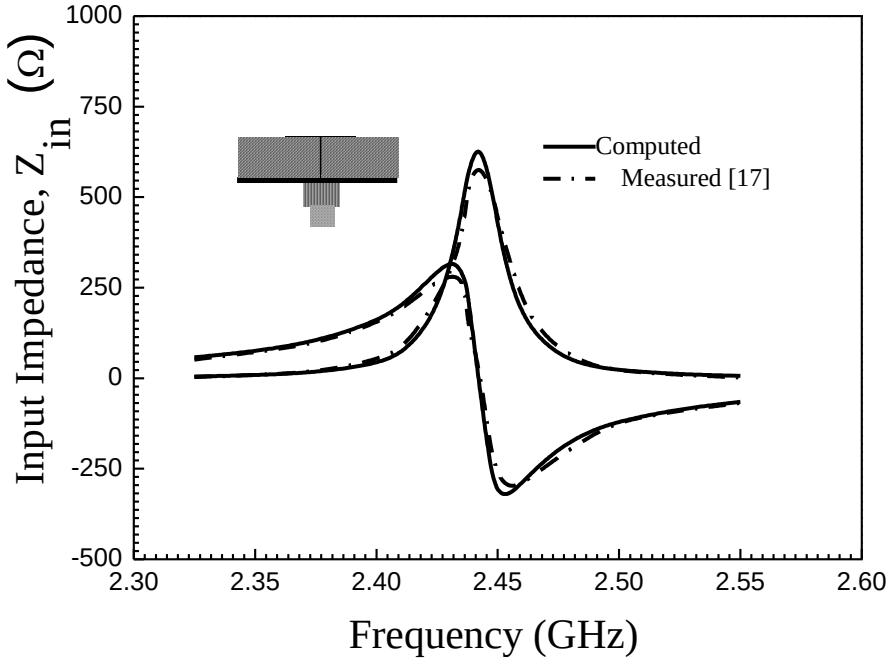

Figure 4.17: Measured [18] and computed TM_{10} mode input impedance as a function of frequency for a RAITPA on single substrate. a = 40 mm, h_1 = 0.0 mm, $h = h_2$ = 0.79 mm, ε_{r1} = 1.0, $\varepsilon_{r2} = \varepsilon_{re}$ = 2.33, ρ = 16 mm, $tan\delta_1$ = 0.000, $tan\delta_2$ = 0.0012.

4.4.4. Gain

The variation of effective side length and gain for a RAITPA on composite (ε_{r1} = 4.4, $tan\delta_1$ = 0.0035) and suspended substrate (ε_{r1} = 1.0, $tan\delta_1$ = 0.000) as a function h_1 is depicted in Fig. 4.18. Theoretical curve for gain employing the present model is compared with simulated [22] data and good agreement is revealed between them. This study shows that with the increase of h_1/h, the gain is increased for suspended substrate and decreased for composite substrate. This is based on the fact that the effective permittivity becomes lowered (Fig. 4.4) for a suspended substrate patch with the increase of h_1, fringing field effect increases (Fig. 4.4), effective aperture area increases, and

therefore the gain is increased. The exactly opposite behavior occurs for an antenna on composite substrate.

In the above studies, we conclude that the change of resonant frequency, bandwidth and gain is possible by changing the h_1 without altering the antenna parameters. This is the advantage of two layered antenna structure.

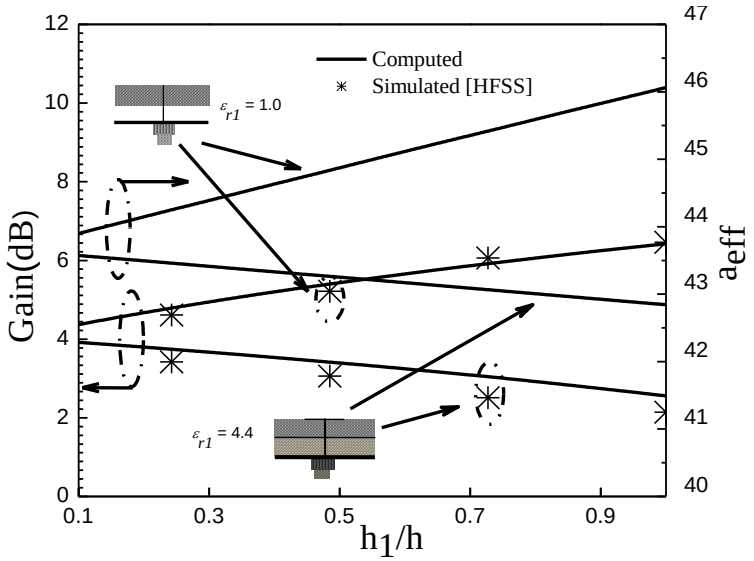

Figure 4.18: Theoretical variation of effective side length and gain of a RAITPA on composite (ε_{r1} = 4.4, $tan\delta_1$ = 0.0022) and suspended substrate. (ε_{r1} = 1.0, $tan\delta_1$ = 0.000) as a function of h_1. a = 40 mm, ε_{r2} = 2.4, ρ = 16 mm.

4.5. Conclusions

In this effort, an accurate expression for the effective permittivity, effective side length, quality factor, input impedance and gain for a probe fed RAITPA on double layered substrate is reported. The present model shows very close agreement with measured and software computed results compared to other models. To the best of our knowledge, this is the first time the effect of composite and suspended substrate on resonant frequency, input impedance, gain and bandwidth of a RAITPA has been investigated. The present model is well valid for wide variation of composite and suspended substrate parameters as well as patch dimension. The superiority of this model is that it is also quite valid for the entire range of thickness and permittivity of the substrate. This model is very useful for design and practical implementation of a RAITPA on composite, suspended and single substrate.

REFERENCES:

[1] K. J.-S. Hong and M.J. Lancaster, "Theory and experiment of dual-mode microstrip triangular patch resonators and filters," *IEEE Trans. Microw. Theory Tech.*, vol. 52, pp. 1237- 1243, Apr. 2004.

[2] J. T. S. Sumantyo, K. Ito, and M. Takahashi, "Dual-band circularly polarized equilateral triangular-patch array antenna for mobile satellite communications," *IEEE Trans. Antennas Propagat.*, vol. 53, pp. 3477- 3485, Nov. 2005.

[3] K. F. Lee, K. M. Luk, and J. S. Dahele, "Characteristics of the equilateral triangular patch antenna," *IEEE Trans. Antennas Propagat.*, vol. 36, pp. 1510-1518, Nov. 1988.

[4] M. Biswas and A. Mandal, "CAD model to compute the input impedance of an equilateral triangular microstrip patch antenna with radome, " *Prog. Electromag. Res. M*, vol. 12, pp. 247-257, 2010.

[5] W. Chen, K. F. Lee, and J. S. Dahele, "Theoretical and experimental studies of the resonant frequencies of equilateral triangular microstrip antenna," *IEEE Trans. Antennas Propagat.*, vol. 40, pp. 1253-1256, Oct. 1992.

[6] D. Karaboğa, K.Güney, N. Karaboğa, and A. Kaplan, "Simple and accurate effective side length expression obtained by using a modified genetic algorithm for the resonant frequency of an equilateral triangular microstrip antenna," *Int. J. Electron.*, vol. 83, pp. 99-108, Jan.1997.

[7] H. R. Hassani and D. M. Syahkal, "Analysis of triangular patch antennas including radome effects," *IEE Proc. H.*, vol. 139, no. 3, pp.251-256, Jun. 1992.

[8] C. S. Gurel and E.Yazgan, "New computation of the resonant frequency of a tunable equilateral triangular microstrip patch," *IEEE Trans. Microw. Theory Tech.*, vol. 48, pp. 334-338, Mar. 2000.

[9] Nasimuddin, K. Esselle, and A.K. Verma, "Resonant frequency of an equilateral triangular microstrip antenna," *Microw. Opt. Tech. Lett.*, vol. 47, no.5, pp.485-489, Dec. 2005.

[10] M. Biswas and D. Guha, "Input impedance and resonance characteristic of superstrate loaded triangular microstrip patch," *IET Microw. Antennas Propagat.*, vol. 3, pp. 92- 98, Feb. 2009.

[11] K. Guney and E. Kurt, "Effective side length formula for resonant frequency of equilateral triangular microstrip antenna," *Int. J. Electron.*, vol. 103, pp. 261-268, 2016.

[12] A. K. Sharma and B. Bhat, "Analysis of triangular microstrip resonator," *IEEE Trans. Microw. Theory Tech.*, vol. 30, no. 11, pp. 2029 -2031, Nov. 1982.

[13] E. F. Keuster and D. C. Chang, "A geometrical theory for the resonant frequencies and Q factors of some triangular microstrip patch antenna," *IEEE Trans. Antennas Propagat.*, vol. 31, pp.27-34, 1983.

[14] Y. Tu, "A study of triangular microstrip antennas," *MS thesis, Boulder (CO) University of Colorado*, Sep. 1983.

[15] P. L. Overfelt and D. J. White, "TE and TM Modes of some triangular cross-section waveguides using superposition of plane waves," *IEEE Trans. Microw. Theory Tech.*, vol. 34, pp. 161-167, Jan 1986.

[16] M. M. Olaimat and N. I. Dib, "A study of 15^0-75^0-90^0 angles triangular patch antenna," *Prog. Electromag. Res. Lett.*, vol. 21, pp. 1-9, Feb. 2011.

[17] S. Maity and B. Gupta, "Accurate resonant frequency of isosceles right-angled triangular patch antenna," *Microw. Opt. Tech. Lett*.", vol. 55, pp. 1306-1308, Jun. 2013.

[18] E. G. Lim, E. Korolkiewicz, S. Scott, A. Sambell, and B. Aljibouri, "An Efficient formula for the input impedance of a microstrip right-angled isosceles triangular patch Antenna," *IEEE Antennas Wireless Propagat. Lett.*, vol. 1, pp. 18-21, Feb. 2002.

[19] V. Losada, R. R. Boix, & M. Horno, "Resonant modes of circular microstrip patches in multilayered substrates," *IEEE Trans. Microw. Theo. Tech*, vol. 47, pp. 488-498, Apr. 1999.

[20] R. M. Nelson, D. A. Rogers, and A. G. D Assuncio, "Resonant frequency of a rectangular microstrip patch on several uniaxial substrates," *IEEE Trans. Antennas Propagat.*, vol. 38, pp. 978-981, Jul. 1990.

[21] H.R. Hassani, and D. M. Syahkal, "Full-wave analysis of stacked rectangular microstrip antennas," *Presented at 6th Int. Conf. Antennas and Propagat., IEE Conf. Publication*, vol. 301, pp. 369-373,Apr. 1989.

[22] High Frequency Structure Simulator: *Ansoft Corp*. 2012. HFSS 13.

[23] J. Zhang and J. Fu, "Comments on`TE and TM modes of some triangular cross-section waveguides using superposition of plane waves," *IEEE Trans. Microw. Theory Tech.*, vol. 39, pp. 612-613, Mar. 1991.

[24] I. Wolff and N. Knoppik, "Rectangular and circular microstrip disk capacitors and resonators," *IEEE Trans. Microw. Theory Tech.*, vol. 22, pp.857-864, Oct. 1974.

[25] F. Abboud, J. P. Damiano, and A. Papiernik, "A new model for calculating the input impedance of coax-fed circular microstrip antennas with and without air gaps," *IEEE Trans. Antennas Propagat.*, vol. 38, pp. 1882-1885, Nov. 1990.

[26] D. M. Pozar, "Microwave engineering," *John Wiley & Sons, Inc.*, USA, 4th edition, ch. 3, pp. 149, 2012.

CHAPTER 5

Investigation of a 30^0-60^0-90^0 Right Angled Triangular Patch Antenna on Single, Composite and Suspended Substrate: Experimental and theoretical study

Content:

5.1. Introduction

Today, the microstrip patch antenna shows great impact on both theoretical research and engineering applications due to its several advantages. It is a thin profile antenna can be used in portable wireless equipments due to light weight, low cost and at the same time being easy to fabricate. Different regular geometries of microstrip patch antennas like rectangular, circular, equilateral triangular, isosceles triangular, right angle isosceles triangular, 30^0-60^0-90^0 right angled triangular etc are available. Among them, 30^0-60^0-90^0 right angled triangular shape is the most attractive patch shape because it has the least area among the entire standard triangular patch operating at the same frequency in the dominant mode [1, table 1]. So it is the most compact compared to other shapes [1, 2]. The antenna with a compact shape is very essential for installation in portable wireless equipments. To get the best outcome from an antenna, a few aspects of antenna have to be considered. First of all the accurate computation of the resonant frequency, input impedance, bandwidth and gain are very important for proper installation of the antenna in portable wireless equipments.

On the other hand, all the antenna parameters need to be changed for every change in resonant frequency. But it is a very difficult process. To avoid this difficulty an air gap is introduced between the substrate and the ground plane. This structure is called suspended type patch antenna. The change in resonant frequency, bandwidth, gain and efficiency is possible by changing the air gap height without altering the other antenna parameters. So the suspended type patch antenna offers the tunability in resonant frequency and also improves the bandwidth, gain and efficiency [3]. The suspended patch antenna is a special type of a patch antenna on composite substrate (i.e. air is replaced by another dielectric layer), which also can play an important role in antenna tunability, described in detail in chapter 2 (sec. 2.1). So, the investigation of patch antenna on composite substrate is also necessary.

Triangular geometry has been widely investigated by several researchers [1-17]. However, among them majority of the studies concentrated only on equilateral shape [1, 3-16]. A very few investigations are available in open literature for 30^0-60^0-90^0 RATPA [1- 2, 15-17]. But the models reported in [1- 2, 15-17] have some drawbacks: i) the effect of fringing fields were not accurately included, ii) the effect of composite and

suspended substrate on resonant frequency was not studied, (iii) employs large and rigorous mathematical steps to compute the quality factors and input impedance of the patch on a single substrate and iv) neither any design guideline nor any experimental results for the input impedance, gain, efficiency and bandwidth of a RATPA on composite and suspended substrate are provided.

Full wave analysis [4, 18-20] and also commercially available simulation softwares [21, 22] can be used to predict the important parameters of patch antennas. But these techniques have enormous complications in design and large computational time constraint. So, the full wave analysis is not ideal for the design oriented interactive computer aided design (CAD) for the direct synthesis of patch antennas. The CAD model takes less computational time and is easy to realize because it consists of a set of closed form expressions. Thus, the CAD model is more suitable than other techniques for direct synthesis of patch antennas.

Considering these issues carefully, the purpose of the work is divided into a two-fold objective: i) we have proposed a set of CAD oriented closed form expressions based on cavity model analysis and single resonant parallel *R-L-C* circuit to predict accurately the resonant frequency, quality factor, bandwidth, input impedance and gain for a probe fed 30^0-60^0-90^0 RATPA printed on a single, composite and suspended substrate. This model is very efficient and capable of computing the above parameters very accurately for wide variation of antenna size and substrate electrical parameters and ii) we have performed a set of experiments with fabricated prototypes to validate the proposed model.

5.2. Theory

This section introduces the expressions for this model including equivalent relative permittivity, dynamic permittivity, effective permittivity, effective side length, quality factors, bandwidth, gain, resonant frequency, resonant resistance and input impedance based on the CAD oriented cavity model and single resonant parallel *R-L-C* circuit.

5.2.1 Resonant frequency

The resonant frequency $f_{r,nml}$ of TM_{nml} modes for 30^0-60^0-90^0 RATPA on composite and suspended substrate can be computed using a simple closed form expression based on cavity model analysis [1, 16 - 17] as:

$$f_{r,nml} = \frac{c}{a\sqrt{3\varepsilon_{re}}}\left(n^2 + nm + m^2\right)^{1/2} \tag{5.1}$$

where, c is the velocity of light in free space, ε_{re} is the equivalent relative permittivity of the medium below the patch, a is the side length of the patch and m, n, l are integers which are never zero simultaneously satisfying the condition $n + m + l = 0$

5.2.2 Equivalent Relative Permittivity

The triangular microstrip patch is modelled as a cavity with a magnetic wall along the edge. This is a two layer cavity (Fig. 5.1): the upper layer has thickness h_2 with relative permittivity ε_{r2} and lower layer has thickness h_1 with permittivity ε_{r1}. In order to give a general formulation for both single and two layer structures, the two-layer structure is modelled as the single-layer one having substrate thickness of $h = h_1 + h_2$ and an equivalent substrate relative permittivity ε_{re} is determined under the cavity model approximations as:

$$\varepsilon_{re} = \frac{\varepsilon_{r1}\varepsilon_{r2}h}{\varepsilon_{r1}h_2 + \varepsilon_{r2}h_1} \tag{5.2}$$

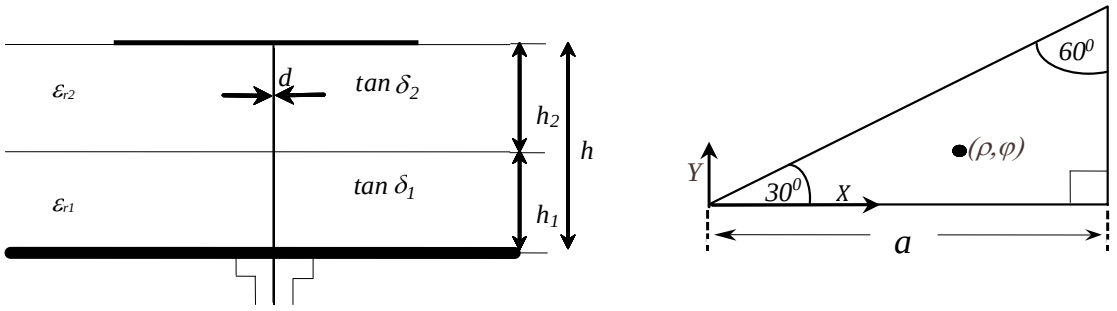

(a) (b)

Figure 5.1: (a). A schematic diagram of a probe-fed 30^0-60^0-90^0 right angle triangular patch antenna (RATPA). (b) Patch shape.

The field distribution in the patch can be divided into two regions: the interior fields and the exterior fields. The exterior fields are the fields outside the cavity region that determine the radiation characteristics of the patch antenna. The interior fields are the fields inside the cavity region, useful in determining the input impedance of the antenna and the currents responsible for the antenna. In practice, the fields are not confined to the patch. A fraction of the field travels outside the physical area ($1/2\sqrt{3}a^2$) of the patch while moving from edge of the patch to ground plane. This is called the fringing field. These fringing fields very much depend on the patch dimension and relative characteristics of substrate. For a low permittivity substrate the fringing fields effect are enhanced and reduced for a high permittivity substrate. The effect of the fringing fields at the edge can be included through the effective dielectric constant $\varepsilon_{r,eff}$ and effective side length a_{eff} [3]. These two parameters are very crucial for determination of resonant frequency. But the effect of fringing fields for computing the effective side length and permittivity was not included properly in the models reported in [1- 2, 15-17]. The model reported in [1, 15-17] did not consider any of these two parameters (a_{eff} and $\varepsilon_{r,eff}$). The model in [2] only considers the a_{eff} and they have employed an approximate formula for a_{eff}. So, the models reported in [1- 2, 15-17] for computing the resonant frequency are inaccurate. We have replaced a and ε_{re} by a_{eff} and $\varepsilon_{r,eff}$ respectively in equation (5.1) to account properly for the effect of fringing fields.

5.2.3. Effective Side Length

The effective side length of the 30^0-60^0-90^0 RATPA on composite and suspended substrate is computed as

$$a_{eff} = a(1+q)^{1/2} \tag{5.3}$$

The q for a circular geometry was reported as [23]:

$$q = q_1 + (1+q_1)(q_2+q_3) \tag{5.4}$$

In (5.3), q arises due to the fringing fields at the edge of the patch. The variables q_1, q_2 and q_3 are derived for this geometry from originally formulated circular geometry of radius r [23, 24] by employing an equivalence relation between them. The equivalence relation between circular and equilateral triangular patches using modal field distribution was reported in [5]. In [5], the equal circumference was considered as the basis of

equivalence. Similar approach has been considered for this geometry. The circumference of circular patch is $2\pi r$ and the circumference of 30^0-60^0-90^0 RATP is ($a + a/\sqrt{3} + 2a/\sqrt{3} = 2.732a$). So the equivalence relation between circular patch and 30^0-60^0-90^0 RATP is obtained as

$$2\pi r = \left(1+\sqrt{3}\right) a \tag{5.5}$$

$$r = \frac{\left(1+\sqrt{3}\right)}{2\pi} a \tag{5.6}$$

Thus the p_1, p_2 and p_3 for a 30^0-60^0-90^0 RATP can be more explicitly written as

$$q_1 = \left(1+\varepsilon_{re}^{-1}\right)\left(2.927\, h/a\right) \tag{5.7}$$

$$q_2 = (2/3)\left\{(0.37+0.63\varepsilon_{re})^{-1}(8+1.367\, a/h)^{-1}\right\} \times \ln\left[\left\{1+0.8(0.435\, a/h)^2+(0.135\, a/h)^4\right\}(1+0.391 a/h)^{-1}\right] \tag{5.8}$$

$$q_3 = \left(4+1.131 a/h+6.667\, h/a\right)^{-1}\left\{(0.37+0.63\varepsilon_{re})^{-1}-1\right\} \tag{5.9}$$

5.2.4. Effective permittivity

The effective permittivity $\varepsilon_{r,eff}$ of this structure can be computed as [25]:

$$\varepsilon_{r,eff} = \frac{4\varepsilon_{re}\,\varepsilon_{r,dyn}}{\left(\sqrt{\varepsilon_{re}}+\sqrt{\varepsilon_{r,dyn}}\right)^2} \tag{5.10}$$

where, ε_{re} is the equivalent relative permittivity defined in (5.2) and $\varepsilon_{r,dyn}$ is the dynamic permittivity. In order to account for the effect of ε_{re} in combination with $\varepsilon_{r,dyn}$, the term $\varepsilon_{r,eff}$ is introduced. The resonant frequency is obtained from (5.1) for considering the $\varepsilon_{r,eff}$ deduced in (5.10) in place of ε_{re} in (5.1).

5.2.5 Dynamic Permittivity

The $\varepsilon_{r,dyn}$ depends on the dimensions, equivalent substrate relative permittivity ε_{re} and field configurations of the mode under study. It can be expressed as [26]:

$$\varepsilon_{r,dyn} = \frac{C_{dyn}\left(\varepsilon = \varepsilon_0\varepsilon_{re}\right)}{C_{dyn}\left(\varepsilon = \varepsilon_0\right)} \tag{5.11}$$

where, $C_{dyn}(\varepsilon)$ is the total dynamic capacitance of the condenser formed by the conducting patch and the ground plane separated by a dielectric of permittivity ε. It takes into account the influence of the fringing field at the edge of the patch. The $C_{dyn}(\varepsilon_0)$ is the total dynamic capacitance when $\varepsilon = \varepsilon_0$. The $C_{dyn}(\varepsilon)$ can be written as

$$C_{dyn}(\varepsilon) = C_{0,dyn}(\varepsilon) + C_{e,dyn}(\varepsilon) \tag{5.12}$$

here, $C_{e,dyn}(\varepsilon)$ and $C_{0,dyn}(\varepsilon)$ are the total dynamic fringe and main field capacitance respectively. Now, $C_{e,dyn}(\varepsilon)$ and $C_{0,dyn}(\varepsilon)$ can be expressed as

$$C_{0,dyn}(\varepsilon) = \gamma_n C_{0,stat} \tag{5.13}$$

$$\begin{aligned} \gamma_n &= 0.3525 \quad for\ n = 1 \\ &= 0.2865 \qquad = 2 \\ &= 0.2450 \qquad = 3 \end{aligned} \tag{5.14}$$

$$C_{e,dyn} = \frac{1}{\delta} C_{e,stat} \tag{5.15}$$

$$\begin{aligned} \delta &= 1 \quad for\ n = 0 \\ &= 2 \qquad n \neq 0 \end{aligned} \tag{5.16}$$

The expression of the static capacitance for a circular patch was reported in [23]. We have employed the equivalence relation (5.5) to compute the static capacitance for this geometry. So, the static capacitance for this geometry becomes as

$$C_e = \frac{\left(1+\sqrt{3}\right)^2}{4\pi} \frac{\varepsilon_0 \varepsilon_{re}\ a^2}{h} (1+q) \tag{5.17}$$

In (5.17), the first term is equal to the static main capacitance $C_{0,stat}$ and the term q arises due to the fringing fields at the edge of the circular disk capacitor. The q for this geometry is defined in (5.4). So, the static fringing capacitance $C_{e,stat}$ is defined as

$$C_{e,stat}(\varepsilon) = C_{0,stat}(\varepsilon).q \tag{5.18}$$

$$C_{0,stat}(\varepsilon) = \frac{\left(1+\sqrt{3}\right)^2}{4\pi} \frac{\varepsilon_0 \varepsilon_{re}\ a^2}{h} \tag{5.19}$$

5.2.6. Input Resistance and Reactance

In order to obtain better efficiency, the better impedance matching between the coaxial probe and radiating patch is required**.** So, it is very essential to compute aaccurately the input impedance for a probe fed 30^0-60^0-90^0 RATPA at a particular feed location. The 30^0-60^0-90^0 RATPA can be treated as a single resonant parallel *R-L-C* circuit (Fig. 5.2). Based on this circuit model the input impedance seen by a coaxial probe located at a distance (ρ, ϕ) as in Fig. 5.1(b) may be computed as [8]:

$$Z_{in} = \frac{R(\rho)}{1+Q_T^2\left[\frac{f_{r,nml}}{f}-\frac{f}{f_{r,nml}}\right]^2} + j\frac{R(\rho)Q_T\left[\frac{f_{r,nml}}{f}-\frac{f}{f_{r,nml}}\right]}{1+Q_T^2\left[\frac{f_{r,nml}}{f}-\frac{f}{f_{r,nml}}\right]^2} \tag{5.20}$$

In equations (5.20), $R(\rho)$ is the input resistance at resonance, $f_{r,nm}$ is given by (5.1), Q_T is the total quality and f is the working frequency.

5.2.7. Input Resistance at resonance and Field Factor

The model reported in [2] has employed large and rigorous mathematical steps to compute $R(\rho)$. But we have proposed a very simple and accurate relation to compute $R(\rho)$ for the structure under study as [3]:

$$R(\rho) = \frac{Q_T}{\omega_r C} \tag{5.21}$$

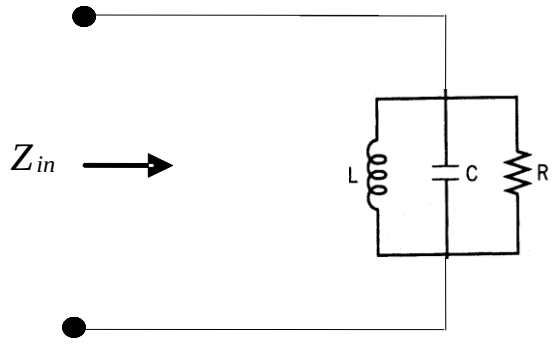

Figure 5.2: Equivalent resonant parallel *R-L-C* circuits of a probe-fed 30^0-60^0-90^0 RATPA.

Where, C is the capacitor of the equivalent parallel resonant circuit (Fig. 5.2) and it is given as [3]:

$$C = \frac{\varepsilon_0 \, \varepsilon_{r,eff} \, a^2}{h} F_{nml}^{-2} \tag{5.22}$$

From (5.21) and (5.22) we get

$$R(\rho) = \left(1.1 + n^{1.8m}\right) \frac{h \, Q_T \, \lambda_{r,nml}}{2\pi a^2 \, \varepsilon_0 \, \varepsilon_{r,eff} \, c} F_{nml} \tag{5.23}$$

There, $\lambda_{r,nml} = c/f_{r,nml}$, $f_{r,nml}$ is calculated from (5.1), $\varepsilon_{r,eff}$ is given by (5.10), Q_T is defined in (5.25) and n and m are the mode indices. F_{nml} is the field factor obtained from [16, 17] as

$$F_{nml} = \left[\cos\frac{\pi l \rho}{a} \cos\frac{\pi (n-m)\phi}{\sqrt{3}a} + \cos\frac{\pi n \rho}{a} \times \cos\frac{\pi (m-l)\phi}{\sqrt{3}a} + \cos\frac{\pi m \rho}{a} \cos\frac{\pi (l-n)\phi}{\sqrt{3}a} \right]^2 \tag{5.24}$$

5.2.8. Quality Factors, Bndwidth and Gain

The total quality factor (Q_T) is obtained as

$$Q_T = \left(\frac{1}{Q_r} + \frac{1}{Q_d} + \frac{1}{Q_c} \right)^{-1} \tag{5.25}$$

here, Q_r is the quality factor due to radiation loss, Q_d is the quality factor due to dielectric loss and Q_c is the quality factor due to conductor loss. For computing the quality factors the model reported in [2] has used large and rigorous mathematical steps.

Here we have employed a very simple and efficient relation to compute the Q_r as proposed in Abboud [27]:

$$Q_r = \frac{2.39}{4\mu_0 \, f_{r,nml} \, h G_r} \tag{5.26}$$

Where G_r is the radiation conductance expressed as [3]:

$$G_r = \frac{3.39}{240 \varepsilon_{re} D(\psi)} \tag{5.27}$$

So, the final expression for Q_r is expressed as

$$Q_r = \frac{60 \times 2.39\, D(\psi)\, \varepsilon_{re}}{3.39\, \mu_0\, f_{r,nml}\, h} \tag{5.28}$$

There, $D(\psi)$ is the directivity, ε_{re} is given by (2), $f_{r,nml}$ is obtained from (5.1). $D(\psi)$ is defined in [28] as

$$D(\psi) = 3.03177 - 0.59251\psi + 4.45509\psi^2 - 5.51485\psi^3 + 5.21473\psi^4 - 1.43543\psi^5 \tag{5.29}$$

$$\psi = \frac{\pi\, f_{r,nml}}{2\, f_{0,nml}\sqrt{\varepsilon_{re}}} \tag{5.30}$$

$$f_{0,nml} = \frac{c}{a\sqrt{3\varepsilon_{re}}}\left(n^2 + nm + m^2\right)^{1/2} \tag{5.31}$$

where, ε_{re} is defined in (5.2), $f_{r,nm}$ is given by (5.1) and n and m are the mode indices.

Q_d for this structure can be computed as [3]:

$$Q_d = \frac{1}{\tan\delta_e} \tag{5.32}$$

where, $tan\delta_e$ is the equivalent loss tangent of a RATPA on two dielectric layer may be defined as

$$\tan\delta_e = \frac{h_1\, \varepsilon_{r1} \tan\delta_1 + h_2\, \varepsilon_{r2} \tan\delta_2}{h\, \varepsilon_{re}} \tag{5.33}$$

The quality factor due to conductor loss Q_c, can be expressed as

$$Q_c = h\sqrt{\pi\, f_{r,nml}\, \mu_0\, \sigma} \tag{5.34}$$

The percentage bandwidth (V.S.W.R < 2) of the antenna is calculated as

$$\frac{1}{\sqrt{2}\, Q_T}\, 100\,\% \tag{5.35}$$

The gain (G) for the structure under study can be expressed as

$$G = \frac{Q_T}{Q_r} D(\psi) \tag{5.36}$$

5.3 Antenna design and experimental tests

The prototypes have been etched on Roggers and Taconic substrates for experimental verification of the theory proposed in section 5.2. The photograph of one of the fabricated prototype is shown in Fig. 5.3. Agilent E 5071B Network Analyzer has been used for the measurement of resonant frequency and input impedance. Two approaches may be used to find the resonant frequency of a patch antenna. (i) Minimum return loss point and (ii) Zero admittance point. Both approaches provide almost same result. But some time during antenna measurement co-axial feed reactance and other unwanted reactive effect provides non-zero admittance at resonant frequency. So, the former approach is considered to measure the resonant frequency.

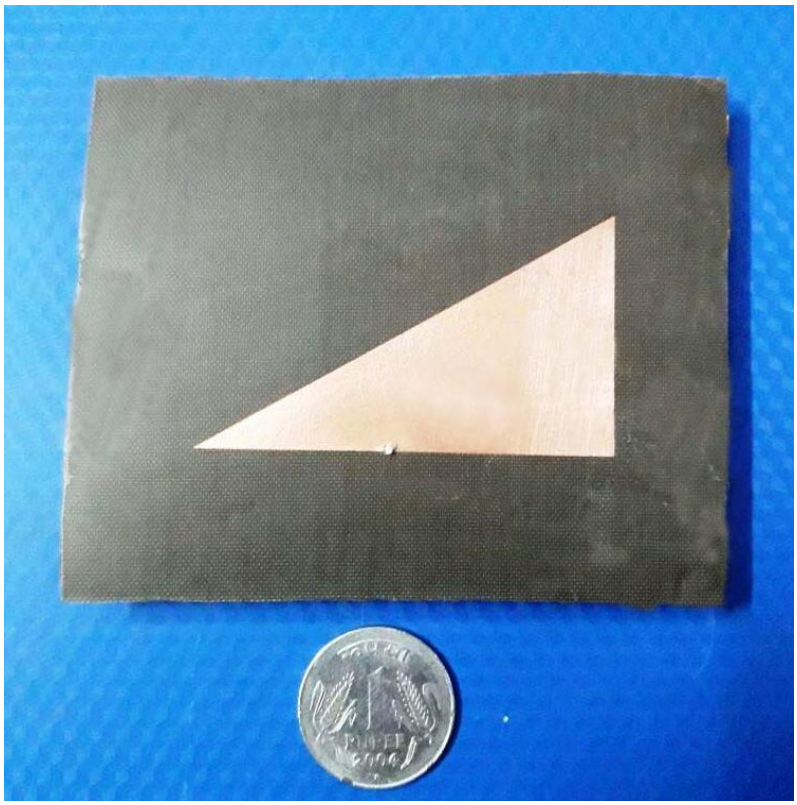

Figure 5.3: Snapshot of the fabricated prototype.

5.4 Results and discussions

5.4.1. Resonant frequency

The theoretical variation of $\varepsilon_{r,eff}$ and $\varepsilon_{r,dyn}$ as a function of side length a with ε_{re} as a parameter is depicted in Fig. 5.4. At very large values of a the $\varepsilon_{r,eff}$ becomes close to $\varepsilon_{r,dyn}$ and the significant difference is observed as a decreases. Thus the $\varepsilon_{r,eff}$ introduced in this work, becomes significant for all large and small value of a.

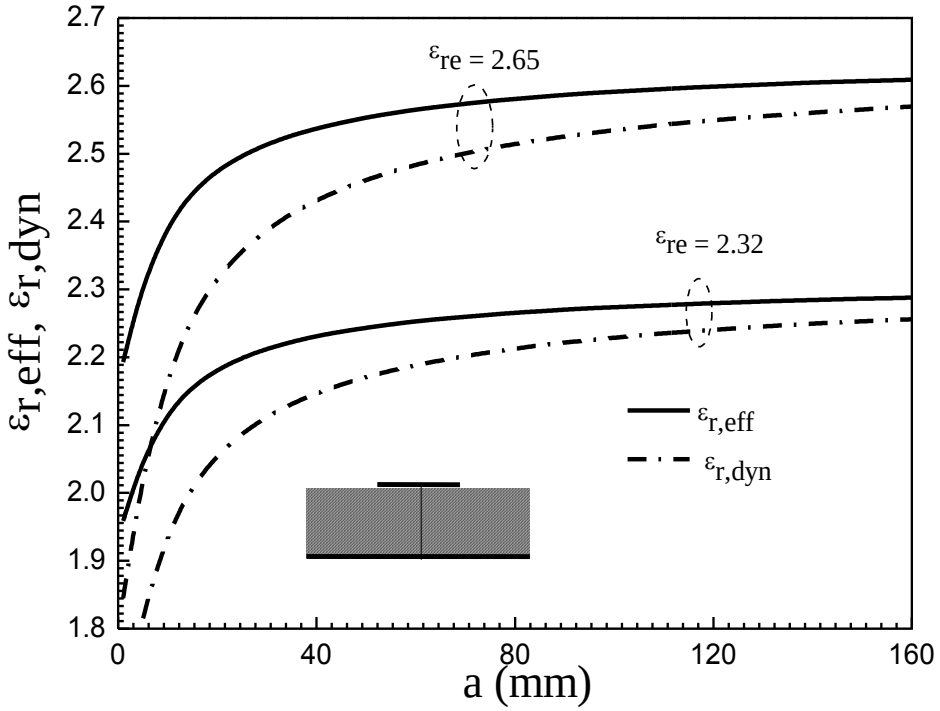

Figure 5.4: Variation of $\varepsilon_{r,dyn}$ and $\varepsilon_{r,eff}$ as a function of side length a for an 30^0-60^0-90^0 RATPA on single substrate. $h = h_2 = 0.8265$ mm.

Theoretically estimated and simulated [21, 22] resonant frequencies for this patch on composite and suspended substrate operated in different modes for different values of h_1 with fixed h_2 are shown in table 5.1. The theoretical and simulated values are quite correlated with each other for different value of h_1.

Theoretical variation of fringing fields factor q and the effective dielectric constant $\varepsilon_{r,eff}$ for this antenna on composite ($\varepsilon_{r1} = 4.4$) and suspended substrate ($\varepsilon_{r1} = 1.0$) as a function of h_1/h clearly depicted in Fig. 5.5. Here h_1 is variable but the total height h is fixed. The $\varepsilon_{r,eff}$ is enhanced for composite substrate and lowered for suspended substrate. Thus, q is reduced for composite substrate and enhanced for

suspended substrate patch antenna. These two parameters play very important roles in the performance of patch antenna and it is clearly established in subsequent study.

TABLE 5.1

COMPUTED AND SIMULATED RESONANT FREQUENCIES OF A RATPA (30^0-60^0-90^0) ON COMPOSITE AND SUSPENDED SUBSTRATE OPERATED IN DIFFERENT MODES.
a/h_2 = 83.4845, h_2 = 0.8265 mm, ε_{r2} = 2.4, $tan\delta_2$ = 0.0022, ρ, ϕ = 69.00, 20.00 mm

		Resonant frequency (GHz)					
h_1 **(mm)**	**Mode**	**Composite Substrate (ε_{r1} = 4.4, $tan\delta_1$ = 0.0035)** 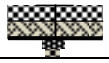			**Suspended Substrate (ε_{r1} = 1.0, $tan\delta_1$ = 0.000)** 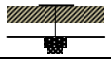		
		Computed	**HFSS [21]**	**IE3D [22]**	**Computed**	**HFSS [21]**	**IE3D [22]**
0.21	**$TM_{1,0,-1}$**	**1.516**	**1.524**	**1.512**	**1.781**	**1.773**	**1.776**
	$TM_{1,1,-2}$	**2.626**	**2.636**	**2.64**	**3.086**	**3.049**	**3.080**
	$TM_{2,0,-2}$	**3.043**	**3.021**	**3.032**	**3.572**	**3.494**	**3.530**
	$TM_{2,1,-3}$	**4.026**	**4.034**	**4.048**	**4.725**	**4.675**	**4.710**
	$TM_{3,0,-3}$	**4.578**	**4.533**	**4.584**	**5.369**	**5.260**	**5.310**
0.42	**$TM_{1,0,-1}$**	**1.463**	**1.477**	**1.480**	**1.886**	**1.877**	**1.869**
	$TM_{1,1,-2}$	**2.534**	**2.553**	**2.568**	**3.266**	**3.216**	**3246**
	$TM_{2,0,-2}$	**2.937**	**2.92**	**2.944**	**3.779**	**3.682**	**3.714**
	$TM_{2,1,-3}$	**3.886**	**3.904**	**3.928**	**5.000**	**4.932**	**4.965**
	$TM_{3,0,-3}$	**4.721**	**4.380**	**4.424**	**5.680**	**5.550**	**5.595**
0.66	**$TM_{1,0,-1}$**	**1.418**	**1.444**	**1.440**	**1.956**	**1.924**	**1.932**
	$TM_{1,1,-2}$	**2.456**	**2.488**	**2.496**	**3.387**	**3.321**	**3.354**
	$TM_{2,0,-2}$	**2.849**	**2.841**	**2.856**	**3.919**	**3.799**	**3.831**
	$TM_{2,1,-3}$	**3.769**	**3.798**	**3.824**	**5.184**	**5.097**	**5.127**
	$TM_{3,0,-3}$	**4.291**	**4.258**	**4.296**	**5.888**	**5.730**	**5.784**
0.8265	**$TM_{1,0,-1}$**	**1.394**	**1.422**	**1.419**	**1.987**	**1.964**	**1.959**
	$TM_{1,1,-2}$	**2.414**	**2.449**	**2.465**	**3.441**	**3.368**	**3.399**
	$TM_{2,0,-2}$	**2.802**	**2.794**	**2.814**	**3.981**	**3.85**	**3.885**
	$TM_{2,1,-3}$	**3.706**	**3.737**	**3.762**	**5.266**	**5.176**	**5.208**
	$TM_{3,0,-3}$	**4.220**	**4.186**	**4.227**	**5.980**	**5.807**	**5.865**

The variation of resonant frequency as a function of h_1/h with fixed h for composite and suspended substrate antenna is shown in Fig. 5.6. The resonant frequency decreases for composite substrate as the effective dielectric constant is enhanced whereas the resonant frequency increases for suspended substrate due to decrease of effective dielectric constant (as shown in Fig. 5.5) . The change of resonant frequency with h_1 provides frequency tunability feature of the antenna. The computed curves are compared with simulated results and shows very close agrement between them.

In table 5.2, we have compared simulated [21, 22] and our experimental resonant frequencies with theoretical values for suspended substrate antenna operated in different modes. The corresponding measured S_{11} (dB) is shown in Fig. 5.7. The computed resonant frequencies are closer to experimental and simulation results.

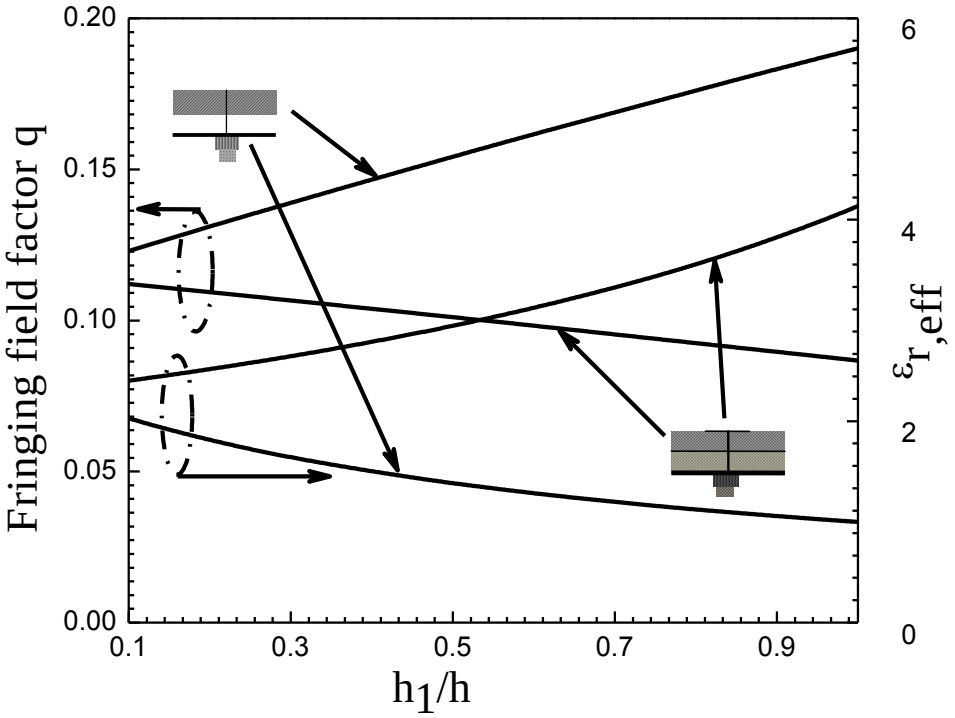

Figure 5.5: Theoretical variation of p and $\varepsilon_{r,eff}$ of a 30^0-60^0-90^0 RATPA on composite (ε_{r1} = 4.4) and suspended substrate (ε_{r1} = 1.0) with the variation of h_1/h. Parameters as in Figure 5.4.

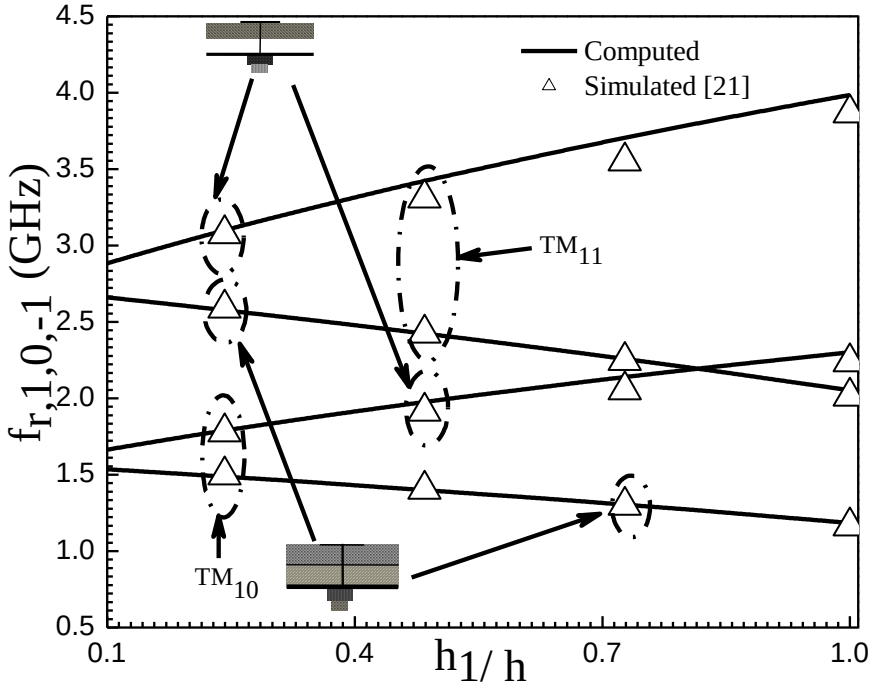

Figure 5.6: Software computational and theoretical variation of resonant frequency of a 30^0-60^0-90^0 RATPA on composite (ε_{r1} = 4.4) and suspended substrate (ε_{r1} = 1.0) operated in $TM_{1,0,-1}$ and $TM_{1,1,-2}$ mode as a function of h_1/h. . a/h = 41.8182, $h = h_1 + h_2$ = 1.65 mm, ε_{r2} = 2.4.

TABLE 5.2

COMPARISON OF EXPERIMENTAL [OUR], SIMULATION AND THEORETICAL RESONANT FREQUENCIES OF A RATPA (30^0-60^0-90^0) ON SUSPENDED SUBSTRATE OPERATED IN DIFFERENT MODES.

a/ h_2 = 83.4846, h_2 = 0.8265 mm, ε_{r1} = 1.0, ε_{r2} = 2.4, ρ, ϕ = 69.00, 20.00 mm

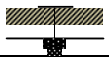

		Resonant frequency (GHz)			
h_1 (mm)	Mode	Exp	HFSS [21]	IE3D [22]	Computed
0.5	$TM_{1,0,-1}$	1.914	1.895	1.894	1.913
	$TM_{1,1,-2}$	3.274	3.305	3.289	3.314
	$TM_{2,0,-2}$	3.728	3.734	3.762	3.835
	$TM_{2,1,-3}$	5.173	5.001	5.026	5.073
	$TM_{3,0,-3}$	5.816	5.630	5.673	5.762
Avg. %Error with respect to Exp					1.401
Avg. %Error with respect to HFSS					1.542
Avg. %Error with respect to IE3D					1.241
1.0	$TM_{1,0,-1}$	2.007	1.986	1.990	2.009
	$TM_{1,1,-2}$	3.415	3.391	3.431	3.480
	$TM_{2,0,-2}$	3.960	3.897	3.915	4.026
	$TM_{2,1,-3}$	5.351	5.233	5.257	5.325
	$TM_{3,0,-3}$	5.983	5.874	5.917	6.047
Avg. %Error with respect to Exp					1.045
Avg. %Error with respect to HFSS					2.359
Avg. %Error with respect to IE3D					1.741

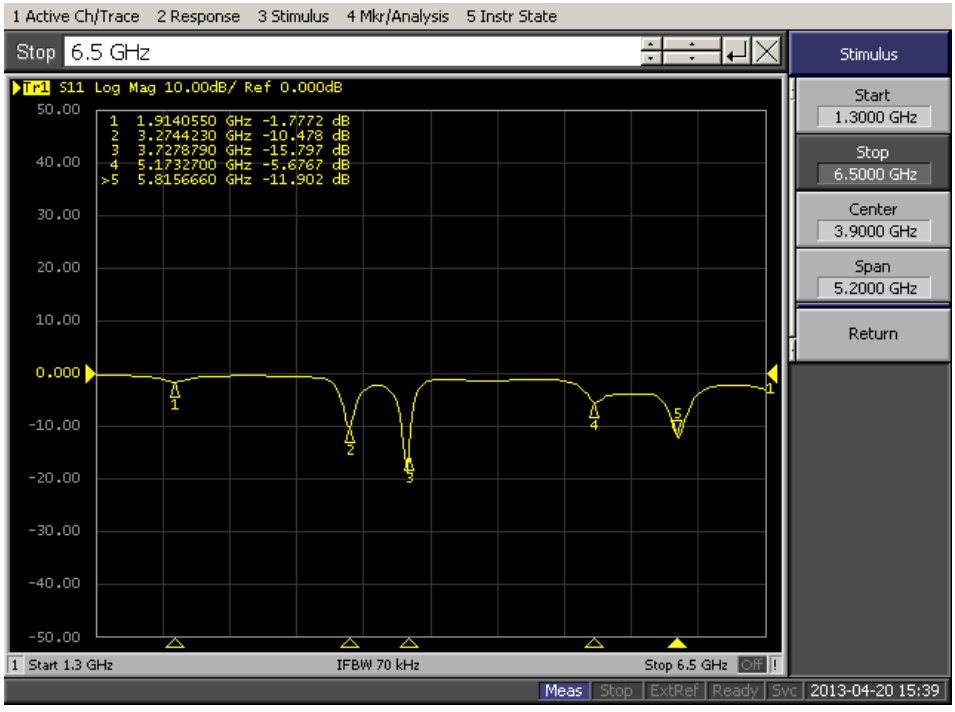

Figure 5.7: Measured S_{11} (dB) for suspended substrate 30^0-60^0-90^0 RATPA. *a*/*h* = 52.0166 mm, h_1 = 0.50 mm, h_2 = 0.8265 mm, $h = h_1 + h_2$, ε_{r1} = 1.0, ε_{r2} = 2.4.

The resonant frequency (f_r) of a patch antenna mainly depends on effective side length a_{eff} and effective permittivity $\varepsilon_{r,eff}$ as described in the section 5.2. So it is essential to compute both the parameters accurately. None of these two parameters was considered in [1] and treated as an inaccurate model. Whereas, the model reported in [2] considers only a_{eff}, so this model is also considered as a less accurate model. But we have considered these two (a_{eff} and $\varepsilon_{r,eff}$) parameters for computation of f_r. table 5.3 shows the comparison of theoretical resonant frequencies obtained by employing the present model and models reported in [1] and [2] for a patch printed on a substrate with simulation [21, 22] and our experimental results. The corresponding measured S_{11} (dB) is depicted in Fig. 5.8. The computed resonant frequencies employing the present model shows closer agreement with simulation and experimental results compared to other models.

TABLE 5.3

COMPARISON OF EXPERIMENTAL [OUR], SIMULATION AND THEORETICAL RESONANT FREQUENCIES OF A RATPA (30^0-60^0-90^0) ON A SUBSTRATE OPERATED IN DIFFERENT MODES.

h_1 = 0.0 mm, $h = h_1 + h_2$, ε_{r1} = 1.0

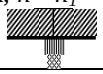

Resonant frequency (GHz)									
a/h	$\varepsilon_{r2} = \varepsilon_{re}$	h_2	**Mode**	**Exp**	**HFSS [21]**	**IE3D [22]**	**Computed**		
							Present	**[1]**	**[2]***
83.4846	2.4	0.8265	$TM_{10,-1}$	1.591	1.598	1.600	1.593	1.620	1.639
			$TM_{11,-2}$	2.765	2.744	2.776	2.759	2.807	2.839
			$TM_{20,-2}$	3.115	3.14	3.192	3.194	3.241	3.279
			$TM_{21,-3}$	4.233	4.209	4.240	4.226	4.287	4.338
			$TM_{30,-3}$	4.684	4.726	4.784	4.803	4.861	4.919
Avg. %Error with respect to Exp							1.116	2.488	3.691
Avg. %Error with respect to HFSS							0.922	2.319	3.521
Avg. %Error with respect to IE3D							0.368	1.324	2.513
81.9048	2.33	0.7875	$TM_{10,-1}$	1.726	1.727	1.735	1.727	1.759	1.779
			$TM_{11,-2}$	2.947	2.971	3.011	2.992	3.047	3.082
			$TM_{20,-2}$	3.426	3.417	3.456	3.464	3.518	3.559
			$TM_{21,-3}$	4.517	4.592	4.600	4.582	4.655	4.709
			$TM_{30,-3}$	5.094	5.141	5.182	5.208	5.278	5.339
Avg. %Error with respect to Exp							1.274	2.932	4.119
Avg. %Error with respect to HFSS							0.721	2.281	3.460
Avg. %Error with respect to IE3D							0.443	1.484	2.654
* ε_{re} is replaced by $\varepsilon_{r,eff}$									

Computed and simulated [21] variation of $TM_{1,0,-1}$ mode resonant frequency as a function of a for a single substrate antenna (h_1 = 0.0, ε_{r1} = 1.0) is visualized in Fig. 5.9. In this study, the antenna parameters are $h = h_2$ = 0.8265 mm and $\varepsilon_{re} = \varepsilon_{r2}$ = 2.4. The theoretical curve is compared with HFSS computational results [21] and the

comparison reveals good correlation between them for all values *a*. So, the present model is valid for a patch whose side length varies from very low to very high value.

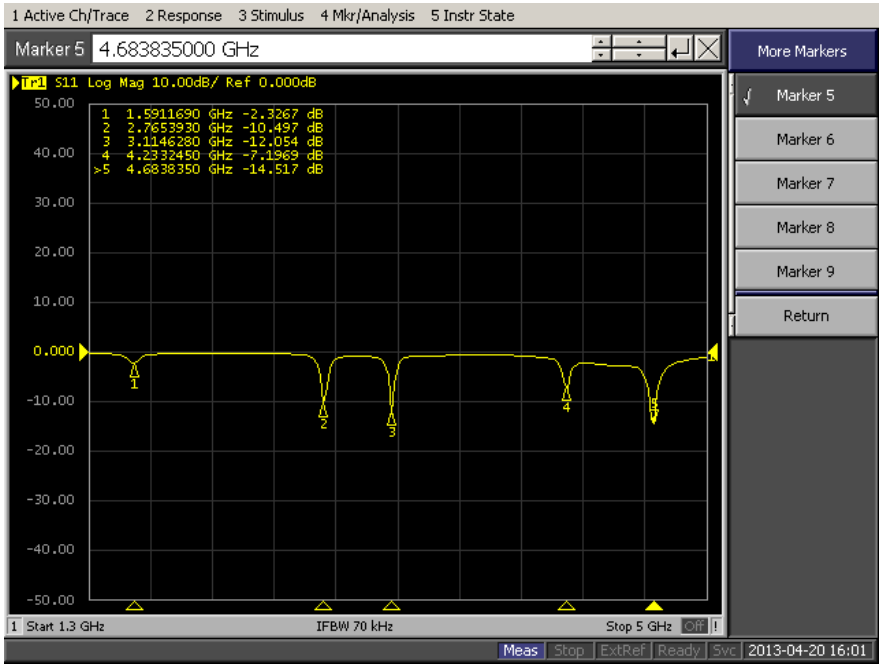

Figure 5.8: Measured S_{11} (dB) for single substrate 30^0-60^0-90^0 RATPA. a/h = 83.4845 mm, h_1 = 0.0 mm, h = h_2 = 0.8265 mm ε_{r1} = 1.0, ε_{re} = ε_{r2} = 2.4.

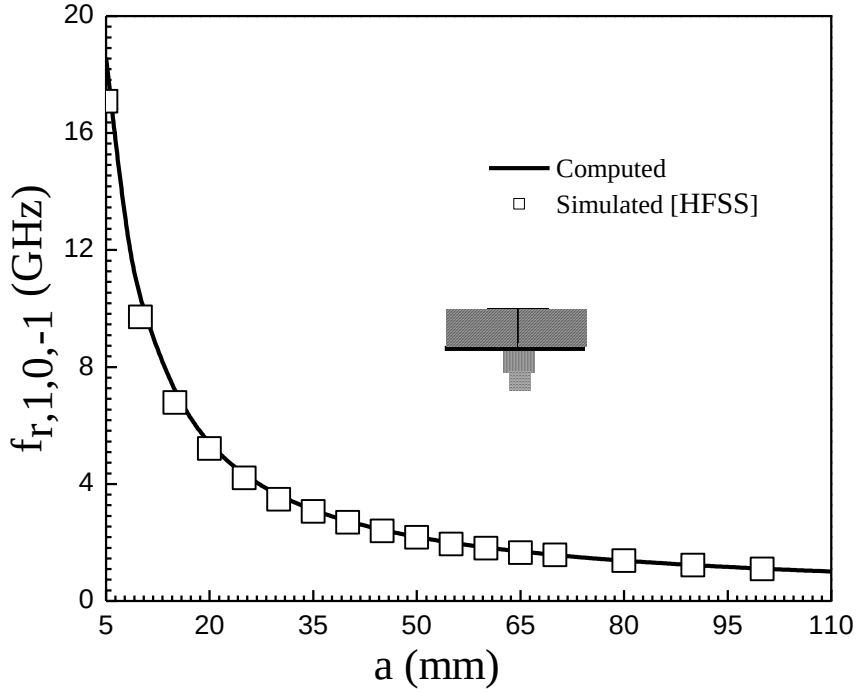

Figure 5.9: Software computational and theoretical variation of resonant frequency as a function of side length a for a 30^0-60^0-90^0 RATPA on single substrate operated in $TM_{1,0,-1}$ mode. h_1 = 0.0 mm, h = h_2 = 0.8265 mm, ε_{r1} = 1.0, ε_{re} = ε_{r2} = 2.4.

In Figure 5.10 we have compared the theoretically predicted resonant frequency curves with HFSS simulation [21] results as a function of substrate thickness $h = h_2$ for different dielectric constants ε_{re} of a single substrate antenna. Theoretical curves are close to the simulation results for wide variations of substrate thickness and permittivity.

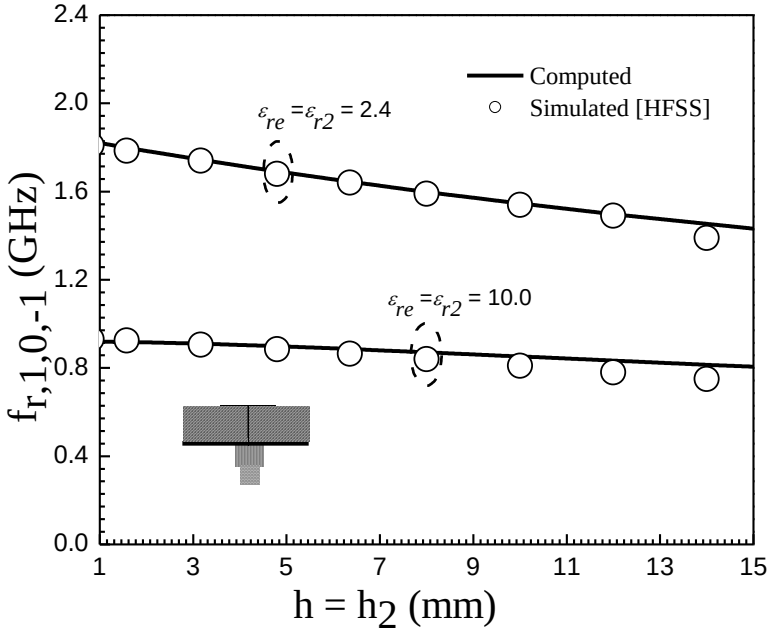

Figure 5.10: Theoretical and simulation variation of $TM_{1,0,-1}$ mode resonant frequency of 30^0-60^0-90^0 RATPA on single substrate as a function of h. a = 60.00 mm, h_1 = 0.0 mm, $h = h_2$, ε_{r1} = 1.0, ε_{r2} variable.

From this study we observe that the present model is well valid for an antenna whose side length a, thickness h and permittivity ε_{re} vary from very low to very high values.

As 30^0-60^0-90^0 RATPA is a resonant type narrow band antenna. So its performance mostly depends on the resonant frequency and its accurate estimation is essential. It is clear from the above observations that the present model is highly suitable for this work.

5.4.2. Quality factor and Bandwidth

The radiation performance of the antenna mainly depends on different loss mechanisms. So, the study of quality factors for different loss mechanisms is very important. Theoretically estimated Q_T and percentage bandwidth ($B.W$) for different values of a/h for composite, suspended and single substrate antenna are presented in

table 5.4. It is clear from this study that Q_T is increasing with the increase in *a/h* and as a result *B.W.* is decreasing. The computed Q_T employing the present model well supports the simulation [21] results for all values of *a/h*. So the present model is valid for an antenna having a side length that varies from very small to very large values.

TABLE 5.4
COMPUTED AND SIMULATED [21] VALUE OF Q_T AND PERCENTAGE B.W FOR DIFFERENT VALUE OF *a/h* 30^0-60^0-90^0 RATPA ON COMPOSITE, SUSPENDED AND SINGLE SUBSTRATE.
h = 1.65 mm, ε_{r2} = 2.4, ρ, ϕ = 69.00, 20.00 mm, $tan\delta_2$ = 0.0022.

a/h	Q_T						% B.W					
	Composite substrate		Suspended substrate		Single substrate		Composite substrate		Suspended substrate		Single substrate	
	I*	II**	I*	II**	I*	II**	I*	II**	I*	II**	I*	II**
6.061	32	30	11	12	22	23	2.21	2.32	6.31	5.89	3.22	3.06
12.121	55	51	23	26	41	43	1.29	1.39	3.12	2.72	1.74	1.64
18.182	73	76	34	38	57	65	0.97	0.93	2.09	1.86	1.23	1.09
24.242	87	89	45	47	72	79	0.81	0.79	1.58	1.49	0.98	0.90
30.303	98	105	55	59	85	91	0.72	0.67	1.29	1.19	0.83	0.78
36.364	107	110	65	71	96	103	0.66	0.64	1.09	0.99	0.74	0.69
42.424	115	116	74	79	106	107	0.62	0.61	0.96	0.90	0.67	0.66
48.485	121	11	82	87	114	116	0.59	0.59	0.86	0.81	0.62	0.61
60.606	130	129	98	105	128	127	0.55	0.55	0.72	0.67	0.55	0.56

I* : Computed
II** : Simulated (HFSS)
i) Composite substrate (ε_{r1} = 4.4, $tan\delta_1$ = 0.0035, h_1 = 1.2 mm, h_2 = 0.45 mm)
ii) Suspended substrate (ε_{r1} = 1.0, $tan\delta_1$ = 0.0, h_1 = 1.2 mm, h_2 = 0.45 mm)
iii) Single substrate (h_1 = 0.0 mm, ε_{r1} = 1.0, $h = h_2$ = 1.65 mm).

The validity of the present model for Q_T and percentage *B.W.* is further verified in Fig. 5.11. The variation of total quality factor Q_T and percentage *B.W.* with the variation of h_1/h for composite and suspended substrate is shown in Fig. 5.11. This study indicates that the quality factor (Q_T) increases for composite substrate and decreases for suspended substrate with the increase of h_1/h. Thus, the *B.W.* is lowered for composite substrate and enhances for suspended substrate with the increase of h_1/h. So, the improvement in bandwidth is observed when the high permittivity substrate is replaced by air substrate. The computed curves are well supported by the simulated [21] values.

The table 5.5 shows a comparison of experimental Q_T obtained from [2, 15] with computed Q_T employing the present model and the model reported in [2]. The model reported in [2] has employed large and rigorous mathematical steps. This comparison indicates that the present model more accurately computes the Q_T.

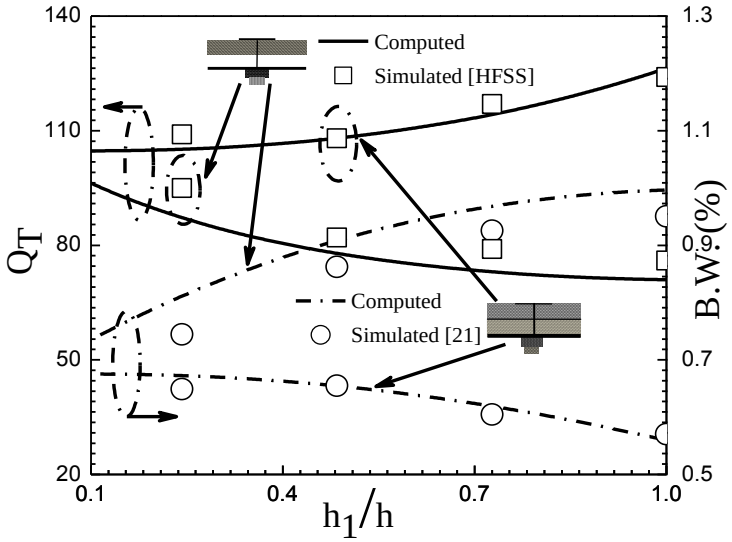

Figure 5.11: Computed and simulated variation of percentage B.W & Q_T with h_1 /h for a 30^0-60^0-90^0 RATPA on composite (ε_{r1} = 4.4, $tan\delta_1$ = 0.0035) and suspended substrate (ε_{r1} = 1.0, $tan\delta_1$ = 0.000). a/h = 41.8182, h = 1.65 mm, ε_{r2} = 2.4, ρ, ϕ = 69.00, 20.00 mm, $tan\delta_2$ = 0.0022.

The variation of Q_T as a function of a for different values of substrate permittivity ε_{re} and thickness h is depicted in Figs. 5.12 (a) and 5.12 (b) respectively. The model is validated with simulation results and good correlation is observed between them.

TABLE 5.5
COMPARISON OF EXPERIMENTAL AND THEORETICAL TOTAL QUALITY FACTORS OF A RATPA (30^0-60^0-90^0) ON A SUBSTRATE OPERATED IN DIFFERENT MODES.
h_1 = 0.0 mm, h= h_1 + h_2, ε_{r1} = 1.0, $tan\delta_1$ = 0.000

Ant.	a (mm)	Mode (m,n,l)	Total quality factor (Q_t)		
			Exp	Computed	
				Present	[2]
I	100	$TM_{1,0,-1}$	136.00	124.00	137.80
		$TM_{1,1,-2}$	126.00	113.00	124.90
		$TM_{2,0,-2}$	109.00	108.40	110.90
		$TM_{2,1,-3}$	111.70	97.60	112.90
		$TM_{3,0,-3}$	93.40	92.40	92.70
II	62.354	$TM_{1,0,-1}$	133.20	139.60	172.0
	60.622	$TM_{1,0,-1}$	126.47	138.30	171.0
	56.292	$TM_{1,0,-1}$	125.47	134.80	169.0
	51.962	$TM_{1,0,-1}$	120.35	130.70	166.0
	47.631	$TM_{1,0,-1}$	116.00	126.00	162.0
Total avg. %Error				7.220	18.239

* ε_{re} is replaced by $\varepsilon_{r,eff}$
I: h= h_2 = 0.762, ε_{r2} = 2.5, $tan\delta_2$ = 0.0035, ρ, ϕ = 10.00, 4.00 mm [2]
II: h= h_2 = 0.76, ε_{r2} = 2.34, $tan\delta_2$ = 0.0018 [15]

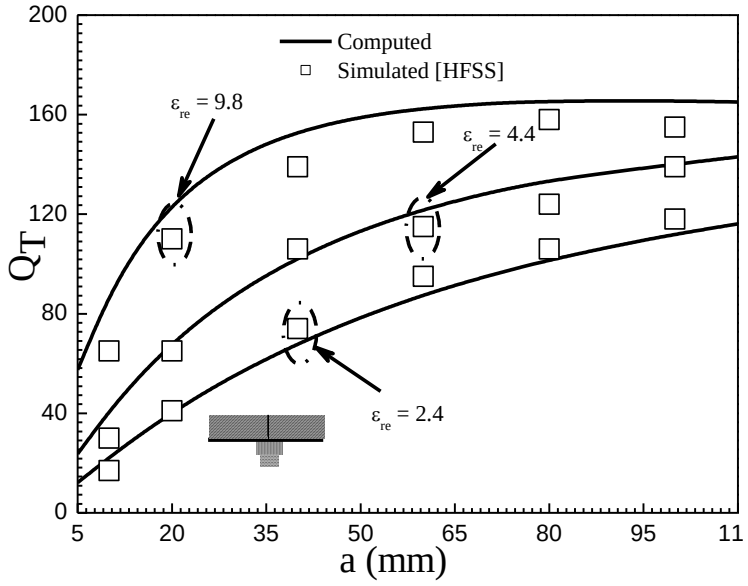

(a)

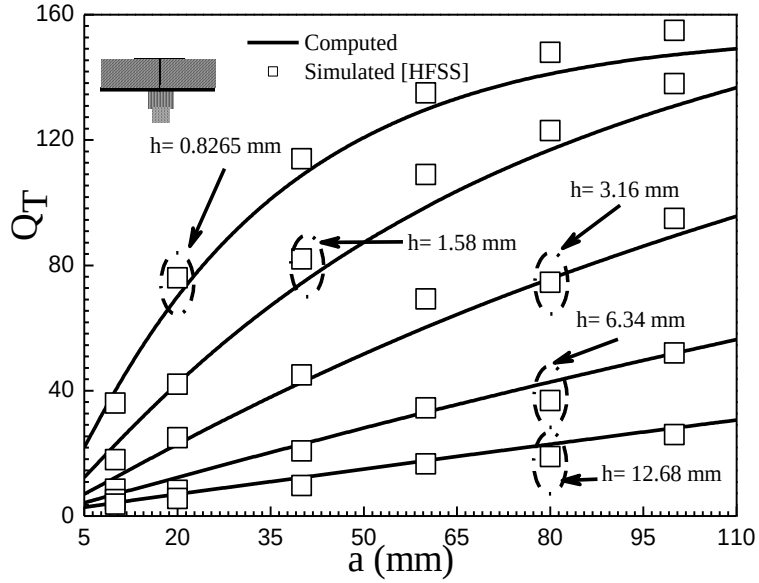

(b)

Figure 5.12: Computed and simulated variation of Q_T as a function of side length a for a 30^0-60^0-90^0 RATPA on single substrate.
(a) For different ε_{re} ($h = h_2 = 1.58$ mm)
(b) For different h ($\varepsilon_{re} = \varepsilon_{r2} = 2.4$)
$h_1 = 0.0$ mm, $h = h_2$, $\varepsilon_{r1} = 1.0$, $\varepsilon_{re} = \varepsilon_{r2}$, $tan\delta_2 = 0.0022$.

From the above studies, we conclude that the model developed for computing Q_T in this chapter is valid for an antenna whose side length a, thickness h and permittivity ε_{re} vary from very low to very high values.

5.4.3. Input impedance

Table 5.6 shows a comparative study of experimental input impedance [2, 15] with the theoretical values obtained by employing the model reported in [2] and the present model. The model reported in [2] has employed large and rigorous mathemateical steps. But here we have proposed a very simple model. The present model shows better accuracy compared to the model in [2].

TABLE 5.6

COMPARISON OF EXPERIMENTAL AND THEORETICAL RESONANT RESISTANCE OF A RATPA (30^0-60^0-90^0) ON A SUBSTRATE OPERATED IN DIFFERENT MODES.
a/h = 131.2335 , h_1 = 0.0 mm, $h = h_1 + h_2$, $h = h_2$ = 0.762, ε_{r1} = 1.0,
ε_{r2} = 2.5, $tan\delta_1$ = 0.000, $tan\delta_2$ = 0.0035, ρ, ϕ = 10.00, 4.00 mm

Mode (m,n,l)	Resonant Resistance(Ω)		
	Measured [2]	Computed	
		Present	[2]
$TM_{1,0,-1}$	1125	1118	1325
$TM_{1,1,-2}$	520	502	595
$TM_{2,0,-2}$	404	385	422
$TM_{2,1,-3}$	449	443	506
$TM_{3,0,-3}$	141	141	151
Avg. %Error		2.03	11.29

The computed TM_{10} mode input impedance curves as a function of frequency for composite substrate antenna are compared with simulated [21] curves in Fig. 5.13. The theoretical curves employing the present model exhibits good agreement with simulated [21] curves.

The input impedance of $TM_{1,0,-1}$ mode as a function of frequency for composite and suspended substrate antenna for different h_1 with fixed h_2 is shown in Fig. 5.14. It is observed that with the increase in h_1 both the resonant frequency and input impedance are considerably changed. The resonant frequency f_r and input impedance both increase for suspended substrate antenna whereas f_r decreases and input impedance increases for an antenna on composite substrate due to increase of h_1.

In Fig. 5.15 (a) and 5.15 (b), the theoretical and experimental $TM_{1,0,-1}$ mode input impedance curves are compared for the antenna printed on suspended substrate and single substrate respectively.

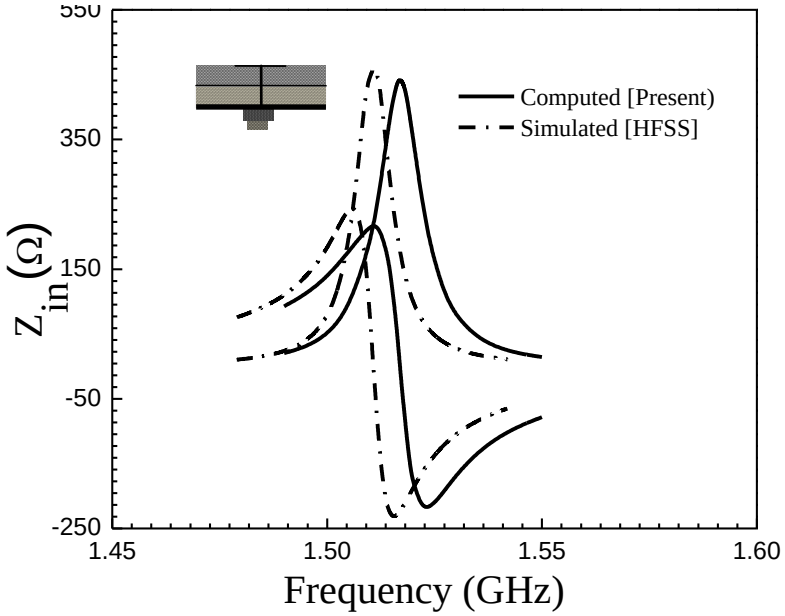

Figure 5.13: TM_{10} mode input impedance as a function of frequency for a 30^0-60^0-90^0 RATPA on composite (ε_{r1} = 4.4, $tan\delta_1$ = 0.0035) substrate. a/h = 66.5702, h_1 =0.21, h_2 = 0.8265 mm, h = 1.0365 mm, ε_{r2} = 2.4, ρ, ϕ = 69.00, 20.00 mm, $tan\delta_2$ = 0.0022.

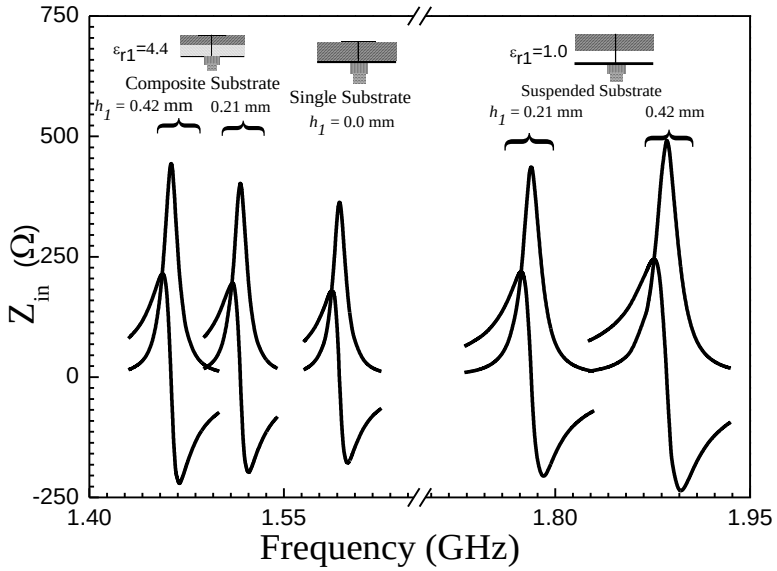

Figure 5.14: $TM_{1,0,-1}$ mode input impedance as a function of frequency for a 30^0-60^0-90^0 RATPA on composite (ε_{r1} = 4.4, $tan\delta_1$ = 0.0035) and suspended substrate (ε_{r1} = 1.0, $tan\delta_1$ = 0.000). a/h_2 = 83.4846, h_2 = 0.8265 mm, h_1 variable, ε_{r2} = 2.4.4, $tan\delta_2$ = 0.0022, ρ, ϕ = 69.00, 20.00 mm.

The parameters for this study are a = 69.00 mm, h_1 = 0.5 mm, h_2 = 0.8265 mm, ε_{r1} = 1.0, ε_{r2} = 2.4, ρ, ϕ = 69.00, 20.00 mm, $tan\delta_2$ = 0.0022. The corresponding measured impedance loci are shown in Fig. 5.16 (a) and 5.16 (b). The close agreement

is observed between them. The theoretical curves employing the present model exhibit very good agreement with experimental curves. It is clear from this study that the present model is not only valid for this patch on composite and suspended substrate but also well valid for a patch on single substrate.

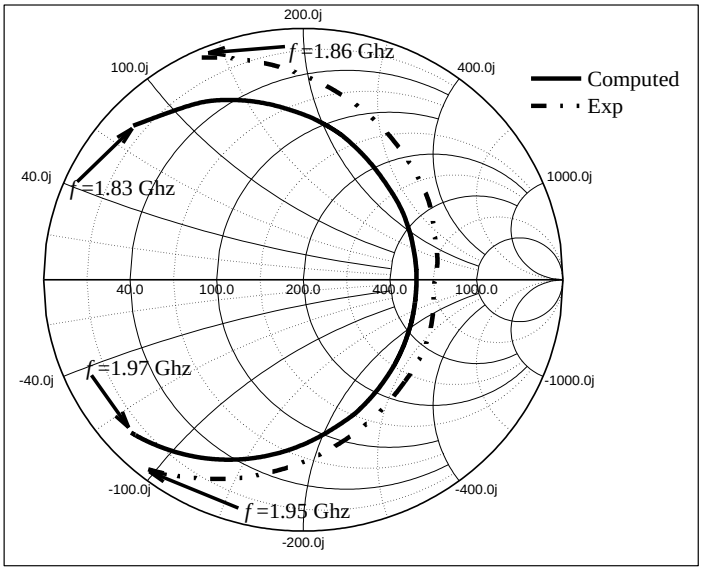

(a)

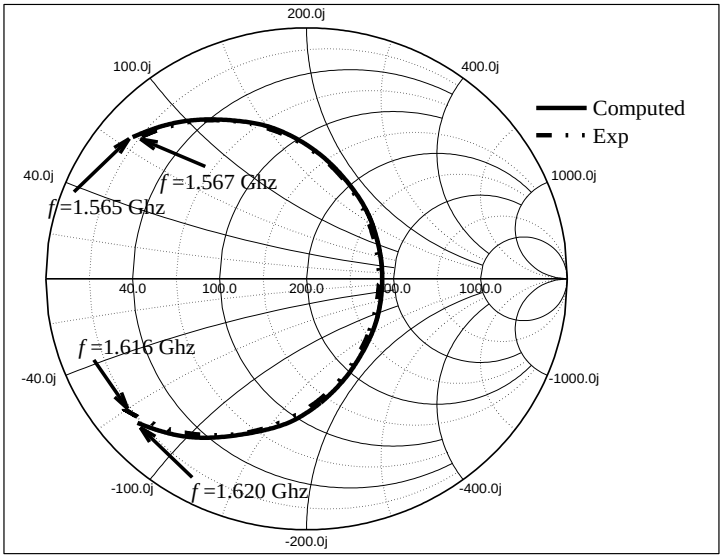

(b)

Figure 5.15: Measured [our] and computed TM_{10} mode input impedance loci of a RATPA on:
(a) Suspended substrate (h_1 = 0.5 mm, a/h = 52.0166)
(b) Single substrate (h_1 = 0.0 mm, a/h = 83.4846)
ε_{r1} = 1.0, ε_{r2} = 2.4, h_2 = 0.8265 mm, $h = h_1 + h_2$, ρ, ϕ = 69.00, 20.00 mm, $tan\delta_1$ = 0.000, $tan\delta_2$ = 0.0022.

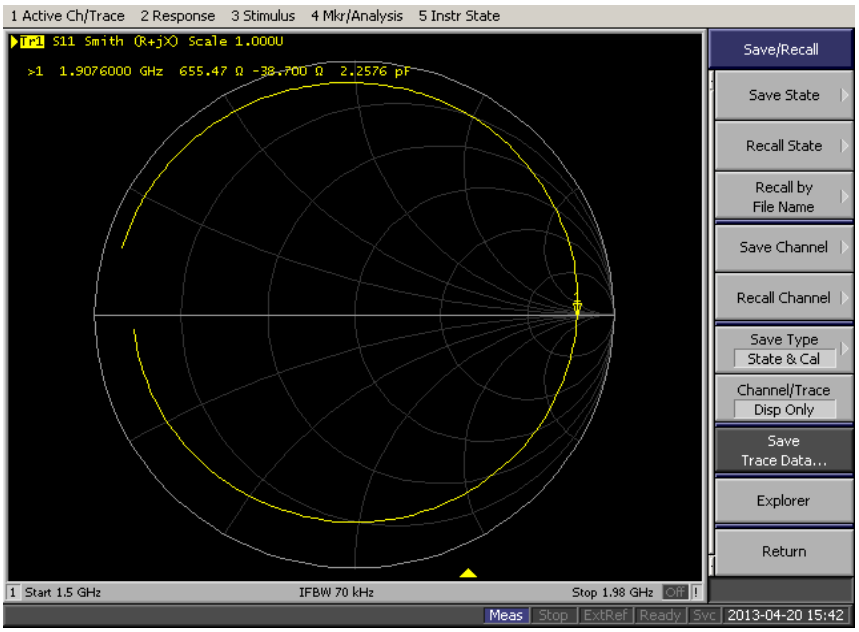

(a)

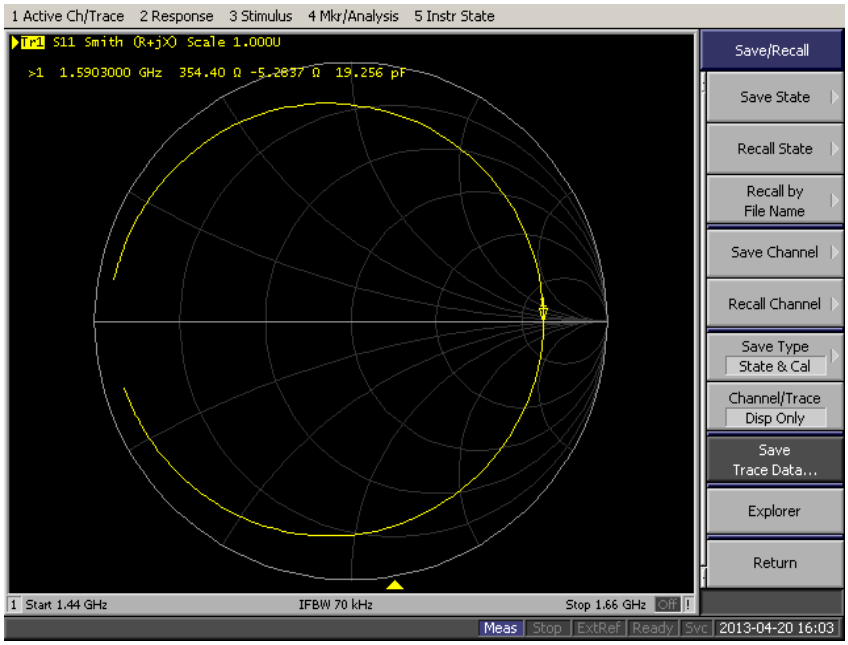

(b)

Figure 5.16: Snapshot of measured [our] input impedance loci of a RATPA on:
(a) Suspended substrate (h_1 = 0.5 mm, a/h = 52.0166)
(b) Single substrate (h_1 = 0.0 mm, a/h = 83.4846)
Parameter as in Fig.5.15

The present model is further verified with another experimental result in Fig. 5.17. This is a comparative study of computed and measured input impedance loci for a patch printed on a single substrate and very close agreement is revealed between them.

The theoretical, simulation and experimental variation of input resistance at resonance as a function of feed location for different modes are depicted in Fig. 5.18. The theoretical curves well support the experimental and simulation results.

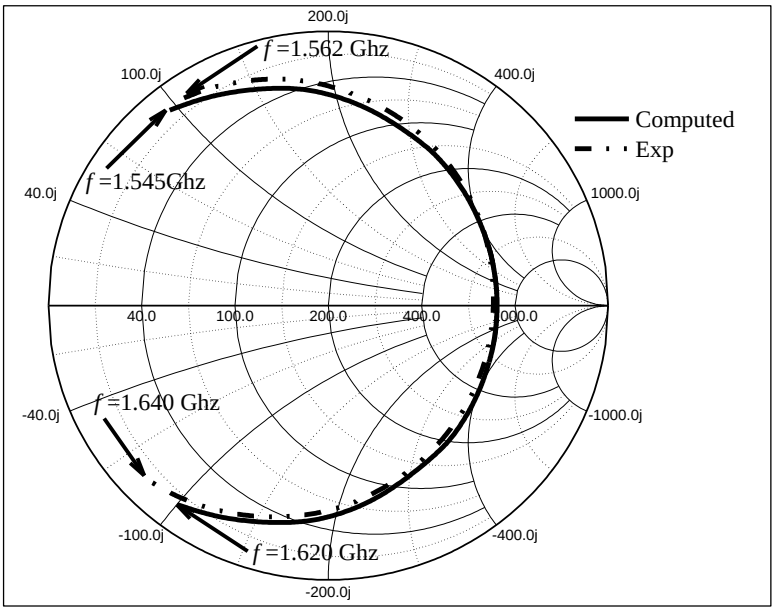

Figure 5.17: Measured [our] and computed TM_{10} mode input impedance loci for a single substrate antenna. a/h = 83.4846 mm, h_1 = 0.0 mm, $h = h_2$ = 0.8265 mm, ε_{r1} = 1.0, $\varepsilon_{re} = \varepsilon_{r2}$ = 2.4, ρ, ϕ = 25.00, 0.00 mm, $tan\delta_1$ = 0.000, $tan\delta_2$ = 0.0022.

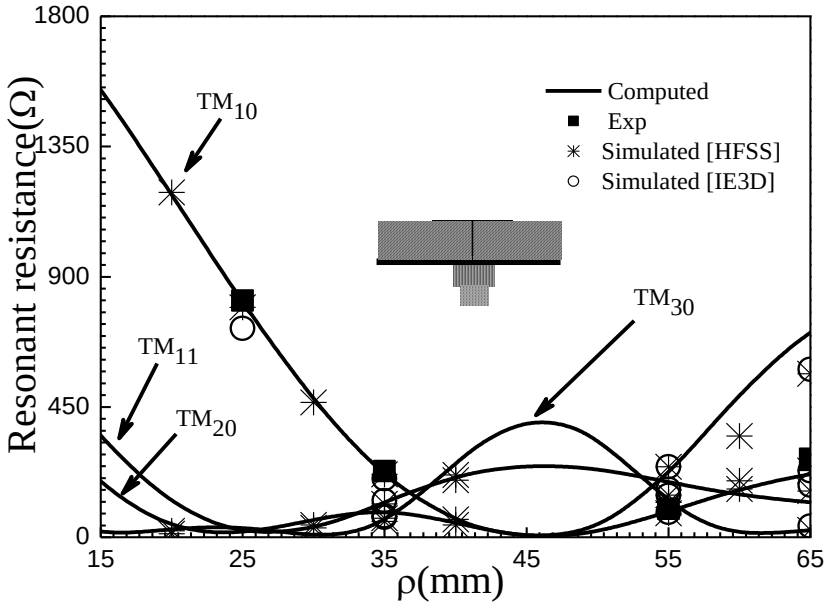

Figure 5.18: Measured [our], simulated and computed resonant resistance as a function of feed location for a single substrate antenna. a/h = 83.4846 mm, h_1 = 0.0 mm, $h = h_2$ = 0.8265 mm, ε_{r1} = 1.0, $\varepsilon_{re} = \varepsilon_{r2}$ = 2.4, ϕ = 0.00 mm, $tan\delta_1$ = 0.000, $tan\delta_2$ = 0.0022.

Some inherent errors occurred which cannot be avoided. These arise due to feed position, BNC connector, unintended fabrication and measurement process. The slight inconsistency is observed between theoretical and experimental results due to these errors.

5.4.4. Gain

Figure 5.19 depicts the variation of gain and effective side length for a 30^0-60^0-90^0 RATPA on composite and suspended substrate as a function of h_1/h. Theoretical curve for gain is compared with simulated [21] values and good correlation is found between them. This study shows that with the increase in h_1/h, the gain is decreased for composite substrate and increased for suspended substrate antenna. This is based on the fact that for the increase of h_1/h fringing field effect increases (as shown in Fig. 5.5); effective side length and aperture area increase, and therefore the gain is increased for suspended substrate. The exactly opposite phenomena is occurred for composite substrate antenna.

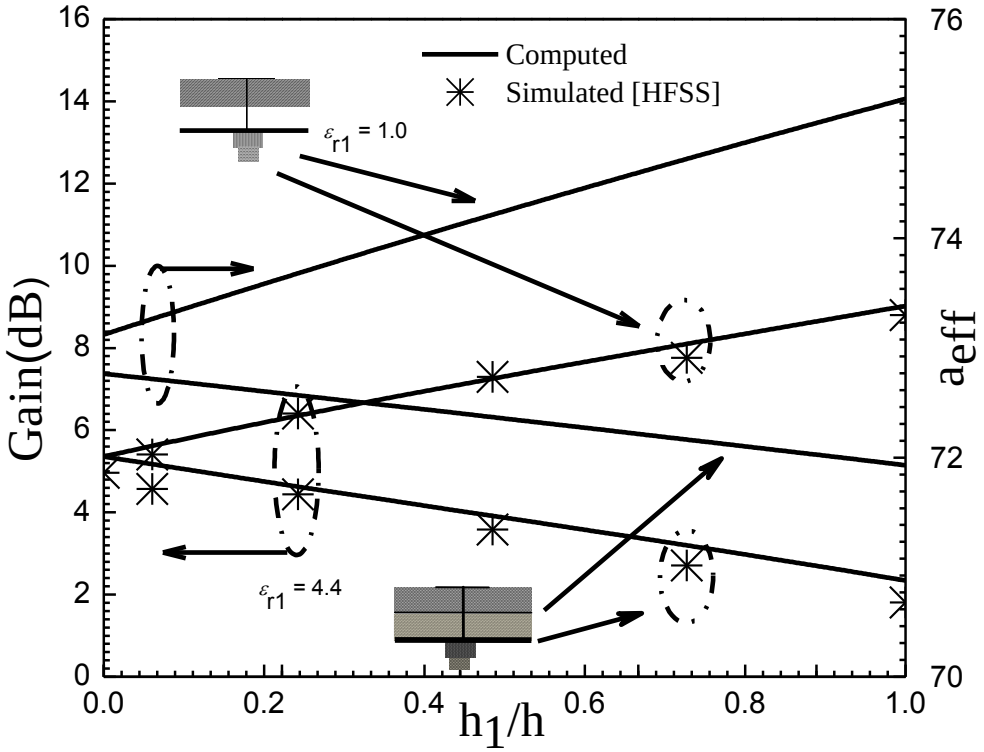

Figure 5.19: Variation of effective side length and gain of a 30^0-60^0-90^0 RATPA on composite (ε_{r1} = 4.4) and suspended substrate (ε_{r1} = 1.0) as a function of h_1/h. Parameter as in Fig.5.5.

In the above studies we conclude that the improvement in gain and bandwidth is possible by controlling the thickness of air gap in between the substrate and ground plane without altering the antenna parameters. This is the advantage of suspended substrate antenna.

5.5. Conclusion

In this chapter, we have presented an improved, fast and efficient CAD model based on cavity model analysis and also parallel resonant *R-L-C* circuit for computing the resonant frequency, quality factor, bandwidth, input impedance and gain of a probe fed 30^0-60^0-90^0 RATPA. In this work, we have properly accounted the fringing fields effect. The computed values employing the present model and other models are compared to experimental results available in open literature and our new experimental results. The present model shows very close agreements compared to the other model. This efficient model is capable of predicting accurately the resonant frequency, quality factor, bandwidth, input impedance and gain for wide variation of antenna size and substrates electrical parameters. This theoretical design guide line is very useful for practical implementation of 30^0-60^0-90^0 RATPA in portable wireless equipment.

REFERENCES

[1] M. M. Olaimat and N. I. Dib, "A study of 15^0-75^0-90^0 angles triangular patch antenna," *Prog. Electromag. Res. Lett.*, vol. 21, pp. 1-9, Feb. 2011.

[2] S. Maity and B. Gupta, "Cavity model analysis of 30°–60°–90° triangular microstrip antenna," *AEU-Int. J. Electron. Comm.*, vol. 69, pp. 923-932, 2015.

[3] Garg, P. Bhartia, I. J. Bahl, and A. Ittipiboon, "Microstrip antenna design handbook," *Artech house*, 2001.

[4] H. R. Hassani and D. M. Syahkal, "Analysis of triangular patch antennas including radome effects" *IEE Proc. H*, vol. 139, no. 3, pp.251-256, Jun. 1992.

[5] M. Biswas and D. Guha, **"**Input impedance and resonance characteristic of superstrate loaded triangular microstrip patch," *IET Microw. Antennas Propagat.*, vol. 3, pp. 92 – 98, Feb. 2009.

[6] K. J.-S. Hong and M.J. Lancaster, "Theory and experiment of dual-mode microstrip triangular patch resonators and filters," *IEEE Trans. Microw. Theory Tech.*, vol. 52, pp. 1237- 1243, Apr. 2004.

[7] J. T. S. Sumantyo, K. Ito, and M. Takahashi, "Dual-band circularly polarized equilateral triangular-patch array antenna for mobile satellite communications," *IEEE Trans. Antennas Propagat.*, vol. 53, pp. 3477- 3485, Nov. 2005.

[8] P. Mythili, A. Das, "Simple approach to determine resonant frequencies of microstrip antennas," *IEE Proc. Microw. Antennas Propagat.,* vol. 145, No. 2, April 1998.

[9] C. S. Gurel and E. Yazgan, "New computation of the resonant frequency of a tunable equilateral triangular microstrip patch," *IEEE Trans. Microw. Theory Tech.*, vol. 48, pp. 334-338, Mar. 2000.

[10] M.Biswas and A. Mandal, "CAD model to compute the input impedance of an equilateral triangular microstrip patch antenna with radome," *Prog. Electromag. Res. M.*, vol. 12, pp. 247-257, 2010.

[11] J. S. Dahele and K. F. Lee, "On the resonant frequencies of the triangular patch antenna," *IEEE Trans. Antennas Propagat.*, vol. 35, pp.100-101, 1987.

[12] K. F. Lee, K. M. Luk, and J. S. Dahele, "Characteristics of the equilateral triangular patch antenna," *IEEE Trans. Antennas Propagat.*, vol. 36, no.11, pp.1510-1518, Nov. 1988.

[13] W. Chen, K. F. Lee, and J. S. Dahele, "Theoretical and experimental studies of the resonant frequencies of equilateral triangular microstrip antenna," *IEEE Trans. Antennas Propagat.*, vol. 40, pp.1253-1256, Oct. 1992.

[14] Nasimuddin, K. Esselle, and A.K.Verma, "Resonant frequency of an equilateral triangular microstrip antenna," *Microw. Opt. Technol. Lett.*, vol. 47, no.5, pp.485-489, Dec. 2005.

[15] Y. Tu, "A study of triangular microstrip antennas," *MS thesis, Boulder (CO) University of Colorado,* Sep. 1983.

[16] P. L. Overfelt and D. J. White, "TE and TM Modes of some triangular cross-section waveguides using superposition of plane waves," *IEEE Trans. Microw. Theory Tech.*, vol. 34, pp. 161-167, Jan 1986.

[17] J. Zhang and J. Fu, "Comments on TE and TM modes of some triangular cross-section waveguides using superposition of plane waves," *IEEE Trans. Microw. Theory Tech.*, vol. 39, pp. 612-613, Mar. 1991.

[18] V. Losada, R. R. Boix, & M. Horno, "Resonant modes of circular microstrip patches in multilayered substrates," *IEEE Trans. Microw. Theory Tech*, vol. 47, pp. 488-498, Apr. 1999.

[19] R. M. Nelson, D. A. Rogers, and A. G. D Assuncio, "Resonant frequency of a rectangular microstrip patch on several uniaxial substrates," *IEEE Trans. Antennas Propagat.*, vol. 38, pp. 978-981, Jul. 1990.

[20] H.R. Hassani, and D. Mirshekar-Syahkal, "Full-wave analysis of stacked rectangular microstrip antennas," *Presented at 6th Int. Conf. Antennas and Propagat., IEE Conf. Publication* , vol. 301, pp. 369-373,Apr. 1989.

[21] HFSS 13: Ansoft's Corp.

[22] Integral Equation Three-Dimensional (IE3D) software.

[23] H. A. Wheeler, "A simple formula for the capacitance of a disc on dielectric on a plane," *IEEE Trans. Microwave Theory Tech.*, vol. 30, pp. 2050-2054, 1982.

[24] M. Biswas and S. Banik, "Characteristics of circular patch antenna with and without air gaps," *Microwave Opt. Technol. Lett.*, vol. 54, pp. 1692-1699, 2012.

[25] D.Guha, "Resonant frequency of circular microstrip antennas with and without air gaps," *IEEE Trans". Antennas and Propagat.*, vol. 49, no. 1, pp. 55-59, 2001.

[26] I. Wolff, N. Knoppik, "Rectangular and circular microstrip disk capacitors and resonators," *IEEE Trans. Microwave Theory Tech.*, vol. 22, pp. 857-864, 1974.

[27] A. G. Derneryd, "Microstrip disc antenna covers multiple frequencies," Microw. J., pp. 77-79, 2001.

[28] J. D. Mahony, "Approximate expressions for the directivity of a circular microstrip-patch antenna," *IEEE Antennas Propagat. Mag.*, vol. 43, no. 4, pp. 88-90, 2001.

CHAPTER 6

Investigation of Equilateral Triangular Patch Covered with Several Dielectric Layers: Resonance, Impedance, Bandwidth and Radiation Characteristics

Content:

6.1. Introduction

Today microstrip patch antenna has become essential component in microwave application due to its compact size, light weight and easy conformability. It finds extensive application in mobile, aircraft radome, missiles, radars, satellites and many useful sensors [1-11]. In outdoor application the patch antenna must be covered with dielectric layer to protect the patch against environmental hazards. The effective permittivity of the microstrip structure is changed due to the application of dielectric cover layer above the patch. Thus, the resonant frequency, quality factor, bandwidth, gain and input impedance are also changed. The antenna designed without consideration of these changes will not perform as expected once installed in wireless devices. The change in frequency of the patch antenna may be used to assess the relative permittivity of any dielectric layer in a multi dielectric structure. So, the accurate computation of resonant frequency is required to use the patch antenna as a sensor. The better impedance matching between co-axial probe and patch is required to obtain the maximum efficiency from the antenna. The input impedance as a function of probe location over its profile, substrate and cover layer parameters is the another basic design parameters. The efficiency may be calculated from the quality factors and the gain is related to the efficiency, the input impedance is related to the quality factor, frequency, resonant resistance and probe location under the patch. Thus, the accurate computation of frequency, quality factor, bandwidth, gain and input impedance of a co-axial probe fed equilateral patch antenna loaded with several dielectric layers are very important to install properly into wireless equipments.

Recently, equilateral triangular patch antenna (ETPA) finds many investigations in different areas of research [12-32]. Among them, most of the investigations have been concentrated on conventional patch printed on single layered [12-25] and double layered (suspended) substrate [26-28]. But triangular patch with dielectric cover layer finds very few investigations [29-32] so far. Among them, a chip resistor-loaded equilateral patch with a dielectric cover layer was reported in [29] for improving the gain. Another group of researchers [30] provides some theoretical results of an ETPA including radome using spectral domain technique analysis. This article [30] does not provide any closed form theoretical design guide line. Very recently, [31, 32] provides

the design guideline and experimental results for resonant frequency and input impedance of an ETPA covered with a dielectric layer. Here the conformal mapping approach and the cavity model analysis are used. These models [31, 32] have employed the rectified filling fraction for effective permittivity computation and minimize the effect of surface wave mode. But the models [31, 32] have some drawbacks: (i) show large error and error increases with the increase of permittivity of the structure, (ii) do not minimize the effect of leaky wave mode (iii) have not considered the effect of dielectric cover layer on the computation of quality factor which plays significant role in input impedance calculation (iv) the models are limited to only one dielectric cover layer. To the best of our knowledge neither any design guideline nor any experimental results for an ETPA with more than one dielectric cover layer is available in open literature.

The important parameters (resonant frequency, quality factor, input impedance bandwidth, directivity and gain) of an equilateral triangular patch antenna covered with one or more dielectric layers are calculated by the full wave method [30] and also by the commercial software [33]. But the full wave methods involve large and rigorous mathematical steps and it is computationally slow. Also, the numerical methods do not provide the closed form expressions and equivalent circuits for analysis. Therefore the numerical methods with high accuracy are not suitable for direct synthesis of patch antennas. The CAD oriented conformal mapping technique and cavity model analysis together are ideal for design purpose because they are very simple, fast and directly applied to the CAD program. The cavity model also provides the closed form expressions for design and equivalent circuits for analysis.

Considering these issues carefully, the purpose of this article is divided into two-fold objectives: i) we have proposed a simple model to determine accurately the resonant frequency, quality factor, bandwidth, gain and input impedance of an ETPA loaded with several dielectric layers. The model is based on the classical methods: (a) effective permittivity to take into account the influence of fringing field at the edge of the patch. We have employed the improved model reported in [5] for computing the effective permittivity of an ETPA in multi-dielectric layer, (b) effective side length to take into account the change of fringing field due to the imposition of dielectric cover layers. The

formula reported in [36] is employed to compute the effective side length of an ETPA loaded with several dielectric layers. We have modified the effective side length expression by incorporating the effect of surface wave as well as leaky wave modes, (c) the cavity model determining the resonant frequency and input resistance at resonance and (d) the equivalent resonant parallel *R-L-C* circuit for determination of input impedance. This model is capable of predicting accurately the resonant frequency, input impedance, quality factor, bandwidth and gain for wide variation of antenna geometric and electrical parameters of dielectric cover layers and (ii) we have performed several experiments to validate the model.

6.2 Theory

In this section a set of closed form expressions have been presented to compute the effective permittivity, effective side length, resonant frequency, quality factor, input impedance, bandwidth and gain for a probe fed ETPA covered with multi-dielectric layer.

6.2.1. Resonant frequency

The resonant frequency for an ETPA covered with several dielectric layers as shown in Fig. 6.1 can be expressed by the following formula for conventional patch as [15]:

$$f_{r,nml} = \frac{c}{a_{eff}\sqrt{3\varepsilon_{reff}}}\left(n^2 + nm + m^2\right)^{1/2} \tag{6.1}$$

where, c is the velocity of light in free space, $\varepsilon_{r,eff}$ is the effective relative permittivity of the multilayered structure , a_{eff} is the effective side length of the patch and m, n, l are the integers which are never zero simultaneously satisfying the condition $m + n + l = 0$.

6.2.2. Effective permittivity $\varepsilon_{r,eff}$

The fringing field between patch and ground plane is modulated due to the imposition of one or more dielectric layers above the patch and that effect is accounted for by the effective permittivity $\varepsilon_{r,eff}$. The effective permittivity for an ETPA covered with several dielectric layers is computed from originally formulated rectangular patch with length L and width W loaded with several dielectric layers [5] by employing an

equivalent relation between rectangular geometry and equilateral triangular geometry of side length a . Here we have used $W = 0.545a$ as considered in [31]. Thus, the $\varepsilon_{r,eff}$ for this structure under study is more explicitly written as [5]:

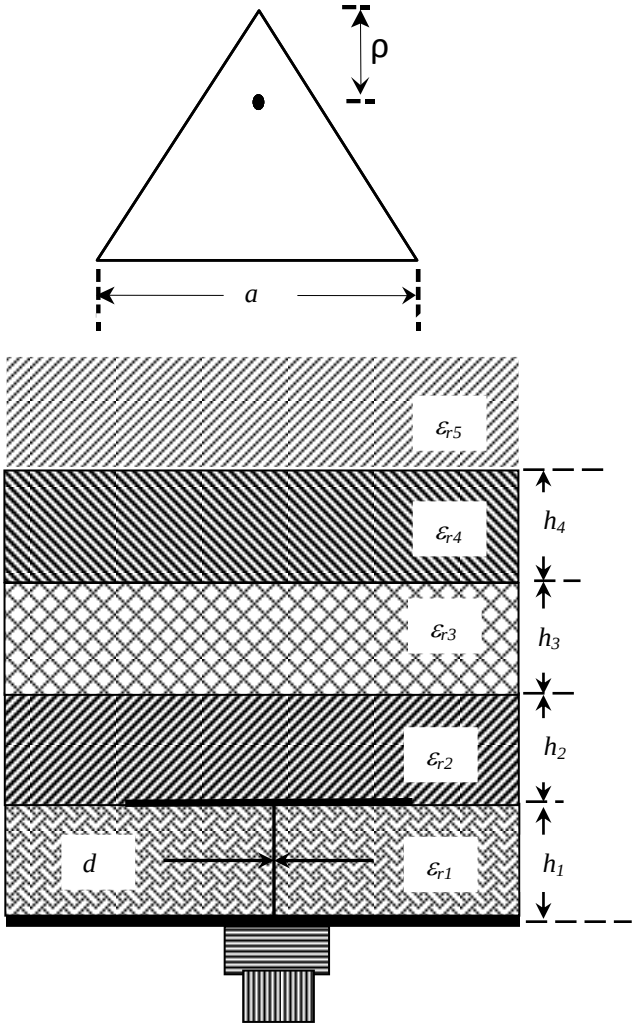

Figure 6.1: A schematic diagram of probe-fed equilateral triangular microstrip patch covered with several dielectric layers.

$$\varepsilon_{r,eff} = \varepsilon_{r1}\, p_{11} + \varepsilon_{r1} u \left(p_{22} + p_{33} + p_{44} + p_{55} + 4\, p_{20}\right)^2 \times \left[\varepsilon_{r1}\left(p_{22} + p_{33} + p_{44} + p_{55} + 3\, p_{20}\right)^2 + u p_{20}\right]^{-1} \tag{6.2}$$

$$u = \varepsilon_{r2}\, p_{22} + \varepsilon_{r2}\left(\varepsilon_{r3} p_{33} + v\right)\left(p_{33} + p_{44} + p_{55} + 3\, p_{20}\right)^2 \times \left[\varepsilon_{r2}\left(p_{33} + p_{44} + p_{55} + 2\, p_{20}\right)^2 + \left(\varepsilon_{r3} p_{33} + v\right) p_{20}\right]^{-1} \tag{6.3}$$

and

$$v = \varepsilon_{r3}\left[\varepsilon_{r4}\, p_{44} + \varepsilon_{r4}\,\varepsilon_{r5}\left(p_{55}+p_{20}\right)^2 \times \left(\varepsilon_{r4}\, p_{55} + \varepsilon_{r5}\, p_{20}\right)^{-1}\right] \times \left(p_{44}+p_{55}+2\,p_{20}\right)^2 \times \left\{\varepsilon_{r3}\left(p_{44}+p_{55}+p_{20}\right)^2 + p_{20} \times \left[\varepsilon_{r4}\, p_{44} + \varepsilon_{r4}\,\varepsilon_{r5}\left(p_{55}+p_{20}\right)^2 \times \left(\varepsilon_{r4}\, p_{55} + \varepsilon_{r5}\, p_{20}\right)^{-1}\right]\right\} \tag{6.4}$$

$$p_{11} = p_1 - 2\,p_{20} - p_{40} \tag{6.5}$$

$$p_{ii} = \left[1 - p_{11} - p_5 - 2p_{20} - p_{30} - p_{40}\right] \times \left(p_i - p_{i0}\right)\left[\sum_{j=2}^{4} p_j - p_{j0}\right]^{-1} \tag{6.6}$$

$i = 2,3,4$

$$p_{55} = 1 - \sum_{j=2}^{4} p_{jj} - p_{11} \tag{6.7}$$

$$p_{i0} = \frac{h_1}{2\Gamma}\left\{\ln\left(\frac{\pi}{h_1}\Gamma - 1\right) - \left(1+g_{i-1}\right) \times \ln\left[\frac{2\Gamma}{h_1}\frac{\cos\left(\frac{\pi}{2}g_{i-1}\right)}{\frac{2h_{i-1}}{h_1} - 1 + g_{i-1}} + \sin\left(\frac{\pi}{2}g_{i-1}\right)\right]\right\} \tag{6.8}$$

$i = 2,3,4$

$$g_i = \frac{2}{\pi}\arctan\left[\frac{\pi}{\frac{\pi}{2}\frac{\Gamma}{h_1} - 2}\left(\frac{h_i}{h_1}\right) - 1\right] \tag{6.9}$$

$$p_1 = 1 - \frac{h_1}{2\Gamma}\ln\left(\frac{\pi}{h_1}\Gamma - 1\right) \tag{6.10}$$

$$p_i = \frac{h_1}{2\Gamma}\left\{\ln\left(\frac{\pi}{h_1}\Gamma - 1\right) - \left(1+g_i\right) \times \ln\left[\frac{2\Gamma}{h_1}\frac{\cos\left(\frac{\pi}{2}g_i\right)}{\frac{2h_i}{h_1} - 1 + g_i} + \sin\left(\frac{\pi}{2}g_i\right)\right]\right\} \tag{6.11}$$

$i = 2,3,4$

$$p_5 = 1 - \sum_{j=2}^{4} p_j - p_1 \tag{6.12}$$

$$\Gamma = \sqrt{\frac{\varepsilon_{re}}{\varepsilon_{r,eff}}}\left[\left\{0.545\,a + 0.882\,h_1 + 0.164\,h_1\,\frac{(\varepsilon_{re}-1)}{(\varepsilon_{re})^2}\right\} + h_1\,\frac{(\varepsilon_{re}-1)}{\pi\varepsilon_{re}}\left\{\ln(0.94 + 0.545\,a/2\,h_1) + 1.451\right\}\right] \tag{6.13}$$

where,

$$\varepsilon_{re} = \frac{2\varepsilon_{r,eff} - 1 + \left(1 + \frac{10h_1}{\Gamma}\right)^{-1/2}}{1 + \left(1 + \frac{10h_1}{\Gamma}\right)^{-1/2}} \tag{6.14}$$

The final value of Γ and ε_{re} are determined by two step iteration as proposed in [35].

6.2.3 Effective side length a_{eff}

The actual side length a of the patch is extended due to the effect of fringing field at the edge of the patch. This fringing field very much depends on relative characteristics of substrate and dielectric cover layer. So, the accurate computation of effective side length a_{eff} is very important. The expression for a_{eff} may be expressed as

$$a_{eff} = a\left(1 + q\right)^{\frac{1}{2}} \tag{6.15}$$

In (6.15), q arises due to the fringing fields at the edge of the patch. The q for an ETPA may be obtained from originally formulated circular patch with radius r [36] by employing an equivalent relation between circular geometry and equilateral triangular geometry. Equal circumference is considered as the basis of equivalence as in [31]. The circumference of circular patch is $2\pi r$ and the circumference of ETPA is $3a$. So the equivalence relation between circular patch and equilateral triangular patch is obtained as $r = 3\,a/2\pi$. Now, based on equivalent relation q may be expressed for this geometry as

$$q = \frac{4h_1}{3a\,\varepsilon_r}\left[\log\left(\frac{3\,a}{4\pi\,h_1}\right) + 1.41\varepsilon_r + 1.77 + \frac{2\pi\,h_1}{3\,a}\left(0.268\,\varepsilon_r + 1.65\right)\right] \tag{6.16}$$

The relative permittivity of the substrate ε_r has been modified by Biswas [31, 32] in terms of fringing field to incorporate the effect of surface wave mode. They [31, 32] proposed an equivalent relative permittivity of the substrate below the patch in effective side length calculation as

$$\varepsilon_r = \frac{\varepsilon_{r1}}{\varepsilon_{r,eff}} \tag{6.17}$$

With this new relative permittivity the model is improved but shows higher error and the error increases with the increase of permittivity of the microstrip structure. Li [5] reported that the accuracy of the model is improved further by the consideration of leaky wave modes and the effect of leaky wave modes may be accounted as a similar manner of surface wave mode. Recently the effect of leaky waves on microstrip structure draws much attention of the researchers [37-40]. These studies show that the leaky wave has significant impact on antenna radiation characteristics. The research group [39, 40] showed that the leaky wave due to the leaky wave mode will be reduced to a great extent when the relative permittivity of dielectric cover layer is larger than substrate for some substrate and dielectric cover layer thickness combination. Based on these facts the leaky wave is also accounted in terms of fringing field. This fringing field very much depends on the relative characteristics of the substrate and dielectric cover layer. Based on these two facts (surface wave and leaky wave modes), we have proposed a new relative permittivity below the patch in terms of fringing field as

$$\varepsilon_r = \frac{\varepsilon_{re}}{\varepsilon_{r,eff}} \tag{6.18}$$

We have put this value of ε_r in equations (6.16).

6.2.4 Input Impedance

The triangular geometry may be treated as a single resonant parallel *R-L-C* circuit as shown in Fig. 6.2 to calculate the input impedance of an ETPA with and without dielectric cover layer. Thus, the input resistance and reactance is seen by a coaxial probe located at a distance ρ from tip of the triangle may be computed as

$$R_{in} = \frac{R_r P_{nml}}{1 + Q_T^2 \left[\frac{f_{r,nml}}{f} - \frac{f}{f_{r,nml}} \right]^2} \tag{6.19}$$

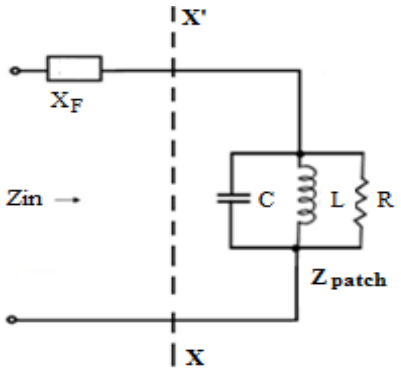

Figure 6.2: Equivalent resonant parallel *R-L-C* circuits of probe-fed equilateral triangular microstrip patch on multilayered structure.

$$X_{in} = X_f(f,\rho) + \frac{R_r P_{nml} Q_T \left[\frac{f_{r,nml}}{f} - \frac{f}{f_{r,nml}}\right]}{1 + Q_T^2 \left[\frac{f_{r,nml}}{f} - \frac{f}{f_{r,nml}}\right]^2} \tag{6.20}$$

where, P_{nml} is field factor and X_f *(f, ρ)* is the probe reactance. These two parameters are computed from equation (3.3) and (3.11) in chapter 3. R_r is the input resistance at resonance expressed as

$$R_r = \left(\frac{\eta\ \pi h_1 \lambda_{r,nm} Q_T}{\sqrt{2}\, a^2 \sqrt{\varepsilon_{r,eff}}}\right) \tag{6.21}$$

6.2.5 Total quality factor Q_T

The Q_T is defined as

$$Q_T = \left(\frac{1}{Q_r} + \frac{1}{Q_d} + \frac{1}{Q_c}\right)^{-1} \tag{6.22}$$

The accurate computation of Q_r is very important because it determines the radiation efficiency. The models reported in [31, 32] did not consider the effect of dielectric cover layers on Q_r. Very recently, the model reported in [34] showed that the Q_r of a rectangular patch antenna decreases with the increase of dielectric cover layer thickness and relative permittivity and vice-versa. This model [34] also provides the expression of Q_r including the dielectric cover layer effect. Based on this concept [34],

we have employed the expression of the Q_r for an ETPA loaded with one or more dielectric layers as:

$$Q_r = \frac{c\,\varepsilon_{r1}}{h_1\, f_{r,nm}\varepsilon_{r,eff}} - \left(\frac{h_4}{h_1}\right)\left(\frac{\varepsilon_{r,eff}}{\varepsilon_{r1}}\right) \tag{6.23}$$

The Q_c can be expressed as

$$Q_c = \frac{\pi\sqrt{\varepsilon_{r,eff}}}{\lambda_{r,nml}\,\alpha_c} \tag{6.24}$$

α_c is the conductor loss and obtained from [41] as

$$\alpha_c = \frac{R_s}{Z\left(\frac{a}{h_1}, h_1, \varepsilon_{reff}\right)0.545a} \tag{6.25}$$

$$Z\left(\frac{a}{h_1}, h_1, \varepsilon_{reff}\right) = \frac{120\pi}{\sqrt{\varepsilon_{reff}}}\left[\frac{0.545a}{h_1} + 1.393 + 0.667\ln\left(\frac{0.545a}{h_1} + 1.444\right)\right]^{-1} \tag{6.26}$$

$$R_s = \sqrt{\frac{\pi\, f_{r,nml}\,\mu_0}{\sigma}} \tag{6.27}$$

where, σ is the conductivity and other variables have usual meaning.

Q_d for this structure can be computed as

$$Q_d = \frac{1}{\tan\delta_e} \tag{6.28}$$

where, $tan\delta_e$ is the equivalent loss tangent of a triangular patch in multilayered media. The $tan\delta_e$ is defined as

$$\tan\delta_e = \frac{p_1\,\varepsilon_{r1}\tan\delta_1 + p_2\,\varepsilon_{r2}\tan\delta_2 + p_3\,\varepsilon_{r3}\tan\delta_3 + p_4\,\varepsilon_{r4}\tan\delta_4}{\varepsilon_{re}} \tag{6.29}$$

ε_{re} is given in (6.14)

6.2.6. Bandwidth and Gain

Percentage bandwidth (V.S.W.R < 2) of the antenna is calculated as

$$\frac{1}{\sqrt{2}Q_T}100\% \tag{6.30}$$

The gain (G) for the structure under study can be expressed as

$$G = \frac{Q_T}{Q_r} D(\delta)\left(\frac{\varepsilon_{re}}{\varepsilon_{r,eff}}\right)^2 \tag{6.31}$$

where, $D(\delta)$ is the directivity of the structure under the study. This can be computed from chapter 2 (equation 2.28).

6.3 Patch fabrication and experimental tests

A number of prototypes of different a have been etched on various dielectric substrates. The dielectric substrates are from Taconic, Rogers, Glass Epoxy and Arlon etc. with different thickness and relative permittivity as given in table 6.1. These materials are also used as a dielectric cover layer. A typical experimental setup with fabricated prototypes with and without dielectric cover layer is shown in Fig. 6.3. The patch was excited with a coaxial probe whose diameter d = 1.24 mm. To validate the model developed in section 6.2. We have performed a series of experiments using Network Analyzer Agilent- E5071B.

TABLE 6.1

RELATIVE PERMITTIVITY AND DIELECTRIC LOSS TANGENT OF THE DIELECTRIC TEST MATERIAL

Sl. No.	Dielectric materials properties		
	Thickness	ε_{r1}	Dielectric loss tangent ($\tan\delta_1$)
1	0.508	2.2	0.0009
2	0.7875	2.33	0.0010
3	1.575	2.33	0.0010
4	0.8265	2.4	0.0022
5	1.58	2.4	0.0022
6	1.51	1.26	0.0008
7	2.33	2.55	0.0016
8	1.63	5.0	0.0200
9	1.4	5.6	0.0200
10	1.63	10.0	0.0035

(a)

(b)

Figure 6.3: Typical experimental setup used for the determination of resonant frequency and input impedance of an ETPA. (a) Fabricated prototype without cover, (b) Fabricated prototype with cover layer.

6.4 Results and discussions

We have presented theoretically predicted, simulated and measured results for the resonant frequency, quality factor, bandwidth, gain and input impedance of an ETPA covered with several dielectric layers.

6.4.1 Resonant frequency

6.4.1.1 Patch covered with three dielectric layers

In table 6.2, 6.3 and 6.4 we have compared simulated (HFSS) and measured resonant frequencies with theoretical values employing the present model of an ETPA covered with three dielectric layers.

Table 6.2 presents the results of an ETPA for different sets of second dielectric cover layer parameters (ε_{r3} and h_3). The results of an ETPA for different sets of top dielectric cover layer parameters (ε_{r4} and h_4) are shown in table 6.3. The accuracy of the present model for an ETPA for different sets of dielectric cover layer parameters is further verified in table 6.4. Here the second dielectric cover layer is replaced by air dielectric whose thickness is wide variable.

TABLE 6.2
COMPARISON OF THEORETICALLY PREDICTED RESONANT FREQUENCIES FOR AN EQUILATERAL TRIANGULAR PATCH COVERED WITH VARIUS THREE LAYER DIELECTRIC STRUCTURES WITH HFSS SIMULATION AND EXPERIMENTAL [OUR] RESULTS. THESE THREE LAYER DIELECTRIC STRUCTURE ARE WITH DIFFERENT a, ε_{r1}, ε_{r2}, ε_{r3}, ε_{r4}, h_1, h_2, h_3, h_4, ε_{r5} = 1.0

a (mm)	ε_{r1} ε_{r2} ε_{r4}	h_1 h_2 h_4 (mm)	ε_{r3}	h_3 (mm)	Resonant frequency(GHz)		
					EXP.	HFSS [33]	Model
42.00	ε_{r1} = 2.4 ε_{r2} = 2.33 ε_{r4} = 2.4	h_1 = 0.8265 h_2 = 0.7875 h_4 = 0.8265	2.2	0.508	2.885	2.870	2.887
			2.4	0.8265	2.884	2.862	2.884
			2.4	1.58	2.875	2.853	2.881
			2.33	1.575	2.866	2.854	2.882
			5.0	1.63	2.834	2.796	2.836
			10.0	1.63	2.726	2.713	2.761
23.00	ε_{r1} = 1.30 ε_{r2} = 2.4 ε_{r4} = 2.33	h_1 = 1.58 h_2 = 0.8265 h_4 = 0.7875	2.2	0.508	5.897	5.901	5.891
			5.6	1.40	5.38	5.434	5.436
			2.33	1.575	5.739	5.772	5.813
			5.0	1.63	5.421	5.441	5.455
			10.0	1.63	4.947	4.985	4.957
			2.55	2.33	5.642	5.729	5.733
	ε_{r1} = 1.30 ε_{r2} = 2.4 ε_{r4} = 2.33	h_1 = 1.58 h_2 = 0.8265 h_4 = 1.575	2.2	0.508	5.873	5.830	5.859
			5.6	1.40	5.39	5.398	5.435
			2.33	1.575	5.773	5.797	5.788
			5.0	1.63	5.451	5.509	5.452
			10.0	1.63	4.939	5.023	4.982
			2.55	2.33	5.681	5.695	5.713

It is clear from these comparison that the computed resonant frequencies employing the present model shows excellent agreement with HFSS and experimental results for wide variation of dielectric cover layer thickness and permittivity ($(1.0 \leq \varepsilon_r \leq 10.0)$.

TABLE 6.3

COMPARISON OF THEORETICALLY PREDICTED RESONANT FREQUENCIES FOR AN EQUILATERAL TRIANGULAR PATCH COVERED WITH VARIUS THREE LAYER DIELECTRIC STRUCTURES WITH HFSS SIMULATION AND EXPERIMENTAL [OUR] RESULTS. THESE THREE LAYER DIELECTRIC STRUCTURE ARE WITH DIFFERENT a ε_{r1}, ε_{r2}, ε_{r3}, ε_{r4}, h_1, h_2, h_3, h_4

a (mm)	ε_{r1} ε_{r2} ε_{r3}	h_1 h_2 h_3 (mm)	ε_{r4}	h_4 (mm)	Resonant frequency (GHz)		
					Exp.	HFSS [33]	Model
42.00	ε_{r1} = 2.4 ε_{r2} = 2.33 ε_{r3} = 2.4	h_1 = 0.8265 h_2 = 0.7875 h_3 = 0.8265	2.2	0.508	2.891	2.863	2.887
			2.4	0.8265	2.884	2.862	2.884
			2.4	1.58	2.862	2.851	2.881
			2.33	1.575	2.876	2.854	2.882
			5.0	1.63	2.844	2.82	2.850
			10.0	1.63	2.795	2.766	2.800
23.00	ε_{r1} = 1.30 ε_{r2} = 2.33 ε_{r3} = 2.4	h_1 = 1.58 h_2 = 0.7875 h_3 = 0.8265	2.2	0.508	5.812	5.915	5.885
			2.4	0.8265	5.808	5.871	5.858
			2.33	1.575	5.795	5.818	5.836
			2.55	2.33	5.693	5.743	5.782
			5.0	1.63	5.585	5.557	5.560
			5.6	1.4	5.577	5.551	5.541
			10.0	1.63	5.235	5.195	5.178
ε_{r5} = 1.0							

TABLE 6.4

COMPARISON OF THEORETICALLY PREDICTED RESONANT FREQUENCIES FOR AN EQUILATERAL TRIANGULAR PATCH COVERED WITH VARIUS THREE LAYER DIELECTRIC STRUCTURES WITH HFSS SIMULATION AND EXPERIMENTAL [OUR] RESULTS. THESE THREE LAYER DIELECTRIC STRUCTURE ARE WITH DIFFERENT a, ε_{r1}, ε_{r4}, h_1, h_3.

a (mm)	ε_{r1}	h_1 (mm)	ε_{r4}	h_4 (mm)	h_3 (mm)	Resonant frequency (GHz)		
						Exp.	HFSS [33]	Model
23.0	1.3	1.58	2.33	1.575	2	5.866	5.935	5.955
					3	5.882	5.953	5.973
					5	5.887	5.981	6.003
					7	5.917	6.004	6.027
					9	5.991	6.010	6.044
			5.6	1.4	2	5.694	5.832	5.768
					3	5.851	5.908	5.808
					5	6.012	6.030	5.873
					7	6.050	6.062	5.923
					9	6.058	6.070	5.961
42.0	2.4	0.8265	2.33	1.575	2	2.885	2.869	2.901
					5	2.893	2.875	2.910
					7	2.896	2.876	2.915
					9	2.921	2.877	2.918
			5.6	1.4	2	2.881	2.857	2.882
					5	2.883	2.869	2.897
					7	2.887	2.871	2.904
					9	2.910	2.873	2.909
h_2 = 1.575 mm, ε_{r2} = 2.33, ε_{r3} = ε_{r5} = 1.0								

6.4.1.2 Patch covered with two dielectric layers

In table 6.5, we have compared simulated (HFSS) and measured resonant frequencies with theoretical values for an ETPA having variable side length printed on different substrate covered with two dielectric layers. Here the wide variations of second

cover layer permittivity (ε_{r3}) have been taken. It is observed that the computed resonant frequencies employing the present model are in close correlation with simulation and experimental results.

TABLE 6.5

COMPARISON OF THEORETICALLY PREDICTED RESONANT FREQUENCIES FOR AN EQUILATERAL TRIANGULAR PATCH COVERED WITH VARIUS TWO LAYER DIELECTRIC STRUCTURES WITH HFSS SIMULATION AND EXPERIMENTAL [OUR] RESULTS. THESE TWO LAYER DIELECTRIC STRUCTURES ARE WITH DIFFERENT a, ε_{r1}, ε_{r2}, ε_{r3}, h_1, h_3.

a (mm)	ε_{r1}	h_1 (mm)	ε_{r2}	h_2 (mm)	ε_{r3}	h_3 (mm)	Resonant frequency (GHz)		
							Exp.	HFSS [33]	Computed Present
42.0	2.4	0.8265	2.33	0.7875	2.4	0.8265	2.844	2.878	2.893
					2.55	2.33	2.864	2.863	2.882
			5.0	1.63	2.33	0.7875	2.828	2.753	2.798
					2.4	1.58	2.807	2.713	2.796
32.0	2.4	1.58	2.2	0.508	5.0	1.63	3.515	3.464	3.440
					5.6	1.4	3.524	3.462	3.427
					2.33	1.575	3.615	3.602	3.575
					2.55	2.33	3.587	3.569	3.553
			2.33	1.575	2.2	0.508	3.592	3.594	3.575
					2.33	1.575	3.57	3.561	3.562
					2.55	2.33	3.547	3.536	3.547
					10	1.63	3.405	3.382	3.339
			5.6	1.4	2.2	0.508	3.435	3.335	3.367
					2.33	1.575	3.405	3.318	3.366
					10	1.63	3.225	3.050	3.135
					2.55	2.33	3.367	3.297	3.356
23.0	1.3	1.58	2.33	0.7875	2.2	0.508	5.993	6.039	5.985
					2.4	0.8265	5.887	5.979	5.937
					2.33	1.575	5.875	5.893	5.891
					2.55	2.33	5.720	5.781	5.802
					5	1.63	5.473	5.497	5.489
					5.6	1.40	5.527	5.586	5.463
					10	1.63	4.988	5.070	4.938
$\varepsilon_{r4} = \varepsilon_{r5} = 1.0$									

The accuracy of the present model for an ETPA covered with two dielectric cover layers for different substrates and dielectric cover layer combination is further verified in table 6.6. Here first dielectric cover layer is considered as an air dielectric. Comparison shows that the theoretical results are in good correlation with HFSS and experimental results.

6.4.1.3. Patch covered with single dielectric layer

In table 6.7, the computed resonant frequencies employing the present model and model reported in [31] for an ETPA covered with single dielectric layer has been compared with simulated (HFSS) and experimental results. This comparison shows that computed resonant frequencies employing the present model are in good agreement with

simulation and measured results compared to [31]. Here the average error with respect to experiment for the model reported in [31] is near about 9%, whereas the average error employing present model is 0.8%. So, excellent improvement in computation of resonant frequency is achieved in the present work. This is based on the following facts: (i) the model reported in [31] has been employed an effective permittivity expression reported in [35], which shows better result for low permittivity structure but shows higher error for higher permittivity structure. But the present model employs the model reported in [5] for effective permittivity calculation which shows less error for both low and high permittivity structures and (ii) the model [31] only minimized the effect of surface wave modes. We have previously stated that the effect of leaky wave modes also significant for higher permittivity structure. But the previous model [31] does not consider the effect of leaky wave mode. We have minimized the effect of leaky wave as well as surface wave modes. So, the more improvement in results occurs.

TABLE 6.6

COMPARISON OF THEORETICALLY PREDICTED RESONANT FREQUENCIES FOR AN EQUILATERAL TRIANGULAR PATCH COVERED WITH VARIUS TWO LAYER DIELECTRIC STRUCTURES WITH HFSS SIMULATION AND EXPERIMENTAL [OUR] RESULTS. THIS TWO LAYER DIELECTRIC STRUCTURE ARE WITH DIFFERENT a, h_1, h_2, h_3, ε_{r3}.

a (mm)	ε_{r1}	h_1 (mm)	ε_{r2}	h_2 (mm)	ε_{r3}	h_3 (mm)	Resonant frequency (GHz)		
							Exp.	HFSS [33]	Computed Present
42	2.4	0.8265	1.0	3	2.4	0.8265	2.95	2.961	2.949
				3	5	1.63	2.941	2.947	2.927
				7	5	1.63	2.957	2.958	2.947
32	2.4	1.58	1.0	6	2.4	0.8265	3.765	3.748	3.712
				6	2.4	1.58	3.763	3.774	3.708
				6	5.0	1.63	3.749	3.752	3.672
				10	2.4	0.8265	3.771	3.786	3.731
				10	2.4	1.58	3.77	3.781	3.727
				10	5.0	1.63	3.759	3.778	3.703
23	1.3	1.58	1.0	2	2.33	1.575	6.251	6.275	6.240
				6	2.33	1.575	6.370	6.372	6.325
				6	1.4	5.6	6.317	6.384	6.364
				10	2.33	1.575	6.325	6.356	6.366
				10	1.4	5.6	6.382	6.392	6.396
$\varepsilon_{r4} = \varepsilon_{r5} = 1.0$									

6.4.1.4. Patch without covered layer

The validity of the present model for a conventional ETPA without any cover layer is shown in Fig. 6.4. Here the variation of dominant mode resonant frequency with side length is depicted. The computed curve employing the present model is compared with our experimental and simulated (HFSS) values. This comparison shows that the

present model well supports the measured and simulated values. Thus, the present model is well valid for an ETPA with and without dielectric cover layer.

TABLE 6.7
COMPARISON OF THEORETICAL, HFSS SIMULATION AND EXPERIMENTAL [OUR] RESONANT FREQUENCIES OF AN EQUILATERAL TRIANGULAR PATCH COVERED WITH SINGLE DIELECTRIC LAYER. THESE DIELECTRIC TOP LAYERS ARE WITH DIFFERENT ε_{r2} AND h_2.

ε_{r2}	h_2 (mm)	Resonant frequency (GHz)										
		Exp.	HFSS [33]	Computed								
				Present						Biswas & Guha [31]		
				$\varepsilon_r = \varepsilon_{re}/\varepsilon_{reff}$			$\varepsilon_r = \varepsilon_{r1}/\varepsilon_{reff}$					
				Calc. f_r	% Error with respect to EXP	% Error with respect to HFSS	Calc. f_r	% Error with respect to EXP	% Error with respect to HFSS	Calc. f_r	% Error with respect to EXP	% Error with respect to HFSS
2.2	0.508	6.157	6.216	6.126	0.499	1.448	6.039	1.917	2.848	6.500	-5.571	-4.569
2.4	0.8265	6.108	6.112	6.044	1.049	1.113	5.938	2.775	2.839	6.425	-5.190	-5.121
2.4	1.58	5.908	5.946	5.968	-1.014	0.370	5.846	1.047	1.679	6.338	-7.278	-6.593
2.33	0.7875	6.14	6.118	6.064	1.241	0.883	5.963	2.886	2.537	6.439	-4.870	-5.247
2.33	1.575	5.915	5.971	5.987	-1.224	0.268	5.870	0.764	1.694	6.352	-7.388	-6.381
2.55	2.33	5.771	5.776	5.867	-1.665	1.575	5.724	0.809	0.895	6.249	-8.283	-8.189
5.0	1.63	5.347	5.349	5.341	0.105	0.150	5.093	4.749	4.785	5.938	-11.053	-11.011
5.6	1.4	5.307	5.308	5.273	0.637	0.659	5.012	5.568	5.586	5.913	-11.419	-11.398
10.0	1.63	4.515	4.530	4.518	-0.075	0.265	4.116	8.841	9.143	5.448	-20.664	-20.265
Total Average % Error					0.834	0.746		3.262	3.556	-	9.079	8.753
a = 23 mm, ε_{r1} = 1.3, $\varepsilon_{r3} = \varepsilon_{r4} = \varepsilon_{r5}$ = 1.0, h_1 = 1.58, $h_3 = h_4$ = 0.0 mm.												

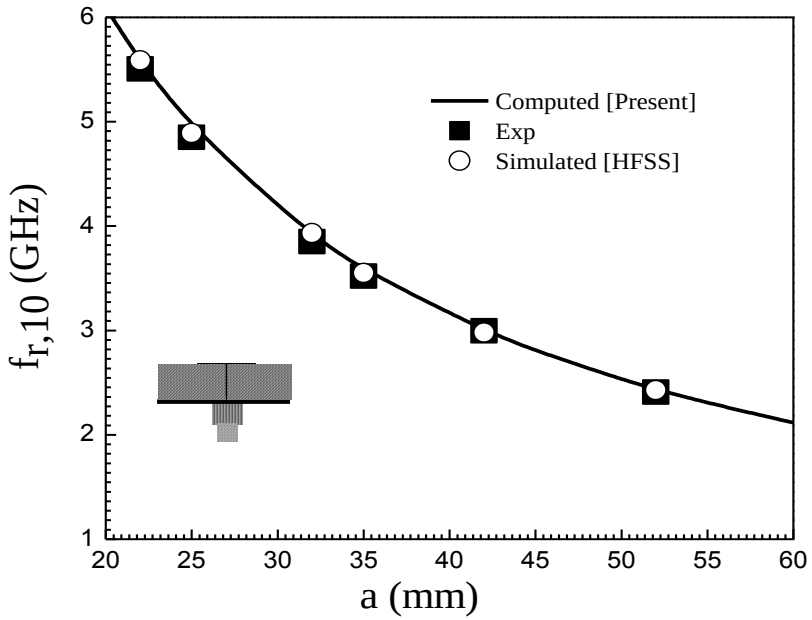

Figure 6.4: Computed, simulated and measured [our] dominant mode resonant frequency of an ETPA without cover layer. h_1 = 1.58 mm, $h_2 = h_3 = h_4$ = 0.0 mm, ε_{r1} = 2.4, $\varepsilon_{r2} = \varepsilon_{r3} = \varepsilon_{r4}$ = 1.0, $tan\delta_1$ =0.002, $tan\delta_2 = tan\delta_3 = tan\delta_4$ = 0.00.

6.4.2. Input impedance

6.4.2.1 Patch covered with three dielectric layers

Comparison of theoretical, HFSS simulation and experimental values of input impedance and total quality factor (Q_T) of an ETPA covered with three dielectric layers

is shown in table 6.8. This comparison shows that the computed input impedance and Q_T employing the present model are closely correlated with simulation and experimental results.

A comparison of computed and measured input impedance for a probe-fed ETPA covered with three dielectric layers is depicted in Fig. 6.5. Theoretical curve shows excellent agreement with measured curve.

TABLE 6.8

COMPARISON OF THEORETICAL, HFSS SIMULATION AND EXPERIMENTAL [OUR] VALUES OF INPUT IMPEDANCE AND TOTAL QUALITY FACTOR OF AN ETPA COVERED WITH MULTILAYERED DIELECTRICS.

Superstrate Parameters						Input impedance (Ω)			Total quality factor (Q_T)		
ε_{r2}	h_2 (mm)	ε_{r3}	h_3 (mm)	ε_{r4}	h_4 (mm)	Exp.	HFSS [33]	Present	Exp.	HFSS [33]	Present
2.33	0.7875	1.0	0.0	1.0	0.0	105.0	93.6	103.2	82	91	86.3
2.4	1.58	1.0	0.0	1.0	0.0	98.0	90.8	101.9	79	90	85.3
5.6	1.4	1.0	0.0	1.0	0.0	82.3	78.0	83.9	72	74	70.2
2.33	0.7875	2.4	0.8265	1.0	0.0	103.5	86.0	102.3	82	91	85.5
		2.4	1.58	1.0	0.0	102.0	89.3	101.6	87	89	84.9
		5.6	1.4	1.0	0.0	89.0	80.0	92.2	81	81	77.1
2.33	0.7875	2.4	0.8265	2.33	1.575	96.5	89.0	101.9	80	88	85.3
				2.4	1.58	101.0	87.0	101.6	84	88	84.9
				5.6	1.4	92.0	84.0	92.2	83	83	87.12
a = 42 mm, ε_{r1} = 2.4, h_1 = 0.8265, ρ = 19.1 mm											

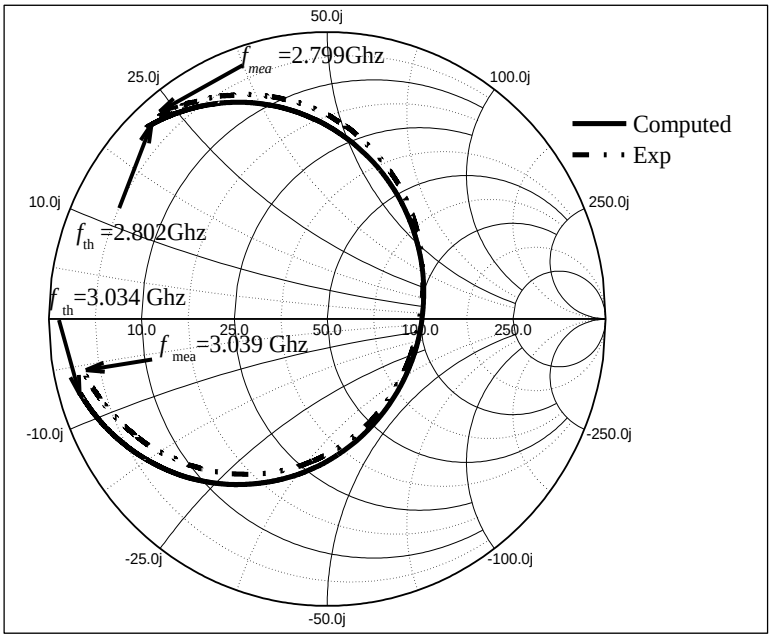

Figure 6.5: Experimental [our] and theoretical input impedance for a probe-fed ETPA covered with three dielectric cover layers. a = 42 mm, h_1 = 0.8265 mm, h_2 = 0.7875 mm, h_3 = 0.8265 mm, h_4 = 1.58 mm, ε_{r1} = 2.4, ε_{r2} = 2.33, ε_{r3} = 2.4, ε_{r4} = 2.4, $tan\delta_1$ = 0.0022, $tan\delta_2$ = 0.001, $tan\delta_3$ = 0.0022, $tan\delta_4$ = 0.0022, ρ = 19.10 mm, d = 1.24 mm.

The effect of top cover layer parameters (ε_{r4}, h_4) on input impedance and resonant frequency of a probe-fed ETPA covered with three dielectric layers is shown in Fig. 6.6. Both the resonant frequency and input impedance changes with the change of top dielectric cover layer parameters.

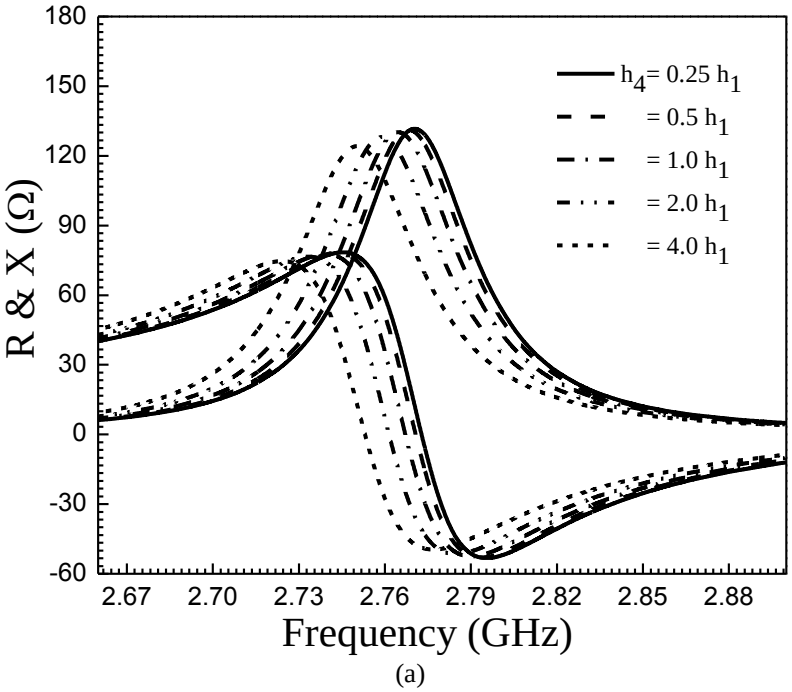

(a)

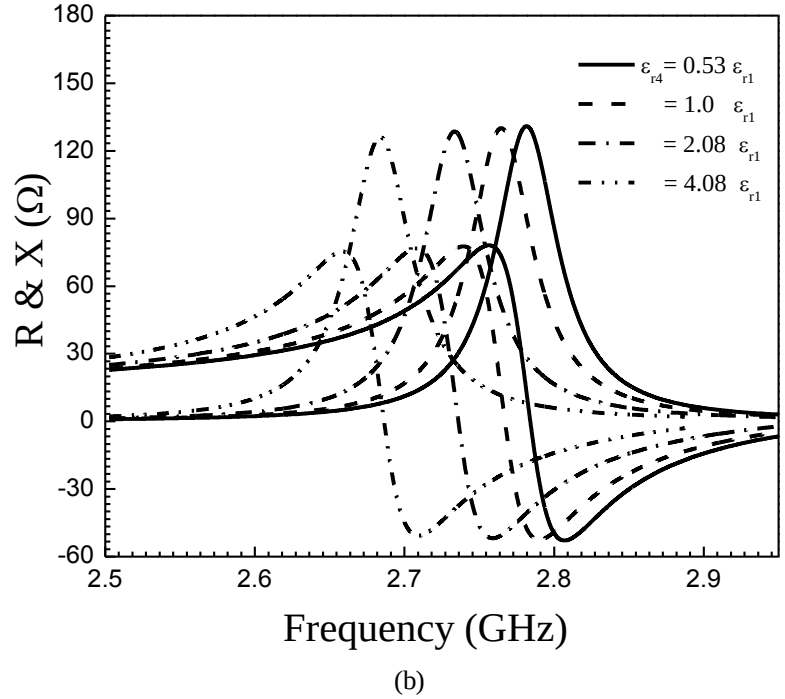

(b)

Figure 6.6: Variation of input impedance with the variation of top dielectric cover layer parameter h_4 and ε_{r4}. (a) ε_{r4} = 2.4, h_4 variable(b) h_4 = 1.58, ε_{r4} variable. a = 42 mm, $h_1 = h_2 = h_3$ = 1.58 mm, $\varepsilon_{r1} = \varepsilon_{r2} = \varepsilon_{r3}$ = 2.4, $tan\delta_1 = tan\delta_2 = tan\delta_3 = tan\delta_4$ = 0.0022. ρ = 19.10 mm.

6.4.2.2 Patch covered with two dielectric layers

Figure 6.7 depicts the Experimental and theoretical input impedance for a probe-fed ETPA covered with two dielectric layers. It is observed that both theoretical and experimental curves are closely correlated.

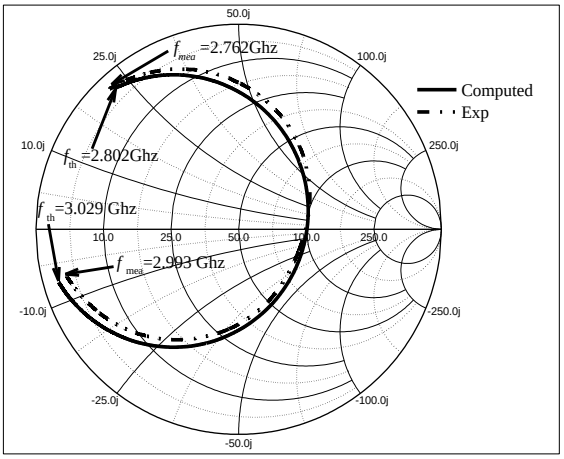

Figure 6.7: Experimental [our] and theoretical variation input impedance for a probe-fed ETPA covered with two dielectric layers. a = 42 mm, h_1 = 0.8265 mm, h_2 = 0.7875 mm, h_3 = 0.8265 mm, h_4 = 0.0 mm, ε_{r1} = 2.4, ε_{r2} = 2.33, ε_{r3} = 2.4, ε_{r4} = 1.0, $tan\delta_1$ = 0.0022, $tan\delta_2$ = 0.001, $tan\delta_3$ = 0.0022, $tan\delta_4$ = 0.00, ρ = 19.10 mm, d = 1.24 mm.

The effect of second cover layer parameters (ε_{r3}, h_3) on input impedance and resonant frequency of a probe-fed ETPA is shown in Fig. 6.8. The changes in resonant frequency and input impedance are occured with the change of second dielectric covers layer parameters.

6.4.2.3 Patch covered with single dielectric layer

Experimental and theoretical input impedance for a probe-fed ETPA covered with single dielectric layer are shown in Fig. 6.9. The close agreement is revealed between the theoretical curves employing present model and experimental curves.

The accuracy of the present model for a probe-fed ETPA covered with single dielectric layer is further verified in table 6.9. Here computed resonant resistance employing the present model and model reported in [31] is compared with simulated values for wide variation of dielectric cover layer permittivity and thickness. It is observed that the present model shows good agreement with simulation results compared to [31]. This is due to the fact that the model reported in [31] did not include the

dielectric cover layer effect on quality factor calculation which has significant impact on resonant resistance.

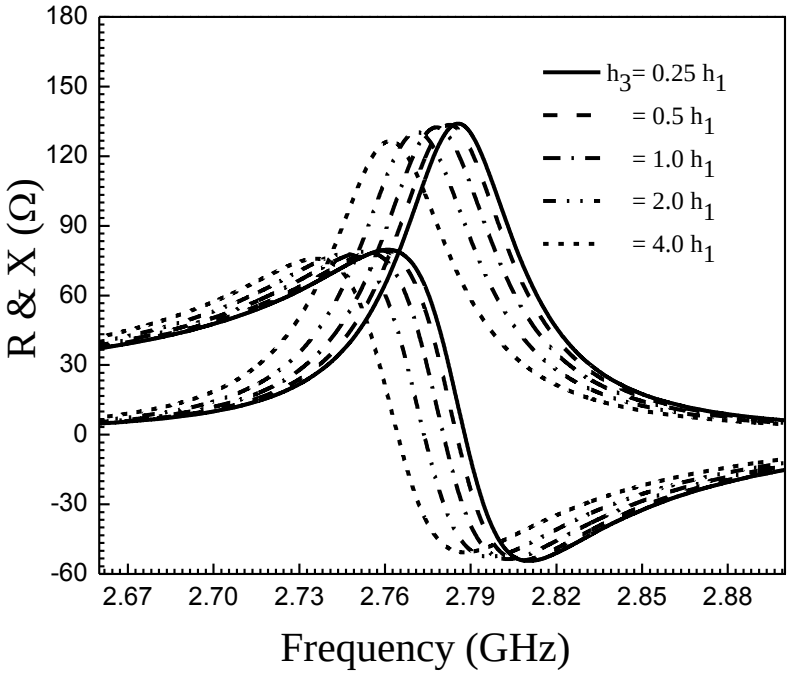

(a)

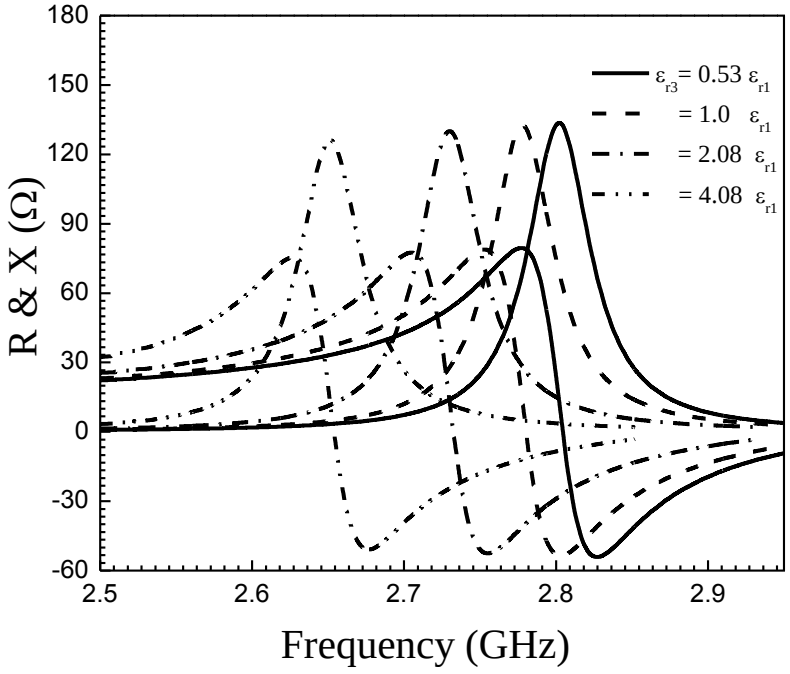

(b)

Figure 6.8: Variation of input impedance as a function of frequency with the variation of superstrate parameter h_3 and ε_{r3}. (a) ε_{r3}= 2.4, h_3 variable (b) h_3 = 1.58, ε_{r3} variable, other parameters are a = 42 mm, h_1 = h_2 = 1.58 mm, ε_{r1} = ε_{r2} = 2.4, $tan\delta_1$ = $tan\delta_2$ = $tan\delta_3$ = 0.0022. ρ = 19.10 mm, h_4 = 0.0 mm, ε_{r4} = 1.0, $tan\delta_4$ = 0.00.

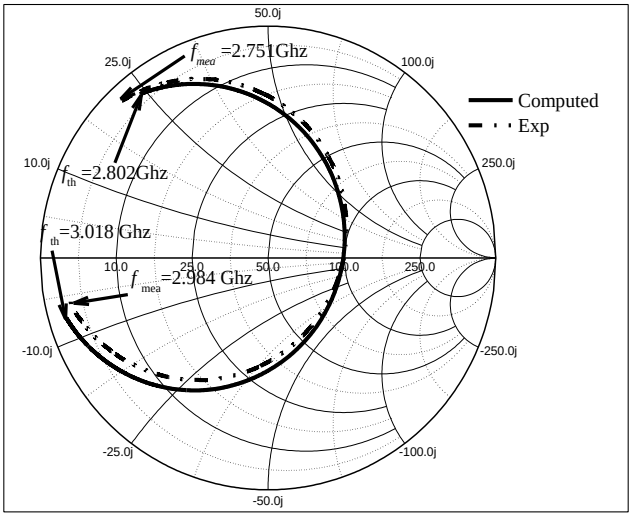

Figure 6.9: Experimental [our] and theoretical input impedance for a probe-fed ETPA covered with one dielectric layer. a = 42 mm, h_1 = 0.8265 mm, h_2 = 0.7875 mm, $h_3 = h_4$ = 0.0 mm, ε_{r1} = 2.4, ε_{r2} = 2.33, $\varepsilon_{r3} = \varepsilon_{r4}$ = 1.0, $tan\delta_1$ = 0.0022, $tan\delta_2$ = 0.001, $tan\delta_3 = tan\delta_4$ = 0.00, ρ = 19.10 mm, d = 1.24 mm.

TABLE 6.9

COMPARISON OF THEORETICALLY PREDICTED AND HFSS SIMULATED RESONANT RESISTANCES FOR A TRIANGULAR PATCH COVERED WITH SINGLE DIELECTRIC COVER FOR WIDE RANGE OF VARIATION OF THICKNESS (h_2) AND PERMITTIVITY (ε_{r2}).

Dielectric cover parameter		Resonant resistance		
h_2/h_1	$\varepsilon_{r2}/\varepsilon_{r1}$	HFSS [33]	Present	Biswas [31]
0.5	0.5	97.4	101.9	148.0
	1.0	95.7	100.3	146.0
	1.25	95.5	99.6	145.1
	2.0	95.2	97.5	142.6
1.0	0.5	96.6	101.5	147.9
	1.0	93.5	99.4	144.8
	1.25	92.8	98.5	143.5
	2.0	90.4	95.8	139.9
2.0	0.5	95	100.5	147.7
	1.0	87.7	97.8	143.4
	1.25	86.4	96.6	141.6
	2.0	85	93.0	136.7
4.0	0.5	92.3	98.5	147.4
	1.0	83.4	94.9	141.9
	1.25	80.5	93.3	139.6
	2.0	78	88.6	133.6
0.5	0.5	97.4	101.9	148.0
1.0		96.6	101.5	147.9
2.0		95	100.5	147.7
4.0		92.3	98.5	147.4
0.5	1.0	95.7	100.3	146.0
1.0		93.5	99.4	144.8
2.0		87.7	97.8	143.4
4.0		83.4	94.9	141.9
0.5	1.25	95.5	99.6	145.1
1.0		92.8	98.5	143.5
2.0		86.4	96.6	141.6
4.0		80.5	93.3	139.6
0.5	2.0	95.2	97.5	142.6
1.0		90.4	95.8	139.9
2.0		85	93.0	136.7
4.0		78	88.6	133.6
a = 42 mm, ε_{r1} = 2.4, h_1 = 1.58, ρ = 19.8 mm,, $tan\delta_1 = tan\delta_2$ = 0.0022				

The change in input impedance and resonant frequency with the change of dielectric cover layer thickness (h_2) and relative permittivity (ε_{r2}) for a probe-fed ETPA is shown in Fig. 6.10. Both input impedance and resonant frequency decrease with the increase of cover layer thickness and permittivity. The variation becomes noteworthy for higher values of thickness and relative permittivity of dielectric cover layer.

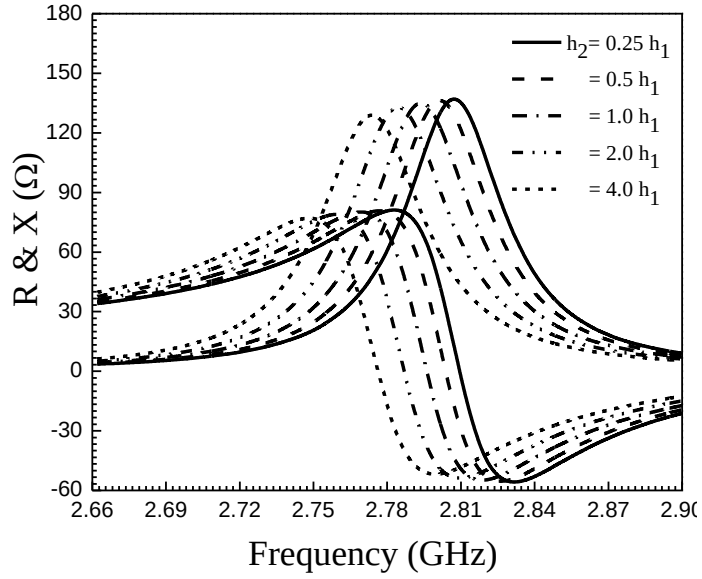

(a)

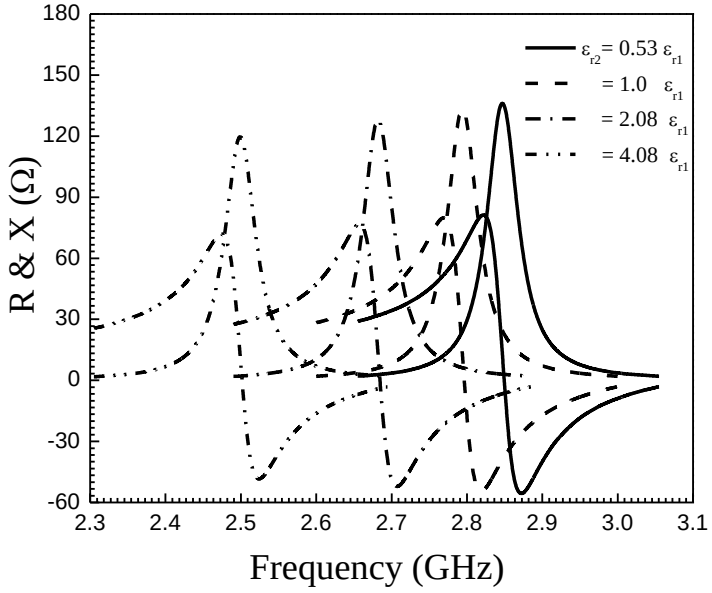

(b)

Figure 6.10: Variation of input impedance as a function of frequency with the variation of superstrate parameter h_2 and ε_{r2}. (a) $\varepsilon_{r2} = 2.4$, h_2 variable (b) $h_2 = 1.58$, ε_{r2} variable. $a = 42$ mm, $h_1 = 1.58$ mm, $h_2 = 0.7875$ mm, $h_3 = h_4 = 0.0$ mm, $\varepsilon_{r1} = 2.4$, $\varepsilon_{r3} = \varepsilon_{r4} = 1.0$, $tan\delta_1 = tan\delta_2 = 0.0022$, $tan\delta_3 = tan\delta_4 = 0.00$, $\rho = 19.10$ mm.

The significant point is that, the change in input impedance and resonant frequency are maximum in Fig. 6.10, intermediate in Fig. 6.8 and least amount in Fig. 6.6. Now it is clear that the effect of h_2 on both input impedance and resonant frequency is more significant than h_3 and h_4.

Thus with the above study it is clear that the tuning of an ETPA is possible by varying the dielectric cover layer parameter without any change in antenna parameters.

6.4.2.4 Patch without cover layers

The variation of dominant mode input impedance as a function of frequency for an ETPA without cover ($h_2 = h_3 = h_4 = 0.0$ mm) is depicted in Fig. 6.11. The computed input impedance using present model is compared with our experimental results and excellent correlation is found between them. Thus, the present model is also well valid for an ETPA printed on single substrate without any cover layer.

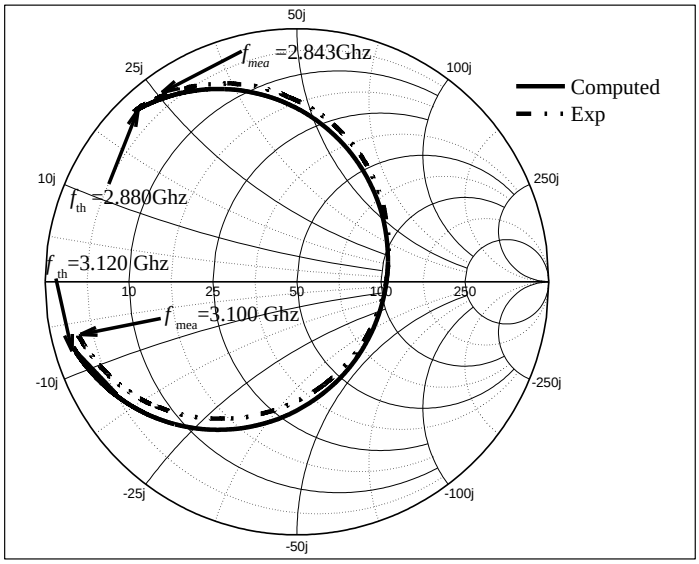

Figure 6.11: Experimental [our] and theoretical variation of input impedance as a function of frequency for a probe-fed ETPA without cover layer. Parameters are a = 42 mm, h_1 = 0.8265 mm, $h_2 = \infty$, $h_3 = h_4 =$ 0.0 mm, ε_{r1} = 2.4, $\varepsilon_{r2} = \varepsilon_{r3} = \varepsilon_{r4}$ = 1.0, $tan\delta_1$ = 0.0022, $tan\delta_2 = tan\delta_3 = tan\delta_4$ = 0.00, ρ = 19.10 mm.

6.4.3. Bandwidth and gain

Comparison of theoretical and HFSS simulation values of bandwidth (% BW) and gain of an ETPA covered with several dielectric layers with different parameter is shown in table 6.10. The bandwidth increases and gain decreases with the increase of cover layer thickness and permittivity. The computed Bandwidth and gain employing the present model shows close correlation with simulated values.

TABLE 6.10
COMPARISON OF THEORETICAL, HFSS SIMULATION VALUES OF % BW AND GAIN OF AN ETPA COVERED WITH MULTILAYERED SUBSTRATE.

Superstrate Parameters						%BW			Gain	
ε_{r2}	h_2 (mm)	ε_{r3}	h_3 (mm)	ε_{r4}	h_4 (mm)	Exp.	HFSS [33]	Present	HFSS [33]	Present
2.33	0.7875	1.0	0.0	1.0	0.0	0.862	0.777	0.819	6.236	6.244
2.4	1.58	1.0	0.0	1.0	0.0	0.895	0.789	0.829	6.170	6.209
5.6	1.4	1.0	0.0	1.0	0.0	0.982	0.952	1.006	4.919	5.172
2.33	0.7875	2.4	0.8265	1.0	0.0	0.862	0.781	0.826	6.140	6.221
		2.4	1.58	1.0	0.0	0.813	0.792	0.832	6.124	6.217
		5.6	1.4	1.0	0.0	0.873	0.871	0.917	5.850	5.697
2.33	0.7875	2.4	0.8265	2.33	1.575	0.884	0.801	0.829	6.110	6.233
				2.4	1.58	0.842	0.807	0.832	6.160	6.217
				5.6	1.4	0.852	0.852	0.917	6.035	5.697
a = 42 mm, ε_{r1} = 2.4, h_1 = 0.8265, ρ = 19.1 mm										

It is already seen that the effect of first cover layer is most significant on the resonant frequency and input impedance of an ETPA. Now more explicitly the effect of the first dielectric cover layer on gain of an ETPA is depicted in Fig. 6.12. Here the variation of gain as a function of ε_{r2} for different value of cover thickness h_2 is depicted. It is observed that the gain decreases with the increase of ε_{r2} and h_2. It is noteworthy to mention that the change of gain is maximum when the cover thickness is half of the substrate thickness. This information is very significant for analysis the characteristics of an ETPA with cover.

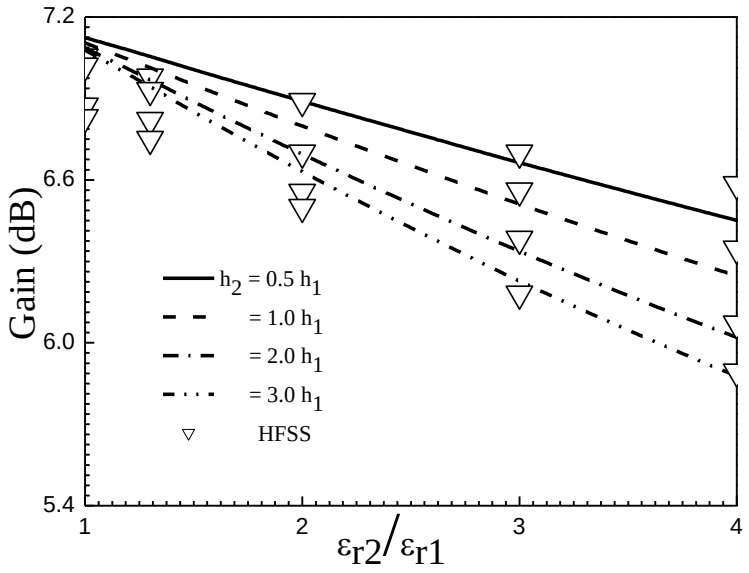

Figure 6.12: Variation of gain as a function of ε_{r2} for a probe-fed ETPA for different dielectric covers thickness h_2. Parameters are a = 42 mm, h_1 = 1.58 mm, $h_3 = h_4$ = 0.0 mm, ε_{r1} = 2.4, = $\varepsilon_{r3} = \varepsilon_{r4}$ = 1.0, $tan\delta_1 = tan\delta_2$ = 0.0022, $tan\delta_3 = tan\delta_4$ = 0.00.

Measured and simulated *E*- plane and *H*-plane gain pattern of a probe-fed ETPA with and without multi dielectric cover layer is shown in Fig. 6.13 and 6.14 respectively.

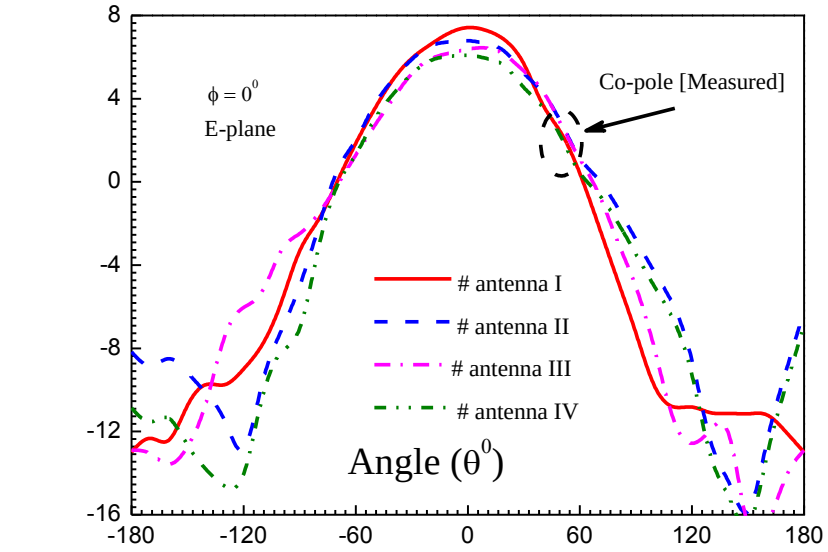

(a)

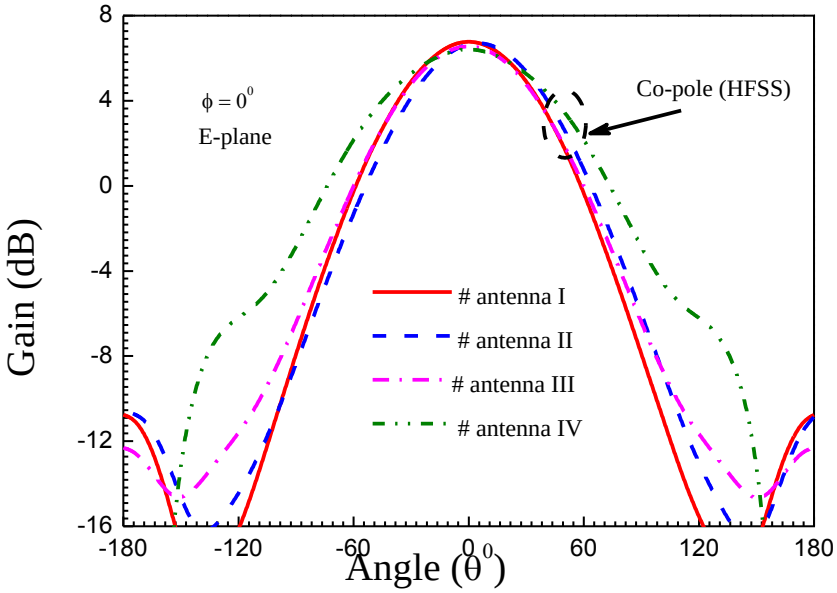

(b)

Figure 6.13: (a) Measured [our] and (b) HFSS simulated E- plane co-polar gain pattern of an ETPA covered with multidielectric layer. a = 22 mm, h_1 = 1.58 mm, ε_{r1} = 2.4, $tan\delta_1$ =0.0022.

#Antenna –I: $h_2 = h_3 = h_4 = 0.0$, $\varepsilon_{r2} = \varepsilon_{r3} = \varepsilon_{r4} = 1.0$, $tan\delta_2 = tan\delta_3 = tan\delta_4 = 0.00$.

#Antenna –II: h_2 = 1.575 mm, $h_3 = h_4$ = 0.0 mm ε_{r2} = 2.33, $\varepsilon_{r3} = \varepsilon_{r4}$ = 1.0, $tan\delta_2$ =0.001, $tan\delta_3 = tan\delta_4$ = 0.00.

#Antenna –III: h_2 = 1.575 mm, h_3 = 1.4 mm, h_4 = 0.0 mm, ε_{r2} = 2.33, ε_{r3} = 5.6, ε_{r4} = 1.0, $tan\delta_2$ = 0.001, $tan\delta_3$ = 0.02, $tan\delta_4$ = 0.00.

#Antenna –IV: h_2 = 1.575 mm, h_3 = 1.4 mm, h_4 = 1.63 mm, ε_{r2} = 2.33, ε_{r3} = 5.6, ε_{r4} = 5.0, $tan\delta_2$ = 0.001, $tan\delta_3$ = 0.02, $tan\delta_4$ = 0.02.

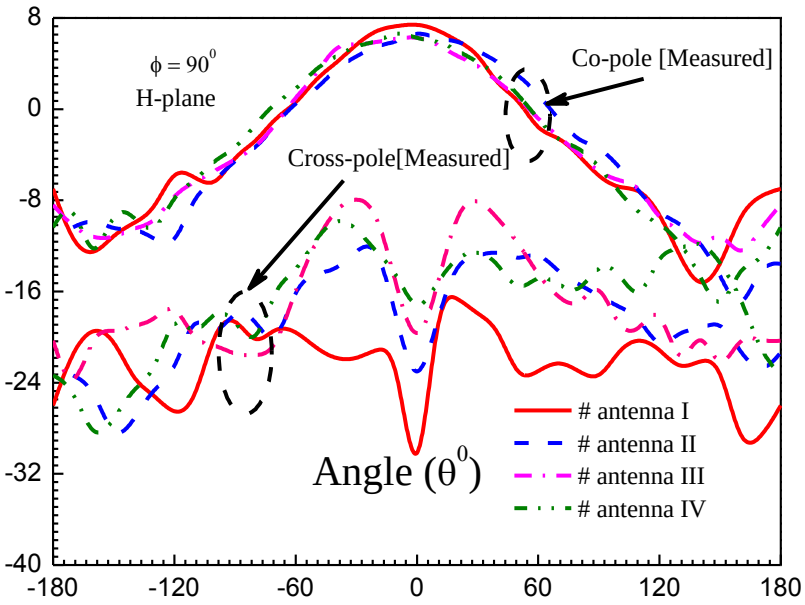

(a)

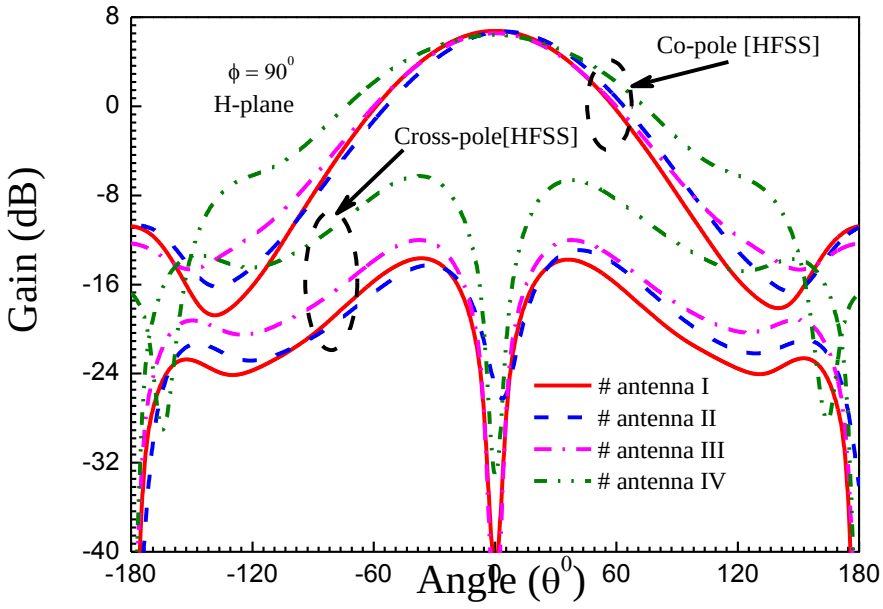

(b)

Figure 6.14: (a) Measured [our] and (b) HFSS simulated H- plane co-polar and cross polar gain pattern of an ETPA covered with multi dielectric layer. a = 22 mm, h_1 = 1.58 mm, ε_{r1} = 2.4.

#Antenna –I: $h_2 = h_3 = h_4 = 0.0$, $\varepsilon_{r2} = \varepsilon_{r3} = \varepsilon_{r4} = 1.0$, $tan\delta_2 = tan\delta_3 = tan\delta_4 = 0.00$.

#Antenna –II: $h_2 = 1.575$ mm, $h_3 = h_4 = 0.0$ mm $\varepsilon_{r2} = 2.33$, $\varepsilon_{r3} = \varepsilon_{r4} = 1.0$, $tan\delta_2 = 0.001$, $tan\delta_3 = tan\delta_4 = 0.00$.

#Antenna –III: $h_2 = 1.575$ mm, $h_3 = 1.4$ mm, $h_4 = 0.0$ mm, $\varepsilon_{r2} = 2.33$, $\varepsilon_{r3} = 5.6$, $\varepsilon_{r4} = 1.0$, $tan\delta_2 = 0.001$, $tan\delta_3 = 0.02$, $tan\delta_4 = 0.00$.

#Antenna –IV: $h_2 = 1.575$ mm, $h_3 = 1.4$ mm, $h_4 = 1.63$ mm, $\varepsilon_{r2} = 2.33$, $\varepsilon_{r3} = 5.6$, $\varepsilon_{r4} = 5.0$, $tan\delta_2 = 0.001$, $tan\delta_3 = 0.02$, $tan\delta_4 = 0.02$.

It is observed that effect dielectric cover layer on gain is negligible though the effect on resonant frequency is more significant. The gain slightly reduces with the increase of dielectric cover layer. The beam width is increased with the addition of dielectric layer for the co-polar gain pattern. Both measured and simulated pattern are showing similar impact of cover layer on the gain characteristics.

6.5. Conclusions

In this article, a very simple, fast, efficient and accurate model is presented to determine the resonant frequency, input impedance, gain and bandwidth of an equilateral triangular patch antenna covered with several dielectric layer. This model is based on conformal mapping technique, cavity model analysis and single resonant parallel *R-L-C* circuit. The drawback of the prior works for resonant frequency computation has been eliminated by employing the new improved effective permittivity formula. Also, more tuning in resonant frequency result is achieved by considering the surface wave and leaky wave modes in effective side length calculation. The effect of dielectric cover layer has also been incorporated in total quality factor expression to account accurately the effect of dielectric cover layer on input impedance. This efficient model is capable of predicting accurately the resonant frequency, input impedance, gain, bandwidth etc. for wide range of variation of substrate and dielectric cover layer parameters. To validate the model we have performed several experiments. We have measured the radiation patterns of different multilayered structure. Electromagnetic software is also employed to generate simulated data. The computed values employing the present model is very close to the experimental and simulation results. This information is very useful for practical implementation of an ETPA with one or more dielectric cover layers to install properly in wireless equipments.

REFERENCES

[1] R. Garg, P. Bhartia, I. J. Bahl, and A. Ittipiboon, "Microstrip antenna design handbook," *Artech house*, 2001.

[2] G. Kumar and K. P. Ray, "Broadband microstrip antennas," *Artech House,* 2003.

[3] M. Biswas and M. Sen, "Design and development of rectangular patch antenna with superstrates for the application in portable wireless equipments and aircraft radome," *Microw. Optical Technol. Lett.* vol. 56, PP. 883-893, 2014.

[4] E. Nyfors and P. Vainikainen, "Industrial microwave sensors," *Artech House*, 1989.

[5] Y. Li and N. Bowler, "Resonant frequency of a rectangular patch sensor covered with multilayered dielectric structures," *IEEE Trans. Antennas Propagat.*, vol. 58, pp. 1883-1889, 2010.

[6] H. Baltes , W. G.opel, and J. Hesse, " Sensors update," *Wiley Vch*, Germany, vol. 7, 2000.

[7] Zucchelli, M. Chimenti, and E. Bozzi, "Application of a coaxial-fed patch to microwave non-destructive porosity measurements in low-loss dielectrics," *Progr. Electromagn. Res.*, vol. 5, pp.1–14, 2008.

[8] M. Bogosanovich, "Microstrip patch sensor for measurement of the permittivity of homogeneous dielectric materials," *IEEE Trans. Instrum. Meas.*, vol. 49, pp. 1144–1148, Oct. 2000.

[9] A. K. Verma, Nasimuddin, and A. S. Omar, "Microstrip resonator sensors for determination of complex permittivity of materials in sheet, liquid and paste forms," *Proc. Inst. Elect. Eng.*, vol. 152, pp. 47–54, 2005.

[10] A. Cataldo, G. Monti, E. De Benedetto, G. Cannazza, and L. Tarricone, "A noninvasive resonance-based method for moisture content evaluation through microstrip antennas," *IEEE Trans. Instrum. Meas.*, vol. 58, pp. 1420–1426, May 2009.

[11] M. Biswas and A. Mandal, "Design and development of an equilateral patch sensor for determination of permittivity of homogeneous dielectric medium," *Microw. Opt. Technol. Lett.***,** vol. 56, pp. 1097-1104, May. 2014.

[12] Q. Luo et al, "Dual circularly polarized equilateral triangular patch array*," IEEE Trans. Antennas Propagat.*, vol. 64, pp. 2255-2262, 2016.

[13] J. T. S. Sumantyo, K. Ito, and M. Takahashi, "Dual-band circularly polarized equilateral triangular-patch array antenna for mobile satellite communications," *IEEE Trans. Antennas Propagat.*, vol. 53, no. 11, pp. 3477 – 3485, Nov. 2005.

[14] J. - S. Hong and M. J. Lancaster, "Theory and experiment of dual-mode microstrip triangular patch resonators and filters," *IEEE Trans. Microw. Theory Tech.*, vol. 52, no. 4, pp. 1237 – 1243, Apr. 2004.

[15] J. Helszajn and D. S. James, "Planar triangular resonators with magnetic walls," *IEEE Trans. Microw. Theory Tech.*, vol. MTT-26, pp. 95-100, Feb. 1978.

[16] A. K. Sharma and B. Bhat, "Analysis of triangular microstrip resonator," *IEEE Trans. Microw. Theory Tech*., vol. 30, no. 11, pp. 2029 – 2031, Nov. 1982.

[17] E. F. Keuster and D. C. Chang: 'A geometrical theory for the resonant frequencies and Q factors of some triangular microstrip patch antenna', *IEEE Trans. Antennas Propagat.*, vol. 31, pp.27-34, 1983.

[18] J. S. Dahele and K. F. Lee: 'On the resonant frequencies of the triangular patch antenna', *IEEE Trans. Antennas Propagat.*, vol. 35, pp.100-101, 1987.

[19] K. F. Lee, K. M. Luk, and J. S. Dahele, "Characteristics of the equilateral triangular patch antenna," *IEEE Trans. Antennas Propagat.*, vol. 36, no.11, pp.1510-1518, Nov. 1988.

[20] X. Gang 'On the resonant frequencies of microstrip antennas', *IEEE Trans. Antennas Propagat.*, vol. 37, pp. 245-247, 1989.

[21] W. Chen, K. F. Lee, and J. S. Dahele, "Theoretical and experimental studies of the resonant frequencies of equilateral triangular microstrip antenna," *IEEE Trans. Antennas Propagat.*, vol. 40, pp.1253-1256, Oct. 1992.

[22] D. Karaboğa, K.Güney, N. Karaboğa, and A. Kaplan, "Simple and accurate effective side length expression obtained by using a modified genetic algorithm for the resonant frequency of an equilateral triangular microstrip antenna,"*Int. J. Electron.*, vol. 83, pp.99-108, Jan.1997.

[23] M. M. Olaimat and N. I. Dib, "Improved formulae for the resonant frequencies of triangular microstrip patch antennas," *Int. J. Electron.*, vol. 98, pp. 407-424, 2011.

[24] M. M. Olaimat and N. I. Dib, "A study of 15^0-75^0-90^0 angles triangular patch antenna," *Progr. Electromagn. Res. Lett.*, vol. 21, pp. 1-9, 2011.

[25] K. Guney and E. Kurt, "Effective side length formula for resonant frequency of equilateral triangular microstrip antenna," *Int. J. Electron.*, vol. 103, pp. 261-268, 2016.

[26] D. Guha and J.Y. Siddiqui, "Resonant frequency of equilateral triangular microstrip patch antenna with and without air gaps," *IEEE Trans. Antennas Propagat.*, vol. 52, no.8, pp. 2174-2177, Aug. 2004.

[27] Nasimuddin, K. Esselle, and A. K.Verma, "Resonant frequency of an equilateral triangular microstrip antenna," *Microwav. Opt. Technol. Lett.*, vol. 47, no.5, pp.485-489, Dec. 2005.

[28] C. S. Gurel and E.Yazgan, 'New computation of the resonant frequency of a tunable equilateral triangular microstrip patch', *IEEE Trans. Microw. Theory Tech.*, vol. 48, pp. 334-338, 2000.

[29] C. - S. Hong, "Gain-enhanced broadband microstrip antenna," *Proc. Natl. Sci. Counc. Rep. China A*, vol. 23, no. 5, pp. 609–611, 1999.

[30] H. R. Hassani and D. Mirshekar Syahkal, "Analysis of triangular patch antennas including radome effects" *IEE Proc. H*, vol. 139, no. 3, pp.251-256, Jun. 1992.

[31] M. Biswas and D. Guha, "Input impedance and resonance characteristic of superstrate loaded triangular microstrip patch," *IET Microw. Antennas Propagat.*, vol. 3, pp. 92 – 98, Feb. 2009.

[32] M. Biswas and A. Mandal, "CAD model to compute the input impedance of an equilateral triangular microstrip patch antenna with radome," *Progr. Electromag. Res. M.*, vol. 12, pp. 247-257, 2010.

[33] High Frequency Structure Simulator: Ansoft Corp. 2012.

[34] M. Biswas and A. Mandal, "Experimental and theoretical investigation to predict the effect of superstrate on the impedance, bandwidth, and gain characteristics for a rectangular patch antenna," *J. Electromagn. Waves Applicat.*, vol. 29, no. 16, pp. 2093-2109, 2015.

[35] J. T. Bernhard and C. J. Tousignant, "Resonant frequencies of rectangular microstrip antennas with flush and spaced dielectric superstrates," *IEEE Trans. Antennas Propagat*., vol. 47, pp. 302–308, 1999.

[36] F. Abboud, J. P. Damiano, A. Papiernik, "A new model for calculating the input impedance of coax-fed circular microstrip antennas with and without air gaps," *IEEE Trans. Antennas Propagat*., vol. 38, pp. 1882–1885, 1990.

[37] F. Mesa, D. R. Jackson, and M. J. Freire, "Evolution of leaky modes on printed-circuit lines," *IEEE Trans Microw. Theory Tech.,* vol. 50, pp. 94–104, 2002.

[38] D. Nghiem, J. T. Williams, D. R. Jackson, and A. A. Oliner, "Existence of a leaky dominant mode on microstrip line with an isotropic substrate: Theory and measurements," *IEEE Trans. Microw. Theory Tech.*, vol. 44, pp. 1710–1715, 1996.

[39] C. Peixeiro and A. M. Barbosa, "Leaky and surface waves in anisotropic printed antenna structures," *IEEE Trans. Antennas Propagat*., vol. 40, pp. 566-569, 1992.

[40] D. R. Jackson and A. A. Oliner, "A leaky-wave analysis of the high-gain printed antenna configuration," *IEEE Trans. Antennas Propagat.*, vol. 36, pp. 905-910, 1988.

[41] D. M. Pozar, "Microwave engineering," *John Wiley & Sons Inc*, 4th edition, 2012.

CHAPTER 7

Coax-Fed Electromagnetically Coupled Stacked Equilateral Triangular Patch Antenna: Theoretical and Experimental Studies on Resonance Frequency and Input Impedance

Content:

7.1. Introduction

Recently, the microstrip patch antenna draws the interest of many researchers due to its extensive application in mobile, aircraft radome, missiles, radars, satellites and many useful sensors [1-11]. The equilateral triangular patch antenna (ETPA) is more compact than other microstrip geometries with good radiation characteristics [12]. But the Q-factor of an ETPA is very high and the bandwidth is very low. This narrow impedance bandwidth of ETPA is a serious limitation which restricts its application in many areas. The patches in stacked configuration are a good choice for improving the bandwidth up to 6-20% without degrading the other antenna performances [13]. The patch antennas in stacked configurations for different patch geometries have been reported in [13-25]. The triangular geometry has been investigated by many researchers [12-15, 26-42] but stacked ETPA find very little investigations [13-15] till now. The article [13] provides only the experimental results for resonant frequency, bandwidth, input impedance and radiation pattern of electromagnetically coupled stacked ETPA (EMCSETPA). The article [14] has employed the full wave technique for computing the different parameters of stacked ETPA and provides some experimental results also. The article [15] is based on experiments. To the best of our knowledge any theoretical closed form expressions are not reported till now for EMCSETPA.

The useful parameters of EMCSETPA may be computed by the full wave method [14] and also by the commercial software [43]. But the full wave methods involve large and rigorous mathematical steps and require huge computational time. Also, the numerical methods do not provide the closed form expressions and equivalent circuits for analysis. Therefore the numerical methods with high accuracy are not suitable for direct synthesis of EMCSETPA. The CAD oriented cavity model analysis is ideal for design purpose because they are very simple, fast and directly applied to the CAD programs and at the same time, the cavity model also provides the closed form expressions for design and equivalent circuit for analysis.

Keeping these in view, the purpose of this article is divided into two-fold objectives: i) we have proposed a fast and accurate model based on conformal mapping technique, cavity model and single parallel resonant *R-L-C* circuit to determine the resonant frequency, quality factor, input impedance and bandwidth of an EMCSETPA,

and (ii) we have performed several experiments to validate the proposed model. We have also employed electromagnetic software to validate the model. The proposed model is capable of predicting accurately the resonant frequency, input impedance, quality factor and bandwidth for wide variation of antenna size and dielectric layers electrical parameters.

7.2 Theory

The structure of a three layered EMCSETPA is shown in Fig. 7.1. Here we have considered that the middle layer as air substrate (Foam) and both top and bottom layer as dielectric substrate (PTFE). For theoretical analysis the structure under investigation is divided into two cavities: lower and upper cavities [16]. The patch of the lower cavity is called the driven patch which is excited by a coaxial probe. The upper patch is termed as a parasitic patch which is not directly connected with co-axial probe, but it is excited by the field radiated from the lower patch through electromagnetic coupling. Both cavities have their own resonant frequency, quality factor and input impedance but a coupling exists between these two cavities [25].

7.2.1 Lower cavity

The lower cavity is considered as the ETPA covered with several dielectric layers as shown in Fig. 7.2. The set of closed form expressions have been proposed to compute resonant frequency, quality factor, input impedance and bandwidth of an ETPA covered with several dielectric layers.

7.2.1.1 Resonant frequency

The resonant frequency for an ETPA covered with several dielectric layers (Fig. 7.2) in dominant mode can be expressed as [29]:

$$f_{r1} = \frac{2c}{3a_{1eff}\sqrt{\varepsilon_{r,eff1}}} \tag{7.1}$$

where, c is the velocity of light in free space, $\varepsilon_{r,eff1}$ is the effective relative permittivity of the multilayered structure and a_{1eff} is the effective side length of the patch.

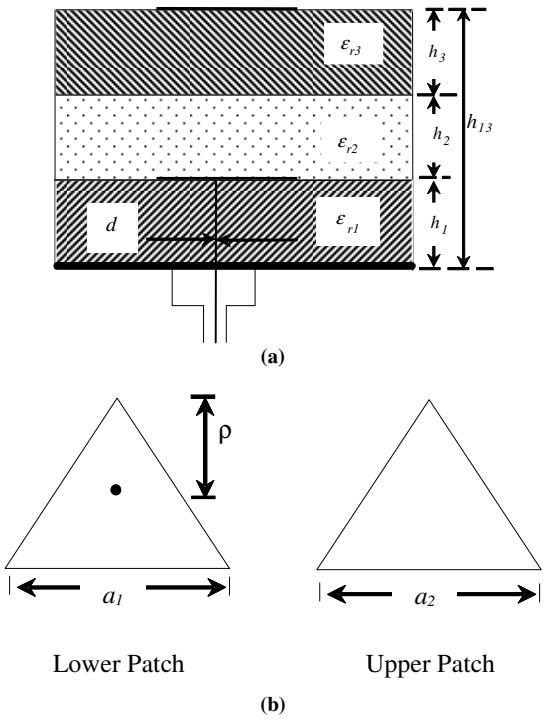

Figure 7.1: a) A schematic diagram of probe-fed equilateral triangular microstrip patches in stacked configuration. b) Patch geometries

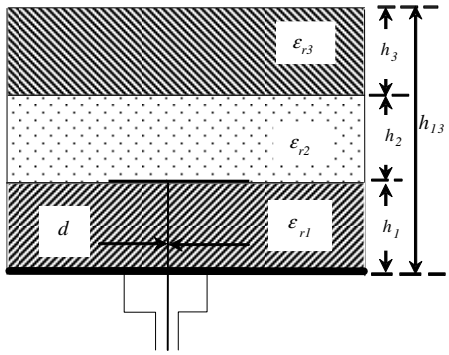

Figure 7.2: Configuration of the lower cavity

7.2.1.2. Effective permittivity

The effective permittivity for an ETPA covered with several dielectric layers is computed from originally formulated rectangular patch with length b_1 and width w_1 loaded with four dielectric layers [5] by employing an equivalent relation between rectangular geometry and equilateral triangular geometry of side length a_1. Here we have used $w_1 = 0.545\ a_1$ and $b_1 = 0.955\ a_1$ [34]. The five layer structure of Li [5] is used to compute the effective permittivity (ε_{reff1}) of four layer structure as:

$$\varepsilon_{r,eff1} = \varepsilon_{r1} q_{11} + \varepsilon_{r1} E \left(q_{22} + q_{33} + q_{44} + 4 q_{20} \right)^2 \times \left[\varepsilon_{r1} \left(q_{22} + q_{33} + q_{44} + 3 q_{20} \right)^2 + E q_{20} \right]^{-1} \tag{7.2}$$

$$E = \varepsilon_{r2} q_{22} + \varepsilon_{r2} \left(\varepsilon_{r3} q_{33} + F \right) \left(q_{33} + q_{44} + 3 q_{20} \right)^2 \times \left[\varepsilon_{r2} \left(q_{33} + q_{44} + 2 q_{20} \right)^2 + \left(\varepsilon_{r3} q_{33} + F \right) q_{20} \right]^{-1} \tag{7.3}$$

and

$$F = \varepsilon_{r3} \left[\left(q_{44} + q_{20} \right)^2 \times \left(q_{44} + q_{20} \right)^{-1} \right] \times \left(q_{44} + 2 q_{20} \right)^2 \times \left\{ \varepsilon_{r3} \left(q_{44} + q_{20} \right)^2 + q_{20} \times \left[\left(q_{44} + q_{20} \right)^2 \times \left(q_{44} + q_{20} \right)^{-1} \right] \right\} \tag{7.4}$$

$$q_{11} = q_1 - 2 q_{20} - q_3 \tag{7.5}$$

$$q_{ii} = \left[1 - q_{11} - q_4 - 2 q_{20} - q_{30} \right] \times \left(p_i - p_{i0} \right) \left[\sum_{j=2}^{3} q_j - q_{j0} \right]^{-1} \tag{7.6}$$

$i = 2, 3$

$$q_{44} = 1 - \sum_{j=2}^{3} q_{jj} - q_{11} \tag{7.7}$$

$i = 2, 3$

$$q_{i0} = \frac{h_1}{2S} \left\{ \ln \left(\frac{\pi}{h_1} S - 1 \right) - \left(1 + g_{i-1} \right) \times \ln \left[\frac{2S}{h_1} \frac{\cos \left(\frac{\pi}{2} S_{i-1} \right)}{\frac{2 h_{i-1}}{h_1} - 1 + g_{i-1}} + \sin \left(\frac{\pi}{2} g_{i-1} \right) \right] \right\} \tag{7.8}$$

$i = 2, 3$

$$g_i = \frac{2}{\pi} \arctan \left[\frac{\pi}{\frac{\pi}{2} \frac{S}{h_1} - 2} \left(\frac{h_i}{h_1} \right) - 1 \right] \tag{7.9}$$

$$q_1 = 1 - \frac{h_1}{2S} \ln \left(\frac{\pi}{h_1} S - 1 \right) \tag{7.10}$$

$$q_i = \frac{h_1}{2S}\left\{\ln\left(\frac{\pi}{h_1}S-1\right)-(1+g_i)\times\ln\left[\frac{2S}{h_1}\frac{\cos\left(\frac{\pi}{2}g_i\right)}{\frac{2h_i}{h_1}-1+g_i}+\sin\left(\frac{\pi}{2}g_i\right)\right]\right\} \tag{7.11}$$

$$q_5 = 1-\sum_{j=2}^{4} q_j - q_1 \tag{7.12}$$

$$i = 2,\ 3$$

$$S = \sqrt{\frac{\varepsilon_{re}}{\varepsilon_{r,eff}}}\left[\left\{0.545a+0.882h_1+0.164h_1\frac{(\varepsilon_{re}-1)}{(\varepsilon_{re})^2}\right\} + h_1\frac{(\varepsilon_{re}-1)}{\pi\varepsilon_{re}}\{\ln(0.94+0.545a/2h_1)+1.451\}\right] \tag{7.13}$$

where,

$$\varepsilon_{re} = \frac{2\varepsilon_{r,eff}-1+\left(1+\frac{10h_1}{S}\right)^{-1/2}}{1+\left(1+\frac{10h_1}{S}\right)^{-1/2}} \tag{7.14}$$

The final value of S and ε_{re} are determined by two step iteration as proposed in [44].

7.2.1.3. Effective side length

The expression for effective side length is given as [34]:

$$a_{eff1} = a_1\left(1+p_{a1}\right)^{\frac{1}{2}} \tag{7.15}$$

In equation (7.15), p_{a1} arises due to the fringing fields at the edge of the patch. The p_{a1} for a ETPA may be obtained from originally formulated circular patch with radius r_1 [45] by employing an equivalent relation between circular geometry and equilateral triangular geometry of side length a_1 as provided in [34]. The equivalent relation between circular patch and ETPA is obtained as $r_1 = 0.4775a_1$. Now, p_{a1} can be computed as

$$p_{a1} = p_{11}+(1+p_{11})(p_{12}+p_{13}) \tag{7.16}$$

$$p_{11} = \left(1+\varepsilon_r^{-1}\right)\left(4h_1/0.4775\pi a_1\right) \tag{7.17}$$

$$p_{12} = (2/3)\left\{\left(0.37+0.63\varepsilon_r\right)^{-1}\left(8+0.4775\pi a_1/h_1\right)^{-1}\right\} \times \ln\left[\left\{1+0.8\left(0.4775 a_1/h_1\right)^2+\left(0.148 a_1/h_1\right)^4\right\}\left(1+0.4297\ a_1/h_1\right)^{-1}\right] \tag{7.18}$$

$$p_{13} = \left(4+1.2415 a_1/h_1+2.9 h_1/0.4775 a_1\right)^{-1}\left\{\left(0.37+0.63\varepsilon_r\right)^{-1}-1\right\} \tag{7.19}$$

$$\varepsilon_r = \frac{\varepsilon_{re}}{\varepsilon_{r,eff}\,1} \tag{7.20}$$

7.2.1.4. Input Impedance

The triangular patch of lower cavity may be treated as a single resonant parallel R_1-L_1-C_1 circuit as shown in Fig. 7.3 to calculate the input impedance of an ETPA covered with dielectric layers. Thus, the input resistance and reactance seen by a coaxial probe located at a distance ρ from tip of the triangle may be computed as

$$Z_{in1} = R_{in1} + j\,X_{in1} \tag{7.21}$$

$$R_{in1} = \frac{R_{r1} P_{nml1}}{1+Q_{T1}^2\left[\dfrac{f_{r1}}{f}-\dfrac{f}{f_{r1}}\right]^2} \tag{7.22}$$

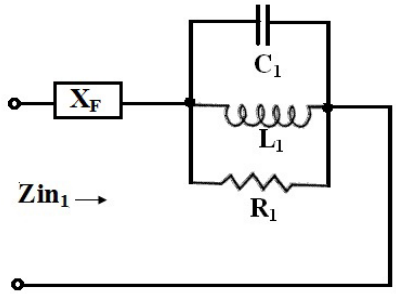

Figure 7.3: Equivalent resonant parallel R_1-L_1-C_1 circuit to compute the input impedance of the lower patch.

$$X_{in1} = X_f(f,\rho) + \frac{R_{r1} P_{nml1} Q_{T1}\left[\dfrac{f_{r1}}{f}-\dfrac{f}{f_{r1}}\right]}{1+Q_{T1}^2\left[\dfrac{f_{r1}}{f}-\dfrac{f}{f_{r1}}\right]^2} \tag{7.23}$$

R_{r1} is the input resistance at resonance, P_{nml1} is field factor and $X_f(f, \rho)$ is the probe reactance has been computed from equation (3.11) in chapter 3. The R_{r1} is taken as

$$R_{r1} = \left(\frac{\eta \, \pi h_1 \lambda_{r1} \, Q_{T1}}{\sqrt{2} \, a_{1eff}^2 \sqrt{\varepsilon_{r,eff\,1}}} \right) \tag{7.24}$$

where, η is the intrinsic impedance of the medium, Q_{T1} is the total quality factor and wave length $\lambda_{r1} = c/f_{r1}$.

$$P_{nml1}(\rho) = (5\pi)^{-1} \left[\cos\frac{2\pi l \rho}{\sqrt{3}\, a_1} + \cos\frac{2\pi n \rho}{\sqrt{3}\, a_1} + \cos\frac{2\pi m \rho}{\sqrt{3}\, a_1} \right]^2 \tag{7.25}$$

where, m, n, l are the integers which never zero simultaneously satisfying the condition $m + n + l = 0$.

7.2.1.5. Total Quality factors

The Q_{T1} is defined as

$$Q_{T1} = \left(\frac{1}{Q_{r1}} + \frac{1}{Q_{d1}} + \frac{1}{Q_{c1}} \right)^{-1} \tag{7.26}$$

Based on concept reported in [46] we have proposed a very simple expression to compute the Q_{r1} of an ETPA loaded with one or more dielectric layer as:

$$Q_{r1} = \frac{c \, \varepsilon_{r1}}{\sqrt{3} h_1 \, f_{r1} \, \varepsilon_{r,eff\,1}} \left(\frac{h_1}{h_{13}} \right) \tag{7.27}$$

The $Q_{c1,}$ can be expressed as

$$Q_{c1} = h_1 \sqrt{\pi f_{r1} \mu_0 \sigma} \tag{7.28}$$

Q_{d1} for this structure can be computed as

$$Q_{d1} = \frac{1}{\tan \delta_{e1}} \tag{7.29}$$

where, $tan\delta_{e1}$ is the equivalent loss tangent of the structure. The $tan\delta_{e1}$ is defined as

$$\tan\delta_{e1} = \frac{q_1 \varepsilon_{r1} \tan\delta_1 + q_2 \varepsilon_{r2} \tan\delta_2 + q_3 \varepsilon_{r3} \tan\delta_3}{\varepsilon_{re}} \tag{7.30}$$

The percentage bandwidth (V.S.W.R < 2) of the antenna is calculated as

$$\frac{1}{\sqrt{2}\, Q_{T1}} \, 100 \, \% \tag{7.31}$$

7.2.2 Upper cavity

7.2.2.1. Resonant frequency

Here the driven patch (lower patch) is considered as the ground plane of the upper parasitic patch. The structure of upper cavity is analyzed as the ETPA on two layered substrate. Based on cavity model analysis, the resonant frequency of an ETPA on two layered substrate (Fig. 7.4) operated in dominant mode may be computed from [29] as

$$f_{r2} = \frac{2c}{3a_{2eff}\sqrt{\varepsilon_{r,eff\,2}}} \tag{7.32}$$

where, a_{2eff} is the effective side length of the upper ETPA , $\varepsilon_{r,eff2}$ is the effective relative permittivity of the medium below the lower patch.

7.2.2.2. Effective permittivity $\varepsilon_{r,eff}$

The $\varepsilon_{r,eff2}$ for this two layered structure is written as

$$\varepsilon_{r,eff\,2} = \varepsilon_{re2} - \frac{\varepsilon_{re2} - \varepsilon_{r,dyn2}}{1 + G\left(f_a / f_p\right)^2} \tag{7.33}$$

where, G is purely empirical term, $\varepsilon_{r,dyn2}$ is the dynamic permittivity which depends on the dimensions, equivalent substrate relative permittivity ε_{re2}, field configurations of the mode under study and f_a is the frequency without fringing fields. The G, f_a and f_p are computed as

$$G = \sqrt{\frac{\varepsilon_{r,dyn2}}{\varepsilon_{re2}}} \tag{7.34}$$

$$f_a = \frac{2c}{3a_2\sqrt{\varepsilon_{re2}}} \tag{7.35}$$

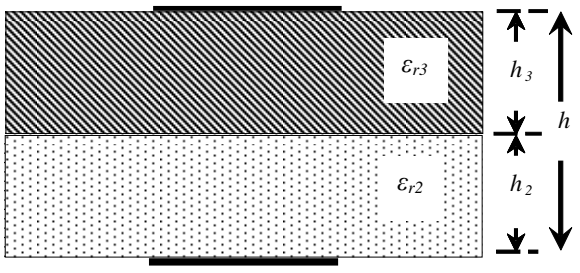

Figure 7.4: Configuration of the upper cavity.

$$f_p = \frac{Z\left(\frac{a_2}{h}, h, \varepsilon_{re2}\right)}{2\mu_0 h} \tag{7.36}$$

The $Z\ (a_2/h,\ h,\ \varepsilon_{re2})$ is the characteristic impedance. The $Z\ (a_2/h,\ h,\ \varepsilon_{re2})$ for an ETPA is obtained from originally formulated equation of rectangular geometry [1] by employing the similar equivalent relation between an equilateral triangular (side length a_2) and a rectangular geometry (width w_2 and length b_2) as taken for lower cavity (w_2 = 0.545 a_2 and b_2 = 0.955 a_2).Thus the $Z\ (a_2/h,\ h,\ \varepsilon_{re2})$ for an ETPA can be written as

$$Z\left(\frac{a_2}{h}, h, \varepsilon_{re2}\right) = \frac{120\pi}{\sqrt{\varepsilon_{rp}}}\left[\frac{0.545a_2}{h} + 1.393 + 0.667\ln\left(\frac{0.545a_2}{h} + 1.444\right)\right]^{-1} \tag{7.37}$$

$$\varepsilon_{rp} = \frac{\varepsilon_{re2}+1}{2} + \frac{\varepsilon_{re2}-1}{2}\left(1 + \frac{12h}{0.545a_2}\right)^{-1/2} \tag{7.38}$$

The ε_{re2} for this two-layer structure is modeled as the single-layer one having substrate thickness of $h = h_2 + h_3$. The upper layer has thickness h_3 with relative permittivity ε_{r3} and lower layer has thickness h_2 with permittivity ε_{r2}. The ε_{re2} can be computed as

$$\varepsilon_{re2} = \frac{\varepsilon_{r2}\varepsilon_{r3}h}{\varepsilon_{r2}h_3 + \varepsilon_{r3}h_2} \tag{7.39}$$

The $\varepsilon_{r,dyn}$ for this structure is computed as

$$\varepsilon_{r,dyn} = \frac{C_{dyn}(\varepsilon = \varepsilon_0\varepsilon_{re2})}{C_{dyn}(\varepsilon = \varepsilon_0)} \tag{7.40}$$

The $C_{dyn}(\varepsilon)$ can be calculated as

$$C_{dyn}(\varepsilon) = C_{0,dyn}(\varepsilon) + C_{e,dyn}(\varepsilon) \tag{7.41}$$

The total dynamic fringe field capacitance $C_{e,dyn}(\varepsilon)$ for this structure is written as

$$C_{e,dyn}(\varepsilon) = \frac{1}{2}\left[\frac{Z\left(a_2/h, h, \varepsilon_{re2}=1\right)0.955a_2}{cZ^2\left(a_2/h, h, \varepsilon_{re2}\right)} - C_{0,stat}(\varepsilon)\right] \tag{7.42}$$

$$C_{0,stat}(\varepsilon) = \frac{\sqrt{3}\,\varepsilon_0 \varepsilon_{re2}\, a_2^{\,2}}{4h} \tag{7.43}$$

The total dynamic main field capacitance $C_{0,dyn}(\varepsilon)$ is taken for the structure under study as

$$C_{0,dyn}(\varepsilon) = \gamma_{nm}\, C_{0,stat}(\varepsilon) \tag{7.44}$$

γ_{nm} = 0.3525, for n = 1

= 0.2865 = 2

= 0.2450 = 3

7.2.2.3 Effective side length a_{eff2}

The actual side length a_2 *i*s enhanced due to the effect of fringing field at the edge of the patch. This new side length termed as effective side length $a_{eff2.}$ The a_{eff2} is expressed as

$$a_{eff\,2} = a_2 \left(1 + p_{a2}\right)^{\frac{1}{2}} \tag{7.45}$$

In equation (52), p_{a2} arises due to the fringing field at the edge of the patch. The p_{a2} for an ETPA may be obtained from originally formulated circular geometry with radius r_2 [47] by employing an equivalent relation between circular geometry and equilateral triangular geometry of side length a_2, as taken for lower cavity (r_2 = 0.4775a_2). Thus p_{a2} can be written as

$$p_{a2} = \frac{2h}{\pi 0.4775 a_2\, \varepsilon_{re2}} \left(\log\left(\frac{0.4775 a_2}{2h} \right) + 1.41\varepsilon_{re2} + 1.77 + \frac{h}{0.4775\, a_2} \left(0.268\varepsilon_{re2} + 1.65\right) \right) \tag{7.46}$$

where, ε_{re2} is the equivalent relative permittivity of the medium below the patch. The ε_{re2} for a two layered structure is defined in (7.39).

7.2.2.4 Input Impedance

The lower patch can be treated as a resonant cavity modeled by a single resonant parallel of R_2-L_2-C_2 circuit. The equivalent resonant parallel L_2, C_2 and R_2 circuit of an ETPA is shown in Fig. 7.5. Here no direct co-axial feed is used to excite the upper patch. The model reported in [17] has been considered to determine the feed location of the upper patch for calculating of input impedance. The feed location of upper patch ρ' can be calculated as [17]:

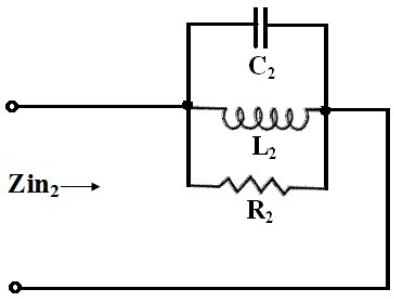

Figure 7.5: Equivalent resonant parallel R_2-L_2-C_2 circuit to compute the input impedance of the upper patch.

$$\rho' = \rho + \sqrt{3}(a_2 - a_1)/4 \tag{7.47}$$

Thus, the input resistance and reactance for upper patch may be written as

$$Z_{in2} = \frac{R_2(\rho')}{1 + Q_{T2}^2 A^2} + \frac{R_2(\rho') Q_{T2} A}{1 + Q_{T2}^2 A^2} \tag{7.48}$$

$$A = \left[\frac{f_{r2}}{f} - \frac{f}{f_{r2}} \right] \tag{7.49}$$

where, $R_2(\rho')$ is the input resistance at resonance, Q_{T2} is the total quality factor, f_{r2} is the resonant frequency defined in (7.32), f is the working frequency.

$R_2(\rho')$ is the resonant resistance of the microstrip element which varies with ρ' as:

$$R_2(\rho') = R_{r2} P_{nml2}(\rho') \tag{7.50}$$

Where, $p_{lnm2}(\rho')$ is the field factor and R_{r2} is the radiation resistance.

We have employed a simple and efficient expression to compute R_{r2} from [48] as

$$R_{r2} = \left(\frac{2\eta h Q_{T2}}{\pi a_{2eff} \sqrt{\varepsilon_{r,eff\,2}}} \right) \tag{7.51}$$

Where, Q_{T2} is the total quality factor, $\varepsilon_{r,eff2}$ is effective dielectric constant defined in (7.33) The field factor $p_{lnm2}(\rho')$ may be computed as

$$P_{nml2}(\rho') = 0.1076 \left[\cos\frac{2\pi l \rho'}{\sqrt{3}\, a} + \cos\frac{2\pi n \rho'}{\sqrt{3}\, a} + \cos\frac{2\pi m \rho'}{\sqrt{3}\, a} \right]^2 \tag{7.52}$$

7.2.2.5 Total quality factor Q_T

The total loss (Q_{T2}) is defined as

$$Q_{T2} = \left(\frac{1}{Q_{r2}} + \frac{1}{Q_{d2}} + \frac{1}{Q_{c2}} \right)^{-1} \tag{7.53}$$

Here we have taken a very simple and efficient expression to compute Q_{r2} as

$$Q_{r2} = \frac{30\, D(\delta)\, \varepsilon_{re2}}{\mu_0\, f_{r2}\, h} \tag{7.54}$$

where, first term is the mode dependent factor. ε_{re2} is defined in (7.39), f_{r2} is given by (7.32) and $D(\delta)$ is the directivity.

Here we have taken the new curve fitting formula for computing the directivity as proposed in:

$$D(\delta) = 3.194 - 0.482\,\delta + 3.042\,\delta^2 - 3.213\,\delta^3 + 4.924\,\delta^4 - 1.526\,\delta^5 \tag{7.55}$$

where,

$$\delta = \frac{\pi\, f_{r2}}{2\, f_{20}\, \sqrt{\varepsilon_{re2}}} \tag{7.56}$$

and

$$f_{20} = \frac{2c}{3a_2\, \sqrt{\varepsilon_{re2}}} \tag{7.57}$$

The quality factor due to conductor loss Q_{c2} can be expressed as

$$Q_{c2} = \frac{\pi \sqrt{\varepsilon_{r,eff\,2}}}{\lambda_{r2}\, \alpha_c} \tag{7.58}$$

α_c is the conductor loss and obtained from [49] as

$$\alpha_c = \frac{R_s}{Z\left(\frac{a_2}{h}, h, \varepsilon_{re2}\right) 0.545 a_2} \tag{7.59}$$

$$R_s = \sqrt{\frac{\pi\, f_{r2}\, \mu_0}{\sigma}} \tag{7.60}$$

where, σ is the conductivity and other variables have usual meaning.

Q_{d2} for this structure can be computed as

$$Q_{d2} = \frac{1}{\tan \delta_{e2}} \tag{7.61}$$

where, $tan\delta_{e2}$ is the equivalent loss tangent of a triangular patch on two dielectric layer may be defined as

$$\tan\delta_{e2} = \frac{h_2 \varepsilon_{r2} \tan\delta_2 + h_3 \varepsilon_{r3} \tan\delta_3}{h \varepsilon_{re2}} \tag{7.62}$$

The percentage bandwidth (V.S.W.R < 2) of the antenna is calculated as [1]

$$\frac{1}{\sqrt{2}\, Q_{T2}} 100\ \% \tag{7.63}$$

Since the patch of the lower cavity acts as a ground plane for the patch of the upper cavity and significant coupling also exist between two cavities, so the total input impedance of the EMCSETPA under study can be computed as the series connection of the impedances of the upper and lower cavities. Base on this fact, the total input impedance of the EMCSETPA can be expressed as

$$Z_{in}(f) = Z_{in1}(f) + \left(\frac{h_1}{h}\right)^{1/2} Z_{in2}(f) \tag{7.64}$$

Where, the term $(h_1/h)^{1/2}$ considered as the coupling factor between two cavity.

7.3 Patch fabrication and experimental tests

The prototypes of different side length have been etched on a Rogers dielectric substrates with two thickness (0.8265 & 1.58 mm), $\varepsilon_{r1} = \varepsilon_{r2} = 2.4$ and $tan\delta_1 = tan\delta_3 = 0.0022$. The lower patch was excited with a coaxial probe whose diameter $d = 1.24$ mm. To validate the model developed in section II we have performed a series of experiments using Network Analyzer Agilent- E5071B. Snapshot of a typical stacked configuration is shown in Fig. 7.6.

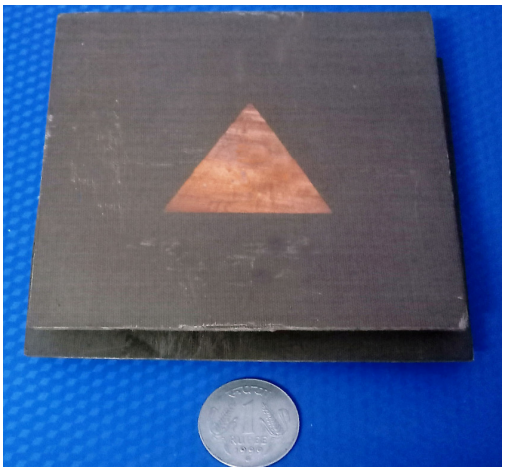

Figure 7.6: Snapshot of a typical ETPA in stacked configuration.

7.4 Results and discussions

We have presented the theoretically predicted, simulated and measured results for the resonant frequency and input impedance of an EMCSETPA under study. Here the first resonance is considered for lower patch and second resonance for upper patch [25].

A. Three layered structure

In table 7.1 and Fig. 7.7, we have compared simulated (HFSS) and measured [13] resonant frequencies with theoretical values employing the present model for different value of h_2 of an EMCSETPA with $a_1 = a_2 = 37$ mm, $\varepsilon_{r1} = \varepsilon_{r3} = 2.55$, $\varepsilon_{r2} = 1.0$, $h_1 = h_3 = 1.6$ mm. Comparison shows that the theoretical results are in close agreement with both HFSS and experimental results.

The validity of the present model for an EMCSETPA for different values of h_2 is further verified with simulation and our experimental results in Fig. 7.8. Here the thickness h_2 is varied using foam spacer. Comparison shows that the theoretical curves are in good correlation with HFSS and experimental results. From both table 7.1 and Figs. 7.7 and 7.8 we observe that the change of second resonant frequency is much significant with the change of h_2, whereas the change of first resonant frequency is negligible. The resonant frequency of the upper patch increases initially with h_2 but after a certain value of h_2 resonant frequency f_r decreases gradually.

TABLE 7.1

COMPARISON OF THEORETICALLY PREDICTED RESONANT FREQUENCIES FOR A THREE LAYERED STACKED EQUILATERAL TRIANGULAR PATCHES WITH HFSS SIMULATION AND EXPERIMENTAL RESULTS.

Foam thickness (h_2)	First resonance			Second resonance		
	Measured [13]	Simulated [43]	Computed	Measured [13]	Simulated [43]	Computed
0.0	3.1	3.083	3.050	3.54	3.218	3.236
1.5	3.12	3.104	3.109	3.81	3.769	3.858
3	3.135	3.116	3.129	3.77	3.732	3.825
4	-	3.122	3.137	3.72	3.662	3.744
5	-	3.134	3.143	3.61	3.591	3.652
6	-	3.143	3.148	3.56	3.514	3.556
Avg. %Error with respect to Exp			0.719	Avg. %Error with respect to Exp		2.203
Avg. %Error with respect to HFSS			0.427	Avg. %Error with respect to HFSS		1.754
$a_1 = a_2 =$ 37 mm, $\varepsilon_{r1} = \varepsilon_{r3} = 2.55$, $\varepsilon_{r2} = 1.0$, $h_1 = h_3 = 1.6$ mm.						

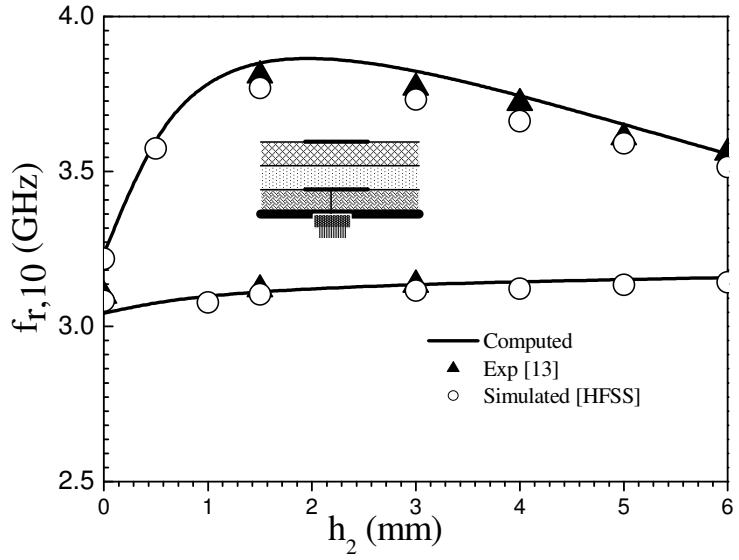

Figure 7.7: Computed, simulated and measured [13] dominant mode resonant frequency of ETPAs in three layered stacked patch configuration. $a_1 = a_2 = 37.0$ mm, $h_1 = h_3 = 1.60$ mm, $h_2 =$ variable, $\varepsilon_{r1} = \varepsilon_{r3} = 2.55$, $\varepsilon_{r2} = 1.0$, $tan\delta_1 = tan\delta_3 = 0.0025$, $tan\delta_2 = 0.00$.

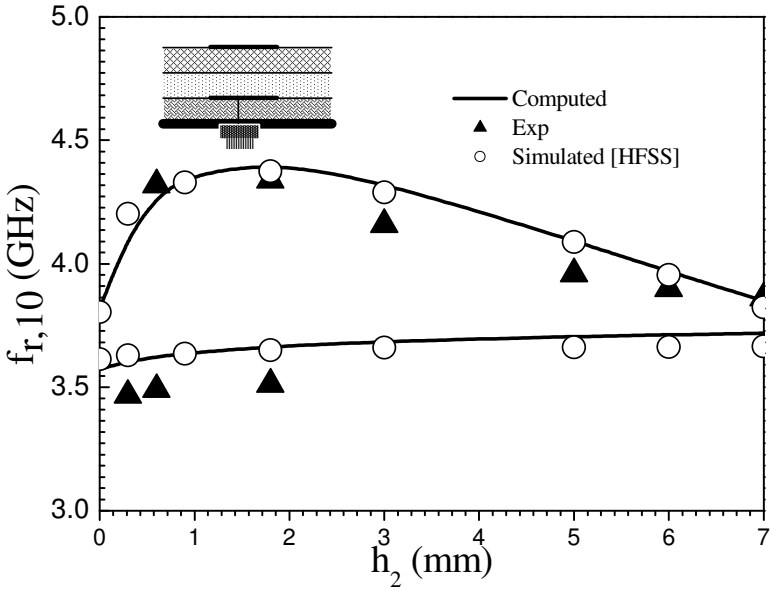

Figure 7.8: Computed, simulated and measured [our] dominant mode resonant frequency of ETPAs in three layered stacked patch configuration. $a_1 = a_2 = 32.0$ mm, $h_1 = 1.58$ mm, $h_2 =$ variable, $h_3 = 1.58$ mm, $\varepsilon_{r1} = \varepsilon_{r3} = 2.4$, $\varepsilon_{r2} = 1.0$, $tan\delta_1 = tan\delta_3 = 0.0022$, $tan\delta_2 = 0.00$.

Comparison of theoretical and experimental values of input impedance of a three layered EMCSETPA is shown in Table 7.2. Comparison shows that the computed input impedance employing the present model shows close agreement with experimental results.

TABLE 7.2
COMPARISON OF THEORETICALLY PREDICTED RESONANT RESISTANCE FOR A THREE LAYERED STACKED EQUILATERAL TRIANGULAR PATCHES WITH EXPERIMENTAL RESULTS.

Ant.	Foam thickness	Maximum resistance (First resonance)			Maximum resistance (Second resonance)		
	(h_2)	Measured		Computed	Measured		Computed
I	0.0	150.0	[13]	163.0	90.0	[13]	103.7
	1.5	150.0		116.0	55.0		63.8
	3	75.0		89.8	48.0		55.1
	4	-		78.0	52.0		52.6
	5	-		68.9	55.0		51.3
	6	-		61.7	62.5		50.6
II	0.0	229.0	[our]	226.0	150.0	[our]	162.0
	0.6	185.0		187.0	127.0		122.0
	1.2	161.0		159.0	82.0		106.0
	1.8	125.0		138.0	73.0		96.6

I: $a_1 = a_2 = 37$ mm, $\varepsilon_{r1} = \varepsilon_{r3} = 2.55$, $\varepsilon_{r2} = 1.0$, $h_1 = h_3 = 1.6$ mm, $tan\delta_1 = tan\delta_3 = 0.0025$, $tan\delta_2 = 0.00$, $\rho = 13.5$ [13]. II: $a_1 = a_2 = 35$ mm, $\varepsilon_{r1} = \varepsilon_{r3} = 2.4$, $\varepsilon_{r2} = 1.0$, $h_1 = 0.8265$ mm, $h_3 = 1.58$ mm, $tan\delta_1 = tan\delta_3 = 0.0022$, $tan\delta_2 = 0.00$, $\rho = 9.0$.

The theoretical, HFSS simulation and experimental variation of the input impedance of three layered EMCSETPA is depicted in Fig. 7.9. Theoretical curve shows excellent correlation with measured and simulated curve.

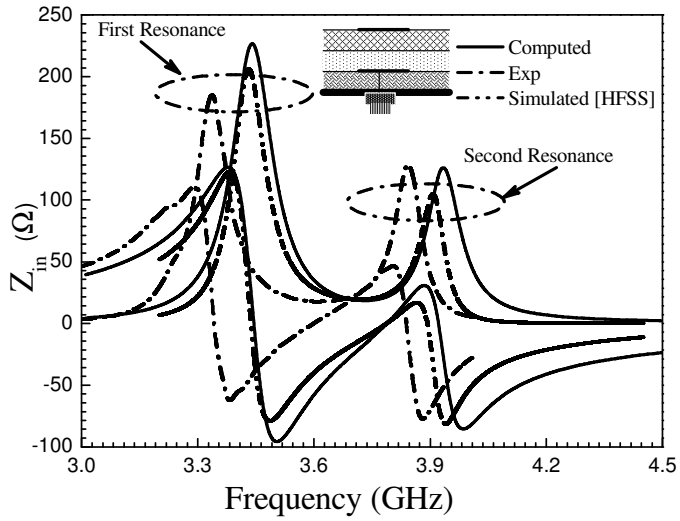

Figure 7.9: Computed, simulated and measured [our] dominant mode input impedance for probe-fed ETPAs in three layered stacked patch configuration. $a_1 = a_2 = 35.0$ mm, $h_1 = 0.8265$ mm, $h_2 = 0.6$ mm, $h_3 = 1.58$ mm, $\varepsilon_{r1} = \varepsilon_{r3} = 2.4$, $\varepsilon_{r2} = 1.0$, $tan\delta_1 = tan\delta_3 = 0.0022$, $tan\delta_2 = 0.00$, $\rho = \rho' = 9.0$ mm.

The variation of input impedance as a function of frequency for different values of h_2 is depicted in Fig. 7.10. It is observed that the input impedance decreases with the increase of h_2 but the change in resonant frequency is not significant for first resonance but the change in resonant frequency is more significant for second resonance.

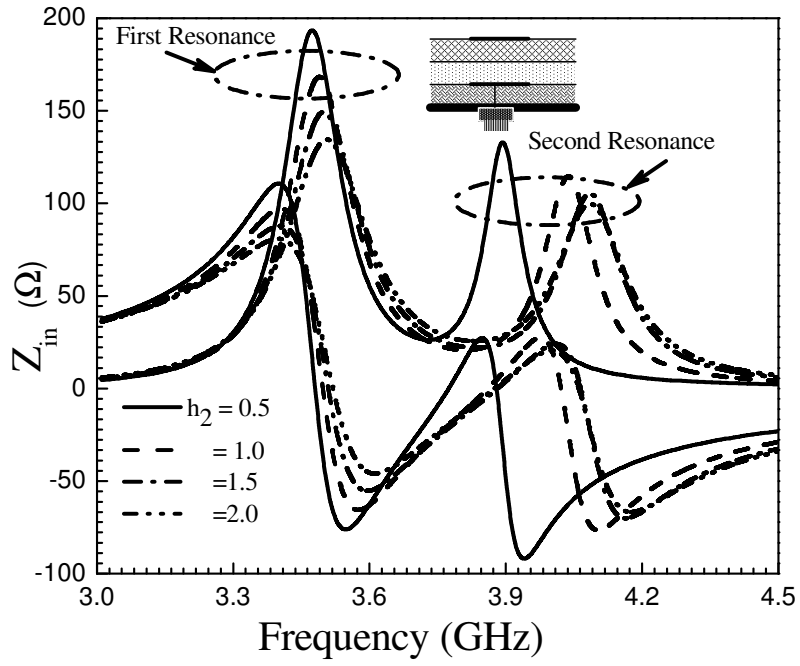

Figure 7.10: Variation of dominant mode input impedance for probe-fed ETPAs in stacked patch configuration as a function of frequency for different h_2. Other parameter as in Fig. 7.9.

The variation of resonant resistance as a function of feed location of three layered EMCSETPA is depicted in Fig. 7.11. Here we have compared computed curve with simulated (HFSS) values. Theoretical curve shows good agreement with simulated curve.

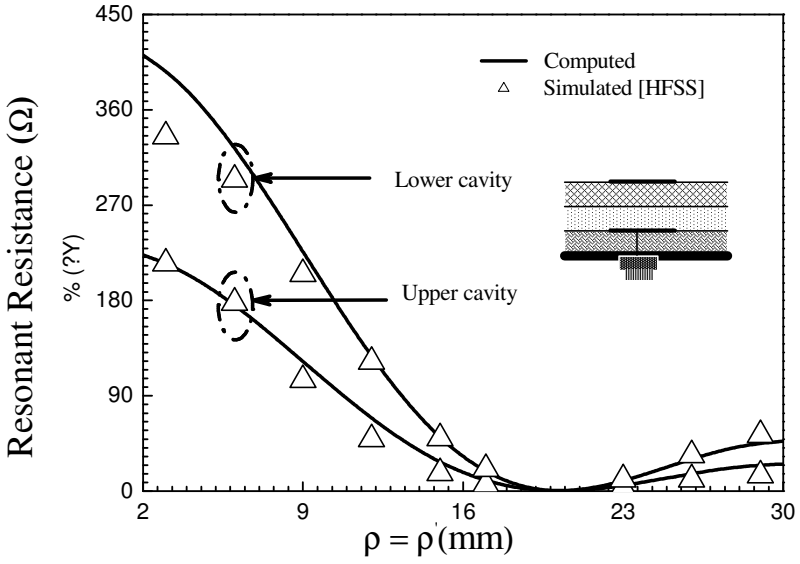

Figure 7.11: Computed and simulated variation of resonant resistance as a function of probe location for ETPAs in three layered stacked patch configuration. $a_1 = a_2 = 35.0$ mm, $h_1 = 0.8265$ mm, $h_3 = 1.58$ mm, $h_2 = 0.6$ mm, $\varepsilon_{r1} = \varepsilon_{r3} = 2.4$, $\varepsilon_{r2} = 1.0$, $tan\delta_1 = tan\delta_3 = 0.0022$, $tan\delta_2 = 0.00$.

Figure 7.12 depicts S_{11} (dB) variation as a function of an ETPA with and without stacked configuration. It is observed that ETPA without stacked configuration shows narrowband response where as ETPA with stacked configuration shows broad band response. Here the estimated bandwidth is about 16%. So, for improving the band width the ETPAs in stacked configuration is a good choice.

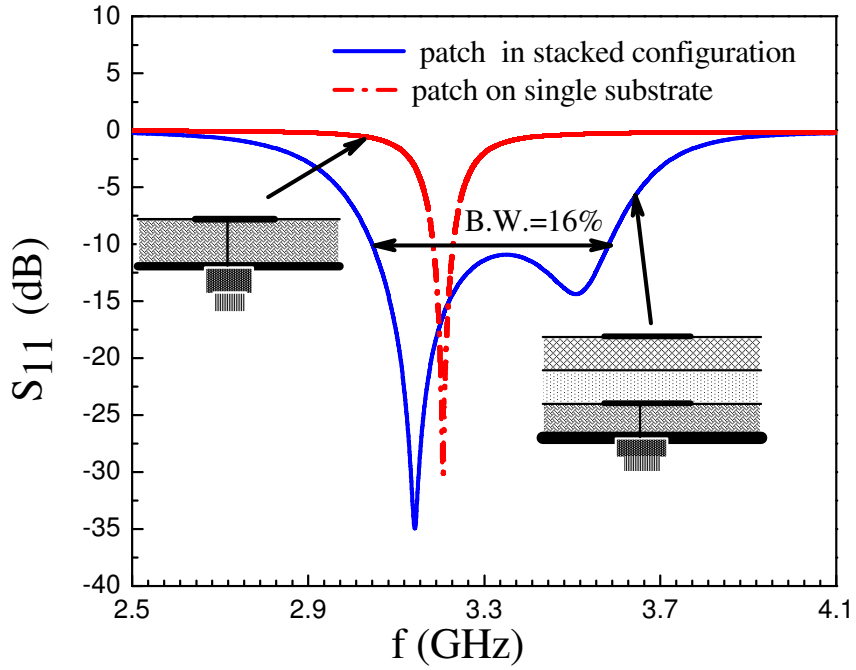

Figure 7.12: S_{11} (dB) as a function frequency of an ETPA with and without stacked configuration. $a_1 = a_2 =$ 37.0 mm, $h_1 = h_3 =$1.59 mm, $h_2 =$ 7.0 mm, $\varepsilon_{r1} = \varepsilon_{r3} =$ 2.4, $\varepsilon_{r2} =$ 1.0, $tan\delta_1 = tan\delta_3 =$ 0.0022, $tan\delta_2 =$ 0.00, $\rho = \rho' =$ 13.5 mm.

B. Two layered structure

In Table 7.3, we have compared theoretical resonant frequencies employing the present model with simulated (HFSS) values with for different values of ε_{r1} and ε_{r3} for a two layered EMCSETPA with $a_1 = a_2 =$ 37 mm, $\varepsilon_{r2} =$ 1.0, $h_1 = h_3 =$ 1.6 mm, $h_2 =$ 0.0 mm. Comparison shows that the theoretical results are in close agreement with simulated values.

The theoretical variation of input impedance for a two layered EMCSETPA as a function of frequency is shown in Fig. 7.13. Here we have compared the theoretical curve employing the present model with HFSS simulated and measured [14] curve. The theoretical curve shows small deviation from the measured and simulated curve. This is

due to the fact that a little air gap between the dielectric layers is present and that cannot be avoided. The slight air gap can causes a change in effective permittivity as well as resonant frequency of the structure.

TABLE 7.3

COMPARISON OF THEORETICALLY PREDICTED RESONANT FREQUENCIES FOR A TWO LAYERED STACKED EQUILATERAL TRIANGULAR PATCHES WITH HFSS SIMULATION RESULTS.

ε_{r1}	ε_{r3}	First resonance		Second resonance		BW%	
		Simulated [43]	Computed	Simulated [43]	Computed	Simulated [43]	Computed
2.5	2.5	3.024	3.078	3.263	3.264	7.603	5.866
2.4	2.4	3.075	3.137	3.321	3.324	7.692	5.789
2.33	2.33	3.121	3.180	3.373	3.367	7.761	5.713
2.2	2.2	3.202	3.265	3.426	3.452	6.759	5.568
2.5	2.4	3.075	3.084	3.321	3.324	7.692	7.491
2.5	2.33	3.0427	3.087	3.359	3.367	9.882	8.677
2.5	2.2	3.065	3.094	3.445	3.452	11.674	10.938
$a_1 = a_2 =$ 37 mm, $\varepsilon_{r2} = 1.0$, $h_1 = h_3 = 1.6$ mm, $h_2 = 0.0$ mm.							

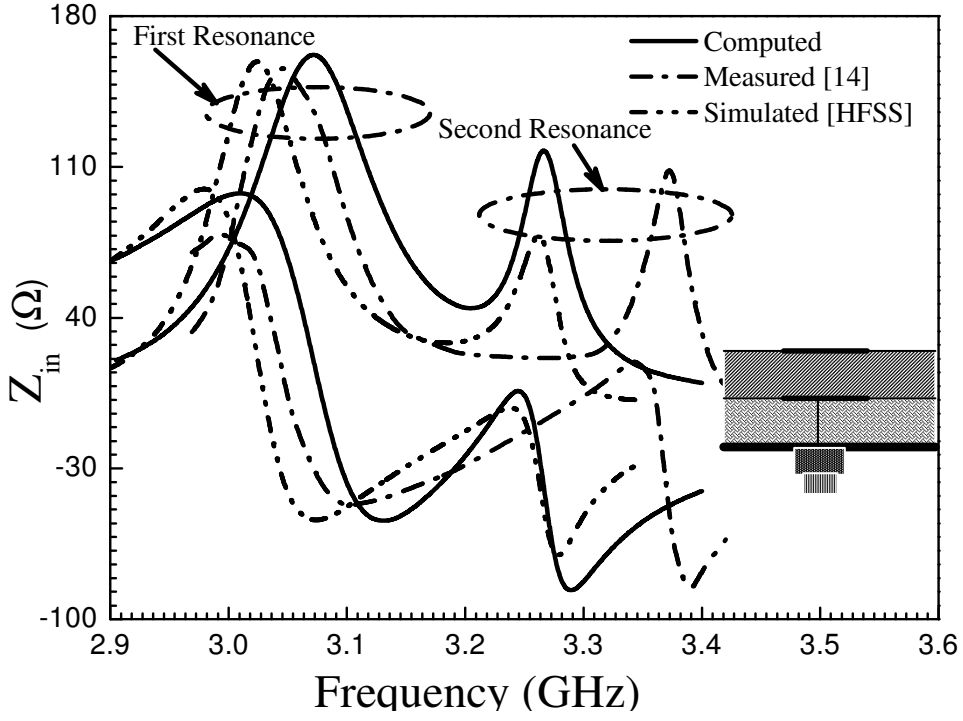

Figure 7.13: Computed, simulated and measured dominant mode input impedance for probe-fed ETPAs in stacked configuration. $a_1 = a_2 = 37.0$ mm, $h_1 = h_3 = 1.59$ mm, $h_2 = 0.0$ mm, $\varepsilon_{r1} = \varepsilon_{r3} = 2.4$, $\varepsilon_{r2} = 1.0$, $tan\delta_1 = tan\delta_3 = 0.0022$, $tan\delta_2 = 0.00$, $\rho = \rho' = 13.5$ mm.

6.5. Conclusions

In this article, a very simple and accurate model is presented to determine the resonant frequency, input impedance of an electromagnetically coupled stacked equilateral triangular patch antenna. This model is based on conformal mapping technique, cavity model analysis and single resonant parallel *R-L-C* circuit. The computed values employing the present model is compared with experimental results available in open literature and our new experimental results. Electromagnetic simulation software (HFSS) also used to validate the present model. The computed values employing the present model is very close to the experimental and simulation results. This information is very useful for practical implementation of electromagnetically coupled stacked equilateral triangular patch antenna in different microwave and wireless applications.

REFERENCES

[1] R. Garg, P. Bhartia, I. J. Bahl, and A. Ittipiboon, "Microstrip antenna design handbook," *Artech house*, 2001.

[2] G. Kumar and K. P. Ray, "Broadband microstrip antennas," *Artech House,* 2003.

[3] M. Biswas and M. Sen, "Design and development of rectangular patch antenna with superstrates for the application in portable wireless equipments and aircraft radome," *Microw. Optical Technol. Lett.* vol. 56, PP. 883-893, 2014.

[4] E. Nyfors and P. Vainikainen, "Industrial microwave sensors," *Artech House*, 1989.

[5] Y. Li and N. Bowler, "Resonant frequency of a rectangular patch sensor covered with multilayered dielectric structures," *IEEE Trans. Antennas Propagat*., vol. 58, pp. 1883-1889, 2010.

[6] H. Baltes , W. G.opel, and J. Hesse, " Sensors update," Wiley– Vch, Germany, Vol. 7, 2000.

[7] M. Bogosanovich, "Microstrip patch sensor for measurement of the permittivity of homogeneous dielectric materials," *IEEE Trans. Instrum. Meas.*, vol. 49, pp. 1144–1148, Oct. 2000.

[8] Zucchelli, M. Chimenti, and E. Bozzi, "Application of a coaxial-fed patch to microwave non-destructive porosity measurements in low-loss dielectrics," *Progr. Electromagn. Res*., vol. 5, pp.1–14, 2008.

[9] A. K. Verma, Nasimuddin, and A. S. Omar, "Microstrip resonator sensors for determination of complex permittivity of materials in sheet, liquid and paste forms," *Proc. Inst. Elect. Eng.*, vol. 152, pp. 47–54, 2005.

[10] A. Cataldo, G. Monti, E. De Benedetto, G. Cannazza, and L. Tarricone, "A noninvasive resonance-based method for moisture content evaluation through microstrip antennas," *IEEE Trans. Instrum. Meas.*, vol. 58, pp. 1420–1426, May 2009.

[11] M. Biswas and A. Mandal, "Design and development of an equilateral patch sensor for determination of permittivity of homogeneous dielectric medium," *Microw. Optical Technol. Lett.,* vol. 56, pp. 1097-1104, May. 2014.

[12] K. F. Lee, K. M. Luk, and J. S. Dahele, "Characteristics of the equilateral triangular patch antenna," *IEEE Trans. Antennas Propagat*., vol. 36, no.11, pp.1510-1518, Nov. 1988.

[13] P. S. Bhatnagar, J. P. Daniel, K. Mahdjoubi, and C. Terret, "Experimental study on stacked triangular microstrip antennas," *Electron. Lett*., vol. 22, no. 16, pp. 864-865, July 31, 1986.

[14] D. Mirshekar-Syahkal and H. R. Hassani, "Characteristics of stacked rectangular and triangular patch antennas for dual band applications," *1993 Eighth Int. Conf. on Antennas and Propagat.*, Edinburgh, vol. 2, pp. 728-731, 1993.

[15] J. Anguera, C. Puente, and C. Borja, "A procedure to design stacked microstrip patch antennas based on a simple network model," *Micro. Opt. Technol. Lett.*, vol. 30, 149–151, Aug. 2001.

[16] H. R. Hassani and D. M. Syahkal, "Study of electromagnetically coupled stacked rectangular patch antennas," *IEE Proc. Microw. Antennas Propagat.*, vol. 142, 7–13, Feb. 1995

[17] J. G. Tagle and C. G. Christodoulou, "Extended cavity model analysis of stacked microstrip ring antennas," IEEE Trans. Antennas Propagat., vol. 45, 1626–1635, Nov. 1997.

[18] M. Edimo, K. Mahdjoubi, A. Sharaiha, C. Terret, "simple circuit model for coax-fed stacked rectangular microstrip patch antenna," *IEE Proc.-Microw. Antennas Propagat.*, vol. 145, pp. 268-272, June 1998.

[19] Z. Wang, S. Fang, S. Fu, and S. Lü, "Dual-band probe-fed stacked patch antenna for GNSS applications" *IEEE Antennas Wireless Propagat. Lett.*, vol. 8, pp. 100-103. 2009.

[20] Z. Wang, S. Fang, S. Fu, and S. Jia, "Single-fed broadband circularly polarized stacked patch antenna with horizontally meandered strip for universal UHF RFID applications," *IEEE Trans. Microw. Theory Tech.*, vol. 59, pp. 1066–1073. 2011.

[21] O. P. Falade, M. U. Rehman, Y. Gao, X. Chen, and C. G. Parini, "Single stacked patch circular polarized antenna for triple band GPS receivers" *IEEE Trans. Antennas Propagat.*, vol. 60, pp. 4479–484, 2012.

[22] Q. Zhu, S. Yang, and Z. Chen, "Modified corner-fed dual-polarised stacked patch antenna for micro-base station applications" *Electron. Lett.*, vol. 51, pp. 604–06, 2015.

[23] Y. Gao, R. Ma, Y. Wang, Q. Zhang, and C. Parini, "Stacked patch antenna with dual-polarization and low mutual coupling for massive MIMO," *IEEE Trans. Antennas Propagat.*, vol. 64, pp. 4544–549, 2016.

[24] J. Hu, Z-C. Hao and W. Hong, "Design of a wideband quad-polarization reconfigurable patch antenna array using a stacked structure," *IEEE Trans. Antennas Propagat.*, vol. 65, pp. 3014–3023, 2017.

[25] M. Biswas and M. Sen, "Design and development of coax-fed electromagnetically coupled stacked rectangular patch antenna for broad band application' *Prog. Electromag. Res. B.*, vol. 79, pp. 21–44, 2017.

[26] Q. Luo et al, "Dual circularly polarized equilateral triangular patch array*," IEEE Trans. Antennas Propagat.*, vol. 64, pp. 2255-2262, 2016.

[27] J. T. S. Sumantyo, K. Ito, and M. Takahashi, "Dual-band circularly polarized equilateral triangular-patch array antenna for mobile satellite communications," *IEEE Trans. Antennas Propagat.*, vol. 53, no. 11, pp. 3477 – 3485, Nov. 2005.

[28] J. - S. Hong and M. J. Lancaster, "Theory and experiment of dual-mode microstrip triangular patch resonators and filters," *IEEE Trans. Microw. Theory Tech.*, vol. 52, no. 4, pp. 1237 – 1243, Apr. 2004.

[29] J. Helszajn and D. S. James, "Planar triangular resonators with magnetic walls," *IEEE Trans. Microw. Theory Tech*., vol. MTT-26, pp. 95-100, Feb. 1978.

[30] A. K. Sharma and B. Bhat, "Analysis of triangular microstrip resonator," *IEEE Trans. Microw. Theory Tech*., vol. 30, no. 11, pp. 2029 – 2031, Nov. 1982.

[31] J. S. Dahele and K. F. Lee: 'On the resonant frequencies of the triangular patch antenna', *IEEE Trans. Antennas Propagat.*, vol. 35, pp.100-101, 1987.

[32] W. Chen, K. F. Lee, and J. S. Dahele, "Theoretical and experimental studies of the resonant frequencies of equilateral triangular microstrip antenna," *IEEE Trans. Antennas Propagat.*, vol. 40, pp.1253-1256, Oct. 1992.

[33] D. Karaboğa, K.Güney, N. Karaboğa, and A. Kaplan, "Simple and accurate effective side length expression obtained by using a modified genetic algorithm for the resonant frequency of an equilateral triangular microstrip antenna,"*Int. J. Electron.,* vol. 83, pp.99-108, Jan.1997.

[34] D. Guha and J.Y. Siddiqui, "Resonant frequency of equilateral triangular microstrip patch antenna with and without air gaps," *IEEE Trans. Antennas Propagat.*, vol. 52, no.8, pp. 2174-2177, Aug. 2004.

[35] M. M. Olaimat and N. I. Dib, "Improved formulae for the resonant frequencies of triangular microstrip patch antennas," *Int. J. Electron.,* vol. 98, pp. 407-424, 2011.

[36] M. M. Olaimat and N. I. Dib, "A study of 15^0-75^0-90^0 angles triangular patch antenna," *Progr. Electromagn. Res. Lett.*, vol. 21, pp. 1-9, 2011.

[37] K. Guney and E. Kurt, "Effective side length formula for resonant frequency of equilateral triangular microstrip antenna," *Int. J. Electron.,* vol. 103, pp. 261-268, 2016.

[38] Nasimuddin, K. Esselle, and A. K.Verma, "Resonant frequency of an equilateral triangular microstrip antenna," *Microwav. Opt. Technol. Lett.,* vol. 47, no.5, pp.485-489, Dec. 2005.

[39] C. S. Gurel and E.Yazgan, 'New computation of the resonant frequency of a tunable equilateral triangular microstrip patch', *IEEE Trans. Microw. Theory Tech.*, vol. 48, pp. 334-338, 2000.

[40] P. Mythili, A. Das, "Simple approach to determine resonant frequencies of microstrip antennas," *IEE Proc. Microw. Antennas Propagat.,* vol. 145, No. 2, April 1998

[41] M. Biswas and D. Guha, "Input impedance and resonance characteristic of superstrate loaded triangular microstrip patch," *IET Microw. Antennas Propagat.,* vol. 3, pp. 92 – 98, Feb. 2009.

[42] M.Biswas and A. Mandal, "CAD model to compute the input impedance of an equilateral triangular microstrip patch antenna with radome," *Progr. Electromag. Res. M*., vol. 12, pp. 247-257, 2010.

[43] High Frequency Structure Simulator: Ansoft Corp. 2012.

[44] J. T. Bernhard and C. J. Tousignant, "Resonant frequencies of rectangular microstrip antennas with flush and spaced dielectric superstrates," *IEEE Trans. Antennas Propagat*., vol. 47, pp. 302–308, 1999.

[45] M. Biswas and S. Banik, "Characteristics of circular patch antenna with and without air gaps," *Microwave Opt. Technol. Lett*., vol. 54, pp. 1692-1699, 2012.

[46] M. Biswas and A. Mandal, "Experimental and theoretical investigation to predict the effect of superstrate on the impedance, bandwidth, and gain characteristics for a rectangular patch antenna," *J. Electromagn. Waves Applicat.*, vol. 29, no. 16, pp. 2093-2109, 2015.

[47] F. Abboud, J. P. Damiano, A. Papiernik, "A new model for calculating the input impedance of coax-fed circular microstrip antennas with and without air gaps," *IEEE Trans. Antennas Propagat*., vol. 38, pp. 1882–1885, 1990.

[48] A. Khellaf, D. Thouroude, J. P. Daniel, "Simple expression of rectangular patch's resistance at resonance," *Electron Lett*., vol. 26, pp. 1188–190, 1990.

[49] A.G. Derneryd, "Analysis of the microstrip disk antenna element," *IEEE Trans. Antennas Propagat*., vol. 27, pp. 660–664, 1979. D. M. Pozar, "Microwave engineering D. M. Pozar, "Microwave engineering," *John Wiley & Sons Inc*, 4th edition, 2012.

.

CHAPTER 8

Summary and Scope for Future Studies

Content:

8.1. Introduction

This treatise embodies the endeavour of the author towards contribution to incremental knowledge on the design and development of triangular patch antennas in multi-layered substrates. In this dissertation several models are proposed to alleviate lacunae of knowledge related to practical design and implementation of different triangular patch antennas. This chapter describes in details the summary of works carried out throughout the thesis; and hence suggest open areas related to this dissertation.

8.2. Summary

The **chapter 1** describes the outline of the chronological research and development of microstrip patch antennas during last few decades. It also highlighted the necessity, relevance and the motivating factor for carrying out this work as well as describes the outline of the studies which was worked out in the subsequent chapters.

The coaxial probe fed equilateral triangular microstrip patch antenna on single and double layered substrate has been thoroughly investigated in **Chapter 2.** Here an improved design guideline based on CAD oriented cavity model has been proposed to predict accurately the resonant frequency, quality factor, bandwidth and gain of the equilateral triangular patch antenna (ETPA). A simple equivalent single resonant parallel *R-L-C* circuit is employed for computation of input impedance. The superiority of the proposed model includes fast computation, mathematical simplicity and low computational cost. Only very few measured results of ETPA are hitherto reported. A number of prototypes of different side lengths were etched on different substrates like Rogers, Glass epoxy, Arlon etc. for experimental verification of the proposed model. We have performed a series of experiments using Network Analyzer Agilent- E5071B. Two commercial softwares (HFSS and CFDTD) are also used to validate proposed model. The proposed model shows close agreement with all the measured values and simulated results. From the studies carried out in chapter 2, we have found few important information: i) the tunability in resonant frequency and all other antenna parameters can be achieved very easily for an ETPA on double layered structure ii) the resonant frequency of ETPA decrease with the increase of patch side length, thickness and relative permittivity of the substrate, (iii) the total quality factor and the input impedance

is higher for a patch printed on composite substrate and lower for suspended substrate compared to patch printed on single substrate, (iv) the input impedance is higher for the feed location near the tip of the triangle and decreases with the increases of feed location from tip, and (v) both the gain and band width is low for an patch printed on composite substrate and high for suspended substrate compared to patch printed on single substrate. The information provided in this chapter is important for practical implementation of ETPA on single and double layered substrate.

The calculation of input impedance will be imperfect without consideration of the probe reactance. So, as a continuation of chapter 2, in **chapter 3** a closed form analytical formula is proposed to compute the probe reactance of an equilateral triangular patch antenna (ETPA) as a function of probe location and substrate electrical parameters. To the best of our knowledge, this is the only model available for computation of probe reactance of an ETPA. From this study in we observe that the probe reactance increases with the increase of frequency and decrease in patch size and decreases with the increase in substrate relative permittivity. The probe reactance is negligible when probe is located near the edge of the patch and become significant when probe is near the center of the patch and thickness of the substrate is high. The computed values of probe reactance employing the present model are verified with performed experiments using a Network Analyzer Agilent- E5071B. HFSS is also employed for validation of proposed model. The computed values employing present model is closely correlated with both experimental and simulated results.

Chapter 4 embodies the analysis of right angle isosceles triangular patch antenna (RAITPA) varying patch size, substrate electrical parameters and probe location. RAITPA finds very little investigation till now and also they did not provide accurate results. So, the effort of this work is to eradicate the drawbacks of the models reported earlier. To the best of our knowledge this is the first time RAITPA on both single and double layered (composite and suspended) has been investigated. A set of fast and accurate CAD oriented cavity model and single resonant parallel *R-L-C* circuit has been proposed to predict the resonant frequency, input impedance, quality factor, bandwidth and gain of a (RAITPA) as a function of patch size, substrate electrical parameters and probe location. From these studies we have observed that: both the resonant frequency

and input impedance significantly changes with the change of composite and suspended substrate thickness. The resonant frequency (f_r) and resonant resistance (R_r) increases for a RAITPA on suspended substrate, while f_r decreases and R_r increases for the antenna on composite substrate with respect to the single substrate antenna. The change in the total quality factor, bandwidth and gain is also possible with the change of substrate thickness for a RAITPA on double layered substrate. For experimental verification of the proposed theoretical model, a prototype has been fabricated on Roggers substrate whose thickness is 0.8265 mm, relative permittivity 2.4 and dielectric loss tangent 0.0022. The measurements were performed using an Agilent E 5071B Network Analyzer. HFSS is also used to validate the present model. The proposed model shows good agreement with the measured and simulated results compared to other reported model.

In **Chapter 5,** another triangular patch: the 30^0-60^0-90^0 right angled triangular patch antenna (RATPA) printed on a single, composite and suspended substrate is studied both theoretically and experimentally**.** A set of closed form expression based in cavity model is proposed to compute resonant frequency, quality factor, bandwidth and gain of 30^0-60^0-90^0 RATPA. Both the dynamic and effective permittivity has been considered to accurately take into account the influence of fringing field at the edge of the patch. In this studies we have seen that: (i) both the resonant frequency and input impedance are considerably changed with the change of composite and suspended substrate thickness and (ii) the improvement of gain and bandwidth is possible by controlling the thickness of air gap in between the substrate and ground plane without altering the antenna parameters. The proposed theoretical model is verified with the measured values found from previous literature and our performed experiments with the fabricated prototypes on Roggers (relative permittivity 2.4 and dielectric loss tangent 0.0022) and Taconic substrate (relative permittivity 2.33 and dielectric loss tangent 0.001). Simulated results obtained from HFSS and IE3D have also been employed to verify the theory. Present theoretical results shows excellent agreement with the measured and simulated results compared to other reported models. This theoretical design guide line is very useful for practical implementation of 30^0-60^0-90^0 RATPA in portable wireless equipment.

In outdoor applications of the patch antenna, it must be covered with dielectric layers to protect the patch against environmental peril. But so far triangular patch with dielectric cover layer finds very few investigations and they shows huge errors for high dielectric substrate. So, to rise above this problem, in **chapter 6,** a set of fast and accurate closed-form expressions based on conformal mapping, cavity model and the equivalent resonant parallel *R-L-C* have been presented to compute the parameters of a triangular patch antenna covered with several dielectric layers. The dielectric cover layer has significant effect on total quality factor. So, here improved formulae are considered to compute the quality factors including the effect of cover layers. From the studies of chapter 6 we have found that: (i) the resonant frequency change with the change of cover layer parameter i.e. the resonant frequency tuning of an ETPA is possible by varying the dielectric cover layer parameter without any change in main antenna parameters, (ii) the effect of first cover layer on both input impedance and resonant frequency is more significant than other higher cover layer, (iii) the change of gain is maximum when the cover thickness is half of the substrate thickness and (iv) the effect dielectric cover layer on gain is negligible though the effect on resonant frequency is more significant. The gain slightly reduces with the increase of dielectric cover layer. For the co-polar gain pattern, increase in the beam width is noticed with the addition of dielectric layer. For experimental verification, a series of experiments is performed with designed prototypes using a Network Analyzer Agilent- E5071B. HFSS has been also employed to validate the model. Present theoretical results shows good agreement with the measured and simulated results.

As, the triangular geometry shows narrow band response so, improvement in band width is the essential requirement. The ETPAs in stacked configuration can improve the bandwidth reasonably (≈ 20%) without degrading the other antenna performances. Now, for practical implementation of ETPA in stacked configuration, a closed form theoretical model is required but hitherto unreported. To the best of our knowledge this is the first time (described in **Chapter 7)**, an accurate CAD oriented closed form expressions have been proposed to compute resonant frequency, quality factor, band width, input impedance of an ETPA in stacked configuration. This model is based on transmission line model and cavity model analysis and single parallel *R-L-C* circuit. Here we have

studied the following facts: (i) the variation of dominant mode resonant frequency and input impedance as a function of foam thickness (h_2) for an ETPA in three layered stacked patch configuration, (ii) S_{11} variation as a function of frequency for a probe-fed ETPA in stacked configuration (iii) the variation of dominant mode resonant frequency and input impedance as a function of frequency of an ETPA in two layered stacked patch configuration. From the above studies we examined that (i) the change of both lower and upper resonance take place for the change of substrate superstrate electrical parameters for two layered and three layered stacked configuration, (ii) the dual resonance is absent for higher value of foam thickness (only upper resonance is present), and (iii) the input impedance decreases with the increase of h_2 and resonant frequency changes slightly in first resonance but the change in resonant frequency is more significant for the second resonance, and (iv) S_{11} plot of an ETPA shows that the band width is improved in stacked configuration (≈16%) in a specific configuration of substrate and superstrate. Theoretical results employing present model are compared with reported measured results and our performed experiments with fabricated prototypes. Commercial software HFSS has also been employed for validation of the proposed model. Present theoretical results shows excellent agreement with the measured and simulated results.

From the studies described in this thesis one can understand the implication of the present studies, their application in different area of microwave and wireless communication and the future scope of research.

8.3 Scope for Future Studies :

In future the research may be carried out in few areas which are related to this thesis. These are listed below:

(i) Investigation of probe reactance for right angled isosceles as well as 30^0-60^0-90^0 right angled triangular microstrip patch antenna on single layered and double layered substrate.

(ii) Investigation of right angled isosceles and 30^0-60^0-90^0 right angled triangular microstrip patch antenna covered dielectric superstrate.

(iii) Investigation of right angled isosceles and 30^0-60^0-90^0 right angled triangular microstrip patch antenna in stacked configuration.